

## DOCTOR OF PHILOSOPHY

### Semi-Active Nonlinear Predictive Suspension Control for Off-Road Vehicles

Ballard, Brandon

*Award date:*  
2022

*Awarding institution:*  
Coventry University

[Link to publication](#)

#### **General rights**

Copyright and moral rights for the publications made accessible in the public portal are retained by the authors and/or other copyright owners and it is a condition of accessing publications that users recognise and abide by the legal requirements associated with these rights.

- Users may download and print one copy of this thesis for personal non-commercial research or study
- This thesis cannot be reproduced or quoted extensively from without first obtaining permission from the copyright holder(s)
- You may not further distribute the material or use it for any profit-making activity or commercial gain
- You may freely distribute the URL identifying the publication in the public portal

#### **Take down policy**

If you believe that this document breaches copyright please contact us providing details, and we will remove access to the work immediately and investigate your claim.

# **Semi-Active Nonlinear Predictive Suspension Control for Off-Road Vehicles**

by

**Brandon Lee James Ballard**

**Doctor of Philosophy**

November 2021



Institute for Future Transport and Cities

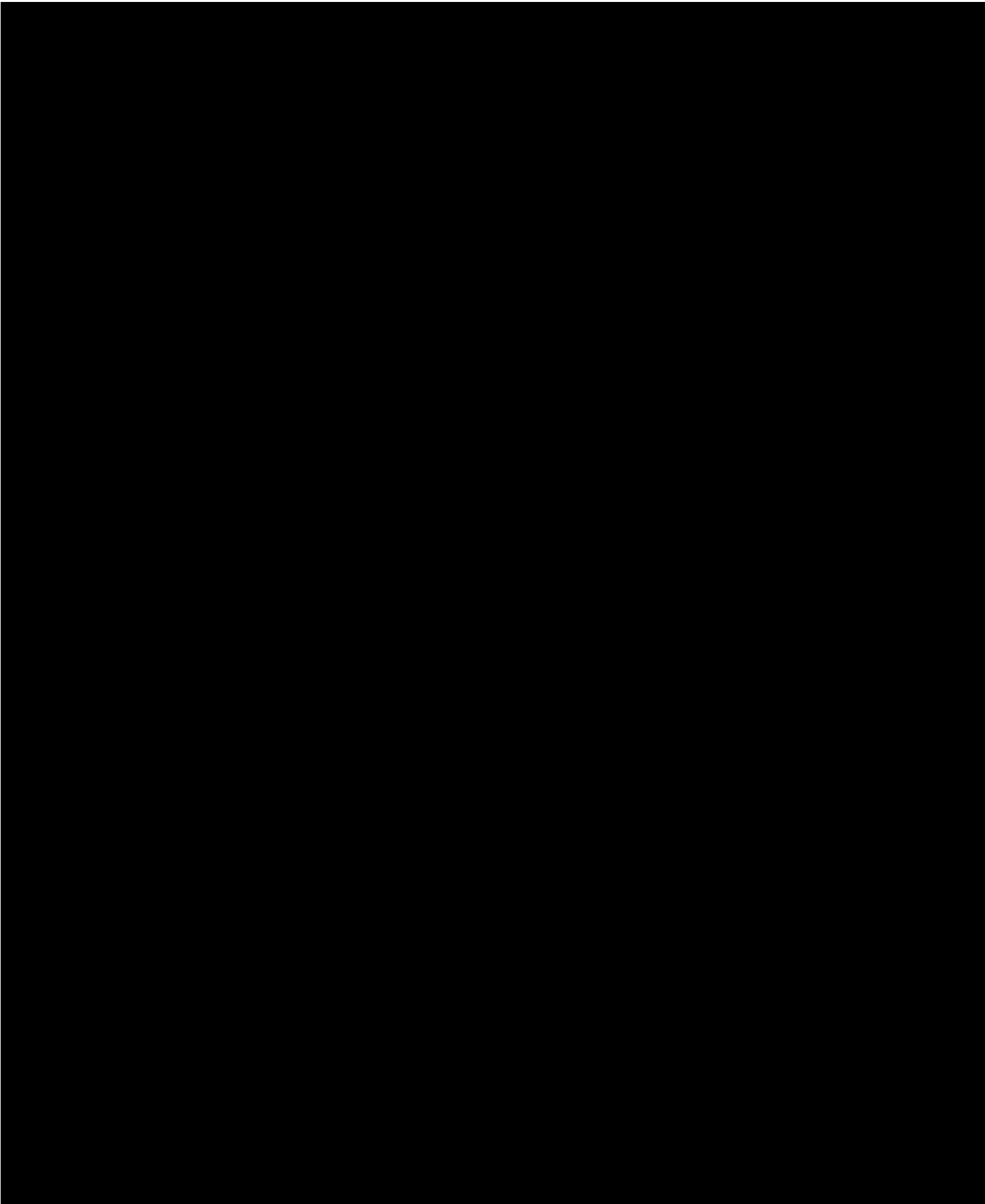


## Certificate of Ethical Approval

Applicant: Brandon Ballard  
Project Title: Semi-Active Nonlinear Predictive Suspension Control for Off-Road Vehicles

This is to certify that the above named applicant has completed the Coventry University Ethical Approval process and their project has been confirmed and approved as Low Risk

Date of approval: 05 Oct 2020  
Project Reference Number: P110838





## **Acknowledgements**

I would like to acknowledge the following people who have helped and advised me in the development of this thesis.

Firstly, I am extremely grateful to Dr. Olivier Haas for his role as my current Director of Studies and who has been instrumental in the writing and revising process. There was many a long nights spent revising and redrafting this thesis and without him this thesis would never have been completed. His constructive advice on the development and tuning of the PID and NMPC controllers helped solidify my understanding of control theory.

I am also extremely grateful to Prof. Mike V. Blundell for his help as part of my supervisory team and who has been fundamental in the development of my knowledge of tyre modelling and vehicle dynamics. His practical insight into the development of the vehicle dynamics assessment process and the useful contributions he has made to the development of the off-road tyre-soil interaction model has been fundamental to the development of the off-road studies conducted herein.

I cannot begin to express my thanks to Dr. Arash M. Dizqah for his help as my previous Director of Studies and without whom, I would not have started this journey of discovery into a new subject area. His help and support during the early stages of my PhD journey cannot be overstated, with his knowledge in optimisation techniques and the opportunities he has provided me to develop my experience of presenting at conferences and producing high quality conference/journal papers.

I am also grateful to Dr. Stratis Kanarachos who provided help and technical support with issues related to the development of my MATLAB code, and the information he has provided towards the development of the literature review.

I would also like to extend my sincere thanks to Prof. Vladimir Vantsevich and the team of international researchers, who were involved in the NATO Agile Tyre Mobility in Severe Terrain Environments multi-year project. The research into off-road tyre-soil interaction as part of the project has helped develop my understanding of tyre-soil interaction modelling and offered opportunities to present my research to a wider audience.

Special thanks to Dr. Georgios Mavros for the helpful discussion we had on the development of the tyre-soil interaction model and the guidance you have provided with respect to off-road tyre modelling.

Finally, I would like to express my thanks to my family, to my parents who helped support me during the late nights and early mornings spent writing this thesis. To my brother who has been helpful during our discussions on lean coding for physical applications and thanks to my girlfriend Kun Zhao for all her support during the tough times. Thanks also to my friends and fellow PhD students who have all helped with advice and emotional support, throughout the PhD process.

I hope that you all will continue to offer your support to me going forward...

## **Abstract**

Off-road vehicle suspension systems are needed for the safe and comfortable traversal of off-road terrain. The use of semi-active suspension for off-road has previously been only considered using existing on-road techniques. However, the behaviour of tyres on soft-soils changes considerably when considering the sinkage of the tyre into the soil. The focus of this thesis is the proposal of a nonlinear model predictive controller which is capable of being used for the control of semi-active magnetorheological damper based suspension on off-road soft soils. This thesis proposes modifications to existing nonlinear damper models to improve the accuracy of the damper forces used during simulations. Utilising the newly modified damper models this thesis proposes formulations of two vehicle models; quarter car, and full car. These formulations are utilised in the composition and simulation of a simulated nonlinear model predictive controller for on-road performance assessment against other controller formulations. A computationally effective controller is also proposed, namely an adaptive proportional-integral-derivative controller. It adjusts its gains in proportion to the normalised suspension deflection and relative velocity. It is combined with cascade control techniques for the case of full car suspension controller. The controllers are tuned to manipulate the current supply to a magnetorheological damper to achieve a reduction in the vertical accelerations of the vehicle body in order to improve vehicle ride comfort. The nonlinear model predictive controller was also modified and utilised for off-road soft soil suspension control on both flat and gently sloping terrain. The soft soil behaviour of the tyre is modelled using a modified tyre-soil interaction model which is adapted here to improve the speed of calculation through the use of lookup tables. The simulation studies conducted herein show that the nonlinear model predictive controller can perform far better than the proportional-integral-derivative (PID) controllers when operated on-road due to its ability to predict the behaviour of the vehicle response to incoming disturbances. The PID based controllers are tuned for a specific scenario. The nonlinear model predictive controller have the advantage of being able to adapting to a change in scenarios. However, the improvement seen for the controller on soft soils is marginally better and suggestions for further research into both the tuning process for the controller and the method of integration between the tyre-soil interaction model and the vehicle model are proposed in the conclusion.



# Table of contents

|  |            |
|--|------------|
| <b>List of figures</b>                                     | <b>xv</b>  |
| <b>List of tables</b>                                      | <b>xix</b> |
| <b>Nomenclature</b>  | <b>xxi</b> |
| <b>1 Introduction</b>                                      | <b>1</b>   |
| 1.1 Background to the Project . . . . .                    | 1          |
| 1.2 Project Aim . . . . .                                  | 2          |
| 1.3 Research Questions . . . . .                           | 2          |
| 1.4 Technical Objectives . . . . .                         | 3          |
| 1.5 Research Methodology . . . . .                         | 3          |
| 1.6 Contributions to Existing Knowledge . . . . .          | 4          |
| 1.7 Outline of Thesis Structure . . . . .                  | 6          |
| <b>2 Literature Review</b>                                 | <b>11</b>  |
| 2.1 Introduction . . . . .                                 | 11         |
| 2.2 Vehicle Ride Comfort and Handling . . . . .            | 12         |
| 2.3 Vehicle Modelling . . . . .                            | 14         |
| 2.4 Magnetorheological Damper Modelling . . . . .          | 17         |
| 2.4.1 Nonlinear Hysteretic Biviscous Model . . . . .       | 17         |
| 2.4.2 Nonlinear Viscoelastic Plastic Model . . . . .       | 19         |
| 2.4.3 Bouc-Wen and Modified Bouc-Wen Models . . . . .      | 19         |
| 2.5 Control of Active and Semi-Active Suspension . . . . . | 22         |
| 2.5.1 Closed Loop Control . . . . .                        | 22         |
| 2.5.2 Semi-Active Suspension Control in Industry . . . . . | 25         |
| 2.5.3 Preview Information and Predictive Control . . . . . | 27         |
| 2.6 Terrain Modelling and Terramechanics . . . . .         | 28         |
| 2.6.1 On-Road Conditions . . . . .                         | 28         |

|          |  |           |
|----------|--|-----------|
| 2.6.2    | On-road Tyre Models and Contact Point Formulation . . . . .              | 29        |
| 2.6.3    | Off-Road Conditions . . . . .  | 32        |
| 2.6.4    | Tyre-Soil Interaction Models . . . . .                                   | 33        |
| 2.6.5    | Terrain Parameters and Characteristics . . . . .                         | 36        |
| 2.7      | Concluding Remarks . . . . .   | 37        |
| <b>3</b> | <b>Nonlinear Magnetorheological Damper Modelling</b>                     | <b>41</b> |
| 3.1      | Introduction . . . . .   | 41        |
| 3.2      | Modified Nonlinear Hysteretic Biviscous Model . . . . .                  | 42        |
| 3.3      | Modified Nonlinear Viscoelastic Plastic Model . . . . .                  | 44        |
| 3.4      | Model Fitting and Parameterisation . . . . .                             | 47        |
| 3.4.1    | Experimental Setup . . . . .   | 47        |
| 3.4.2    | Model Fit Accuracy and Comparison to Other Available Models . . . . .    | 50        |
| 3.5      | Applications for Semi-Active Suspension Behaviour Modelling . . . . .    | 52        |
| 3.6      | Concluding Remarks . . . . .   | 56        |
| <b>4</b> | <b>Vehicle Dynamics System Modelling</b>                                 | <b>59</b> |
| 4.1      | Introduction . . . . .   | 59        |
| 4.2      | Nonlinear Quarter Car Vehicle Model . . . . .                            | 60        |
| 4.2.1    | Method 1: Single State Space Quarter Car Vehicle Model . . . . .         | 62        |
| 4.2.2    | Method 2: Coupled State Space Quarter Car Vehicle Model . . . . .        | 65        |
| 4.3      | Nonlinear Full Car Vehicle Model . . . . .                               | 68        |
| 4.3.1    | Method 1: Single State Space Full Car Vehicle Model . . . . .            | 69        |
| 4.3.2    | Method 2: Coupled State Space Full Car Vehicle Model . . . . .           | 75        |
| 4.4      | Modified Automotive Simulation Model (ASM) for Vehicle Dynamics Analysis | 79        |
| 4.4.1    | Modifications to the ASM Vehicle Dynamics Model . . . . .                | 83        |
| 4.4.2    | Comparison of Standard ASM Model and Modified ASM models . . . . .       | 84        |
| 4.5      | Concluding Remarks . . . . .   | 87        |
| <b>5</b> | <b>Tyre-Soil Interaction Modelling for Off-Road System Analysis</b>      | <b>89</b> |
| 5.1      | Introduction . . . . .   | 89        |
| 5.2      | Wheel Velocity and Slip Ratio . . . . .                                  | 90        |
| 5.3      | Rigid Wheel Tyre-Soil Interaction Modelling . . . . .                    | 93        |
| 5.3.1    | Pressure-Sinkage Relationship . . . . .                                  | 95        |
| 5.3.2    | The Computational Algorithm . . . . .                                    | 96        |
| 5.4      | Tyre-Soil Interaction Model Parameterisation . . . . .                   | 99        |
| 5.5      | Pre-Lookup Method Development . . . . .                                  | 99        |

---

|          |   |            |
|----------|---|------------|
| 5.5.1    | Generating Lookup Tables for Tyre-Soil Interaction . . . . .      | 100        |
| 5.5.2    | Lookup Table versus Pre-Lookup Method . . . . .                   | 101        |
| 5.6      | Sloped Terrain Tyre-Soil Interaction Modelling . . . . .          | 105        |
| 5.7      | Model Integration with Vehicle Models . . . . .                   | 110        |
| 5.7.1    | Quarter Car Off-Road Vehicle Model . . . . .                      | 110        |
| 5.8      | Concluding Remarks . . . . .                                      | 115        |
| <b>6</b> | <b>Nonlinear Quarter-Car Semi-Active Damper Controller Design</b> | <b>117</b> |
| 6.1      | Introduction . . . . .  | 117        |
| 6.2      | Constant Current Control . . . . .                                | 118        |
| 6.2.1    | MRPassive - Hard . . . . .  | 118        |
| 6.2.2    | MRPassive - Soft . . . . .  | 118        |
| 6.3      | PID Controller . . . . .  | 119        |
| 6.3.1    | Tuning of the PID Controller Gains . . . . .                      | 120        |
| 6.4      | Adaptive PID . . . . .  | 123        |
| 6.4.1    | Tuning of the Adaptive PID Controller Gains . . . . .             | 124        |
| 6.5      | Standard MPC . . . . .  | 126        |
| 6.6      | Nonlinear MPC . . . . .   | 127        |
| 6.6.1    | Defining the Quadratic Problem (QP) . . . . .                     | 129        |
| 6.6.2    | Controller Output Sampling Time . . . . .                         | 136        |
| 6.6.3    | Controller Tuning and Horizon Lengths . . . . .                   | 139        |
| 6.6.4    | Adapting the Controllers for Off-Road Use . . . . .               | 141        |
| 6.7      | Concluding Remarks . . . . .                                      | 144        |
| <b>7</b> | <b>Nonlinear Full Car Semi-Active Damper Controller Design</b>    | <b>145</b> |
| 7.1      | Introduction . . . . .  | 145        |
| 7.2      | PID and Adaptive Cascade PID Controllers . . . . .                | 146        |
| 7.2.1    | Full Car PID Controller . . . . .                                 | 146        |
| 7.2.2    | Adaptive Cascade PID Controller . . . . .                         | 147        |
| 7.2.3    | PID and Adaptive Cascade PID Tuning . . . . .                     | 148        |
| 7.3      | Nonlinear MPC . . . . .   | 149        |
| 7.3.1    | Defining the Quadratic Problem (QP) . . . . .                     | 150        |
| 7.3.2    | Controller Sample Time . . . . .                                  | 151        |
| 7.4      | Concluding Remarks . . . . .                                      | 156        |
| <b>8</b> | <b>Simulation and Discussion of Results</b>                       | <b>159</b> |
| 8.1      | Introduction . . . . .  | 159        |

|          |  |            |
|----------|--|------------|
| 8.2      | Simulation Study Setup . . . . .   | 160        |
| 8.3      | Simulation Study 1: The Influence of Damper Model on Controller Performance                      | 162        |
| 8.3.1    | Quarter Car Control . . . . .  | 163        |
| 8.3.2    | Full Car Control . . . . .   | 171        |
| 8.3.3    | Overall Findings for Simulation Study 1 . . . . .  | 176        |
| 8.4      | Simulation Study 2: The Influence of Preview Length on Controller Performance                    | 177        |
| 8.4.1    | Quarter Car Preview Length Testing . . . . .   | 178        |
| 8.4.2    | Full Car Preview Length Testing . . . . .  | 179        |
| 8.4.3    | Optimum Preview Horizon for NMPC . . . . .   | 181        |
| 8.5      | Simulation Study 3: The Influence of Tyre Model for Off-Road Controller<br>Performance . . . . . | 181        |
| 8.6      | Concluding Remarks . . . . .   | 183        |
| <b>9</b> | <b>Conclusions</b>   | <b>187</b> |
| 9.1      | Conclusions . . . . .  | 187        |
| 9.2      | Recommendations for Future Work . . . . .  | 189        |
|          | <b>Appendices</b>  | <b>191</b> |
| <b>A</b> | <b>Model Fitting Application</b>   | <b>193</b> |
| <b>B</b> | <b>MR Damper Vehicle Model Damping Tech Sheet</b>  | <b>195</b> |
| <b>C</b> | <b>MR Damper Model Fitting All Cases</b>   | <b>197</b> |
| <b>D</b> | <b>Convergence Time vs Tolerance</b>   | <b>223</b> |
| <b>E</b> | <b>PID Tuning Application</b>  | <b>225</b> |
| <b>F</b> | <b>NMPC Controller Iteration Limitations Supporting Evidence</b>                                 | <b>231</b> |
|          | <b>References</b>  | <b>233</b> |

# List of figures

|     |  |    |
|-----|--|----|
| 1.1 | Flow Chart Diagram showing the logical progression of content in this thesis   | 7  |
| 2.1 | A Diagram of the trade-off between Vehicle Ride Comfort and Vehicle Handling Based on the work from (Heißing and Ersoy 2010)   | 13 |
| 2.2 | Examples of Vehicle Models   | 14 |
| 2.3 | A Diagram Showing the Three Mechanisms of the Nonlinear Viscoelastic Plastic Model Based on the Work in (Snyder et al. 2001)   | 20 |
| 2.4 | Model Fit Accuracy Comparison two MR Damper Models to the Experimental Data from (Snyder et al. 2001; Spencer et al. 1997)   | 21 |
| 2.5 | Diagram of a Linear PID controller with System Feedback Loop   | 23 |
| 2.6 | PID Controlled Semi-Active Suspension Responding to step bump of 0.1 m ( $t = 5$ s) in height (Jamil et al. 2018)  | 24 |
| 2.7 | Diagram showing the Skyhook and Groundhook system representations (Heißing and Ersoy 2010)   | 25 |
| 2.8 | Diagram showing contact point formulation (Rill and Castro 2020)   | 31 |
| 2.9 | A graphical representation of the substitute circle method (Bekakos et al. 2016b; Harnisch et al. 2005)  | 35 |
| 3.1 | Diagram of the Modified Nonlinear Hysteretic Biviscous Model (modNonlin-HBV)   | 42 |
| 3.2 | Example plot of the force-velocity relationship curve produced by the NVEP and modNVEP models for the Passive Soft condition of the MR Damper during a simulation of a bump of 0.05m in height and at a velocity of $90\text{km.h}^{-1}$ . | 46 |
| 3.3 | LORD RD-8041 MR Damper Connected to INSTRON Fatigue and Tensile Testing Machine for Sinusoidal Testing using a LVDT for displacement sensing.  | 48 |
| 3.4 | Experimental Data of Sinusoidal Testing of Lord RD-8040-1 MR Damper at 1Hz for multiple current values.  | 49 |
| 3.5 | Comparison between damper models and measured data from testing at 1Hz 0A  | 51 |

|      |  |     |
|------|--|-----|
| 3.6  | Interpolated Parameter Fit Compared Against Real Data and Best Fit for 1 Hz<br>0.5 A Test Case . . . . .   | 54  |
| 3.7  | Subplots of the modNonlinHBV Damper Model Parameters Lookup Tables . . . . .   | 55  |
| 3.8  | The output of the transfer function with time constant 0.003 seconds with<br>respect to the response time to reach each of the table values. . . . .   | 56  |
| 4.1  | Quarter Car Vehicle Model Diagram . . . . .  | 61  |
| 4.2  | Simulink Connection Diagram for Quarter Car Vehicle Model using Method 1 . . . . .   | 65  |
| 4.3  | Simulink Connection Diagram for Quarter Car Vehicle Model Using Method 2 . . . . .   | 66  |
| 4.4  | Full Car Vehicle Model Diagram . . . . .   | 70  |
| 4.5  | Simulink Connection Diagram of the Full Car Model from Method 1 . . . . .  | 76  |
| 4.6  | Simulink Connection Diagram for Full Car Coupled State Space System . . . . .  | 78  |
| 4.7  | A Diagram Showing the Main Structure of the ASM Vehicle Dynamics Model<br>( <a href="#">dSPACE GmbH 2020</a> ) . . . . .   | 80  |
| 4.8  | A Simplified Diagram Showing the High Level Elements that form the Vehicle<br>Dynamics Subsystem . . . . .   | 82  |
| 4.9  | The simulated response of the ASM and 7DoF vehicle models to the step bump<br>road profile of height 0.02m at $90 \text{ km.h}^{-1}$ ( $25 \text{ m.s}^{-1}$ ) . . . . .   | 86  |
| 5.1  | The three angular velocity profiles using the predefined method. . . . .   | 92  |
| 5.2  | Diagram of a Rigid Wheel Model . . . . .   | 94  |
| 5.3  | A Diagram illustrating the computational process used in the semi-analytical<br>Bekakos model ( <a href="#">Bekakos et al. 2016b</a> ) . . . . .   | 97  |
| 5.4  | A Simplified Block Diagram of the Pre-Lookup Method . . . . .  | 102 |
| 5.5  | A Comparison Between the Pre-Lookup Method and the Lookup Table Longi-<br>tudinal Force versus Slip Ratio Curve for $R_u = 0.4 \text{ m}$ , $b = 0.2 \text{ m}$ and $F_z = 5000$<br>N for Dry Sand (Soil 1). . . . . | 103 |
| 5.6  | A Comparison Between the Pre-Lookup Method and the Lookup Table Longi-<br>tudinal Force versus Vertical Load at the Wheel Centre . . . . .   | 104 |
| 5.7  | A Diagram of the Sloped Terrain and the Reference Directions of the Sloped<br>Terrain Modifications . . . . .  | 106 |
| 5.8  | Longitudinal Force ( $F_x$ ) with respect to time for multiple inclines of sloped Dry<br>Sand terrain with a vertical load of 4000N . . . . .  | 108 |
| 5.9  | Longitudinal Velocity for sloped Dry Sand with a vertical load of 4000N . . . . .  | 109 |
| 5.10 | Slip Ratio of Sloped Dry Sand cases with 4000N of vertical load at wheel centre . . . . .  | 110 |
| 5.11 | Modified Quarter Car Vehicle Model for Off-Road . . . . .  | 111 |

|      |  |     |
|------|--|-----|
| 5.12 | A Simplified Block Diagram of the Tyre-Soil Integration with the Quarter Car Vehicle Model . . . . .   | 113 |
| 5.13 | Expanded Quarter Car System Block Diagram . . . . .  | 114 |
| 6.1  | A Simplified Block Diagram of the Quarter Car Vehicle PID Controller . . . .   | 120 |
| 6.2  | A Simplified Block Diagram for the Quarter Car Vehicle Adaptive PID Controller   | 125 |
| 6.3  | A Diagram showing the three horizons of a standard model predictive controller   | 127 |
| 6.4  | An example showing the NMPC as part of the MR Damper based Semi-Active suspension system for quarter car suspension control . . . . .  | 128 |
| 6.5  | A Process Flow Chart Detailing the Proposed Computational Algorithm . . . .  | 131 |
| 6.6  | Quarter Car Controlled Response over time for the two sampling time methods with a preview length of 0.1 seconds . . . . .   | 138 |
| 6.7  | Nonlinear Model Predictive Controller with Prediction/Preview Horizon of 500 steps (0.5 seconds), $m_s = 500$ [kg], $m_{us} = 50$ [kg], $K_c = 21300$ [N/m], $K_t = 270000$ [N/m], Vehicle Velocity = $90 \text{ km.h}^{-1}$ ( $25 \text{ m.s}^{-1}$ ), $Q = [0,0,0,0,0,0,1000]$ , $R = 0.1$ . . . . . | 139 |
| 6.8  | A Comparison between the NMPC Controller for bump step of height 0.02 m travelling at a velocity of $90 \text{ km.h}^{-1}$ . . . . .   | 141 |
| 7.1  | A Block Diagram of the Full Car PID Controller . . . . .   | 146 |
| 7.2  | A Simplified Block Diagram of the Adaptive Cascade PID Controller . . . . .  | 148 |
| 7.3  | The Full Car NMPC Algorithm . . . . .  | 152 |
| 7.4  | Vehicle Body Mass Displacement over time for the two sampling time methods with a preview length of 0.030 seconds . . . . .  | 154 |
| 7.5  | Vehicle Body Vertical 'Heave' Acceleration for two sampling time methods with a preview length of 0.030 seconds . . . . .  | 155 |
| 7.6  | Pitch Response of Full Car Model to Bump 0.02 m at 30 mph in comparison to the Dual-rate sampled controller . . . . .  | 156 |
| 8.1  | The bump road profile height displacements used in this thesis for the quarter car (left) and full car (right) models. . . . .   | 161 |
| 8.2  | Results of the MR Damper NMPC controllers for 30 mph . . . . .   | 164 |
| 8.3  | Results of the MR Damper NMPC controllers for 50 mph . . . . .   | 168 |
| 8.4  | Results of the MR Damper NMPC controllers for 30 mph round bump disturbance.   | 170 |
| 8.5  | Frequency Response of the modNVEP controlled case in comparison with the MRPassive case. . . . .   | 172 |
| 8.6  | Full Car Vehicle Response to step bump input . . . . .   | 173 |
| 8.7  | Full Car Vehicle Response to step bump input . . . . .   | 174 |

|      |  |     |
|------|--|-----|
| 8.8  | Frequency Response of the Full Car Vehicle Model as a result of a step bump  | 175 |
| 8.9  | Damper Current Supply for step bump input using NMPC strategy controllers  | 176 |
| 8.10 | Comparison between the passive ASM model and the ASM model with NMPC controller using the millisecond interval sampling . . . . .                        | 177 |
| 8.11 | NMPC Controller output for ASM Vehicle model test to step bump . . . . .   | 178 |
| 8.12 | A Comparison between the quarter car response for a preview controller and a controller without preview supplied . . . . .                               | 179 |
| 8.13 | Vehicle Body Vertical Displacement for Different Preview Lengths of the NMPC 10 millisecond Interval Controller . . . . .                                | 180 |
| 8.14 | Vehicle Body Heave Acceleration for Different Prediction/Preview Lengths measured in steps of 0.01 seconds using the Dual-Rate Sampling Method . . . . . | 181 |
| 8.15 | A Comparison between the full car responses of the modNVEP controlled cases for a bump at 30 mph. . . . .  | 182 |
| 8.16 | A comparison between the velocity of the vehicle and the sprung mass acceleration for both uncontrolled and modNVEP controlled cases. . . . .            | 183 |
| 8.17 | Sprung Mass Acceleration of Quarter Car Vehicle on off-road Dry Sand with NMPC dual-rate sampled controller using 10 steps of preview . . . . .          | 184 |
| 8.18 | Passive and semi-active responses for the unsprung mass displacement on Dry Sand (Soil 1) and Upland Sandy Loam (Soil 2) . . . . .                       | 184 |
| 8.19 | The output current of the NMPC current using 10 steps of preview on Dry Sand (Soil 1) and Upland Sandy Loam (Soil 2) . . . . .                           | 185 |
| 8.20 | The Sprung Mass Displacement of the NMPC and Passive responses on Dry Sand (Soil 1) and Upland Sandy Loam (Soil 2) . . . . .                             | 185 |
| A.1  | Model Fitting Application Example . . . . .  | 193 |
| D.1  | A graph showing the Error and Convergence Time of Discrete Tests at 4000 N (Cold Start) for different tolerance values . . . . .                         | 223 |
| E.1  | PID Tuning Application PID Page View . . . . .   | 227 |
| E.2  | PID Tuning Application Control Current Changes . . . . .   | 228 |
| E.3  | PID Tuning Application Adaptive PID Page View . . . . .  | 229 |
| F.1  | The plotfcn output for an arbitrary test case with $N_p = 29$ . . . . .  | 231 |

# List of tables

|     |  |     |
|-----|--|-----|
| 2.1 | Comparison Table of Parametric Models for MR Damper Modelling . . . . .  | 18  |
| 2.2 | Soil Parameters for Tyre-Soil Interaction Modelling . . . . .  | 36  |
| 3.1 | Starting Parameters for Nonlinear Least Squares Optimisation . . . . .   | 50  |
| 3.2 | Root Mean Squared Error (RMSE) Force Values for each of the damper models for the 1Hz cases . . . . .  | 52  |
| 4.1 | Quarter Car Vehicle Parameters Based on the Front-Left Corner Static Weight Distribution of the ASM Vehicle Model (dSPACE GmbH 2020) . . . . . | 62  |
| 4.2 | Full Car Ride Model Parameters based on the ASM Vehicle Model (dSPACE GmbH 2020) . . . . .   | 69  |
| 4.3 | ASM Vehicle Model Parameters - Using Built-In Active Suspension Block (dSPACE GmbH 2020) . . . . .   | 85  |
| 5.1 | Soil Parameters for Tyre-Soil Interaction Modelling . . . . .  | 99  |
| 6.1 | Influence of Controller Gains on System Response . . . . .   | 123 |
| 8.1 | Quarter Car Model Parameters . . . . .   | 162 |
| 8.2 | Full Car Model Parameters . . . . .  | 162 |
| 8.3 | Settling Time of Sprung Mass Displacement for Quarter Car Vehicle Model During Test 1 . . . . .  | 165 |
| 8.4 | A table highlighting the energy consumed by the MR Damper assuming a constant control voltage of 12 Volts, 30 mph . . . . .                    | 167 |
| 8.5 | A table highlighting the energy consumed by the MR Damper assuming a constant control voltage of 12 Volts, 50 mph . . . . .                    | 169 |
| 8.6 | Settling Time of Sprung Mass Displacement for Quarter Car Vehicle Model During Test 3 . . . . .  | 169 |
| 8.7 | A table highlighting the energy consumed by the MR Damper assuming a constant control voltage of 12 Volts, 30 mph round bump . . . . .         | 171 |

|      |   |     |
|------|---|-----|
| 8.8  | Quarter Car Key Performance Index Values for the Different Damper Models used in the Formulation of the NMPC Controller . . . . . | 171 |
| 8.9  | Full Car Key Performance Index Values for the Different Damper Models used in the Formulation of the NMPC Controller . . . . .    | 173 |
| 8.10 | A Comparison between the Prediction/Preview Length and the Key Performance Index Values . . . . .                                 | 180 |
| A.1  | Available Robust Methods for use with Nonlinear Least Squares for Parameter Fitting . . . . .                                     | 194 |
| D.1  | Bisection Method Convergence Times in seconds for Cold Start Tests . . . . .  | 224 |
| E.1  | Adaptive PID Controller Gain Component Influence on System Response . . . . .   | 226 |

# Nomenclature

## Acronyms

|              |                                      |
|--------------|--------------------------------------|
| <b>7DoF</b>  | Seven Degrees of Freedom Model       |
| <b>ADC</b>   | Analogue to Digital Converter        |
| <b>AS2TM</b> | AESCO Soft Soil Tire Model           |
| <b>ASM</b>   | Automotive Simulation Models         |
| <b>ATV</b>   | All Terrain Vehicle                  |
| <b>DAC</b>   | Digital to Analogue Converter        |
| <b>DEM</b>   | Discrete Element Method              |
| <b>ECU</b>   | Electronic Control Unit              |
| <b>FAS</b>   | Full Active Suspension               |
| <b>FEM</b>   | Finite Element Method                |
| <b>GIRF</b>  | Ground Inertial Reference Frame      |
| <b>ISO</b>   | International Standards Organisation |
| <b>KPI</b>   | Key Performance Index/Indices        |
| <b>LAR</b>   | Least Absolute Residuals Method      |
| <b>LiDAR</b> | Light Detection and Ranging          |
| <b>LQR</b>   | Linear Quadratic Regulator           |
| <b>LUT</b>   | Lookup Table                         |

- modBoucWen** Modified Bouc-Wen Damper Model
- modNonlinHBV** Modified Nonlinear Hysteretic Biviscous Damper Model
- modNVEP** Modified Nonlinear Viscoelastic Plastic Damper Model
- MPC** Model Predictive Control
- MR Damper** Magnetorheological Damper
- MR Fluid** Magnetorheological Fluid
- MRPassive** The behaviour of the MR Damper when no current is applied, see Section [6.2](#)
- MV** Manipulated Variable
- NLS** Nonlinear Least Squares
- NMPC** Nonlinear Model Predictive Control
- NonlinHBV** Nonlinear Hysteretic Biviscous Damper Model
- NVEP** Nonlinear Viscoelastic Plastic Damper Model
- P-LUT** Pre-Lookup
- PID** Proportional-Integral-Derivative
- PV** Process Variable
- QP** Quadratic Problem/Program
- RMS** Root Mean Squared
- SP** Setpoint
- STRF** Sloped Terrain Reference Frame

## Symbols

- $\dot{v}$  Damper Piston Acceleration
- $\varepsilon_c$  Smoothing Parameter
- $\varepsilon_y$  Smoothing Parameter

---

|                           |  |
|---------------------------|--|
| $\rho$                    | Density of the Soil [ $kg/m^3$ ]               |
| $\mathbf{0}_{i \times j}$ | Zeros matrix with i rows and j columns.        |
| $\mathbf{I}_{i \times j}$ | Identity matrix with i rows and j columns.     |
| $\varphi$                 | Angle of Internal Resistance of the Soil [deg] |
| $b$                       | Width of Plate/Tyre [m]                        |
| $c$                       | Cohesion of the Soil [ $kN/m^2$ ]              |
| $c_i$                     | Force Shifting Parameter                       |
| $C_{po}$                  | Post-yield Damping Coefficient                 |
| $C_{pr}$                  | Pre-yield Damping Coefficient                  |
| $C_{ve}$                  | Pre-yield Damping Coefficient                  |
| $C_{vi}$                  | Post-yield Damping Coefficient                 |
| $F_c$                     | Yield Force Constant                           |
| $f_c$                     | Yield Force Component                          |
| $F_d$                     | Force Generated by Damper                      |
| $F_y$                     | Yield Force                                    |
| $f_{po}$                  | Post-yield Force                               |
| $f_{pr}$                  | Pre-yield Force                                |
| $f_{ve}$                  | Viscoelastic Force Component                   |
| $f_{vi}$                  | Viscous Force Component                        |
| $k_c, k_\varphi$          | Bekker Soil Parameters                         |
| $K_{ve}$                  | Pre-yield Stiffness Coefficient                |
| $n$                       | Exponent                                       |
| $p$                       | Pressure on Soil [Pa]                          |
| $R_u$                     | Unloaded Radius [m]                            |

---

|           |   |
|-----------|---|
| $R_u^*$   | Larger Substitute Circle Radius [m]                                     |
| $S_{ve}$  | Pre-yield Shaping Function  |
| $S_{vi}$  | Post-yield Shaping Function   |
| $u_0$     | Rebound Height of Soil [m]  |
| $v$       | Damper Piston Velocity  |
| $V_0$     | Zero Force Velocity Intercept   |
| $v_i$     | Velocity Shifting Parameter   |
| $v_y$     | Yield Velocity  |
| $x_t$     | State Vector for Method 1: Single State Space Quarter Car Vehicle Model |
| $z$       | Sinkage of Plate/Tyre into Soil [m]                                     |
| $z_0$     | Sinkage of Tyre into Soil [m]   |
| $z_{def}$ | Tyre Deflection [m]   |

# Chapter 1

## Introduction

This chapter introduces the research topic and provides a brief background to justify the need for this work. Following a brief introduction to the background to this research and its motivation, this chapter highlights the research questions that will be addressed as part of this research before identifying the project objectives. The chapter then continues to explain the research methodology and finally concludes with an outline of the thesis structure.

### 1.1 Background to the Project

Active suspension is a technology used to improve the ride comfort of a vehicle while maintaining the vehicle's handling performance during disturbances from the tyre-terrain contact. Active suspension generates forces between the wheel and vehicle body based on the control input demand from the chosen control strategy. Semi-active suspension is similar to active suspension in that it adjusts forces between the wheel and vehicle body, but the main difference is that semi-active suspension cannot inject additional energy into the system and instead focus on the adjustment of the damping coefficient of the suspension.

Ride comfort is the subjective assessment of a vehicle's ability to minimise the vibrations from the tyre road/terrain contact patch being transmitted to the passengers/driver of a vehicle leading to the feeling of discomfort. This thesis focuses on the minimisation of the accelerations of the vehicle body which are linked to the motions of the passengers/driver and the overall ride comfort of the vehicle. Section [2.2](#) explains in more detail the trade off that is managed by the suspension controller and how this influences the requirements of the suspension system.

Preview information or 'Preview' is used in this thesis to provide the controller with information about the road/terrain ahead of the vehicle to allow for an informed decision about the necessary control action to improve the ride comfort of the vehicle now and in the future. The information provided to the controllers of this study is different for the on-road and off-road

cases but generally the information is the road/terrain height profile measured ahead of the vehicle.

This thesis investigates the improvements of ride comfort for a quarter car model of a 2010 Maserati GranTurismo based on the motion of the front-left corner of the vehicle. The off-road studies focus on slow speed motion over sand and loam which are surfaces common for some off-road parking such as beach parking or small event parking where the vehicle may be used as a primary form of transport. On-road studies are performed at higher speeds for roads such as motorways which have good infrastructure and are more likely to have short impulse disturbances between the segments of road. The on-road studies also identify controller performance using a full vehicle model which is validated using a commercially available full car model.

## 1.2 Project Aim

The overall aim of this project is to create a nonlinear model predictive controller, which improves vehicle ride comfort, through the manipulation of a semi-active suspension system. The developed controller would be capable of improving ride comfort for both on-road and off-road terrain. This project focuses on ride improvement as opposed to vehicle handling as the limited actuator bandwidth of semi-active dampers often makes it challenging to deal with the higher frequencies of wheel dynamics, instead focusing on the lower frequency oscillations of the vehicle body which lie within the working range of frequencies of semi-active dampers.

## 1.3 Research Questions

The thesis focuses on the key areas of the interaction between tyre and soil, semi-active damper behaviour in response to low frequency oscillations and the influence the controller design plays on the energy efficiency of the semi-active suspension system. This thesis addresses the following research questions:

- How can semi-active MR Damper based suspension systems be modelled using nonlinear modelling and system identification techniques to achieve more accurate models of their behaviour?
- How does the tyre model and terrain response affect the ride performance of the proposed model predictive control strategy?
- How does increasing the prediction horizon influence the performance of the controller for both on-road and off-road applications?

- How does the proposed nonlinear predictive controller compare to other reactive and adaptive controllers?
- How does the amount and quality of the preview information supplied to the controller improve its effectiveness at reducing vehicle body accelerations while reducing the current supplied to the damper and therefore improve its energy efficiency?

## 1.4 Technical Objectives

To achieve the project aim, and answer the research questions the following technical objectives were defined:

- To develop models of semi-active vehicle suspension systems to evaluate the proposed control algorithms.
- To improve the accuracy of existing nonlinear models of a semi-active Magnetorheological Damper (MR Damper) for the purpose of modelling the system and controlling its behaviour.
- To develop and evaluate a modified tyre-soil interaction model that can calculate an estimate of the tyre response on sloped off-road terrain and remains compatible with the quarter car vehicle model.
- To design and evaluate a cascade adaptive proportional-integral-derivative (PID) controller specifically designed for semi-active suspension control.
- To design and evaluate the performance of a nonlinear model predictive controller that operates effectively on both on-road and off-road terrain.
- To critically evaluate nonlinear model predictive control against the computationally efficient cascade adaptive PID.
- To assess the energy demand of the control strategies through the use of the current and length of time it is supplied to the MR Damper based suspension.

## 1.5 Research Methodology

The models to be developed during this research project will be compared against previous works to highlight the differences and identify the benefits of the proposed models. The

improved fit of the proposed Nonlinear MR Damper models are assessed through a direct comparison of the force-velocity relationship curves following the previous methodology from (Snyder et al. 2001) and the new methodology proposed in Chapter 3.

The vehicle models from Chapter 4 are compared to the validated commercial Automotive Simulation Models (ASM) provided by dSPACE (dSPACE GmbH 2020) to show that they accurately reproduce the vehicle body accelerations for a given input disturbance of the road height profile.

In addition, the use of a lookup table based method is proposed in Chapter 5 which improves the calculation time of the tyre-soil behaviour, as shown in the comparisons of the calculation time between the original model and the newly proposed method.

The proposed controller is formulated for each of the vehicle models discussed in Chapter 4 as shown in Chapters 6 and 7 which are compared to the PID and adaptive PID controller responses as part of the simulation studies in Chapter 8. The overall performance of the proposed controller shall be assessed through a direct comparison of the simulation studies data to identify how the use of the models and the resulting changes to the controller formulation result in improved efficiency through a reduction of the current supplied to the damper over time. The performance improvement of vehicle ride comfort is also assessed through a comparison of the vehicle body accelerations of the uncontrolled and controlled responses of the vehicle with an overall reduction of the acceleration values showing an improved response.

Furthermore, frequency analysis of the acceleration values is conducted to show how particular frequencies of oscillation are damped more than others, to show how the controller reduces frequencies that are uncomfortable for the driver and any passengers in the vehicle.

## 1.6 Contributions to Existing Knowledge

The work conducted as part of this research project led to the following contributions to existing knowledge:

- *The creation of modified nonlinear magnetorheological damper models*

The modified nonlinear damper models described in Chapter 3 were created to address the problem of fitting pre-existing models to data that was asymmetrical around the force-velocity origin. This unmodelled asymmetry resulted in less accurate estimations of the damping forces produced by the damper during operation. The proposed approach uses a set of parameters to shift, about the true origin, the force-velocity relationship curves introduced in (Snyder et al. 2001). The proposed modified models provided a better fit to the numerical data than the original models, even when the force data are normalised to accommodate for force offset seen in the physical data.

- *The creation of a modified tyre-soil interaction model that reduces calculation speed and is capable of estimating the response of a tyre on gently sloped terrain.*

The model introduced in Sections 5.2 to 5.5 was created to offer near to real-time calculation of the forces generated by the tyre at the tyre-soil interface. The model utilises the theory introduced in (Senatore and Sandu 2011) and (Bekakos et al. 2016b) and expands it utilising lookup tables generated through simulated scenarios to obtain the sinkage values for any given operating condition. It improved the speed of calculation of the forces based on the improved initial estimate of the sinkage into the soil. The model also introduces coordinate transformations to calculate the response of the tyre on gently sloping terrain. This allows to model the response of the tyre-soil to follow the response of a rigid wheel and the pressure distribution without being negatively affected by the slope.

- *The creation of a nonlinear model predictive controller that utilises the nonlinear magnetorheological damper models introduced in Chapter 3*

A nonlinear model predictive controller that calculates the predicted response of the vehicle through the use of the nonlinear damper models, was created to better reflect the true response of the vehicle. The various nonlinear damper models introduced in Chapter 3 are each utilised and the overall impact on the control decisions of the controller can be seen in Section 8.3. The nonlinear model predictive controller is designed to take the damper force as the control input with the input disturbances being the wheel hub displacement rather than the road height measurement which is typically given. This allows for the calculations of the wheel hub motion and resulting damping force to be isolated from the controller and therefore reduces the need for the controller to consider the high frequency dynamics of the wheel and the effect it has on the vehicle response which is often beyond the capabilities of the magnetorheological damper.

- *The creation of a modified nonlinear model predictive controller for use on off-road soft soils*

The controller proposed in Section 6.4 was modified to model the impact of the soft soil response when loaded by the tyre. This is accomplished through combining the response of the vehicle with the modified tyre-soil interaction model shown in Chapter 5. The controller is compared against the PID controllers seen in Section 6.2 to identify the improvements in the ride comfort the newly proposed controller provides the user. The results of these findings are discussed in Section 8.3.

### **Publications**

Some research was conducted in support of the following publications, which while not

directly related to the research topic, provided some useful insight and background information surrounding the development and integration of the tyre-soil interaction models discussed in Section 2.6.4.

- Dizqah, A. M., Ballard, B., Blundell, M., Kanarachos, S., and Innocente, M. (2020) ‘A Non-Convex Control Allocation Strategy as Energy-Efficient Torque Distributors for On-Road and Off-Road Vehicles’. *Control Engineering Practice*. 95

Research contributions: This paper highlights the use of a Non-Convex Control Allocation Strategy for Torque Distribution between two different drivetrains. The two drivetrains in question are an Internal Combustion Engine (ICE) and Electric Motors. The novelty in this research is the torque distribution is applied to vehicles for both on-road and off-road using tyre-soil interaction modelling.

- Dizqah, A. M., Blundell, M., Vantsevich, V., Kanarachos, S., and Ballard, B. (2017) ‘Fast Energy-Efficient Torque Distribution Amongst Multiple Drivetrains’. *Proceedings of the 19th International & 14th European-African Regional Conference of the ISTVS*. Budapest, Hungary: International Society for Terrain-Vehicle Systems.

Research contributions: This paper proposes an Energy-Efficient method of distributing the torque generated by a hybrid electric powertrain. The torque demand was shown to shift from the front to an even distribution of the torque over all four corners of the vehicle using the novel control allocation technique which was proposed.

## 1.7 Outline of Thesis Structure

This thesis structure outline explains the general layout of the remaining sections of this thesis. Figure 1.1 shows the logical connections between each of the topics discussed in this thesis. The black lines show the fundamental connections between the different chapters and the blue lines are used to represent the additional information needed for the logical flow of the thesis. Chapters may be read sequentially or individually as the cross-links to required content can be found in the text. A brief summary of each chapter is provided below along with the full chapter titles instead of the abbreviated versions used in Figure 1.1.

### *Chapter 2: Literature Review*

This chapter introduces the key literature that is relevant to the development of the various models used in Chapter 3 and the controllers developed in Chapters 6 and 7. A brief discussion is conducted about the different types of vehicle models currently being utilised in industry to simulate and assess the dynamic performance of the vehicles. The models rely on both the

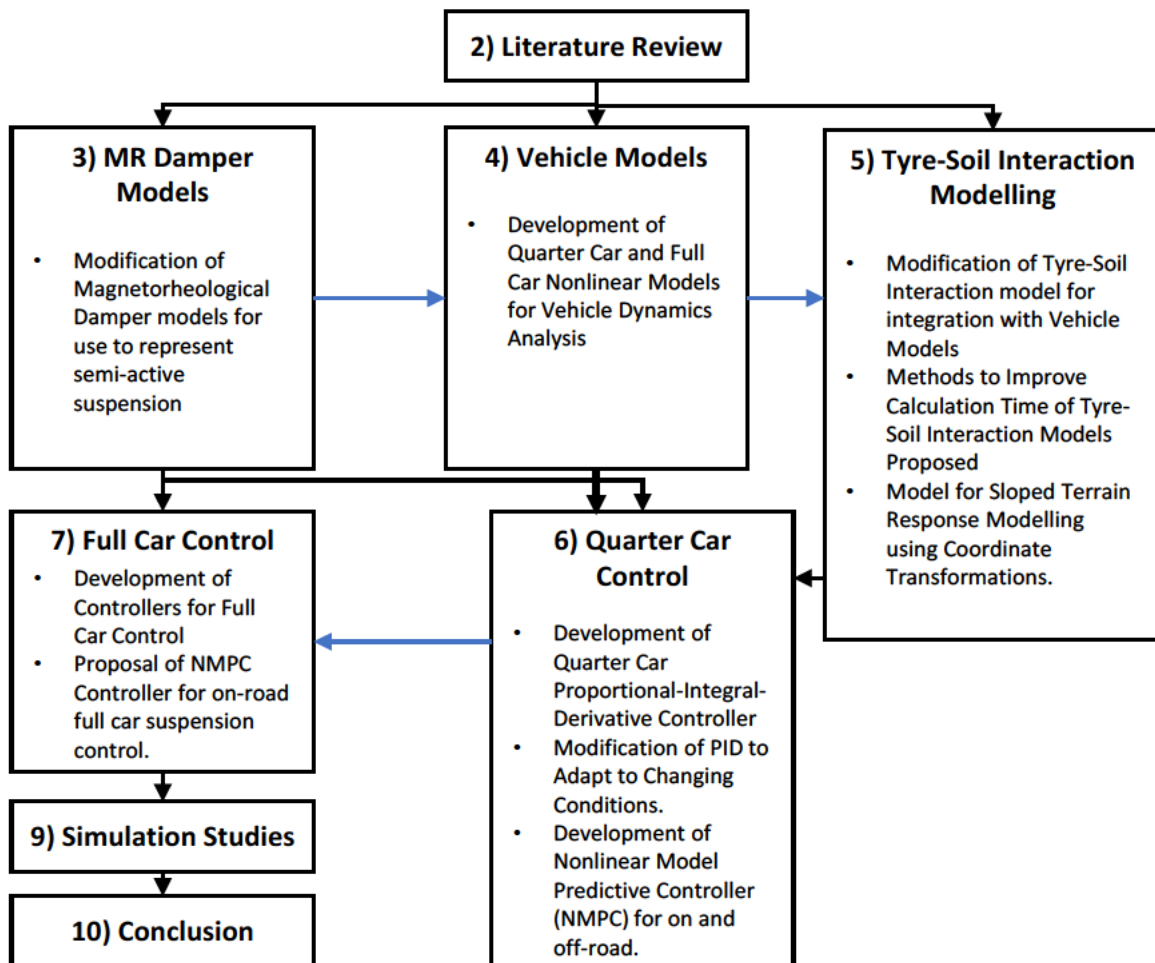


Fig. 1.1 Flow Chart Diagram showing the logical progression of content in this thesis

suspension system being modelled and the tyre dynamics that are present in the model. In addition, more in-depth discussions on the controllers currently being proposed in existing literature and those controllers that have been developed for physical implementation on passenger vehicles are highlighted and evaluated.

### *Chapter 3: Nonlinear Magnetorheological Damper Modelling*

This chapter describes the changes made to the Nonlinear Hysteretic Biviscous and Nonlinear Viscoelastic Plastic models which were introduced in Chapter 2. The chapter also proposes the use of a new method to adapt the models for use within a vehicle model to simulate the behaviour of Magnetorheological Damper (MR Damper) based suspension.

### *Chapter 4: Vehicle Dynamics System Modelling*

This chapter describes the formulations of the nonlinear vehicle models used in the simulation studies in Chapter 8. The chapter proposes two quarter car and two full car models, which are used in the creation of the Nonlinear Model Predictive Controllers (NMPC) from Chapters 6 and 7 for on-road and Chapter 8 for off-road. This chapter also proposes modifications to the Automotive Simulation Models (ASM) from dSPACE (dSPACE GmbH 2020) to verify the response of the full car model and compare the response to a digital clone of a mid-sized vehicle.

#### *Chapter 5: Tyre-Soil Interaction Modelling for Off-Road System Analysis*

This chapter presents modifications to the tyre-soil interaction model from (Bekakos et al. 2016b) which is adapted for use in the simulation of a vehicle on off-road soft soils. This chapter proposes the use of a pre-lookup method to evaluate the static sinkage of the tyre into the soil, in addition to the development of a coordinate transformation for the calculation of the tyre's response on gently sloping terrain which is defined here as having an angle of less than  $\pm 10^\circ$ . This model is used for the assessment of the off-road response of the quarter car and full car models from Chapter 4 and proposes the necessary modifications needed for off-road vehicle modelling.

#### *Chapter 6: Nonlinear Quarter-Car Semi-Active Damper Controller Design*

This chapter proposes three different controllers for use with the MR Damper based semi-active suspension within the nonlinear quarter car model from Chapter 4. The chapter describes the formulation of a Proportional-Integral-Derivative (PID) controller that is largely based on existing research shown in Chapter 2 before adapting the controller so that the gains used to determine the controller action are related to the nonlinearity of the MR Damper suspension as part of an Adaptive PID controller. The chapter also proposes the formulation of a Nonlinear Model Predictive Controller (NMPC) that focuses on the minimisation of the sprung mass acceleration of the quarter car vehicle model which is linked to the ride comfort experienced by passengers.

#### *Chapter 7: Nonlinear Full Car Semi-Active Damper Controller Design*

This chapter proposes adaptations to the controllers from Chapter 6 for the application to full car vehicles fitted with semi-active MR Damper based suspension. The controller utilises a similar PID controller for the control of all four corners of the vehicle in order to minimise the vertical heave acceleration of the vehicle body. Cascade control techniques which are typically used in existing research shown in Chapter 2 for the control of other systems, were adapted to the semi active suspension control problem. the cascade control approach combines the PID controller and the Adaptive PID from Chapter 6 for the adaptive control of each corner of the

vehicle. This proposed scheme is labelled as the Adaptive Cascade PID controller and is a new controller to minimise the vertical heave acceleration and angular acceleration in the pitch and roll directions. The final controller is the Nonlinear Model Predictive Controller (NMPC) which is developed to minimise the vertical heave acceleration of the vehicle body, in addition to the angular acceleration in the pitch and roll directions. The system relies on accurate modelling of the vehicle to calculate the ideal current to be supplied at each calculation time. It differs from other controllers mentioned in Chapter 2 that typically calculate ideal control forces.

#### *Chapter 8: Simulation and Discussion of Results*

This chapter conducts several simulation studies that are investigated in detail to determine the use of controllers for both on and off-road quarter car model simulations and the use of the controllers with full car models for both on-road and off-road conditions.

#### *Chapter 9: Conclusion*

This chapter concludes the findings of the research conducted as part of this thesis and identify key areas of research for future work to investigate. In addition the conclusion will determine whether the main aim and objectives of the research project have been met and as a result determine whether the project has accomplished its original goals.



# Chapter 2

## Literature Review

### 2.1 Introduction

This thesis focuses on how Magnetorheological Damper (MR Damper) based semi-active suspensions can be used to improve the ride comfort of off-road vehicles. This chapter critically reviews the various models used for simulating vehicle dynamics on off-road terrain. The first part discusses the vehicle models currently used in the literature for the simulation of vehicle dynamics including how they are used as part of control systems formulation and performance evaluation of ride comfort and vehicle handling for both on-road and off-road vehicles.

The second part of this chapter, highlights the gaps in existing research surrounding modelling semi-active suspensions and control strategies. Semi-active suspensions are used to minimise vibrations, that are a result of tyre-terrain contact and motion, which when delivered to the passengers could potentially result in the subjective ride comfort of the vehicle being considered uncomfortable or harmful. This part discusses the techniques used to model MR Dampers, semi-active continuously variable dampers that produce nonlinear damping forces. In addition this part reviews the various control strategies, which determine the required forces for optimal damping and improved ride comfort.

The third part compares the on-road conditions that a typical passenger car may encounter and evaluates the difficulties in simulating a vehicle on off-road terrain. This section further discusses the numerous tyre-soil interaction models used for simulating a wheel on soft soils and highlights the processes involved with parameterising these models and the various assumptions they make about the tyre and soil.

This chapter concludes by justifying the selection of the models and controllers used as the basis for the developments detailed in the remainder of this thesis. The resulting models and controllers enable to simulate a vehicle on off-road sloped terrain and control a nonlinear model of an MR Damper with the proposed Nonlinear Model Predictive Controller.

## 2.2 Vehicle Ride Comfort and Handling

Vehicle Ride Comfort can be referred to as a subjective measure of a passenger/driver to the discomfort of vibrations transferred to the human body from the vehicle at various frequencies. Ride comfort assessment fundamentally result from the review of a vehicle's comfort level by a group of individuals, which depending on the study are either a panel of expert assessors as seen in (Anderson and Harty 2010), or through customer feedback once a vehicle is in production. Other studies (Cardinale and Pope 2003; Griffin 2001) however, have been performed to identify and show how the human body is sensitive to particular frequencies when different parts of the body are vibrated as seen in (Griffin 2007).

Key Performance Indices (KPI) such as those described in (Anderson and Harty 2010) and later in Section 6.2.1 approximate the ride comfort of a vehicle based on the Root Mean Squared (RMS) Vertical Heave Body Acceleration. The KPI used in Section 6.2.1 are comparable to the Cooper-Harper Rating Scale for pilot rating and evaluation seen in (Cooper and Harper 1969) with a range typically within zero to ten, and approximate the ride comfort rating of the vehicle based on two sets of frequency ranges referred to in the literature (Blundell and Harty 2014) as primary and secondary ride frequencies.

Blundell and Harty (2014) describe Primary ride frequencies as being within the 0.5Hz to 3Hz range and are related to the motion of the vehicle body in response to an excitation from the long duration undulations of the road/terrain surface. The authors from (Blundell and Harty 2014) also explain that secondary ride frequencies are usually in the 6Hz to 15Hz range and are excited due to short impulse motions of the masses, such as hitting a pothole or speed bump.

Handling of the vehicle may be referred to as the responsiveness of a vehicle to a user's control input and how it moves along the road/terrain (Rill and Castro 2020). A slow response of the vehicle to control inputs (particularly steering and braking inputs) is often undesirable as the user could potentially be unable to avoid obstacles before a collision/accident. However, a vehicle which is too sensitive to control inputs is equally demanding on the user as they are required to constantly correct for errors (however small) in their controls which could likely result in an unstable driving condition.

Vehicle handling is the transient handling behaviour of the vehicle as explained in (Blundell and Harty 2014; Fenton 2013; Rill and Castro 2020). To minimise the variation of the vehicle's transient handling behaviours suspension systems are configured to allow for consistent control qualities across varying road/terrain which is linked to the normalised force/pressure on each wheel.

The requirement for the suspension system to maximise the normalised force/pressure on the tyre to ensure ground contact ensures wheel hop does not occur. However, this is in competition with the requirement to improve the ride comfort of the vehicle. Figure 2.1 shows

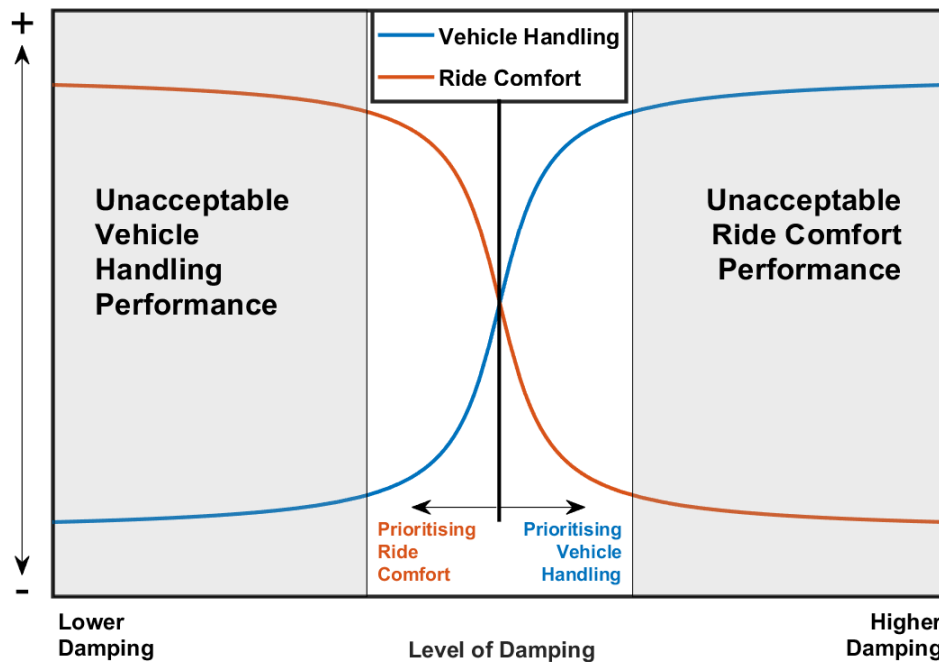
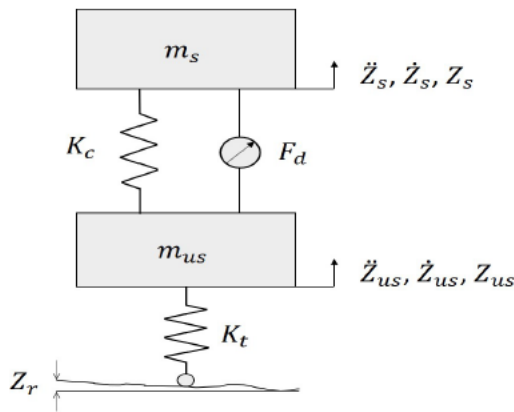


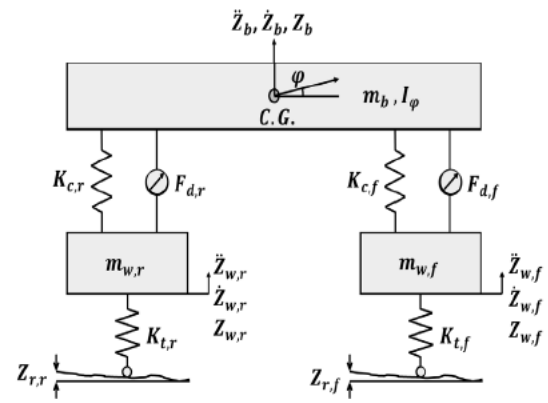
Fig. 2.1 A Diagram of the trade-off between Vehicle Ride Comfort and Vehicle Handling Based on the work from (Heißing and Ersoy 2010)

the trade off relationship between the level of damping and the requirements for ride comfort and handling.

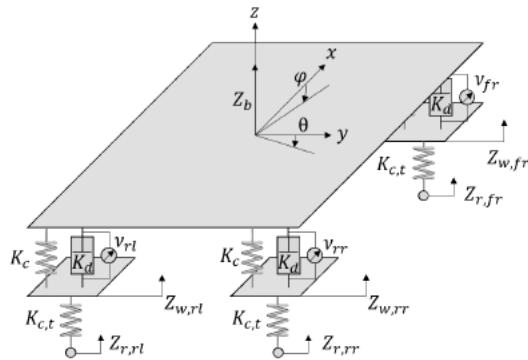
As the level of damping is increased the ride comfort is reduced as the stiffer suspension transmits more vibrations to the passengers/driver. Meanwhile, the vehicle handling improves as there is generally more contact pressure between the tyre and road/terrain. A vehicle manufacturer typically designs a vehicle within a set of acceptable performance values, which differ from company to company. However, these values determine what is considered as unacceptable in terms of vehicle handling performance and ride comfort as illustrated in Figure 2.1. The window of acceptable values typically results in the prioritisation of one of the two objectives with some companies opting to focus more on the ride comfort and others more on the handling performance. This thesis focuses on the ride comfort of a vehicle and the improvements that can be made through the use of vehicle models and vehicle modelling techniques which can inform particular controller design strategies about the potential future response of the vehicle.



(a) Quarter Car Vehicle Model



(b) Half Car Vehicle Model



(c) Full Car Vehicle Ride Model

This item has been removed due to 3rd Party Copyright. The unabridged version of the thesis can be found in the Lanchester Library, Coventry University.

(d) Automotive Simulation Models (ASM) (dSPACE GmbH 2020)

Fig. 2.2 Examples of Vehicle Models

### 2.3 Vehicle Modelling

There are various methods to model the dynamic behaviour of a vehicle and the changing system states, with one of the simplest methods being the two degrees of freedom quarter car model. The quarter car vehicle model as described in the literature (Blundell and Harty 2014; Guglielmino et al. 2008; Prokop and Sharp 1995) and shown in Figure 2.2a simulates the behaviour of a single corner of a vehicle focusing on the vertical motion of the sprung (body) and unsprung (wheel) masses. Quarter Car Vehicle Models are computationally inexpensive and relatively cheap to validate when compared to some of the other more complex vehicle models explained later. The model can be configured to utilise both linear and nonlinear spring and damping components, but it is usually typical for the damper behaviour to be linearised to remove the hysteretic effects of the damper. Meanwhile, studies like (Yao et al. 2002) use models which utilise nonlinear modelling techniques to allow for a more accurate representation of the damper behaviour as explained in Section 2.4.

Nonlinear modelling techniques are also utilised in some vehicle models to determine and predict the behaviour of the tyre, as explained in Section 2.6.2, which increases the complexity and number of degrees of freedom of the system. Compared to some of the other vehicle models in the literature (Canale et al. 2006; Guglielmino et al. 2008; Zhu and Ayalew 2014) the two degrees of freedom quarter car model is limited to the assessment of ride comfort and durability simulations, but it can also be useful for determining the effectiveness of semi-active/active suspension system controllers like that seen in (Prokop and Sharp 1995).

Figure 2.2 also shows some other examples of vehicle models that are convenient to simulate and predict the behaviour of a vehicle. Among the models shown is the half car model which is also used by the authors in (Canale et al. 2006; 2005) (see Figure 2.2b). The half car vehicle model is an extension of the quarter car vehicle model in that the suspension and tyres typically are represented by spring and damper components. This model adds an additional degree of freedom to describe either the roll or the pitch motion of the vehicle body. The additional motion of the vehicle as part of the half car model can be used to categorise the behaviour of the suspension to a change in the pitch or roll of the vehicle body. The inclusion of this motion in the model allows for the generation of controllers for suspension systems, to minimise not only the vertical heave acceleration, but also the angular acceleration in either the roll or pitch directions.

The half car model is used primarily as a means to analyse ride comfort and durability since the simple tyre model only provides a limited amount of information on the tyre. The model is limited in that there is no degree of freedom for longitudinal or lateral motion of the vehicle. This can be improved by adding more complexity to the model but it is still limited to modelling a bicycle with vertically mounted suspension as there is no modelling of the suspension kinematics.

Full Car Vehicle models can be divided into three subcategories; ride only, handling only, or ride and handling. While the term Full Car Model can refer to a particular type of model it usually refers to a model which in some way models the motion of the vehicle body and its wheels. Ride only models typically focus on the motion of the masses in the vertical heave direction in addition to the angular motion of the body mass in pitch and roll. For the input disturbance to the system the ride models use a predetermined or measured road/terrain height profile, which displaces the wheel hub through the compression or extension of the tyre in relation to the overall load force on each wheel.

Full Car Ride Only models like that shown in Figure 2.2c can have a minimum of seven degrees of freedom as seen in (Gohrle et al. 2013). These models link the motion of each corner to the centre of mass and use similar spring and damper components as those seen in the quarter car and half car models. Similar to the other models previously discussed the full car

ride model is unable to effectively be used for handling as the longitudinal and lateral motion is not modelled.

Alternatively, Handling only models usually focus on the motion of the masses in the longitudinal and lateral directions in addition to the angular motion of the vehicle in yaw like that seen in (Guiggiani 2018). While these motions are important in control applications for traction control and adaptive cruise control the use of such models for semi-active/active suspension control is not suitable as in many cases the vertical forces applied to the suspension are not represented clearly.

Ride and Handling models can have elements of both and vary in complexity but there are a number of commercially available models that combine these aspects. The Automotive Simulation Models (ASM) available as a software package from dSPACE (see Figure 2.2d) (dSPACE GmbH 2020) and IPG CarMaker (IPG Automotive GmbH 2020) offer higher complexity models with both ride and handling modelling of the vehicle. These multibody full car models are useful for the development of complex systems, that integrate with the many on-board vehicle systems currently in use on commercial vehicles. However, while these models are capable of being used to validate control systems in preparation for final deployment of the the controller hardware, one of the main downsides of these models at present are that off-road simulation of vehicles are not included as part of the software packages.

Many of the the vehicle models shown in Figure 2.2 and readily available in the wider literature (Canale et al. 2006; Gohrle et al. 2014; Guglielmino et al. 2008) calculate the system response using the tyre response determined through the use of either a spring component or a combination of spring and damper components. However, as discussed in Section 2.5, the wheel hub motion does not rely on purely the spring and damper effects of the tyre for off-road simulations. The lack of flexibility in modifying the wheel hub motion in current formulations of vehicle models results in the need for a new formulation of vehicle model to enable easy integration of tyre-terrain interaction models.

One of the other key areas that vary between vehicle models are how the dynamic forces of the spring and damper are considered. For many passive system representations the spring and damper components are linearised (Blundell and Harty 2014). However, semi-active and full active suspension adopt different methods to model the forces which can vary considerably from model to model. It is common in the literature for fast active suspension to be modelled with a continuously variable force that is directly manipulated by the controller as seen in (Gohrle et al. 2013). While semi-active dampers, including Magnetorheological Dampers, are typically integrated into the vehicle models by the summation of both the passive response of the damper and the control force produced by a change in electrical current (Yakub and Mori 2013).

## 2.4 Magnetorheological Damper Modelling

MR Dampers utilise Magnetorheological Fluid, to modify the yield force of the damper when an electrical current is supplied to an electromagnet housed within the damper structure (Snyder et al. 2001). Unlike Electrorheological Fluids, the yield stress of Magnetorheological Fluids is often much higher typically in the region of 50-100 kN.m<sup>-2</sup> (Snyder et al. 2001). Their ability to be adjusted, through a change in the supply of electrical current, make MR Dampers particularly suited for use in semi-active suspension applications. However, accurately modelling the nonlinear behaviour of the damper under changing operating conditions poses a challenge. Due to the presence of hysteresis in both the low velocity and high velocity regions, magnetorheological damper models typically follow one of two groups of modelling methods: parametric or non-parametric models. Non-parametric models utilise analytical expressions to match the forces observed during testing of the damper. Parametric models utilise spring and damper components to describe the overall behaviour of the damper.

This thesis focuses on the use of parametric models and their use for describing the behaviour of a semi-active magnetorheological damper. Table 2.1 lists a number of parametric models with the number of parameters used and the features each model has. This thesis focuses on Nonlinear Hysteretic Biviscous, Nonlinear Viscoelastic Plastic, Bouc-Wen and Modified Bouc-Wen models due to their ability to closely match the results from physical testing of MR Dampers as shown in (Snyder et al. 2001; Talatahari et al. 2012).

### 2.4.1 Nonlinear Hysteretic Biviscous Model

The Nonlinear Hysteretic Biviscous Model was first proposed in (Wereley et al. 1998) as a means to represent the behaviour of Electrorheological Dampers (ER Dampers). Since both ER Dampers and MR Dampers show similarities in their hysteretic behaviour, the models were implemented in (Snyder et al. 2001) for modelling MR Damper Characteristic Behaviour.

The model comprises six conditional cases that determine the damper force by relating the damper piston velocity and acceleration with the yield force, pre-yield and post-yield regions. This model is more preferable than the Bingham Plastic and Nonlinear Biviscous models as it includes the gradient and hysteresis of the low velocity, pre-yield region. This introduction of the hysteresis in the pre-yield improves the fit to the force-velocity data. However, similarly to Nonlinear Biviscous model, it assumes that the force-velocity relationship transitions is immediate when the yield force is exceeded.

The model relies heavily on the symmetrical behaviour of the data about the origin. It assumes that the force and velocity data have a mean value of zero or have been normalised to re-centre the data around a value of zero. While normalisation is possible in the case of the

Table 2.1 Comparison Table of Parametric Models for MR Damper Modelling

| Damper Model   | Number of Parameters | Model Features   |
|--|----------------------|--|
| Equivalent Viscous Damping <sup>1</sup>                    | 1                    | Linear Damping Model   |
| Bingham Plastic Model <sup>1, 2</sup>                      | 2                    | Post-Yield Damping Coefficient, Yield Force  |
| Nonlinear Biviscous Model <sup>1, 3</sup>                  | 3                    | Pre-Yield Damping Coefficient, Post-Yield Damping Coefficient, Yield Force   |
| Nonlinear Hysteretic Biviscous Model <sup>1, 4</sup>       | 4                    | Pre-Yield Damping Coefficient, Post-Yield Damping Coefficient, Yield Force, Zero-Force Velocity Intercept (Pre-Yield Hysteresis)   |
| Nonlinear Viscoelastic Plastic Model <sup>1, 5, 6, 7</sup> | 7                    | Pre-Yield & Post-Yield Damping Coefficients, Pre-Yield Stiffness Coefficient, Yield Velocity, Yield Force Constant, Smoothing Parameters   |
| Bouc-Wen <sup>2, 8, 9</sup>                                | 8 - 12               | Material Yield Stress, Spring Stiffness and Damping Coefficients, Hysteretic Deformation (Evolutionary Variable)   |
| Modified Bouc-Wen (Spencer Model) <sup>2, 8</sup>          | 10 - 14              | Material Yield Stress, Spring Stiffness and Damping Coefficients, Hysteretic Deformation (Evolutionary Variable), Accumulator Stiffness Coefficient, Viscous Damping Coefficient |

<sup>1</sup> (Snyder et al. 2001); <sup>2</sup> (Spencer et al. 1997); <sup>3</sup> (Wereley et al. 1998);  
<sup>4</sup> (Wang and Liao 2011); <sup>5</sup> (Kamath and Wereley 1997a); <sup>6</sup> (Kamath and Wereley 1997b);  
<sup>7</sup> (Kamath and Wereley 1997c); <sup>8</sup> (Talatahari et al. 2012); <sup>9</sup> (Kwok et al. 2007)

force data, the parameter values of the model become linked to the normalisation method and require to be de-normalised to offer useful force data for simulation and prediction of the MR Damper behaviour. This makes the process more computationally demanding and relies heavily on the assumption that all values will remain in the normalised region for the model to remain valid.

One benefit of using the Nonlinear Hysteretic Biviscous over some of the other models listed in Table 2.1, is the ability to use graphical hand calculations to discern reasonably accurate values of the parameters required for the model. In addition, the model produces

an energy dissipation relationship that closely matches the energy dissipated by a real MR Damper even though the force-velocity relationship does not always reproduce similar force values when compared to real test data. The modified version of this model introduced in Section 3.2 addresses the issue of reliance on perfectly symmetrical data about the origin of the force-velocity data curve. It is proposed as a viable alternative in order to improve the calculation of parameter values and achieve a better overall fit to real test data.

### 2.4.2 Nonlinear Viscoelastic Plastic Model

Similar to the Nonlinear Hysteretic Biviscous Model the Nonlinear Viscoelastic Plastic Model was first proposed to model the behaviour of ER Dampers as seen in (Kamath and Wereley 1997c) before being used to model MR Dampers in (Snyder et al. 2001).

The model consists of three loading mechanisms which are combined to calculate the overall damper force produced for the given operating conditions. The three mechanisms correspond to the pre-yield region, the post-yield region and the transition points between the two regions in the yield force region. The model utilises hyperbolic tangent shaping functions ( $S_{ve}$ ,  $S_c$  and  $S_{vi}$ ) that help to shape the force components of each region into the characteristic S-shape of the force-velocity hysteresis curve seen during testing of MR Dampers (see Sections 3.4 and (Snyder et al. 2001)).

The Nonlinear Viscoelastic Plastic model, more accurately models the force-velocity curve with piece-wise smooth functions. However, it is more time consuming to achieve an accurate fit than with the Nonlinear Hysteretic Biviscous model. The model is typically fitted to the data using Nonlinear Least Squares Optimisation. Fitting the model to the data involves a similar method to that described in (Snyder et al. 2001), by utilising the Nonlinear Hysteretic Biviscous model parameters for the starting conditions for some of the similar parameter values. This fitting process is later modified for use to parameterise the modified MR Damper models in Section 3.4.

### 2.4.3 Bouc-Wen and Modified Bouc-Wen Models

The Bouc-Wen model was first proposed in (Wen 1976) to model the behaviour of nonlinear hysteretic systems. The simple Bouc-Wen model uses 8 parameters to describe the hysteretic behaviour of a system and has been utilised by previous studies (Peng et al. 2018; Talatahari et al. 2012) for MR Damper modelling.

The model was modified for MR Damper modelling to include the response to the pulse width modulated voltage supplied to the damper in (Talatahari et al. 2012). The method for modifying the model resulted in the number of parameters increasing to 12. An alternative

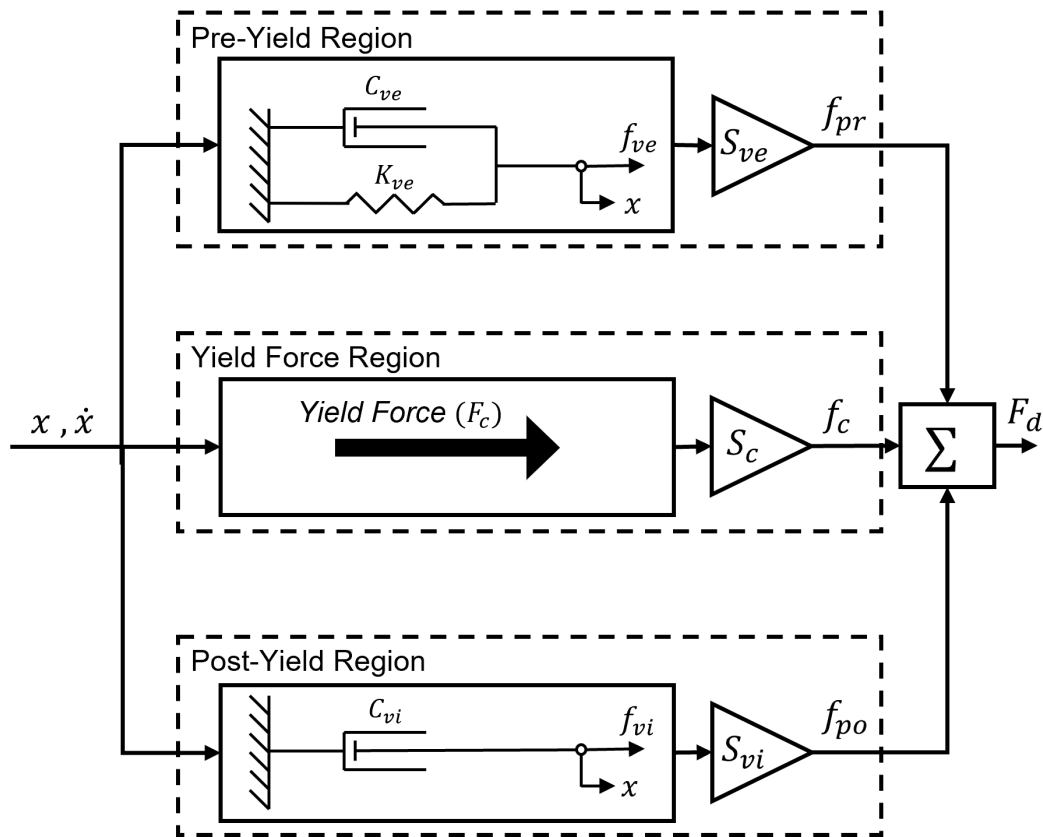


Fig. 2.3 A Diagram Showing the Three Mechanisms of the Nonlinear Viscoelastic Plastic Model Based on the Work in (Snyder et al. 2001)

formulation of the Bouc-Wen model was proposed for use with MR Dampers in (Spencer et al. 1997). This alternative model referred to as the modified Bouc-Wen model typically uses 10 parameters, however this increases to 14 after the modifications stated in (Spencer et al. 1997; Talatahari et al. 2012). Both models have been shown to strongly correlate with the test data from a real MR Damper.

While the charged system search used in (Talatahari et al. 2012) offers an accurate fit to the data, other approaches to fit the model to test data involve particle swarm optimisation (Ab Talib et al. 2020) and nonlinear least squares (Dyke et al. 1998; Spencer et al. 1997). Since the fitting process is not the focus of this Thesis, the nonlinear least squares method has been adopted as it offers reasonable fitting for each of the models discussed in the later sections of this thesis.

Nonlinear Least Squares is a well developed theory that integrates with MATLAB and can be used to determine the confidence intervals of unknown parameters with efficient use of the data (NIST 2013). While Nonlinear Least Squares has many benefits it must be remembered that with the presence of outliers the fit of the parameters can vary greatly (NIST 2013) and

appropriate Robust fitting techniques must be used alongside Nonlinear Least Squares to achieve an acceptable fit result. A short list of the techniques used in this thesis can be found in Table A.1 which were incorporated in the Model Fitting Application mentioned later in Section 3.4.

On visual inspection of the results from (Snyder et al. 2001) and (Spencer et al. 1997) shown in Figure 2.4 the Nonlinear Viscoelastic Plastic (NVEP) model shows that it provides a similar fit to the force-velocity data as the modified Bouc-Wen model. The test data shown in Figure 2.4 is produced from two separate sets of data with similar but not identical test conditions, meaning that a direct comparison of the models is currently not possible with respect to the supporting literature. Therefore, the models must be compared with each other when fit to the same MR Damper test data which is performed later in Section 3.4.2. Figure 2.4 highlights the test conditions for the two models based on the source of the data with specific attention to the current supply ( $I$ ), sinusoidal oscillation frequency ( $\Omega$ ) and the maximum displacement of the damper from the zero point of the respective test ( $x_{max}$ ). The similar performance of the NVEP model when compared to the modified Bouc-Wen model with fewer parameters makes it desirable to adapt and utilise for simulation and prediction of the damper behaviour.

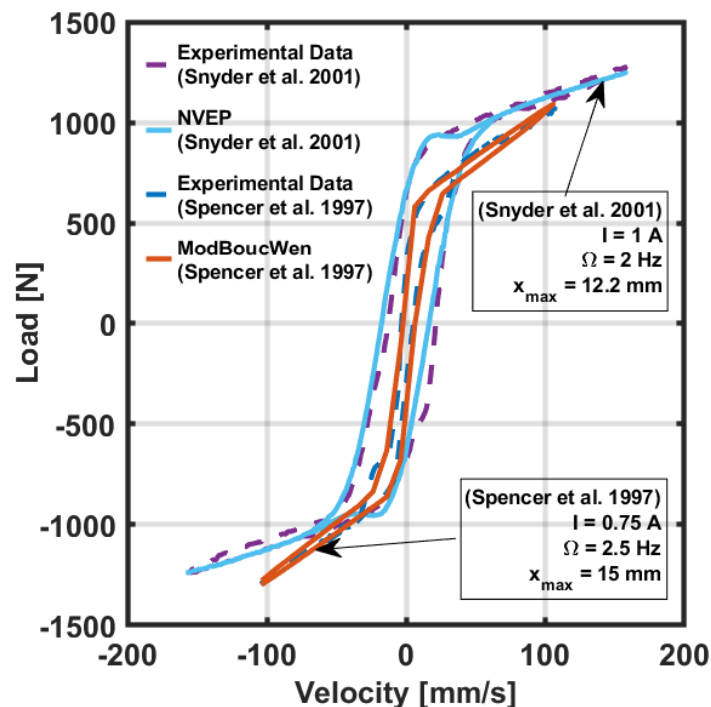


Fig. 2.4 Model Fit Accuracy Comparison two MR Damper Models to the Experimental Data from (Snyder et al. 2001; Spencer et al. 1997)

## 2.5 Control of Active and Semi-Active Suspension

Controllers of semi-active suspension are required to balance the relative importance of ride comfort of the vehicle with the stability and safety of the vehicle. As high damping results in uncomfortable whole body vibrations it is often preferable to reduce the damping to improve ride comfort. The disadvantage of reducing the level of damping is that while the subjective ride comfort of the vehicle is improved, the vehicle handling is impaired resulting in poor stability and safety of the vehicle as illustrated in (Desikan and Kalaichelvi 2015; Macfarlane 2016; Simon 1998).

The need for a compromise has resulted in the proposition of many control strategies that are optimised for use with semi-active suspension to simultaneously improve the ride comfort, stability and safety of a vehicle (Ab Talib and Mat Darus 2013; Desikan and Kalaichelvi 2015; Gohrle et al. 2013; Jamil et al. 2018; Zeinali and Darus 2012). However, the performance of semi-active suspension is limited by the control system's ability, to successfully manipulate the actuator. Developing an optimal control strategy to manipulate the level of damping that effectively controls the system is a challenging problem and a point of focus for the development of semi-active suspension systems.

### 2.5.1 Closed Loop Control

Linear Proportional-Integral-Derivative (PID) controllers are a classical control method which is capable of determining a control action for the system response to force the Process Variable (PV) to meet the desired Set Point (SP), through the minimisation of the error signal equivalent to the difference between the PV and the SP (Altinoz and Yilmaz 2018). As the gains of the controller ( $K_P$ ,  $K_I$ , and  $K_D$ ) are scalar values the controller is typically unsuited to control highly nonlinear systems with external disturbances. However, their speed of actuation, simplicity and suitability with use of linearised models has made them attractive for semi-active suspension applications.

Equation 2.1 shows how the control action ( $u$ ) is calculated using the error ( $e$ ) between the desired SP and the PV at each timestep. The three gains are referred to commonly as the Proportional Gain ( $K_P$ ), the Integral Gain ( $K_I$ ) and the Derivative Gain ( $K_D$ ). The Proportional Gain is used to increase the magnitude of the control action in relation to the magnitude of the error, which as a result typically adjusts the aggressiveness of the control actions. Smaller Proportional gains typically lead to slower rise times of the controlled system when responding to a change in the set point.

$$u(t) = K_P \cdot e(t) + K_I \int_0^t e(t) dt + K_D \frac{de(t)}{dt} \quad (2.1)$$

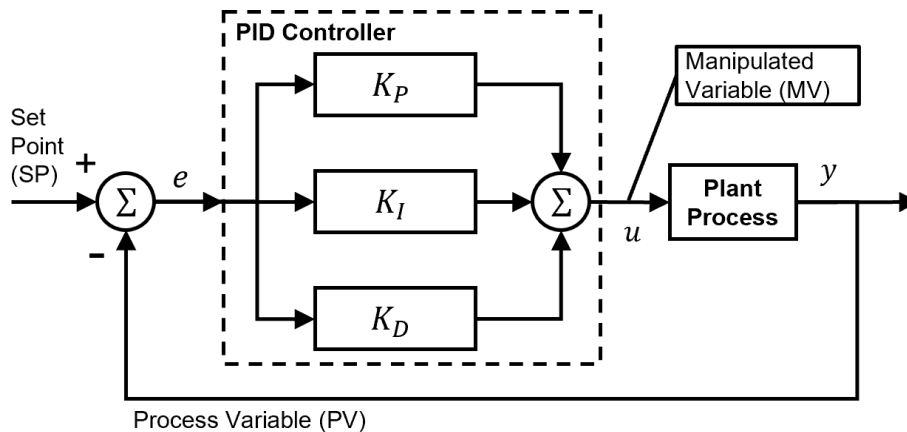


Fig. 2.5 Diagram of a Linear PID controller with System Feedback Loop

The Integral Gain is used to minimise the steady state error of the controlled system with the control action building up as the steady state error increases. Integral Only control is typically avoided due to integral wind-up which occurs when the control action is saturated but the controlled system still has steady state error. Integral anti-wind-up methods such as those described in (Åström and Hägglund 1995) are often utilised to correct for this issue. In addition, the Derivative Gain is used to stabilise the closed loop controller as a result of the time delay between applying the control action and response being visible in the PV.

PID controllers were used in (Rao 2014), with a linearised quarter car model, to determine the control force necessary to improve ride comfort. While the authors in (Jamil et al. 2018) use an adjustable damping coefficient approach which assumes that the damping of the damper is linear with respect to velocity for a constant current value. The authors in (Jamil et al. 2018) used the saturated output of the PID controller to define a damping coefficient value that is used as a means to calculate the damping force. Figure 2.6 shows a comparison of semi-active suspension controlled using the PID Controller and the passive response of a quarter car vehicle on the effective sprung mass displacement from (Jamil et al. 2018).

The gains of a PID controller can be tuned through a number of methods with the simplest through manual tuning. Manual tuning through trial and error is not accurate enough in most cases as the performance of the system is linked directly to how well the controller is tuned. However, several approaches such as the Ziegler-Nichols step response and frequency response methods described in (Åström and Hägglund 1995) are used to improve the accuracy of manual tuning. Among the approaches commonly used for tuning the PID controller is the tuning application that is part of MATLAB\Simulink software as seen in (The MathWorks Inc. 2021). This approaches uses a similar approach to the Ziegler-Nichols tuning method but utilises a proprietary solver to determine the plant and the tuning based on parameters set by the user.

This item has been removed due to 3rd Party Copyright. The unabridged version of the thesis can be found in the Lanchester Library, Coventry University.

Fig. 2.6 PID Controlled Semi-Active Suspension Responding to step bump of 0.1 m ( $t = 5$  s) in height (Jamil et al. 2018)

In cases where PID controllers are used for nonlinear systems tuning may be performed at various operating conditions to determine the conditions when each tuning set can be utilised. Gain scheduling is one particular method where the various tuning characteristics can be applied during predefined control conditions to allow for a more optimal control approach as the controller gains are changed to match the current conditions.

Other studies utilise methods such as self tuning (Ab Talib and Mat Darus 2013) and fuzzy logic (Zeinali and Darus 2012) to adapt the standard PID controller for the nonlinear quarter car system in order to determine the control force necessary to reduce vehicle mass oscillations. Another study (Dangor et al. 2014) proposes the use of Cascade Control with Particle Swarm Optimisation to determine the controller gains for the control of quarter car vehicle suspension.

Robust  $H_\infty$  control was applied to semi-active suspension in (Du et al. 2005; Du and Zhang 2008; Fallah et al. 2010) with the proposed strategy from (Du et al. 2005) resulting in a reduction of RMS Acceleration of the sprung mass by around 70%. While this reduction can be linked to improved ride comfort, reactive control strategies like PID and  $H_\infty$  controllers can perform limited actions to respond to incoming disturbances as they occur. This can be a disadvantage for slower semi-active suspension technologies that have limited bandwidth, preventing the controller to respond in a timely manner to sudden impulse disturbances.

### 2.5.2 Semi-Active Suspension Control in Industry

Semi-active suspension has been in the mass market industry for several years with recent developments focusing on continuously controlled electronic suspension. Among the control strategies that are currently in use commercial systems have utilised versions of Skyhook and Groundhook theory as illustrated in Figure 2.7

This item has been removed due to 3rd Party Copyright. The unabridged version of the thesis can be found in the Lanchester Library, Coventry University.

Fig. 2.7 Diagram showing the Skyhook and Groundhook system representations (Heißing and Ersoy 2010)

The Skyhook Control Theory which was developed in (Crosby and Karnopp 1973) is a control approach based on a theoretically ideal damper which is between the vehicle body mass and the sky as seen in Figure 2.7. The approach allows for switching to occur between the minimal ( $K_{d,min}$ ) and the Skyhook "maximal" damping ( $K_{d,sky}$ ) which is the maximum achievable damping. Switching of the damping is performed when the conditions of the velocity of the vehicle body mass ( $\dot{Z}_b$ ) and the relative velocity of the suspension deflection ( $\dot{Z}_b - \dot{Z}_w$ ) meet the criteria indicated in Equation 2.7 from (Soliman and Kaldas 2019).

$$K_d = \begin{cases} K_{d,min} & \text{if } \dot{Z}_b \cdot (\dot{Z}_b - \dot{Z}_w) \leq 0 \\ K_{d,sky} & \text{if } \dot{Z}_b \cdot (\dot{Z}_b - \dot{Z}_w) > 0 \end{cases} \quad (2.2)$$

The Skyhook approach allows for simple reliable control of a semi-active suspension system and primarily focuses on the minimisation of the body mass acceleration in the vertical

direction. While the Groundhook Control theory is based around the control of the wheel mass acceleration. Similar to the Skyhook theory, Groundhook Control Theory uses an ideal damper, which is connected between the wheel mass and the zero line used as the point of reference for vertical disturbances of the road/terrain height profile. Switching functions similar to those seen in Equation 2.7 are used to control the compression and rebound of the wheel mass motion and the resulting ideal damping coefficient. The switching functions can be seen in Equation 2.3 from (Soliman and Kaldas 2019).

$$K_d = \begin{cases} K_{d,min} & \text{if } -\dot{Z}_w \cdot (\dot{Z}_b - \dot{Z}_w) \leq 0 \\ K_{d,gnd} & \text{if } -\dot{Z}_w \cdot (\dot{Z}_b - \dot{Z}_w) > 0 \end{cases} \quad (2.3)$$

The two approaches address the issue of improving either the ride comfort of the vehicle (Skyhook) or vehicle handling (Groundhook) with respect to the trade off which was explained in Section 2.2. Some approaches combine the two theories of Skyhook and Groundhook control to achieve an improvement of both the ride comfort and vehicle handling. The hybrid approach described in (Soliman and Kaldas 2019) is configured to prioritise the control objective by the ratio ( $\mu$ ) between Skyhook and Groundhook control which is predefined by the user as seen in Equations 2.4 - 2.5 from (Soliman and Kaldas 2019).

$$K_{hyb} = [\mu \cdot K_{d,sky} + (1 - \mu) \cdot K_{d,gnd}] \quad (2.4)$$

$$K_d = \begin{cases} K_{d,min} & \text{if } \dot{Z}_b \cdot (\dot{Z}_b - \dot{Z}_w) \leq 0 \\ K_{d,hyb} & \text{if } \dot{Z}_b \cdot (\dot{Z}_b - \dot{Z}_w) > 0 \\ K_{d,min} & \text{if } -\dot{Z}_w \cdot (\dot{Z}_b - \dot{Z}_w) \leq 0 \\ K_{d,hyb} & \text{if } -\dot{Z}_w \cdot (\dot{Z}_b - \dot{Z}_w) > 0 \end{cases} \quad (2.5)$$

Semi-active suspension in the mass-market typically are focused on vehicles where ride comfort or handling are of particular importance to the end user and as such are only available on specific vehicles.

The Continuously Controlled Electronic Suspension (CES) system developed by Tenneco and Öhlins (Tenneco 2021a;b) is one particular example used on vehicles such as the Volvo S60R and V70R (aftermarketNews 2021). The system utilises sensor data about the vehicle body acceleration and suspension for reliable control of shock absorber valves similar to that seen in (Öhlins 2021) of "up to 100 times a second" (Soliman and Kaldas 2019). Other systems such as the Continuous Damping Control (CDC) system developed by ZF Sachs AG (ZF Sachs AG 2021a;b;c) and the DampTronic-Sky system developed by ThyssenKrupp Bilstein as explained in (Bilstein 2021) are approaches which utilise similar sensor networks. Many

control strategies that utilise preview information and predict the motion of the vehicle are currently still under development however, companies like Clearmotion Inc. (2014) are already utilising predictive control for their own active suspension system which can be outfitted to vehicles as part of an aftermarket purchase option (ClearMotion Inc 2021).

### 2.5.3 Preview Information and Predictive Control

The need to respond to sudden, but predictable, disturbances, whilst making use of low bandwidth actuators, has prompted the use of proactive or predictive control strategies. Such approaches apply control actions calculated based on expected disturbances and inputs that will alter the behaviour of the system response in preparation for the incoming disturbance. Predictions of the expected disturbances have been improved with the use of the collection and analysis of preview information about the terrain surface, ahead of the vehicle (Göhrle et al. 2015; Prokop and Sharp 1995). The collection of the preview information is linked to the understanding of the terrain in front of the vehicle which is discussed more in depth in Section 2.5. The effects related to the amount of preview information supplied to a LQR (Linear Quadratic Regulator) controller about the road surface ahead of the vehicle and its influence on the performance of reducing vertical body accelerations has been previously noted by the authors in (Prokop and Sharp 1995) with specific reference to the bandwidth of the actuator.

In the last decade, research on semi-active and active suspension control has focused on Model Predictive Control (MPC) Strategies (Gohrle et al. 2013; Hu et al. 2015; Nguyen et al. 2016). MPC strategies vary in complexity. It is common for the damper to have the hysteresis removed to simplify the control process. The use of MPC strategies are typically linked directly to half-car and full-car models as seen in (Gohrle et al. 2013; Mehra et al. 1997; Nguyen et al. 2016). MPC methodologies differ in the literature. One methodology is to develop the controller from a quadratic program (QP) problem, since it is both fast to compute and simpler to implement on available hardware. Additionally, it is relatively easy to implement individual weightings on the vehicle response within the cost function as part of the Hessian matrix and its gradient as shown in (Gohrle et al. 2014) which are associated with the parameters that account for the physical limitations of the vehicle model.

Very few studies using MPC to control semi-active suspension have utilised Nonlinear Hysteretic Damper Models such as the Bouc-Wen (Nerbin et al. 2017). One of the possible reasons for this is the difficulty to include the nonlinear hysteretic behaviour within the system state space model as part of a typical QP problem. It is common for the control force to be determined by the controller through optimisation within set limits on the damper displacement and maximum damping force (Gohrle et al. 2013).

The use of the control force instead of the electrical current in the optimisation process is more commonly seen in the literature as this allows the use of an inverse model of the damper model to convert the force to a usable current value (Canale et al. 2006; Gohrle et al. 2013; Gohrle et al. 2014). Inverse modelling allows for faster calculation of the ideal damper current response, but developing an inverse model of the damper is not a straightforward process. The MR Damper model has additional nonlinearities that are present in the response of the MR Damper with regards to the current supplied, thus making inverse modelling a nonlinear non-convex optimisation problem.

One of the important considerations for controllers of semi-active suspension systems is the amount of energy consumed when the actuators are in use. This issue is common with both Full Active Suspension (FAS) and Semi-Active Suspension which has led to research into regenerative Semi-Active (Chen et al. 2018) and FAS systems (Casavola et al. 2018) to reduce the energy demand of using FAS and Semi-Active suspension systems.

Another approach to reducing the energy consumed by semi-active suspension is the reduction of the amount of current supplied to the MR Damper over time, in order to improve the efficiency of the system and result in less wasted electrical energy through sub-optimal damping. This is possible through additional limitations placed on the controller and drives the need for energy efficient suspension control, which is becoming increasingly important as a result of the need, to minimise energy wastage for future electric and hybrid-electric vehicles to ensure that the usable range of the battery can be maximised.

This thesis addresses the issues presented in this section by developing predictive model based controllers that minimise energy usage as well as body vehicle body acceleration to create an effective, yet efficient, solution. The model predictive controller exploits Nonlinear Damper Models to offer a more realistic prediction of the damper forces and the resulting motion of the vehicle body and wheel masses.

## **2.6 Terrain Modelling and Terramechanics**

### **2.6.1 On-Road Conditions**

Terrain modelling for on-road conditions has improved substantially over time, through the use of terrain mapping and improvements to surface geometry detection sensors such as Light Detection and Ranging (LiDAR) and ultrasound. It is often assumed that paved road surfaces are non-deformable rigid mediums as the design of road is to minimise the deformation of the subgrade used under the road surface (Cook et al. 2013:34), there are additional nonlinearities involved between the tyre and road surface. The nonlinearities typically relate to the behaviour

of the tyre and the subsequent generation of forces at the contact patch which serves as the interface between the tyre surface and road surface.

Surface contaminants such as snow, ice, mud, water and in some cases oil, which reduce the magnitude of the friction forces generated, can make calculating the true response of the tyre considerably more difficult. However, many research projects typically relate surface contaminants to the Coulomb Friction Coefficient ( $\mu$ ) to simplify the problem as seen in (Bakker et al. 1987). Other environmental conditions, related to the weather pose challenges to be modelled effectively and can have an impact on the dynamic response of the vehicle. However, for the purpose of this research, environmental conditions have been assumed constant and therefore negligible. In particular, the simulations are carried out for a typically dry day with no wind effects, see Chapter 8.

The main features used in the modelling of a typical road surface are the camber angle, gradient, macro roughness and micro roughness of the road section. In addition to this, potholes and other surface deformities make modelling the terrain surface more complicated when trying to offer a realistic representation of a road surface. Accurately reproducing the features of a specific road can be accomplished through the use of road measurements of the road height profile using vehicle-based LiDAR or ultrasound sensors. However, as explained by the authors in (Karamihis et al. 1999), the measurements would only reflect a snapshot of the shape of the road section, as external conditions would alter the shape of the road with time. In addition, LiDAR and ultrasound suffer from several disadvantages that impact their effectiveness of measuring the road/terrain height profile.

Firstly, is the quantity of data collected, while not necessarily a disadvantage on its own, the amount of computational resources needed to process the data is relatively high when compared to a sensor that samples at a much lower rate. Secondly, unlike some other forms of sensor the absolute measurement of a single point is not guaranteed which links back to the first point of the high quantity of data and the processing required. Finally, due to the amount of data that is required building a LiDAR installation on a vehicle is often quite expensive. The benefit of this though is that some autonomous and semi-autonomous vehicles already incorporate the technology as part of collision avoidance and adaptive cruise control. With all its disadvantages LiDAR does have the ability to provide safe, reliable and fast measurements of varying distances which makes it the ideal sensor for measuring the road/terrain height profile for the collection of preview information.

### 2.6.2 On-road Tyre Models and Contact Point Formulation

A number of on-road tyre models have been developed for studying the tractive behaviour and vehicle dynamics as a result of the tyre contact with the road surface. The most well

known model is the Magic Formula tyre (MF-Tire) model (Pacejka and Bakker 1992) which has had numerous reformulations/versions to improve its ease of use, and accuracy. Among the revisions of the MF-Tire model the Magic Formula - Swift (MF-Swift) tyre model was proposed by the authors in (Besselink et al. 2005) and further compared to the MF-Tire model in (Pacejka 2012).

The MF-Swift tyre model is a version of the MF-Tire model that is adapted to model the higher frequencies of the tyre response with frequencies of up to 100 Hz. The model consists of four elements as explained in (Pacejka 2012) which are the Magic Formula, the contact patch slip model, the rigid ring and the obstacle enveloping model. The first of the four elements is linked in kind to the MF-Tire model with the lateral and longitudinal forces and aligning moment of the tyre calculated using the standard form equation from (Pacejka 2012; Pacejka and Bakker 1992) recreated here as Equation 2.6.

$$y = D \sin [C \arctan \{Bx - E(Bx - \arctan Bx)\}] \quad (2.6)$$

In Equation 2.6 the value  $y$  can be used to represent either the longitudinal force using the longitudinal slip ratio ( $sr$ ) as the value for  $x$  or the lateral force if the value of the lateral slip ( $\tan \alpha$ ) is used as  $x$ . The equation is also capable of producing the aligning moment of the tyre with some minor modification as explained in (Pacejka 2012).

The MF-Tire and MF-Swift models are among a number of commercially available tyre models including the Flexible Structure Tire Model (FTire) (Cosin Scientific Software AG 2020) and CDTire (Gallrein and Bäcker 2007) tyre models which are used in durability testing. The models each are utilised to determine the forces of the tyre but are usually limited by the frequency response of the tyre, for example the FTire software is capable of determining frequencies of up to 200 Hz (Cosin Scientific Software AG 2021). However, detailed testing and analysis of the FTire and CDTire models in terms of the Noise, Vibration and Harshness (NVH) was conducted in (Uhlar et al. 2019) which highlight the frequency response up to 300 Hz.

These models require significant testing of a particular specification of tyre to identify the parameters and achieve an accurate fit of the model. The use of FTire for off-road analysis has also been performed as seen in (Cosin Scientific Software AG 2020; 2021) however, FTire combines several of the approaches used in tyre-soil interaction modelling alongside the parameterisation of the Finite Element Models which are discussed later in Section 2.5.3 that results in larger computational costs and an increase in system complexity with several features that are not required for the purposes of this study.

The method of contact evaluation varies from model to model with some models using point references while others more focus on the change of the contact patch size and area as a

whole. Brush models used by models like the FTire model (Cosin Scientific Software AG 2020) can be utilised that utilise many contact points to calculate an average response of the tyre with accuracy increasing as the density of these points increase. Figure 2.8 shows an example diagram of the contact point formulation used in the calculation of the wheel motion and forces.

This item has been removed due to 3rd Party Copyright. The unabridged version of the thesis can be found in the Lanchester Library, Coventry University.

Fig. 2.8 Diagram showing contact point formulation (Rill and Castro 2020)

Figure 2.8 highlights how the motion of the contact point and the motion of the wheel rim move with respect to the road plane and the fixed inertial reference frame indicated in the directions of  $(x_0, y_0, z_0)$  with the road plane normal indicated by  $z_n$ . The Wheel Carrier (WC) moves in conjunction with the tyre and is generally delayed as the forces between the wheel rim and the tyre build up. This motion differs depending on the model utilised as the tyre can have both spring and damping elements to calculate the motion of the contact point. In (Rill and Castro 2020) the authors explain how the tyre contact motion is calculated with respect to a fixed inertial frame and how other reference frames are used in the calculation of the wheel motion. In general there are typically three other reference frames used in vehicle simulation these are the vehicle, the wheel carrier, and the local road plane or wheel reference frame.

For the simulation of ride comfort however it is more typical to utilise a spring tyre model as illustrated in some of the vehicle models from Figure 2.2 and later in Chapter 4. The spring tyre model is a simplistic model often utilised for on-road simulations where the road surface is assumed to be non-deformable. The model is a computationally inexpensive calculation with the tyre force calculated by the deflection of the tyre and a stiffness constant. It is commonly used in control systems and vehicle dynamics assessments to represent the vertical dynamics of

the tyre for a predefined road/terrain height profile ([Altinoz and Yilmaz 2018](#); [Blundell and Harty 2014](#); [Gohrle et al. 2013](#); [Gohrle et al. 2014](#); [Langlois and Hanna 1991](#)).

The spring model is chosen to be used in the on-road vehicle models for the simulation of the vehicle plant model in Chapter 8 and is also used in the formulation of the controllers which will be proposed later in Chapters 6 and 7. In addition to the spring tyre model, one of the other tyre models which will be used in the later sections of this thesis is the TMeasy tyre model proposed by Dr. Georg Rill ([2021](#)). A parameterised tyre for one of the versions of the TMeasy tyre model is available for use as part of the Automotive Simulation Models (ASM) provided by dSPACE ([dSPACE GmbH 2020](#); [Peperhowe and Schindler 2013](#); [Rill 2020](#); [2021](#)) and is utilised for the on-road full car ASM Vehicle Dynamics model discussed in more detail in Chapter 4.

### 2.6.3 Off-Road Conditions

Off-road terrain modelling requires the the consideration of additional physical behaviour and the parameterisation of variables that are set as constants when modelling on-road conditions.

Even under typical dry conditions, the influence of terrain deformation poses a difficult situation to model. The on-road surface the off-road surfaces/tracks have similar 3D geometrical features such as the camber angle and gradient. However, for off-road these features can vary much more than for a typical road surface. In addition, the presence of soil deformation further complicates this process. The residual stresses in the soil and the multi-pass effect can result in the front tyres travelling across significantly different terrain geometries than the rear tyres.

Soils may be classified based on their composition using the percentage of organic matter in comparison to the overall weight to determine whether the soil is a Organic or Mineral soil. In addition, mineral soils can be further divided into three main groups, Sandy, Clays and Loamy as seen in ([Cranfield University 2021](#)). Soil grain size can be used to categorise whether the soil is a fine grained soil or course grained soil. Fine grained soils typically refer to an average diameter of less than 0.074 mm where 50% or more of the grains by weight as explained in ([Wong 2008](#)). Similarly, a course grained soil like beach or desert soil is considered as soils with average grain sizes larger than 0.074 mm ([Wong 2008](#)).

Terrain types play a crucial part in the terrain modelling process. The first step in order to determine the vehicle's response when travelling on off-road terrain is to determine the terrain's properties and characteristics through physical testing using a bevameter or penetrometer as seen in ([Wong 2009](#)). The results of these test are often freely available and can be used for simulation of terrain behaviour when under loading conditions ([Wong 2008](#); [2009](#)). When modelling the terrain it is common to model the soil as a completely plastic medium, where loading of the soil results in permanent deformation of the soil material and indentation on

the soil surface (Wong 2009). The soil may behave as a plastic medium under certain weather conditions and for soils that are more clay based which can be classified as remouldable soils (STS 2021) but other surface types like dry loose soils have been observed to behave more like an elastic medium (Wong 2009). Other common alternatives to modelling the terrain as a plastic medium include purely elastic models and critical state mechanics modelling (Kurtay and Reece 1970; Roscoe et al. 1958; Schofield and Wroth 1968; Wong 2009) techniques. Critical state mechanics models are typically utilised for modelling the terrain as part of studies in Terramechanics. They have led to the development of Tyre-Soil Interaction Models.

#### 2.6.4 Tyre-Soil Interaction Models

Tyre-Soil Interaction Models were developed to model the complex loading and unloading of a rolling tyre on soil. There are numerous approaches for modelling this behaviour with some of the earliest purely empirical models utilising minimal computational resources to determine whether it was possible to traverse the soil on a 'go' or 'no-go' basis using a number of performance indices. These types of models include the WES VCI model (Rula et al. 1971), STIREMOD model (Allen et al. 1997), and the model proposed by the authors in (Hegazy and Sandu 2013).

Other Physics based models were developed to provide a deeper understanding of the behaviour at the tyre-soil interface utilising Finite Element Methods (FEM) (Shoop 2001) or Discrete Element Methods (DEM) (Smith and Peng 2013). However, the deeper understanding of this behaviour comes at the cost of being both computationally expensive and financially expensive to parameterise. Even 2D FEM or lumped mass models require significant computational resources when compared to purely empirical models.

Semi-empirical models are a compromise between the level of detail and the number of computational resources with some capable of real-time modelling. Semi-empirical Tyre-Soil Interaction Models are typically grouped into two areas; Rigid Wheel and Flexible Tyre. While the two sections are not totally unrelated, it is common for one of the two theories to be valid when describing the behaviour of the tyre on off-road terrain.

Rigid Wheel models assume that the soil is sufficiently soft and as such the tyre is not deflected. Instead the soil undergoes a combination of both plastic and elastic deformation resulting in the wheel creating an indentation in the soil surface. For this to be valid there are several assumptions made about the soil's properties stated in (Wong 2009) including:

- The soil is homogeneous and isotropic.
- The mechanical behaviour of the soil depends only on effective stress, which is defined as the difference between the total stress and the pore water pressure (usually referred to

as pore pressure). The presence or absence of pore pressure or moisture tension alter the effective stress.

- The mechanical behaviour of soil can be described by a macroscopic model. It is not necessary to relate soil behaviour to the properties of individual particles and the interactions between these particles.
- The mechanical behaviour of soil is not time dependent and the soil is not viscous.

Flexible Tyre models assume that the soil stiffness is sufficiently hard to produce a deflection in the tyre surface. they require a new formulation to calculate the pressure distribution at the contact patch. While the assumption that the tyre can behave similarly to a spring is valid when the terrain has a high yield stiffness such as when on tarmac or paved roads, this only is valid if there is no deformation of the terrain surface resulting in the tyre sinking into the supporting terrain. As a result it is often incorrect to assume that the tyre will always behave as a spring for firm off-road terrain.

The effect of the tyre spinning on the soil is highlighted in (Bekakos et al. 2016b) as part of the dynamic slip sinkage. Soils have been observed to show increased tractive forces in the braking condition (negative slip) (Senatore and Sandu 2011) which is generally related to the increase in the soil build up in front of the tyre as the wheel angular velocity is reduced and the vehicle linear velocity exceeds that of the linear velocity at the contact area.

Semi-empirical models offer the best compromise for real-time simulation, therefore the four semi-empirical models are considered; the HSSTM model (Taheri, Sh. et al. 2013), AS2TM (Harnisch et al. 2005), and the models proposed by the authors in (Bekakos et al. 2016b; Senatore and Sandu 2011). Several of these models were included in a review of terramechanics models which was conducted by the authors in (Taheri, Sh. et al. 2015b), which included analysis of the real-time capabilities and computational resources required for some tyre-soil interaction models.

The HSSTM model (Taheri, Sh. et al. 2013) which is mentioned by the authors in (Taheri, Sh. et al. 2015b) is claimed to offer many of the desirable output results expected of tyre-soil interaction models, including bulldozing forces which had not been realised by any other model in their review. However, the process for parameterising the model requires large amounts of physical data on the tyre response to accurately model the tyre behaviour.

The AESCO Soft Soil Tire Model (AS2TM) is a 2D rigid ring tyre model that uses Bekker's suggested approach for a substitute circle of larger radius "to describe the deformed contact patch between the tyre and soil" (Harnisch et al. 2005) as shown in Figure 2.9. The larger radius ( $R_u^*$ ) calculates the static sinkage ( $z_0$ ) and the difference in the sinkage between the

smaller unloaded radius ( $R_u$ ) is used to calculate the tyre deflection ( $z_{def}$ ) with the soil rebound ( $u_0$ ) calculated by the lowest point of the larger circle to the last point in contact with the soil.

It may be noted that while the angles for the two circles may be different the absolute point of contact for entry and exit remain the same for the two radii when using the Earth Reference Frame to mark the vertical and longitudinal positions. This approach is highly reliant on the inflation pressure of the tyre with highly inflated tyres typically represented as rigid wheels with little to no deformation and  $R_u^* = R_u$  (Bekakos et al. 2016b). The AS2TM model also empirically models the terrain and considers the multi-pass effect by applying a modification of Wong's repetitive loading calculations. The slip sinkage effect is also modelled using Steiner's approach and calculates the lateral forces in the tyre-soil system using a combination of the methods investigated in (Grecenko 1967; Schwanghart 1968).

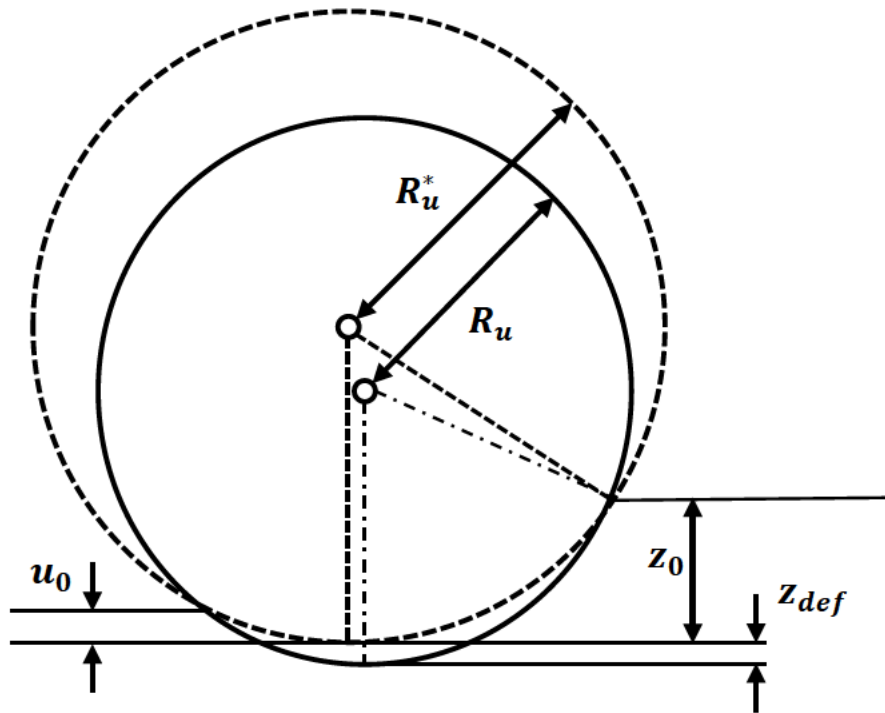


Fig. 2.9 A graphical representation of the substitute circle method (Bekakos et al. 2016b; Harnisch et al. 2005)

The rigid wheel model proposed in (Bekakos et al. 2016b) is one particular application of the theory described in (Bekker 1962; Wong and Reece 1967) for the calculation of the pressure-sinkage distribution curve at the tyre-soil interface. The Bekakos model (Bekakos et al. 2016b) allows for a number of wheel types including: rigid treadless (slick tyres with no deformation), rigid treaded and deformable wheels. The latter provides the static and dynamic sinkage of the tyre which has followed the patterns observed in (Senatore and Sandu 2011).

The models proposed in (Bekakos et al. 2016b; Senatore and Sandu 2011) and the HSSTM model (Taheri, Sh. et al. 2013), use semi-analytical processes to implement two soil failure zones and incrementally discretise the contact patch utilising the theory from (Wong and Reece 1967) that offers an alternative method of calculating the pressure-sinkage curve to that which was presented in (Harnisch et al. 2005) as part of the of the AS2TM model.

The Bekakos model from (Bekakos et al. 2016b) was chosen as the most desirable candidate for the tyre-soil interaction model for use in this thesis. The model offers an efficient approach to calculating the response of the tyre and is computationally inexpensive when compared to the HSSTM model. The tyre-soil interaction model currently only calculates the forces and moments for a tyre on flat soft soils, as such it is proposed that a gentle slope between  $\pm 10$  degrees could be modelled using the proposed modifications shown in Chapter 5.

## 2.6.5 Terrain Parameters and Characteristics

In addition to the rigid wheel model assumption, the choice of terrain parameters are also important. The soil characteristics, properties and the parameters to the pressure-sinkage equation proposed by Bekker in (Bekker 1962) (shown in Equation 2.7) are often easily available in the literature, as the equation provides the basis for many tyre-soil interaction models.

$$p = (k_c/b + k_\phi) z^n = k z^n \quad (2.7)$$

Table 2.2 shows some of the soil parameters for the Bekker equation (Equation 2.7) that are available in the current literature and have been merged from multiple sources to provide a complete set of variables for the modified Bekakos model shown in Chapter 5.

Table 2.2 Soil Parameters for Tyre-Soil Interaction Modelling (Wong 2008; 2009)

| Soil Type                | $n$ [-] | $k_c$<br>[ $kN/m^{n+1}$ ] | $k_\phi$<br>[ $kN/m^{n+2}$ ] | $c$ [ $kN/m^2$ ] | $\phi$ [deg] | $\rho$ [ $kg/m^3$ ] |
|--------------------------|---------|---------------------------|------------------------------|------------------|--------------|---------------------|
| LETE Sand                | 0.79    | 102                       | 5301                         | 1.3              | 31.1         | 1600                |
| Upland<br>Sandy<br>Loam  | 1.10    | 74.6                      | 2080                         | 3.3              | 33.7         | 1557                |
| Rubicon<br>Sandy<br>Loam | 0.66    | 6.9                       | 752                          | 3.7              | 29.8         | 1561                |
| Grenville<br>Loam        | 1.01    | 0.06                      | 5880                         | 3.1              | 29.8         | 1326                |
| Dry Sand                 | 1.1     | 0.99                      | 1528.43                      | 1.04             | 28           | 2000                |
| Soft Soil                | 0.8     | 16.5                      | 911                          | 3.71             | 25.6         | -                   |

Height profile measurements of on-road conditions have been well documented. However, the height profiles of off-road terrain is far less documented, thereby requiring the need for experimental testing or to adopt the assumption that the mean height profile across the terrain is relatively constant. Due to the unavailability of experimental testing equipment, the research presented in this thesis assumed that the height profile of off-road terrain is flat terrain or at a gentle slopes no greater than  $\pm 10$  degrees as highlighted in Chapter 8.

## 2.7 Concluding Remarks

This chapter critically reviewed the literature relevant to the proposed research on off-road semi active control system exploiting the capabilities of MR dampers. It has identified current issues to model tyre soil, damper, vehicle systems and simplifications associated with developing models for the purpose of control. The review has also highlighted the various control strategies previously investigated and identified the most suitable approach. A summary of these findings together with the justification of approaches and accompanying assumptions adopted for this research are now presented:

- Current MR Damper models used in existing research include the Nonlinear Hysteretic Biviscous (NonlinHBV), Nonlinear Viscoelastic Plastic (NVEP), Bouc-Wen and modified Bouc-Wen models. The following models adopted for use and discussion later in this thesis are the NonlinHBV, NVEP and modified Bouc-Wen models. The NonlinHBV and NVEP models are chosen firstly because they offer a representation of the MR Damper that closely resembles the true response of the damper, but also because of the reduced number of parameters when compared to the modified Bouc-Wen model which is included for comparison later in Section 3.4.2. The NonlinHBV and NVEP models need further modifications to their formulation to accommodate for MR Damper test data which does not have a mean force or mean velocity of zero, and could result from either the design of the damper or through measurement error. The modifications proposed later in Chapter 3 will utilise coordinate transformations and translate the force-velocity relationships of the model along the force and velocity axes to achieve a better overall fit to the data.
- Current vehicle models used in the available literature include the quarter car, full car and ASM models which have been chosen to be adopted for use later in this thesis. The quarter car and full car models which are chosen to represent the plant model used in the simulations of the system in Chapter 8 and will be used in the formulation of the Nonlinear Model Predictive Control (NMPC) strategy proposed later in Chapters 6 and 7,

while the ASM model will be used to compare and verify the results of the full car model and assess the performance of the NMPC strategy. The models which have been chosen will be adapted in Chapter 4 to use the nonlinear MR Damper models from Chapter 3 which will replace the linearised dampers used in the original literature, that have no hysteresis modelled as part of the force-velocity damping curve and the proposed changes would produce a more realistic representation of the vehicle response.

- Tyre-Soil Interaction models typically calculate the response of a tyre on flat terrain which limits the possible uses of the model for vehicle dynamics analysis in the vertical direction. A novel approach to modify the Bekakos model from (Bekakos et al. 2016b) in order to calculate the tyre's response on gentle sloping soft soils was discussed which will be presented in Chapter 5 along with approaches to improve the runtime performance of a tyre-soil interaction model through the use of a lookup table. These proposed modifications will allow for the use of the tyre-soil interaction model for the simulation of an off-road vehicle and the lookup table can be utilised further in the prediction of the future vehicle response for use within the NMPC strategy for an off-road vehicle.
- The quarter car and full car vehicle models typically used in the formulation of NMPC strategies for semi-active suspension currently rely on the calculated tyre response to be included within the system model. However, The influence of tyre sinkage requires the wheel hub motion to be calculated separately from the main system as the wheel hub motion is solely dependent on the sinkage in the case of rigid wheel tyre-soil interaction models. Chapters 4 and 5 will propose a novel formulation for calculating the system response of the vehicle for both on-road and off-road, using coupled state space systems in Simulink which will allow the motion of the vehicle body mass and wheel masses to be calculated separately but remain interconnected to ensure that the response of one mass influences the other.
- A critical review of typical control methods for semi-active suspension systems was conducted and PID control and adaptive PID control are chosen as alternative controllers, which will be used to compare controller performance with the proposed NMPC strategy as part of Chapters 6 and 7. Linear PID controllers are typically unsuited to nonlinear control and have mixed results when used to control nonlinear systems, therefore Sections 6.2 and 6.3 propose the use of an alternative method of tuning the PID for the simulations in Chapter 8 in addition to a new formulation of adaptive PID controller which incorporates the displacement and velocity of the MR Damper as seen in Section 6.3.

- Model Predictive Control was discussed as an appropriate control strategy for the semi-active MR Damper based suspension. It was highlighted that current controller formulations use the control force of the MR Damper as the manipulated variable for the improvement of vehicle ride comfort, but generally do not calculate the control current as the optimisation variable until an inverse model is used. The controller proposed in this thesis will differ from previous works in that the current to be supplied to the damper will be the optimisation variable as shown in Chapters 6 and 7 which will form the foundation of Nonlinear Model Predictive Controllers for both on-road and off-road MR Damper suspension control.



# Chapter 3

## Nonlinear Magnetorheological Damper Modelling

### 3.1 Introduction

Accurately predicting and simulating the behaviour of Magnetorheological Dampers (MR Dampers) is a challenging problem, see Chapter 2. This chapter aims to address the problems with current MR Damper models, in particular the way that force offsets present in the data are modelled as part of the dynamic relationship between force and velocity. This chapter proposes two improvements to the Nonlinear Hysteretic Biviscous (NonlinHBV) and Nonlinear Viscoelastic Plastic (NVEP) models, the modified Nonlinear Hysteretic Biviscous model (modNonlinHBV) and the modified Nonlinear Viscoelastic Plastic model (modNVEP).

Sections 3.2 and 3.3 highlight the changes made to the NonlinHBV and NVEP models to accommodate for non-zero mean force and/or mean velocity data. The coordinate transformations first mentioned in Section 2.6 introduced the main concept of the methods employed here. Section 3.4 then continues to explain the processes involved with fitting the modified MR damper models to test data of a particular MR Damper to allow for improved fit to the data.

The fit of the modified models when compared to the original models and the modified Bouc-Wen model is investigated in Section 3.4.2 to show the relative improvements of the modified models. Meanwhile Section 3.5 describes the processes used to utilise the modified models for semi-active suspension modelling when integrated with the vehicle models which are described later in Chapter 4. This chapter concludes by highlighting the key benefits of the proposed changes to the NonlinHBV and NVEP models before showing how the models intend to be utilised in the future chapters of this thesis.

### 3.2 Modified Nonlinear Hysteretic Biviscous Model

A drawback of the current NonlinHBV model is the reliance on data that is symmetrical about the origin for both the force and velocity, see Section 2.4.1. The modified model, referred to as modNonlinHBV, is presented in this section. It uses translated axes to describe the force-velocity relationship rather than the true axes as seen in Figure 3.1. The theoretical axes allow for the same force-velocity relationship curve shape as the original model but with a theoretical origin that does not necessarily correspond to zero.

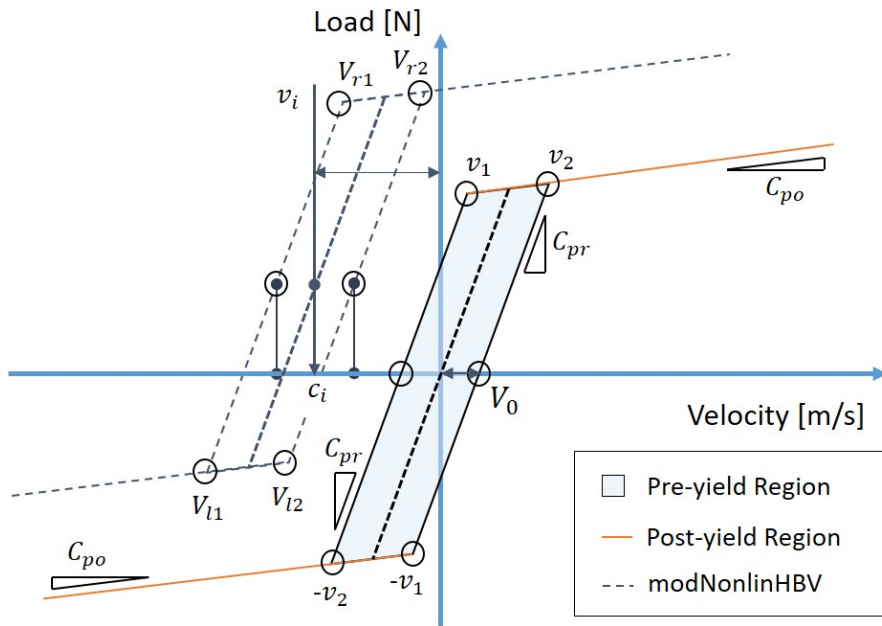


Fig. 3.1 Diagram of the Modified Nonlinear Hysteretic Biviscous Model (modNonlinHBV)

The modNonlinHBV model utilises the shifting parameters  $c_i$  and  $v_i$  to represent the translation of the origin of the force-velocity relationship curve, along the force and/or velocity axes respectively. While the compressive yield velocity  $v_1$  and tensile yield velocity  $v_2$  are calculated the same as in (Snyder et al. 2001) (recreated here as Equations 3.1 and 3.2), the translation of the origin results in the movement of these velocities and the transition of the MR Damper between the post-yield region and the pre-yield region cannot be solely calculated using these values.

The points where the MR Damper transitions from the pre-yield region to the post-yield region and vice versa for both compressive and rebound motions, would usually be defined by the the compressive yield velocity  $v_1$  and tensile yield velocity  $v_2$  and their negative opposites (as seen in Figure 3.1), for the purpose of the explaining the translational movement these points will be referred to as transition points. The transition points of the modified model, as

seen in Equations 3.3 to 3.6, use the offset parameter  $v_i$  to adjust the location of the transition points with respect to the shift of the data along the velocity axis.

$$v_1 = \left( \frac{F_y - C_{pr} \cdot V_0}{C_{pr} - C_{po}} \right) \quad (3.1)$$

$$v_2 = \left( \frac{F_y + C_{pr} \cdot V_0}{C_{pr} - C_{po}} \right) \quad (3.2)$$

$$V_{l1} = -v_2 + v_i \quad (3.3)$$

$$V_{l2} = -v_1 + v_i \quad (3.4)$$

$$V_{r1} = v_1 + v_i \quad (3.5)$$

$$V_{r2} = v_2 + v_i \quad (3.6)$$

The nonlinear forces of the modified damper model are calculated using the six conditional cases shown in Equations 3.7 and 3.8. The nonlinear forces in the pre-yield region are equally spaced apart from the theoretical origin by the zero-force velocity intercept. Similarly to the original model, this is used to model the hysteresis in the pre-yield region of the model. The forces for positive and negative acceleration of the damper piston are given by Equations 3.7 and 3.8 respectively to reflect the damper's transitions between the pre-yield and the post-yield regions.

$$F_d(t) = \begin{cases} C_{po} \cdot (v(t) - v_i) - F_y + c_i & v \leq V_{l2} \\ C_{pr} \cdot (v(t) - v_i - V_0) + c_i & V_{l2} \leq v \leq V_{r2} \\ C_{po} \cdot (v(t) - v_i) + F_y + c_i & V_{r2} \leq v \end{cases} \quad (3.7)$$

where  $\dot{v} > 0$

$$F_d(t) = \begin{cases} C_{po} \cdot (v(t) - v_i) + F_y + c_i & V_{r1} \leq v \\ C_{pr} \cdot (v(t) - v_i + V_0) + c_i & V_{l1} \leq v \leq V_{r1} \\ C_{po} \cdot (v(t) - v_i) - F_y + c_i & v \leq V_{l1} \end{cases} \quad (3.8)$$

where  $\dot{v} < 0$

The parameters of this model can be determined using similar approaches to that for the model from (Snyder et al. 2001). It is possible to determine the parameters from graphical hand calculations, system identification and optimisation methods including nonlinear least squares (see Section 3.4).

### 3.3 Modified Nonlinear Viscoelastic Plastic Model

The NVEP model has similar issues to the NonlinHBV model in that it assumes the data is symmetrical around the origin with a mean of zero for both the force and velocity data. The modNVEP model uses a similar approach to that discussed in the previous section with the introduction of the shifting parameters  $v_i$  and  $c_i$ . The overall model has three components that reflect the mechanisms modelled, namely Pre-yield, Post-yield and Yield Force.

**Pre-yield Mechanism** The Pre-yield Mechanism describes the damping forces in the pre-yield region using spring and damping coefficients. The shaping function  $S_{ve}$  is used to smooth the transition between the Pre-yield region and the Post-yield region as it approaches the Yield Force. The Equations 3.9 to 3.11 are used to calculate the pre-yield force ( $f_{pr}$ ) for a fixed electrical current and oscillating frequency which is combined with the force components from the other mechanisms in Equation 3.17.

$$f_{ve}(t) = K_{ve} \cdot x(t) + C_{ve} \cdot (v(t) - v_i) \quad (3.9)$$

$$S_{ve}(v) = \frac{1}{2} \cdot \left[ 1 - \tanh \left( \frac{|v - v_i| - v_y}{4 \cdot \epsilon_y} \right) \right] \quad (3.10)$$

$$f_{pr}(t) = S_{ve}(v) \cdot f_{ve}(t) \quad (3.11)$$

where  $K_{ve}$  is the Pre-yield Stiffness,  $C_{ve}$  is the Pre-yield Damping Coefficient,  $v_y$  is the Yield Velocity and  $\epsilon_y$  is a smoothing parameter. The key difference between Equations 3.9 - 3.11 and those from (Snyder et al. 2001) is the introduction of the shifting parameter into both the equation for calculating the viscoelastic force component  $f_{ve}$  (Equation 3.9) and the shaping function  $S_{ve}$  (Equation 3.11). By introducing the shifting parameter  $v_i$  into these equations, the damper piston velocity is corrected to remove the impact of the non-zero mean velocity value from each velocity value and calculate the overall response of the damper in the low velocity region.

**Post-yield Mechanism** The Post-yield Mechanism describes the behaviour of the damping force in the high velocity, post-yield region through the use of the Post-yield Damping Coefficient ( $C_{vi}$ ). The same smoothing parameter used in the Pre-yield mechanism is used in Equation 3.13, alongside the yield velocity.

$$f_{vi}(t) = C_{vi} \cdot (v(t) - v_i) \quad (3.12)$$

$$S_{vi}(v) = \frac{1}{2} \cdot \left[ 1 + \tanh \left( \frac{|v - v_i| - v_y}{4 \cdot \epsilon_y} \right) \right] \quad (3.13)$$

$$f_{po}(t) = S_{vi}(v) \cdot f_{vi}(t) \quad (3.14)$$

The viscous force component ( $f_{vi}$ ) determines the change in the viscous force as the fluid behaves similarly to a plastic medium at the higher velocities. The post-yield region has a similar shaping function (Equation 3.13) to that used in Equation 3.10. This ensures a smooth transition between the post-yield region and the pre-yield during the rebound phase, when the load pressure is removed from the damper and the damper extends. Similarly to the Pre-yield Mechanism, the shifting parameter  $v_i$  is added to Equations 3.9 and 3.10 to correct the damper piston velocity values for the high velocity region.

**Yield Force** The Yield Force determines the transition points between the Pre-yield and Post-yield regions. The Yield Force Equation has its own smoothing parameter  $\epsilon_c$  which is introduced into the shaping function  $S_c$  (Equation 3.15) and the yield velocity ( $v_y$ ) term is removed. In addition, the Yield Force Constant ( $F_c$ ) is introduced in place of spring and damping components seen in Equations 3.9 and 3.12. The component of force attributed to the yield force ( $f_c$ ) is calculated using Equation 3.16 which is needed in the final model equation seen in Equation 3.17.

$$S_c(v) = \tanh\left(\frac{v - v_i}{4 \cdot \epsilon_c}\right) \quad (3.15)$$

$$f_c(t) = S_c(v) \cdot F_c \quad (3.16)$$

To ensure that the Yield Force corresponds to the other two mechanisms, the shifting parameter  $v_i$  is introduced into the shaping function  $S_c$ . Adjusting all values associated with the velocity by the shifting parameter  $v_i$  allows to translate the force-velocity curve along the velocity axis.

**Final Model Equation** The resulting model equation seen in Equation 3.17 shows how each of the damper model mechanisms are combined to determine the total force generated by the damper for a given velocity and displacement. The shifting parameter  $c_i$  is added as an additional component of the force to accommodate for the force offset present in some force data as a result of the presence of an accumulator or pressurised gas to avoid cavitation of the MR Fluid.

$$F_d(t) = f_{pr}(t) + f_{po}(t) + f_c(t) + c_i \quad (3.17)$$

The damper force produced by the modNVEP model allows for modelling of the steady state forces with respect to a particular electrical current and sinusoidal oscillation. In addition, the model allows for the dynamic calculation of forces with respect to damper piston displacement

and velocity, provided that the electrical current and the frequency of oscillation are kept constant. A comparison of the force-velocity curve produced using the modified and original models can be seen in Figure 3.2 which uses the bump profile seen later in Figure 8.1 from Chapter 8.

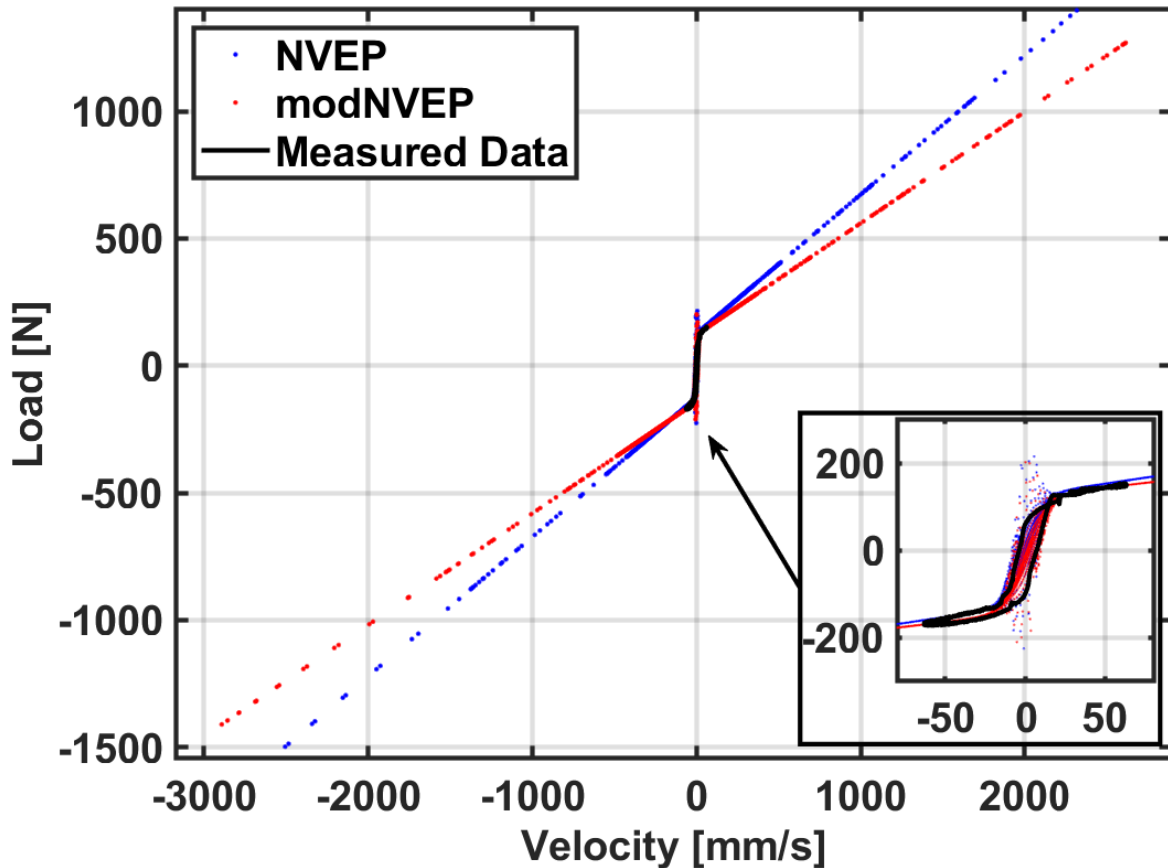


Fig. 3.2 Example plot of the force-velocity relationship curve produced by the NVEP and modNVEP models for the Passive Soft condition of the MR Damper during a simulation of a bump of 0.05m in height and at a velocity of  $90\text{km}\cdot\text{h}^{-1}$ .

Figure 3.2 shows how each of the components combine to produce a force-velocity hysteresis curve which is not too dissimilar to those seen in the real data presented in Section 3.4. Unlike the NonlinHBV and modNonlinHBV models the NVEP and modNVEP models recreate some of the hysteresis seen in the high velocity, post-yield region while keeping the parameters of the model within manageable limits for real-time simulation and damper force predictions.

It may be noted that when both shifting parameters values equal zero the modNonlinHBV and modNVEP model formulations return to match the original formulations presented in (Snyder et al. 2001). The modNonlinHBV and modNVEP models still remain fairly symmetrical with respect to the force curve produced for both compressive and rebound velocities of the

damper piston which is an issue, as it does not account for differences in the shape of the force curve in the post-yield region for compression and rebound of the damper piston.

## 3.4 Model Fitting and Parameterisation

Both of the modified models discussed in sections 3.2 and 3.3 require the model to be parameterised using the same data collected through testing of a real MR damper used in the original models from (Snyder et al. 2001).

### 3.4.1 Experimental Setup

The LORD RD-8041 MR Damper is primarily designed for industrial suspension applications (Lord Corporation 2009), however some research by the authors of (Krauze 2013) have identified its use in vehicle suspension. While the study (Krauze 2013) applies to the suspension of an All Terrain Vehicle (ATV) the equivalent damping of the damper is comparable to that described in (Blundell and Harty 2014) as part of the quarter car vehicle model. In addition, another study (Seong et al. 2011) that has identified that the forces generated by an MR Damper for vehicle suspension applications were found to be comparable to the forces indicated in the technical specifications of the LORD RD-8041 MR Damper (Lord Corporation 2009). This study proposes the damper to be used on a medium sized vehicle comparable to the Maserati GranTurismo and models the damper through model fitting to sinusoidal test data.

Sinusoidal testing of a LORD RD-8041 MR Damper was conducted with a peak displacement amplitude of 10mm. The sinusoidal testing was performed using the INSTRON Fatigue and Tensile Testing Machine at Coventry University for the isolated frequencies of 0.1Hz, 1Hz, 3Hz, and 6Hz with force data being sampled every millisecond. The current supplied to the MR Damper was controlled through the use of a LORD Wonderbox (Lord Corporation 2006) to ensure that the electrical current could be kept constant during sinusoidal testing.

An image of the equipment installed on the INSTRON machine is seen in Figure 3.3 with the damper piston arm connected to the upper moving column. A Linear Variable Differential Transformer (LVDT) was used in parallel to the sensors of the INSTRON machine to ensure that the position measurement data resulted in the desired sinusoidal motion for each test.

The frequency range for the damper testing corresponds to values close to the primary ride frequency, the frequency gaps allow for some interpolation of the raw data to be performed in order to anticipate the reaction of the damper to frequencies in this region. However, it is also common to find literature that tests other dampers in this region allowing for a closer

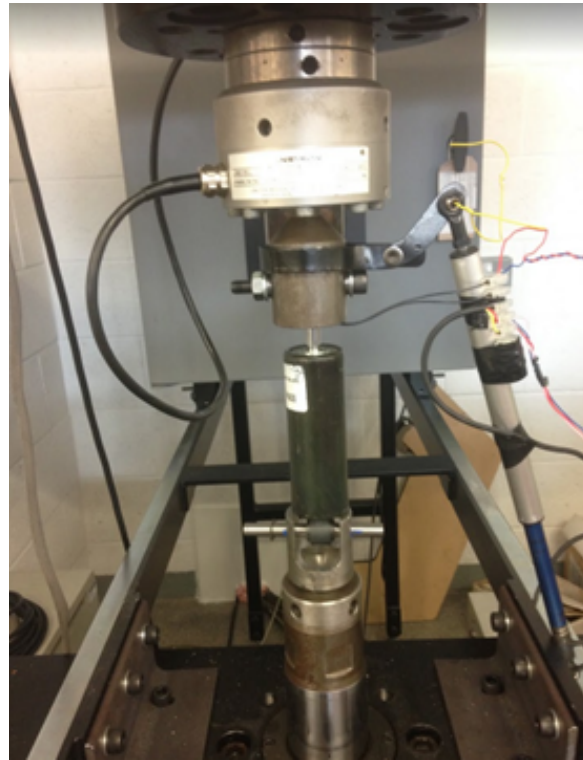


Fig. 3.3 LORD RD-8041 MR Damper Connected to INSTRON Fatigue and Tensile Testing Machine for Sinusoidal Testing using a LVDT for displacement sensing.

comparison between the results from this research to other studies such as ([Kamath and Wereley 1997b](#); [Snyder et al. 2001](#); [Wereley et al. 1998](#)).

Figure 3.4 shows some of the experimental data collected during the sinusoidal testing of the damper at 1Hz when relating the load force of the damper to the damper piston position. The influence of the current on the magnitude of the damper load is clearly visible, in addition to the presence of the force lag that occurs when the acceleration of the damper shifts from positive to negative and vice versa. This force lag is seen when the acceleration of the damper is increasing in magnitude after the peak or trough of the sinusoidal displacement oscillation after the load force has passed through 0 N.

To improve the fit of the models to the data, a tool for visualising the damper model fit, for any given set of parameters, was developed using the MATLAB App Designer. The layout of the graphical user interface for the specifically designed Model Fitting Application is shown in Appendix A. The application allows empirical modelling by adjusting parameters manually. In addition, nonlinear least squares optimisation is employed alongside one of the robust methods listed in Table A.1 of Appendix A to determine the optimum fit to the data in the presence of inconsistencies.

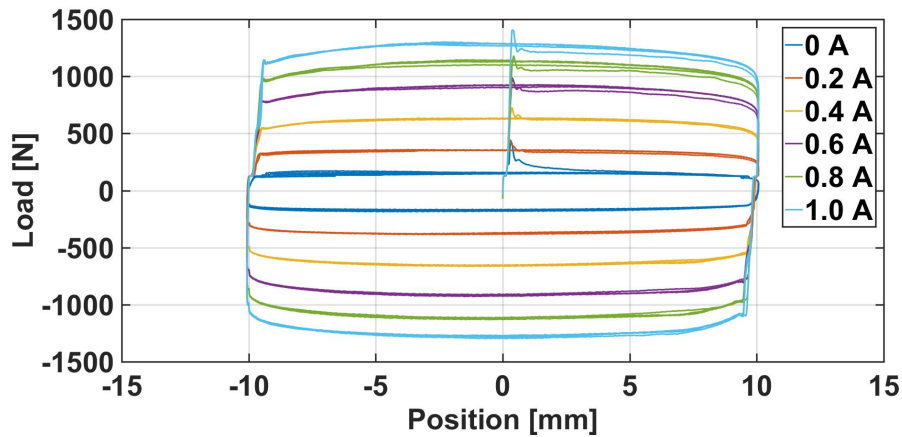


Fig. 3.4 Experimental Data of Sinusoidal Testing of Lord RD-8040-1 MR Damper at 1Hz for multiple current values.

Prior to fitting the model to the data, the velocity of the damper piston is determined through differentiating the damper piston displacement with respect to time. The displacement measurement data from the INSTRON machine could potentially have low amplitude and be contaminated by high frequency noise as a result of imperfect sensors. The process utilised in (Snyder et al. 2001) was adopted to ensure that all the fitted models would produce accurate results whereby the displacement data was filtered by fitting a first order Fourier model to the data prior to differentiation which was to smooth the curve and reflect the true position of the damper piston without noise.

The parameter values of the Nonlinear Hysteretic Biviscous Model (NonlinHBV) and modified Nonlinear Hysteretic Biviscous Model (modNonlinHBV) are easily determined through both manual adjustment in the tool or through the use of optimisation methods. To improve the optimisation process and the accuracy of the fit, the Model Fitting Application, shown in Appendix A, has the option to use manually adjusted parameters as a starting point for the solver to achieve a better overall fit to the data than from the starting points shown in Table 3.1.

Nonlinear Least Squares (NLS) was used to determine the optimal values of the parameters due to it being a nonlinear optimisation problem, and it being a solver which is fully integrated into MATLAB/Simulink. The starting conditions given in Table 3.1 utilise the initial conditions that can be provided to the solver as part of *fmincon* function in MATLAB. The optimisation process for NLS utilises the cost function in Equation 3.18 which calculates the overall cost value ( $J$ ) for the entire cycle of data with  $N$  number of data-points. The measured force of the real MR damper ( $F_d$ ) at time  $t_k$  is compared to the force value calculated by the modified Nonlinear Viscoelastic Plastic model ( $\hat{F}_d$ ).

Table 3.1 Starting Parameters for Nonlinear Least Squares Optimisation

| Parameter       | Starting Value | Units               |
|-----------------|----------------|---------------------|
| $C_{vi}$        | $C_{po}$       | N.m.s <sup>-1</sup> |
| $F_c$           | $F_y$          | N                   |
| $v_y$           | $V_0$          | m.s <sup>-1</sup>   |
| $\varepsilon_y$ | [0 ... 10]     | -                   |
| $\varepsilon_c$ | [0 ... 10]     | -                   |
| $c_i$           | 0              | N                   |
| $v_i$           | 0              | m.s <sup>-1</sup>   |

$$J(C_{ve}, K_{ve}, v_y, \varepsilon_y, F_c, \varepsilon_c, C_{vi}, v_i, c_i) = \sum_{k=1}^N |F_d(t_k) - \hat{F}_d(t_k)|^2 \quad (3.18)$$

The process of fitting the model to the data is identical to the approach used in (Snyder et al. 2001) to allow for a direct comparison between the original and modified models. The only difference between the two approaches is that the shifting parameters are included as part of the variables to be optimised.

### 3.4.2 Model Fit Accuracy and Comparison to Other Available Models

After fitting the parameters of the models to the MR Damper test data, it was necessary to identify the model fit accuracy and determine the improvement of the model fit when compared to the original models and the modified Bouc-Wen model using the 10 parameters of the Spencer Model from (Spencer et al. 1997).

Figure 3.5 shows the forces of the different models for a single 1Hz cycle of oscillation in comparison to the measured data of the real MR damper. The unmodified Nonlinear Hysteretic Biviscous Model (NonlinHBV) and Nonlinear Viscoelastic Plastic Model (NVEP) show a clear mismatch in the magnitude of the force when compared to the measured data. The measured data also illustrates the force offset due to the high pressure nitrogen gas that was stated in the technical specifications of the damper (Lord Corporation 2009).

The differences between the NonlinHBV model and the modNonlinHBV model result in closer tracking of the measured data with the overall difference between the modified model and the measured data being within  $\pm 10$ -20 N of the real value during the peaks and troughs of the cycle. The difference between the NVEP model and the modNVEP model demonstrated the

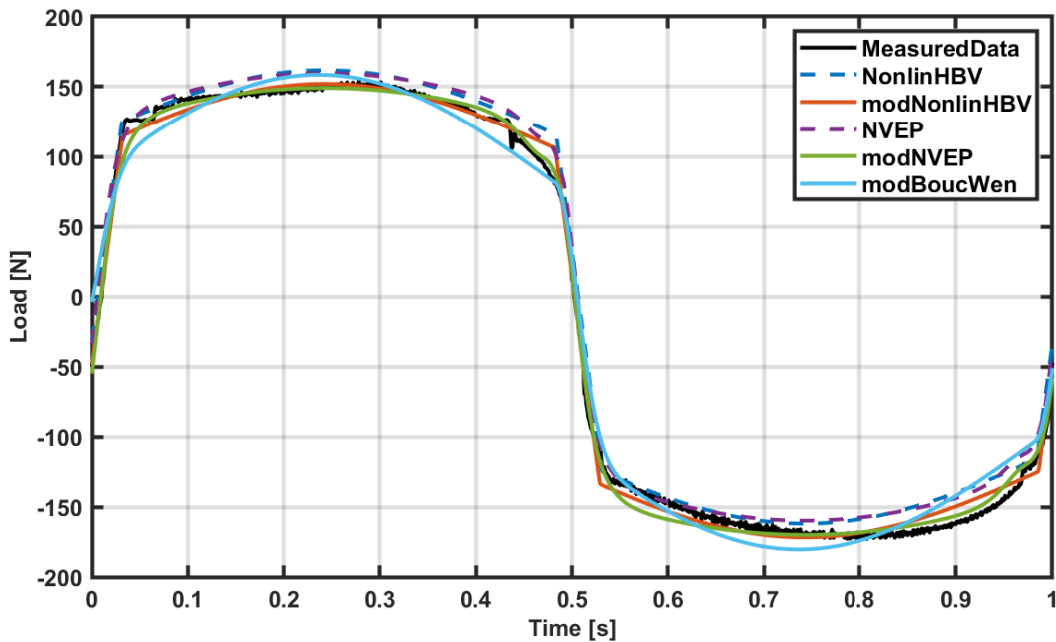


Fig. 3.5 Comparison between damper models and measured data from testing at 1Hz 0A

benefits of the modNVEP model which exhibits improved fitting of the overall magnitude of the force as well as of the shape of the force curve during the peaks and troughs. The differences in the shape of the force curve are due to the calculated parameters for the Pre-Yield Damping Coefficient and the Post-Yield Damping Coefficient as a result of shifting the force value using  $c_i$ .

When comparing the modNonlinHBV with the modNVEP model, the influence the nonlinear shape of the modNVEP has on the overall fit of the model to the data becomes apparent. The force lag effect, observed in the measured data, shows a gradual rise in the magnitude of the force from the start of the peak to the end. The increase and decrease of the force magnitude reproduced by the NonlinHBV and modNonlinHBV models is more symmetrical, highlighting the limitations of the two models in replicating the force lag effect.

As mentioned in Chapter 2 the modified Bouc-Wen model from in (Spencer et al. 1997; Talatahari et al. 2012) offers users the ability to calculate the damper force including the force offset seen in the data. The model has been fitted to the data from the 0.1Hz 0A test case, as seen in Figure 3.5, and shows how the model closely represents the force relationship seen in the real data. The modified Bouc-Wen (modBoucWen) model seen in Figure 3.5 shows the force curve created by a model that is used by several studies (Nerbin et al. 2017; Zhenlei Li et al. 2008) for the purpose of developing controllers for semi-active MR Damper suspension.

The modified Bouc-Wen model and the modNVEP model shown in Figure 3.5 both show forces that very closely match the measured data from the MR Damper. The quantitative evaluation of the models uses the Root Mean Squared Error (RMSE) criteria. Table 3.2 shows the RMSE values of the best fit for each model to the 1Hz 0A test case.

Table 3.2 Root Mean Squared Error (RMSE) Force Values for each of the damper models for the 1Hz cases

| Model Type        | RMSE Force Value [N] at Current |         |        |         |         |         |
|-------------------|---------------------------------|---------|--------|---------|---------|---------|
|                   | 0 A                             | 0.2 A   | 0.4 A  | 0.6 A   | 0.8 A   | 1.0 A   |
| NonlinHBV         | 12.6181                         | 4.7351  | 11.082 | 4.5975  | 5.2759  | 5.9028  |
| modNonlinHBV      | 6.733                           | 3.9778  | 5.3987 | 6.2787  | 7.0501  | 8.0757  |
| NVEP              | 12.1668                         | 11.0765 | 7.5009 | 8.9406  | 11.3099 | 13.7069 |
| modNVEP           | 5.9264                          | 5.4153  | 8.0342 | 10.6854 | 13.6311 | 15.1446 |
| modified Bouc-Wen | 6.3359                          | -       | -      | -       | -       | -       |

The RMSE values from Table 3.2 show that the modNVEP is a capable model at reproducing accurate force calculations for a given displacement and velocity. The added benefit is that even with the additional shifting parameters introduced as part of the modification process, the nine parameters of the model result in the model being a highly competitive alternative to the modified Bouc-Wen model currently used in the literature. While these values show the average error the force velocity curve reflects a relationship where the modNVEP model closely matches the relationship curve with this being evident in Figure 3.6 and the subsequent figures from Appendix C. It is for this reason, that the modNVEP model will be used to represent the true response of the MR damper as part of the vehicle modelling process seen in Chapter 4.

### 3.5 Applications for Semi-Active Suspension Behaviour Modelling

One of the key applications of the modNVEP model is for the modelling of MR Damper behaviour as part of semi-active suspension. The model as shown in the earlier sections offers as a suitable alternative to the modified Bouc-Wen model. Nonlinearities of the MR Damper behaviour with respect to the current supplied and frequency of oscillation, make inverse functions difficult to produce, this issue is also present in the Nonlinear Damper models from (Snyder et al. 2001) and the proposed modifications in Sections 3.2 and 3.3.

Fixed model parameters were identified from data measured during fixed current/frequency testing. These model parameters are however required to be adjusted to calculate the approxi-

mate behaviour of the damper when electrical current to the damper is changing or when the main oscillating frequency is changing.

To calculate the model response to a changing current, the model parameters that were obtained for each test case were used to form two-dimensional lookup tables, one for each of the parameters. Figure 3.7 shows the lookup table values for the modNonlinHBV model with frequency along the x axes, current along the y axes, and the parameter value along the z axis. The two-dimensional lookup tables are created as a means to interpolate the values of the parameters across both the current and frequency ranges.

Through interpolation of the lookup table values it is possible to find acceptable parameter values for each damper model when operating at conditions which were not covered during testing. To formally verify this method the data-point for the 0.5 A, 1 Hz test case was temporarily removed and the lookup table value was queried using the remaining data to find the interpolated value equivalent to the 0.5 A, 1 Hz test case. The results of the fit can be found in Figure 3.6 along with the best fit found using the method from Section 3.4 and the measured data for the real damper. This method was, however, not utilised to model the impact of frequency changes. This was partly due to the unavailability of force data at high sampling rates. The latter led to a less accurate fit at the higher frequencies of 3Hz and 6Hz than at 0.1Hz and 1Hz.

The subplots in Figure 3.7 show the lookup table values and the interpolated surface representing the parameter values at operating conditions not covered during the testing of the damper. It can be observed that the parameter values along the 1Hz line increase gradually as the current value increases but there is less overall variation of the parameter values than the other test frequencies providing more reliable estimations of the damper force at 1Hz throughout the range of current values as seen in Appendix C.

Another key implementation included in the MR Damper model, for use within a semi-active suspension, was the introduction of a lag in the current supply to the damper model. The damper is physically limited to respond to changes in the electrical current within a time of 15 milliseconds (Lord Corporation 2009). However, the damper forces calculated based on the models proposed here refer to the steady state forces with respect to the current, while accommodating for the dynamic behaviour of the displacement and velocity of the damper piston.

To ensure the time lag introduced as the MR Damper begins to respond to the changes in electrical current and the resulting magnetic field, a first order transfer function with a time constant of 0.003 seconds was introduced to slow the rate of increase of the electrical current. While the electrical current in reality would respond almost instantaneously, the output of the

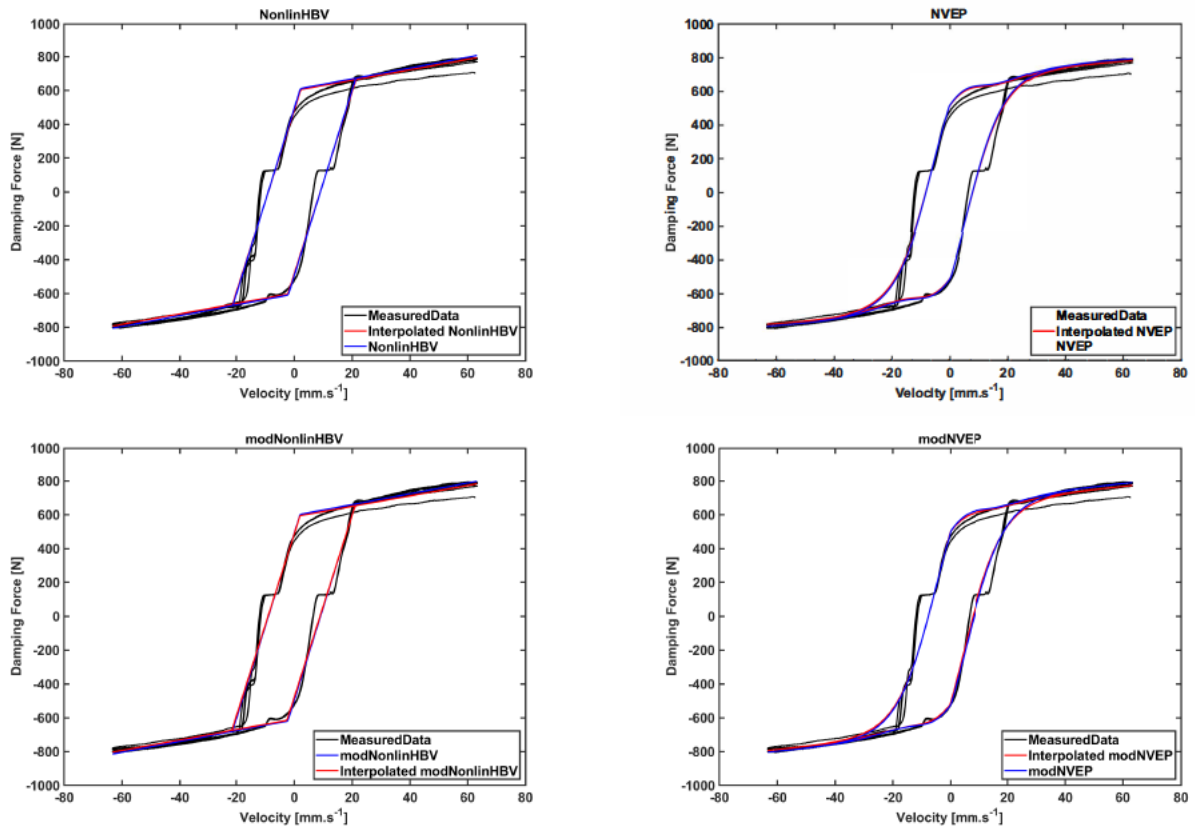


Fig. 3.6 Interpolated Parameter Fit Compared Against Real Data and Best Fit for 1 Hz 0.5 A Test Case

transfer function outputs an equivalent current that represents the dampers transition to the new steady state current value determined by the controller.

The time constant of 0.003 seconds is chosen so that within five times the time constant the system will stabilise within 99% of its final value, which corresponds to the time stated for the damper to respond within in (Lord Corporation 2009). This behaviour is comparable with electrical circuits that include both resistance and capacitance, whereby a capacitor will reach its final charge value within five time constants. Figure 3.8 shows the resulting output of the chosen transfer function in comparison to the step input of 1A with the number of time constants ( $nT$ ) shown in the table with their respective current output values.

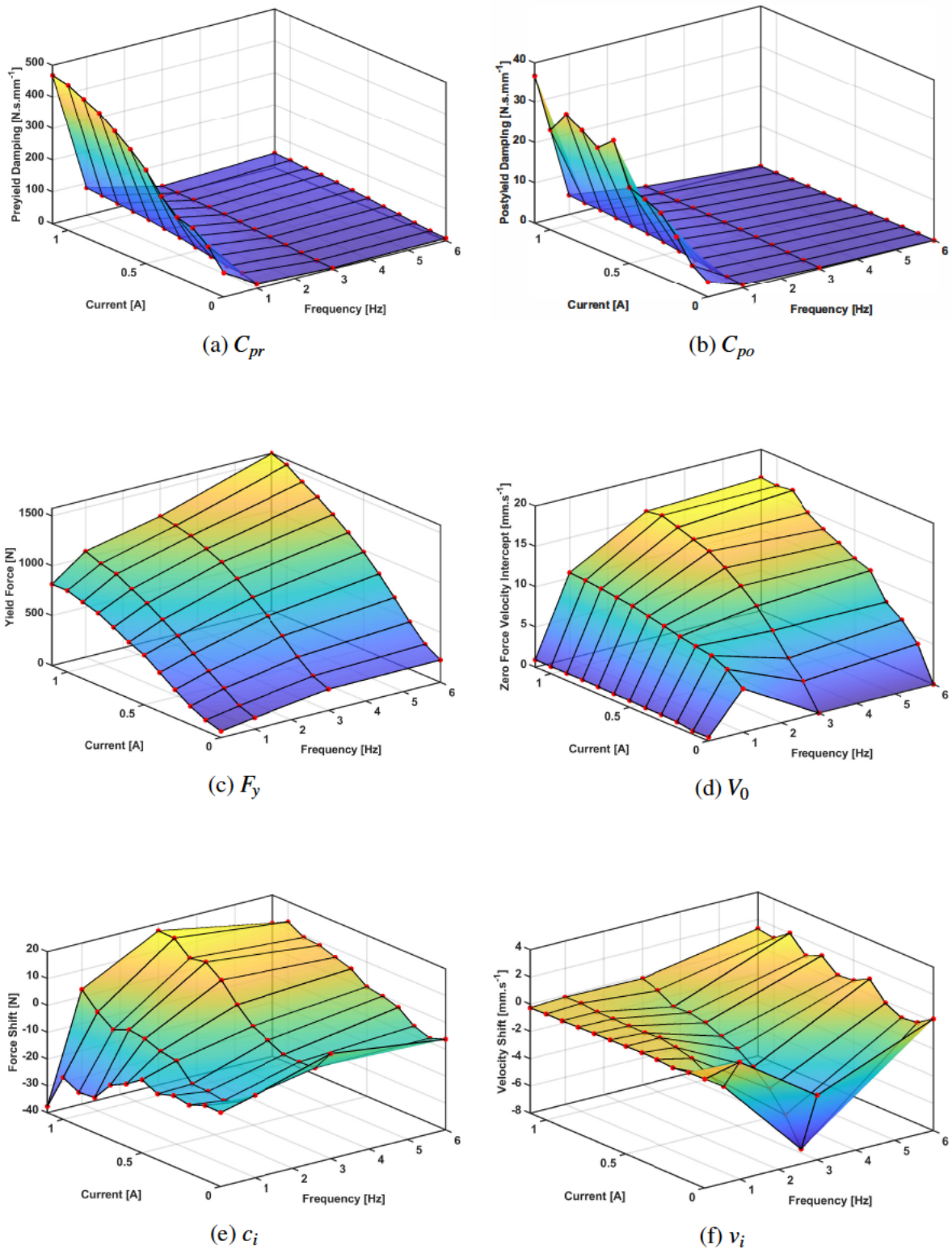


Fig. 3.7 Subplots of the modNonlinHBV Damper Model Parameters Lookup Tables

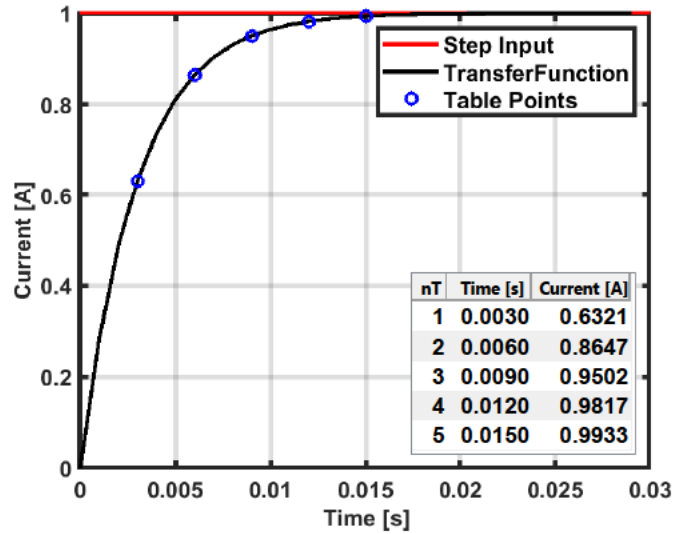


Fig. 3.8 The output of the transfer function with time constant 0.003 seconds with respect to the response time to reach each of the table values.

### 3.6 Concluding Remarks

This chapter detailed the modifications to the NonlinHBV and NVEP models to improve the modelling accuracy for situations when there is non-zero force and/or velocity data. The chapter highlighted how the modifications impacts the process of fitting the models to test data. It demonstrates that the modifications lead to improvement in terms of model fit compared to the original models. A summary of the specific findings is now presented.

- The modNonlinHBV model is typically easier to fit to the test data than the modNVEP model. However, it does not reproduce the force-velocity curve in as much detail as the modNVEP model as there is no hysteresis considered in the Post-Yield region.
- The modNonlinHBV model parameters can be estimated using the approach described in (Snyder et al. 2001). In particular, the model parameters for the NVEP and modNVEP models can be used as the starting point for the parameter fitting optimisation process.
- Lookup tables were used for the MR Damper models parameters to accommodate for varying operating conditions. The resulting models were integrated to the semi-active suspensions within the vehicle models, see Chapter 4.
- Lookup tables used to interpolate the parameter values from the best fit cases of the model fitting optimisation process were found to allow for the estimation of acceptably accurate results when reproducing the nonlinear damper response at operating conditions

not previously tested. This approach was utilised to calculate the response of the damper at operating conditions which lie between current values that have been tested.

- The modNVEP model was found to offer the most accurate representation of the damper behaviour at the test frequencies of 0.1Hz and 1Hz. Therefore, the modNVEP model was chosen to represent the true response of the damper during the simulations in Chapter 8.
- The Model Fitting Application tool developed in the MATLAB App Designer was successfully used to determine the initial parameter values exploited by the optimisation process. In addition, the tool was useful in performing manual adjustments to the parameter values to obtain a better overall fit of the model when compared to using the standard optimising process described previously.
- The optimised force-velocity relationships for the modified models are given in Appendix C in addition to the models from (Snyder et al. 2001) to allow for further comparisons to the 1Hz test data to be made.



# Chapter 4

## Vehicle Dynamics System Modelling

### 4.1 Introduction

To determine the effect that the Nonlinear MR Damper models have on a vehicle's dynamics and to begin formulating the predictive model used by the controller, a vehicle dynamics system model must first be defined. This chapter introduces the three vehicle models used in the simulation studies detailed in Chapter 8; a nonlinear quarter car model, a nonlinear full car model and a modified version of the dSPACE Automotive Simulation Model (ASM) (dSPACE GmbH 2020). In addition, each of the three models is modified to use the nonlinear MR Damper models from Chapter 3 to determine the nonlinear response of a vehicle.

The first part of this chapter describes the two techniques used to formulate a nonlinear quarter car vehicle model used in the analysis of the vertical motion of the vehicle in response to a change in road/terrain height. The first method describes the model represented as a single continuous time invariant state space model. It uses a nonlinear damper force, calculated by the MR Damper models discussed previously in Chapter 3. The second method describes a model split into two state space systems. It describe the motion of each mass separately with the two models coupled to ensure the correct calculation of the displacements of each mass and balance the system.

The second part describes the two techniques used to formulate a nonlinear full car vehicle model. Such model is used for the analysis of the vertical and angular motion of the vehicle body that results from a difference in the terrain height between the four corners of the vehicle. The first method uses a single state space model to describe the behaviour of the vehicle, while the second method describes the process of separating the body mass motion, from the calculation of the wheel masses.

The third part describes the modifications made to the Automotive Simulation Model (ASM) used for full car vehicle dynamics analysis to allow the use of the modified nonlinear MR

Damper models described in Chapter 3. This part also describes the impact of changing the MR Damper model on the system response and shows how the use of a linearised model for vehicle suspension modelling does not offer as accurate results as the nonlinear MR Damper models proposed in Chapter 3.

The chapter concludes with a description of the novelties and purposes of each of the vehicle models introduced in this chapter. It summarises how they are combined to simulate vehicles and predict the vehicle behaviour as part of the nonlinear Model Predictive Controllers proposed in Chapters 6 and 7.

## 4.2 Nonlinear Quarter Car Vehicle Model

The quarter car vehicle model represents a single corner of the vehicle and calculates the motion of a single wheel connected to the quarter mass of the vehicle. The sprung mass (quarter mass of the vehicle) and the unsprung mass (wheel mass) are linked together using spring and damper components which represent the vehicle's suspension and are capable of moving along the vertical axis. The forces generated when there is a change in relative distance between the two masses, are often as a result of external forces being exerted on either of the two masses.

The quarter car vehicle models described in Section 2.3 typically use linear/linearised spring and damper coefficients to determine the vertical dynamic response of the vehicle to changes in the road/terrain height. However, the vertical dynamics of a vehicle are not linear. Therefore, the linearised models used to predict the motion of the vehicle often lead to model-reality mismatches which is a particular issue for predictive controllers that are formulated to use these models.

There have been a number of formulations for nonlinear quarter car vehicle models that use a variable force to represent the forces from semi-active and active suspension systems (Gohrle et al. 2013; Gohrle et al. 2014; Göhrle et al. 2015). These formulations allow for the calculation of the vehicle's vertical response to a road/terrain height disturbance. However, these approaches, typically, do not use models that reproduce the hysteresis of the spring or damping elements.

A formulation of a nonlinear quarter car vehicle model is needed to fully characterise the behaviour of a quarter car vehicle fitted with semi-active MR Damper based suspension. For the purposes of this study, the springs used in the formulations of the quarter car vehicle model are considered to be linear. However, nonlinear damper models that reproduce the hysteresis present in MR Dampers, as described in Chapter 3, are considered to represent a more realistic representation of the damper response and enable the user to predict the response of a quarter car vehicle with improved accuracy.

Figure 4.1 shows a quarter car vehicle model that is a modification of the diagram shown in (Koch and Kloiber 2014) with a continuously variable damping force ( $F_d$ ). The damping force used as part of the model described here is calculated using either the NonlinHBV, modNonlinHBV, NVEP or modNVEP MR damper models which were discussed in Sections 2.3 and 3.

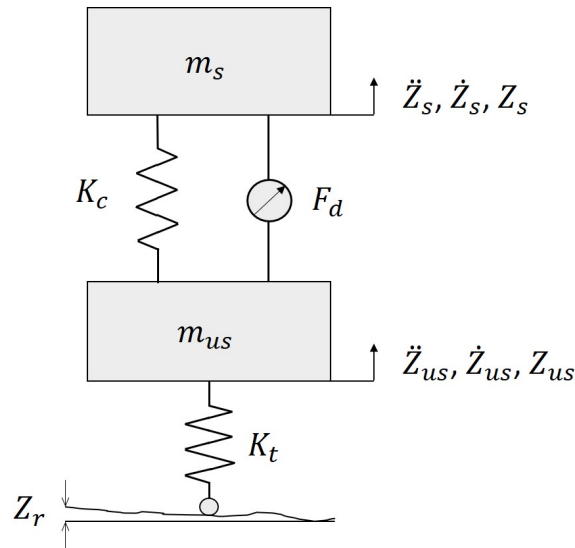


Fig. 4.1 Quarter Car Vehicle Model Diagram

The model utilises a spring with a known stiffness ( $K_t$ ) to represent the response of the tyre to a varying road height profile ( $Z_r$ ). This common assumption underestimates the substantial damping of vertical forces. Such a simplification of the tyre's vertical response overestimates the amount of energy introduced into the system from the road. It represents the worst case situation and is therefore ideal for the purpose of semi-active suspension control design.

The model parameters for the quarter car vehicle model were derived from the static quarter mass distribution of the front-left corner of the ASM vehicle model which is based around the Maserati GranTurismo. The parameters listed in Table 4.1 are utilised in all the quarter car simulations for both on and off-road conditions.

The nonlinear behaviour of the quarter car vehicle for both on and off-road is formulated through one of two methods. The first method described in Section 4.2.1 forms one complete state space system combining the quarter mass of the vehicle body (sprung mass) and the wheel mass (unsprung mass). The second method uses two state space systems to model the motion of each mass separately and then uses Simulink to link the systems together allowing for the adjustment of the motion of the unsprung mass before being given to the other system as explained in Section 4.2.2.

Table 4.1 Quarter Car Vehicle Parameters Based on the Front-Left Corner Static Weight Distribution of the ASM Vehicle Model (dSPACE GmbH 2020)

| Parameter Variable | Value   | Units |
|--------------------|---------|-------|
| $m_s$              | 561     | [kg]  |
| $m_{us}$           | 35      | [kg]  |
| $K_c$              | 130,000 | [N/m] |
| $K_t$              | 270,000 | [N/m] |

### 4.2.1 Method 1: Single State Space Quarter Car Vehicle Model

The first method of modelling the quarter car vehicle involves formulating the model as a single continuous time invariant state space system. The inputs to the system are the nonlinear damping force of the MR Damper ( $F_d$ ) and the road/terrain height profile ( $Z_r$ ). The motion of the sprung mass ( $m_s$ ) is calculated as a function of the damping force and the displacements of the two masses using Equation 4.1.

The model assumes that the motion of the sprung mass, given by Equation 4.1, is only affected by the motion of the unsprung mass. It is assumed that changes in the quarter mass of the vehicle do not occur throughout the simulation. The author acknowledges that such external forces and changes in the quarter loads of the vehicle are common in real world testing of a typical vehicle. However, modelling the stochastic variability in size and timing of these occurrences during a typical journey lies beyond the scope of this study. In this work, the model assumes that the only disturbances introduced into the system are the changes in the vertical displacement of the road/terrain from a fixed reference height.

The Equations 4.1 and 4.2 represent the motion of the sprung mass ( $m_s$ ) and unsprung mass ( $m_{us}$ ) respectively. The motion of one of the masses is linked to the other through the force generated by the MR Damper ( $F_d$ ) and the compression/elongation of a spring that is attached in parallel to the damper, which supports the load force of the vehicle when in equilibrium (shown in Figure 4.1). The spring force is determined by the multiplication of the spring stiffness constant ( $K_c$ ) with the relative suspension deflection, which is calculated by subtracting the displacement of the unsprung mass ( $Z_{us}$ ) from the displacement of the sprung mass ( $Z_s$ ).

$$m_s \ddot{Z}_s = -K_c (Z_s - Z_{us}) - F_d \quad (4.1)$$

$$m_{us} \ddot{Z}_{us} = K_c (Z_s - Z_{us}) + F_d - K_t (Z_{us} - Z_r) \quad (4.2)$$

The equation of motion for the unsprung mass (Equation 4.2) includes the additional terms for the spring tyre deflection ( $Z_{us} - Z_r$ ), which represents the amount the tyre flexes in response to the road/terrain and the load of the vehicle. In an unloaded state the tyre deflection would be

be equal to zero and the radius of the tyre would be equal to the unloaded radius. However, when under loading the tyre deflection typically lies between the unloaded radius and the radius of the wheel rim. Careful consideration of the value of the tyre spring stiffness constant ( $K_t$ ) relative to the sprung mass and the mass of the wheel hub avoids the wheel rim making contact with the road. This is a condition where tyre deflection is extreme enough to result in the wheel rim making contact with the road/terrain surface, an occurrence which rarely occurs during typical operation.

The equations of motion for the two masses are converted to state space form by first defining the vehicle states. The vehicle states are defined by the state vector  $x_t = [Z_s, Z_{us}, \dot{Z}_s, \dot{Z}_{us}]^T$ , with the nonlinear damping force ( $F_d$ ) and the road/terrain displacement introduced as the system inputs ( $u_t$ ) where  $u_t = [F_d, Z_r]^T$ . The first method uses a continuous time-invariant state space model formed around the damper force as the controllable system input. The chosen nonlinear damper model calculates the MR Damper response to the changing relative displacement and velocity of the suspension. The latter can be translated directly into the displacement and velocity of the damper piston since both the the spring and damper are mounted vertically and in parallel to each other and deflect by the same amount.

Including the MR Damper model as part of the calculation for the system inputs allows for the vehicle model to be constructed to account for changes in the electrical current supplied by a controller to the MR damper, in addition to the viscous response of the damper fluid to the displacement and velocity of the damper piston. However, since both the relative displacement and the velocity of the suspension are required to calculate the damping force, the system output vector ( $y_t$ ) must be constructed to include the calculation of the relative suspension displacement ( $Z_s - Z_{us}$ ) and relative suspension velocity ( $\dot{Z}_s - \dot{Z}_{us}$ ).

$$A = \begin{bmatrix} 0 & 1 & 0 & 0 \\ -\frac{K_c}{m_s} & 0 & \frac{K_c}{m_s} & 0 \\ 0 & 0 & 0 & 1 \\ \frac{K_c}{m_{us}} & 0 & -\frac{(K_c + K_t)}{m_{us}} & 0 \end{bmatrix}, \quad B = \begin{bmatrix} 0 & 0 \\ -\frac{1}{m_s} & 0 \\ 0 & 0 \\ \frac{1}{m_{us}} & \frac{K_t}{m_{us}} \end{bmatrix}$$

$$C = \begin{bmatrix} 1 & 0 & 0 & 0 \\ 0 & 0 & 1 & 0 \\ 1 & 0 & -1 & 0 \\ 0 & 1 & 0 & 0 \\ 0 & 0 & 0 & 1 \\ 0 & 1 & 0 & -1 \\ -\frac{K_c}{m_s} & 0 & \frac{K_c}{m_s} & 0 \\ \frac{K_c}{m_{us}} & 0 & -\frac{(K_c + K_t)}{m_{us}} & 0 \end{bmatrix}, \quad D = \begin{bmatrix} 0 & 0 \\ 0 & 0 \\ 0 & 0 \\ 0 & 0 \\ 0 & 0 \\ 0 & 0 \\ -\frac{1}{m_s} & 0 \\ \frac{1}{m_{us}} & \frac{K_t}{m_{us}} \end{bmatrix}$$

$$\dot{x}_t = A x_t + B u_t \quad (4.3)$$

$$y_t = C x_t + D u_t \quad (4.4)$$

The system outputs are given by the output vector  $y_t$  shown in Equation 4.4, where the output matrices  $C$  and  $D$  give the outputs shown in Equation 4.5. The velocities of the sprung ( $\dot{Z}_s$ ) and unsprung ( $\dot{Z}_{us}$ ) masses are used for the calculation of the relative suspension velocity. They are updated at each time step using the system derivatives calculated using Equation 4.3. The vertical accelerations of the sprung ( $\ddot{Z}_s$ ) and the unsprung ( $\ddot{Z}_{us}$ ) masses provide the user with information on the comfort and stability of the vehicle. The sprung mass acceleration in particular is used for the calculation of the Key Performance Indicators (KPI) seen in the analysis of the simulation results in Chapter 8. Such KPI are used to assess the effective performance of semi-active suspension control strategies with respect to vehicle ride comfort.

$$y_t = [Z_s, Z_{us}, (Z_s - Z_{us}), \dot{Z}_s, \dot{Z}_{us}, (\dot{Z}_s - \dot{Z}_{us}), \ddot{Z}_s, \ddot{Z}_{us}]^T \quad (4.5)$$

Figure 4.2 shows a diagram of the connections between the nonlinear MR Damper model and the state space system formulated using Method 1. The feedback loop of the MR Damper

model calculates the updated response of the damper to the change in relative displacement and velocity of the suspension. It supplies a new force value for at each time step. The supply of the current to the MR Damper model, highlighted in blue, shows how the transfer function is used to calculate the Equivalent Current as explained in Chapter 3.

The nonlinear quarter car vehicle model formulated using the first method provides the user with a simple model to calculate the vehicle’s response to a changing road/terrain height disturbance. The disadvantage of this approach is that the wheel dynamics are locked within the state space system and cannot be modified to account for off-road tyre-soil interaction. The latter, introduced in Chapter 5, for off-road simulation of the quarter car system, has prompted the derivation of the second formulation, see Section 4.2.2. It releases the wheel dynamics from the sprung mass response and the vehicle states in order to allow the user to include other tyre models in the calculation of the vehicle response.

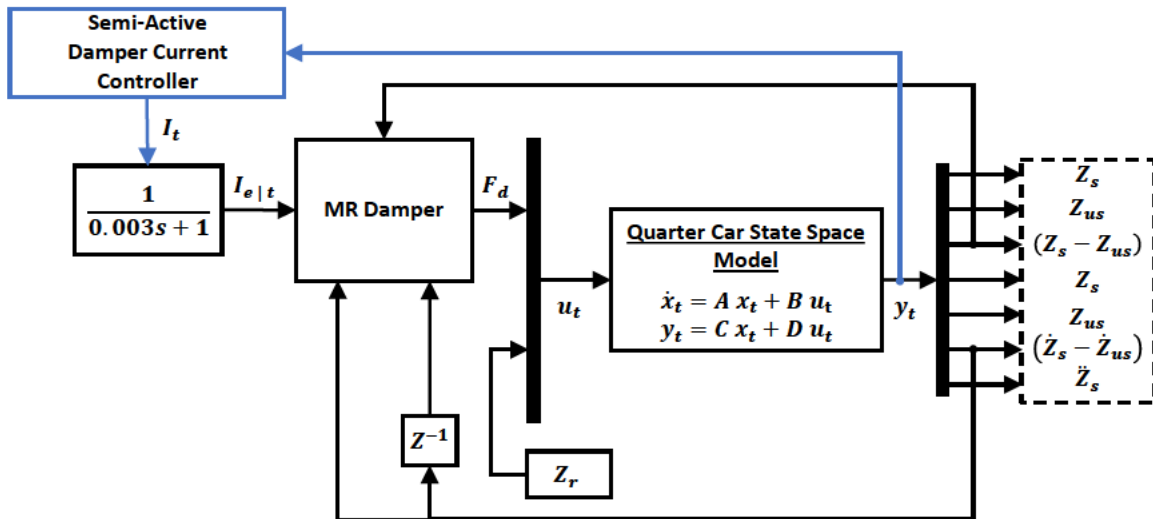


Fig. 4.2 Simulink Connection Diagram for Quarter Car Vehicle Model using Method 1

### 4.2.2 Method 2: Coupled State Space Quarter Car Vehicle Model

The second method for formulating the quarter car vehicle model utilises two state space models, where the motion of each mass is calculated by its own system model. The second method utilises the same equations of motion for the masses as shown by Equations 4.1 and 4.2. However, the state space models for the second method utilise additional matrices to represent the disturbances transferred between each system as seen in Equations 4.6 - 4.9. The state space models are coupled together using Simulink to supply the information from each model as shown in Figure 4.3

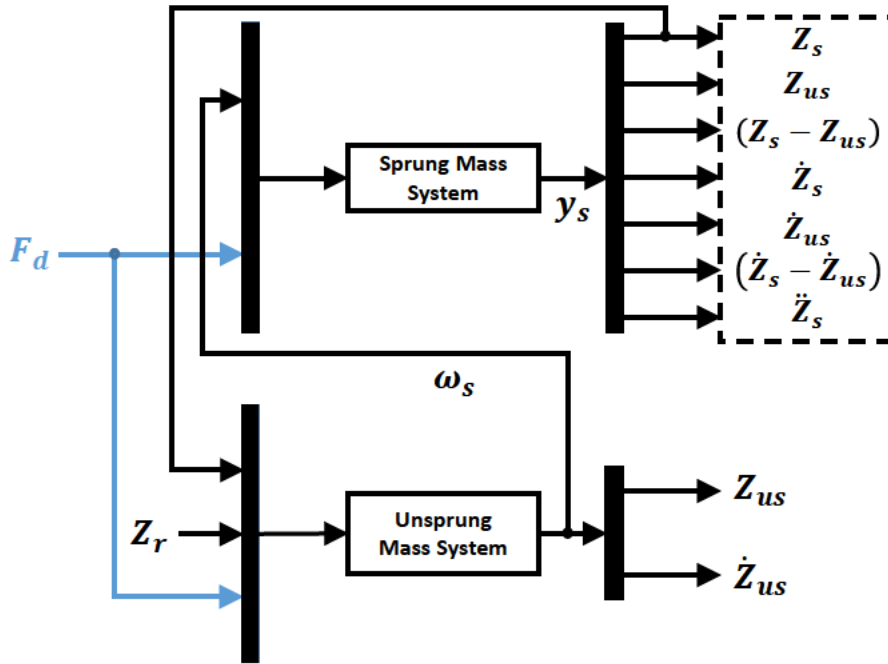


Fig. 4.3 Simulink Connection Diagram for Quarter Car Vehicle Model Using Method 2

Figure 4.3 shows the two distinct systems for sprung and unsprung masses. It highlights the transfer of information between the two systems. Both systems utilise the nonlinear damper force supplied by the MR Damper model. It is connected to the relative displacement and velocity of the suspension, given as an output of the sprung mass system and updated at each time step. The formulation utilises Equations 4.1 and 4.2 from Section 4.2.1 to generate the sprung mass system matrices  $A_s$ ,  $B_s$ ,  $\Gamma_s$ ,  $C_s$ ,  $D_s$ , and  $\Gamma_{s1}$ . These matrices calculate the motion of the sprung mass and use the information provided by the unsprung mass state space model to calculate the future motion of the system. The sprung mass system's state vector  $x_s$  uses two states which consist of the sprung mass displacement ( $Z_s$ ) and the sprung mass velocity ( $\dot{Z}_s$ ). The inputs to the sprung mass system consist of the primary system input ( $u$ ) which is the damping force calculated by the MR Damper model and the disturbance inputs ( $\omega_s$ ), which are the current displacement ( $Z_{us}$ ) and velocity ( $\dot{Z}_{us}$ ) of the unsprung mass. The output vector ( $y_s$ ) for the sprung mass system consists of the same outputs listed for the system described in Section 4.2.1 with the exception of the unsprung mass acceleration ( $\ddot{Z}_{us}$ ).

$$\begin{aligned}
A_s &= \begin{bmatrix} 0 & 1 \\ -\frac{K_c}{m_s} & 0 \end{bmatrix} & B_s &= \begin{bmatrix} 0 \\ -\frac{1}{m_s} \end{bmatrix} & \Gamma_s &= \begin{bmatrix} 0 & 0 \\ \frac{K_c}{m_s} & 0 \end{bmatrix} \\
C_s &= \begin{bmatrix} 1 & 0 \\ 0 & 0 \\ 1 & 0 \\ 0 & 1 \\ 0 & 0 \\ 0 & 1 \\ -\frac{K_c}{m_s} & 0 \end{bmatrix} & D_s &= \begin{bmatrix} 0 \\ 0 \\ 0 \\ 0 \\ 0 \\ 0 \\ -\frac{1}{m_s} \end{bmatrix} & \Gamma_{s1} &= \begin{bmatrix} 0 & 0 \\ 1 & 0 \\ -1 & 0 \\ 0 & 0 \\ 0 & 1 \\ 0 & -1 \\ \frac{K_c}{m_s} & 0 \end{bmatrix}
\end{aligned}$$

$$\dot{x}_{s,t} = A_s x_{s,t} + B_s u_t + \Gamma_s \omega_{s,t} \quad (4.6)$$

$$y_{s,t} = C_s x_{s,t} + D_s u_t + \Gamma_{s1} \omega_{s,t} \quad (4.7)$$

The sprung mass system matrices rearrange the terms for the model so that they correspond to the new locations of the unsprung mass displacement and velocity. This system allows for the calculation of the motion of the sprung mass without the need to balance the forces of the tyre. Therefore, the motion of the sprung mass can be calculated using the wheel displacement and velocity provided by any tyre model. The unsprung mass acceleration was removed from the sprung mass system outputs to remove the need to include the tyre force or tyre spring stiffness ( $K_t$ ) into the formulation of the sprung mass system response. While the unsprung mass acceleration is not included in the sprung mass system formulation, it can be calculated using the unsprung mass system using Equations 4.8 and 4.9.

The unsprung mass system formulation consists of the matrices  $A_u$ ,  $B_u$ ,  $\Gamma_u$ ,  $C_u$ ,  $D_u$ , and  $\Gamma_{u1}$  which are used to determine the motion of the unsprung mass and are derived from Equation 4.2. The unsprung system state vector ( $x_u$ ) is composed of the unsprung mass displacement ( $Z_{us}$ ) and the unsprung mass velocity ( $\dot{Z}_{us}$ ), which are the main outputs of the system determined by the output matrices  $C_u$ ,  $D_u$ , and  $\Gamma_{u1}$ . The optional output of the unsprung mass acceleration ( $\ddot{Z}_{us}$ ) has been included in the definitions for the output matrices beneath the dotted line for reference purposes, which matches the second line of the  $A_u$ ,  $B_u$ , and  $\Gamma_u$  matrices. Similarly to the sprung mass system, the primary system input to the unsprung mass system ( $u$ ) is the damping force produced by the MR Damper model. However, the disturbance inputs given by

$\omega_u$  have been changed to represent the displacement of the sprung mass ( $Z_s$ ) and the terrain height disturbance profile ( $Z_r$ ), instead of the displacement and velocity of the unsprung mass used in the other system.

$$A_u = \begin{bmatrix} 0 & 1 \\ -\frac{(K_c + K_t)}{m_{us}} & 0 \end{bmatrix} \quad B_u = \begin{bmatrix} 0 \\ 1 \\ \frac{1}{m_{us}} \end{bmatrix} \quad \Gamma_u = \begin{bmatrix} 0 & 0 \\ \frac{K_c}{m_{us}} & \frac{K_t}{m_{us}} \end{bmatrix}$$

$$C_u = \begin{bmatrix} 1 & 0 \\ 0 & 1 \\ \dots & \dots \\ -\frac{(K_c + K_t)}{m_{us}} & 0 \end{bmatrix} \quad D_u = \begin{bmatrix} 0 \\ 0 \\ \dots & \dots \\ 1 \\ \frac{1}{m_{us}} \end{bmatrix} \quad \Gamma_{u1} = \begin{bmatrix} 0 & 0 \\ 0 & 0 \\ \dots & \dots \\ \frac{K_c}{m_{us}} & \frac{K_t}{m_{us}} \end{bmatrix}$$

$$\dot{x}_{u,t} = A_u x_{u,t} + B_u u_t + \Gamma_u \omega_{u,t} \quad (4.8)$$

$$y_{u,t} = C_u x_{u,t} + D_u u_t + \Gamma_{u1} \omega_{u,t} \quad (4.9)$$

One of the benefits of splitting the vehicle model into the two systems is that the calculated responses of the systems can be adjusted to accommodate for differences in the tyre model used and allows the user to modify the wheel hub motion to suit the needs of the model. The user is also able to identify the impact of the MR Damper forces on the motion of either of the two masses independently using a step displacement of either the sprung mass or unsprung mass in replacement of the connections shown in Figure 4.3.

### 4.3 Nonlinear Full Car Vehicle Model

This section proposes two nonlinear full car model formulations that utilise some of the methods discussed in Sections 4.2.1 and 4.2.2. The full car models proposed here address the issue of using linear/linearised damper elements in the development of vehicle models which typically remove the presence of hysteresis and simplify the model. The key disadvantage of removing this hysteresis from the vehicle model is that the model introduces inaccuracies between simulated results using the model and real-world test data from a vehicle. Chapter 2 briefly mentioned that there have been several studies (Canale et al. 2006; Gohrle et al. 2013; Krauze 2013) that utilise a variable control force similar to that seen in Figure 4.4 to represent the instantaneous force generated by the semi-active or active suspension system actuators. MR Dampers and the models from Chapter 3 are calculating the response of the damper to changes

in the displacement, velocity and current supplied at each time step. This makes this particular method of integration suited for use with the MR Damper models.

Table 4.2 Full Car Ride Model Parameters based on the ASM Vehicle Model (dSPACE GmbH 2020)

This item has been removed due to 3rd Party Copyright. The unabridged version of the thesis can be found in the Lanchester Library, Coventry University.

Two separate methods of formulating the nonlinear full car models are proposed based on (Gohrle et al. 2014). The first method uses a single state space system model to represent the entirety of the vehicle and expands on the methodology in (Gohrle et al. 2014). It gives a vehicle model capable of integrating well with the nonlinear MR Damper models proposed in Chapter 3. The model is proposed to simulate the vehicle dynamics of a full car model that simulates the vertical and angular motion of the vehicle body in addition to the vertical motion of each wheel mass. Method two uses two state space models to represent the vertical and angular motion of the body mass and the vertical motion of the wheel masses. These separate systems are linked together using Simulink, with the full car version of the process described in Section 4.2.2. This separation of the two masses allows for the controller from Chapter 7 to be designed for the motion of the body mass with limited reliance on the motion of the wheel masses.

### 4.3.1 Method 1: Single State Space Full Car Vehicle Model

The full car vehicle model proposed as part of method one is a single state space continuous time-invariant model which represents the motion of the vehicle body and wheel masses. The system calculates the values of the vertical 'heave' acceleration ( $\ddot{Z}_b$ ) in addition to the angular

accelerations in the pitch ( $\ddot{\phi}$ ) and roll ( $\ddot{\theta}$ ) directions for the vehicle body mass, which are calculated about the vehicle body's centre of mass as shown in Figure 4.4. The motion of each of the four wheel masses are also calculated based on their vertical acceleration. However, the longitudinal and lateral motion of the wheel masses remain excluded from the list of calculated variables. The motion of the vehicle body mass is calculated with respect to the forces generated by the wheels at each corner of the vehicle with positive forces resulting in the rise of the vehicle's respective corner. The angular motion of the vehicle body is linked to the the angular inertia for pitch and roll are given by the variables  $J_\phi$  and  $J_\theta$  respectively.

For the full car vehicle models the vehicle body is referred to by the variable  $M_b$  instead of the sprung mass that was used for the quarter car vehicle model from Section 4.2.1. This new naming convention helps to distinguish between the variables associated with the full and quarter car models. Another change to the naming convention, specific to full car vehicle models, is that the wheel masses are now referred to by variable  $M_{w,ii}$ .  $ii$  denotes the corner of the vehicle the mass is associated with, which is substituted with front-left ( $fl$ ), front-right ( $fr$ ), rear-left ( $rl$ ) or rear-right ( $rr$ ) respectively. The use of underbar in the following equations is used to refer to variables that are associated with each corner of the vehicle. The values are typically represented by either a four by four diagonal matrix or a four by one vector where the values for each corner follow in the order  $fl$ ,  $fr$ ,  $rl$  and  $rr$ . An example of this is the mass matrix  $\Theta_w$  which is used in Equation 4.14 as a diagonal matrix where  $\Theta_w = \text{diag}([M_{w,fl}; M_{w,fr}; M_{w,rl}; M_{w,rr}])$ .

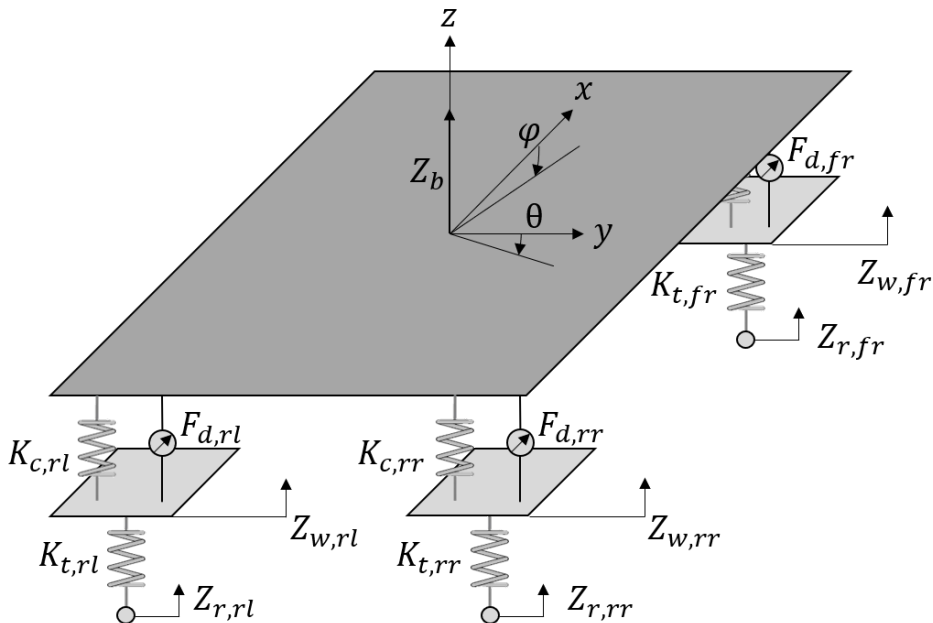


Fig. 4.4 Full Car Vehicle Model Diagram

Equations 4.10 to 4.16 are recreated here from (Gohrle et al. 2014) and provide the fundamental baseline to formulate the nonlinear full car vehicle models described here and in Section 4.3.2. It is important that the assumptions about the product of inertia ( $J_{\phi\theta}$ ) from (Gohrle et al. 2014) are mirrored here to ensure that the model correctly assumes that this can be neglected in the subsequent calculations. Equation 4.10 begins to describe the accelerations of the vehicle body mass with respect to the wheel forces and moments about the vehicle body centre of mass.

The diagonal matrix, consisting of the vehicle body mass ( $M_b$ ) and the angular inertias ( $J_\phi$  &  $J_\theta$ ), is represented by the variable  $\Theta_b$  in subsequent calculations; including in Equation 4.13 and when the inverse matrix ( $\Theta_b^{-1}$ ) is used in the subsequent state space model seen in Equations 4.23 and 4.24. The value of  $T_G$  (Equation 4.11) is used for the coordinate transformation of the forces along the appropriate directions, as indicated in Figure 4.4. The values for  $l_f$  and  $l_r$  represent the distance between the front/rear axle and the vehicle body centre of mass with  $l_{fl}$ ,  $l_{fr}$ ,  $l_{rl}$  and  $l_{rr}$  representing the half track width distances between the centre line and each of the wheel centres.

$$\begin{pmatrix} M_b & 0 & 0 \\ 0 & J_\phi & 0 \\ 0 & 0 & J_\theta \end{pmatrix} \begin{pmatrix} \ddot{Z}_b \\ \ddot{\phi} \\ \ddot{\theta} \end{pmatrix} = -T_G \cdot \begin{bmatrix} F_{w,fl} \\ F_{w,fr} \\ F_{w,rl} \\ F_{w,rr} \end{bmatrix} \quad (4.10)$$

$$T_G = \begin{pmatrix} 1 & 1 & 1 & 1 \\ -l_f & -l_f & l_r & l_r \\ l_{fl} & -l_{fr} & l_{rl} & -l_{rr} \end{pmatrix} \quad (4.11)$$

The matrices  $H_c$  and  $H_d$  used in Equation 4.12 and later calculations refer to the ratios between the spring and damper forces and their influence on the wheel forces given by the vector of wheel forces  $\underline{F}_w$  (seen in Equation 4.10) which consists of the wheel forces at each corner of the vehicle.  $H_c$  and  $H_d$  can be calculated using physical suspension deflection tests. However, values used in the simulations from Chapter 8 typically assume the ratios are four-by-four diagonal matrices with 0.65 along the primary diagonal for both  $H_c$  and  $H_d$ . The relationship created by the aforementioned values produce a similar response to the Automotive Simulation Model shown in Section 4.4.2. This approach assumes that the spring and damper are mounted in parallel with the pre-load of the spring ignored as the vehicle is assumed to start at equilibrium, except when specifically stated.

$$\underline{F}_w = H_c \cdot \underline{F}_c + H_d \cdot \underline{F}_d \quad (4.12)$$

When substituting Equations 4.11 and 4.12 into Equation 4.10 the equation of motion for the vehicle body mass can be obtained as seen in Equation 4.13.  $T_c = T_G H_c$  and  $T_d = T_G H_d$  are used to define the relative displacement of the suspension springs ( $\underline{Z}_{rel,c}$ ) seen in Equation 4.15 and the relative velocity of the dampers  $\dot{\underline{Z}}_{rel,d}$  (Equation 4.16). However, unlike in (Gohrle et al. 2014) the relative displacement and velocity of the damper are not used as part of the equations of motion for either the body mass or the wheel masses (Equation 4.14) and instead are replaced by the calculated damper force provided by one of the nonlinear MR Damper models described in Chapter 3.

$$\Theta_b \begin{pmatrix} \ddot{\underline{Z}}_b \\ \ddot{\phi} \\ \ddot{\theta} \end{pmatrix} = T_d \underline{F}_d + T_c \underline{K}_c \left( T_c^T \begin{pmatrix} \underline{Z}_b \\ \phi \\ \theta \end{pmatrix} - H_c \underline{Z}_w \right) \quad (4.13)$$

The equation of motion for the wheel masses shown in Equation 4.14, calculates the wheel hub accelerations  $\ddot{\underline{Z}}_w$  for each corner of the vehicle. Since there is no need for the coordinate transformations which were used in the body mass acceleration calculations from Equation 4.13, the matrix  $T_G$  is not required in the wheel mass motion calculations. The variable  $\Theta_w$  represents a diagonal matrix which has the mass of each wheel on the primary diagonal and zeros in all other positions forming a four by four matrix. The variable  $\underline{K}_t$  is a diagonal matrix of the spring stiffness constants for each tyre populating the primary diagonal.

$$\Theta_w \ddot{\underline{Z}}_w = -\underline{K}_t (\underline{Z}_w - \underline{Z}_r) + H_c \underline{K}_c \left( T_c^T \begin{pmatrix} \underline{Z}_b \\ \phi \\ \theta \end{pmatrix} - H_c \underline{Z}_w \right) + H_d \underline{F}_d \quad (4.14)$$

The road/terrain height vector  $\underline{Z}_r$ , corresponding to the height disturbance at each corner, is used to calculate the tyre response to the loads on the tyres. Similarly, each corner of the vehicle has its own calculated damper force which form the vector  $\underline{F}_d$ . These forces influence the motion of both the vehicle body mass and the wheel hub mass of its corresponding corner. The damper force is calculated by the nonlinear MR Damper model, chosen to represent the behaviour of the damper, in relation to the relative displacement of the damper at each corner ( $\underline{Z}_{rel,d}$ ) and the relative velocity of the damper piston ( $\dot{\underline{Z}}_{rel,d}$ ). Note that while the damper and suspension spring are mounted in parallel for the subsequent simulations the values of the ratios for  $H_d$  and  $H_c$  will result in differences between the values of the relative displacement of the spring and damper.

$$\underline{Z}_{rel,c} = T_c^T \begin{bmatrix} Z_b \\ \phi \\ \theta \end{bmatrix} - H_c \underline{Z}_w \quad (4.15)$$

$$\underline{Z}_{rel,d} = T_d^T \begin{bmatrix} Z_b \\ \phi \\ \theta \end{bmatrix} - H_d \underline{Z}_w \quad (4.16)$$

$$\dot{\underline{Z}}_{rel,d} = T_d^T \begin{bmatrix} \dot{Z}_b \\ \dot{\phi} \\ \dot{\theta} \end{bmatrix} - H_d \dot{\underline{Z}}_w \quad (4.17)$$

The model begins to diverge from that presented in (Gohrle et al. 2014) with the use of the system states represented by the state vector  $x_t$  shown in Equation 4.18 and the nonlinear damper force used instead of the actuator input described in (Gohrle et al. 2014). The proposed model consists of 14 states with eight system inputs given by the input vector  $u_t$ . The system inputs for this model formulation are the four damping forces at each of the corners given by the damping force vector  $\underline{F}_d$  of the vehicle. These forces are calculated using the previous time step's damper displacement and velocity and the road/terrain heights for each corner of the vehicle for the current time step given by the height profile vector  $\underline{Z}_r$ . The model introduces the sub-matrix variables  $A^*$ ,  $B^*$ ,  $H^*$  and  $T^*$  that are calculated using Equations 4.19 to 4.22 and used to construct the matrices  $A$  and  $B$  which update the system state derivatives ( $\dot{x}_t$ ) at each time step as seen in Equation 4.23.

$$x_t = \left[ Z_b \quad \phi \quad \theta \quad \dot{Z}_b \quad \dot{\phi} \quad \dot{\theta} \quad Z_{w,fl} \quad Z_{w,fr} \quad Z_{w,rl} \quad Z_{w,rr} \quad \dot{Z}_{w,fl} \quad \dot{Z}_{w,fr} \quad \dot{Z}_{w,rl} \quad \dot{Z}_{w,rr} \right]^T \quad (4.18)$$

$$A^* = T_c \underline{K}_c T_c^T \quad (4.19)$$

$$B^* = T_c \underline{K}_c H_c \quad (4.20)$$

$$H^* = H_c \underline{K}_c T_c^T \quad (4.21)$$

$$T^* = H_c \underline{K}_c H_c \quad (4.22)$$

$$A = \begin{bmatrix} \mathbf{0}_{3 \times 3} & \mathbf{I}_{3 \times 3} & \mathbf{0}_{3 \times 4} & \mathbf{0}_{3 \times 4} \\ -\Theta_b^{-1} A^* & \mathbf{0}_{3 \times 3} & \Theta_b^{-1} B^* & \mathbf{0}_{3 \times 4} \\ \mathbf{0}_{4 \times 3} & \mathbf{0}_{4 \times 3} & \mathbf{0}_{4 \times 4} & \mathbf{I}_{4 \times 4} \\ \Theta_w^{-1} H^* & \mathbf{0}_{4 \times 3} & -\Theta_w^{-1} [T^* + \underline{K}_t] & \mathbf{0}_{4 \times 4} \end{bmatrix} \quad B = \begin{bmatrix} \mathbf{0}_{3 \times 4} & \mathbf{0}_{3 \times 4} \\ -\Theta_b^{-1} T_d & \mathbf{0}_{3 \times 4} \\ \mathbf{0}_{4 \times 4} & \mathbf{0}_{4 \times 4} \\ \Theta_w^{-1} H_d & \Theta_w^{-1} \underline{K}_t \end{bmatrix}$$

$$C = \begin{bmatrix} \mathbf{I}_{3 \times 3} & \mathbf{0}_{3 \times 3} & \mathbf{0}_{3 \times 4} & \mathbf{0}_{3 \times 4} \\ \mathbf{0}_{3 \times 3} & \mathbf{I}_{3 \times 3} & \mathbf{0}_{3 \times 4} & \mathbf{0}_{3 \times 4} \\ -\Theta_b^{-1} A^* & \mathbf{0}_{3 \times 3} & \Theta_b^{-1} B^* & \mathbf{0}_{3 \times 4} \\ \mathbf{0}_{4 \times 3} & \mathbf{0}_{4 \times 3} & \mathbf{I}_{4 \times 4} & \mathbf{0}_{4 \times 4} \\ \mathbf{0}_{4 \times 3} & \mathbf{0}_{4 \times 3} & \mathbf{0}_{4 \times 4} & \mathbf{I}_{4 \times 4} \\ \Theta_w^{-1} H^* & \mathbf{0}_{4 \times 3} & -\Theta_w^{-1} [T^* + \underline{K}_t] & \mathbf{0}_{4 \times 4} \\ T_d^T & \mathbf{0}_{4 \times 3} & -H_d & \mathbf{0}_{4 \times 4} \\ \mathbf{0}_{4 \times 3} & T_d^T & \mathbf{0}_{4 \times 4} & -H_d \end{bmatrix} \quad D = \begin{bmatrix} \mathbf{0}_{3 \times 4} & \mathbf{0}_{3 \times 4} \\ \mathbf{0}_{3 \times 4} & \mathbf{0}_{3 \times 4} \\ -\Theta_b^{-1} T_d & \mathbf{0}_{3 \times 4} \\ \mathbf{0}_{4 \times 4} & \mathbf{0}_{4 \times 4} \\ \mathbf{0}_{4 \times 4} & \mathbf{0}_{4 \times 4} \\ \Theta_w^{-1} H_d & \Theta_w^{-1} \underline{K}_t \\ \mathbf{0}_{4 \times 4} & \mathbf{0}_{4 \times 4} \\ \mathbf{0}_{4 \times 4} & \mathbf{0}_{4 \times 4} \end{bmatrix}$$

$$\dot{x}_t = A x_t + B u_t \quad (4.23)$$

$$y_t = C x_t + D u_t \quad (4.24)$$

The sub-matrices are also used to construct the output matrices  $C$  and  $D$  which provide the output vector  $y$  seen in Equations 4.24 and 4.25. The system outputs given by the output matrices result in the output vector shown in Equation 4.25. Among the outputs are the relative displacement and relative velocity of the dampers at each corner of the vehicle. These outputs are required to calculate the damping forces used at the next time step. They are given to the chosen MR Damper model in addition to the electrical current supplied by the controller to each corner of the vehicle. Equation 4.25 shows that the output vector includes the vertical accelerations of the wheel hubs ( $\ddot{Z}_w$ ). It provides information about the changing motion of the wheel and can be used in conjunction with the wheel hub displacement to identify the occurrence of wheel hop during the simulations, see Chapter 8.

$$\begin{aligned}
y_t = & [Z_b, \phi, \theta, \dot{Z}_b, \dot{\phi}, \dot{\theta}, \ddot{Z}_b, \ddot{\phi}, \ddot{\theta}, \dots \\
& Z_{w,fl}, Z_{w,fr}, Z_{w,rl}, Z_{w,rr}, \dot{Z}_{w,fl}, \dot{Z}_{w,fr}, \dot{Z}_{w,rl}, \dot{Z}_{w,rr}, \dots \\
& \ddot{Z}_{w,fl}, \ddot{Z}_{w,fr}, \ddot{Z}_{w,rl}, \ddot{Z}_{w,rr}, Z_{rel,d:fl}, Z_{rel,d:fr}, Z_{rel,d:rl}, Z_{rel,d:rr}, \dots \\
& \dot{Z}_{rel,d:fl}, \dot{Z}_{rel,d:fr}, \dot{Z}_{rel,d:rl}, \dot{Z}_{rel,d:rr}]^T
\end{aligned} \tag{4.25}$$

Figure 4.5 shows the Simulink connections between the state space system and the MR Damper models from Chapter 3. It can be observed that the full car model feeds back the relative displacement and velocity of the MR Damper to the Nonlinear Damper model to calculate the next time step's damping forces for each corner of the vehicle. In addition, the current supplied to the MR Damper model is fed via the transfer function, see 3.4, to represent the time delay of the damper responding to a change in the current supplied by one of the controllers from Chapters 6 and 7.

### 4.3.2 Method 2: Coupled State Space Full Car Vehicle Model

The Coupled State Space Full Car Vehicle Model utilises two state space models to calculate the motion of the vehicle body separately from the wheel masses using a similar process to the one used for the quarter car model in Section 4.3.2. The method utilises Equations 4.10 to 4.16 from Section 4.3.1 to begin the new formulation of the state space models. Equation 4.26 defines the values of the vehicle states for the vehicle body system. It can be noted that the wheel displacements and velocities have been moved from the vehicle body states ( $x_s$ ) and are instead included in the disturbance inputs to the system ( $\omega_s$ ).

$$x_b = [Z_b, \phi, \theta, \dot{Z}_b, \dot{\phi}, \dot{\theta}]^T \tag{4.26}$$

The vehicle body state space system shown in Equations 4.27 and 4.28 is constructed using the system matrices  $A_s$ ,  $B_s$  and  $\Gamma_s$  which correspond to the update function used to calculate the vehicle body system state derivatives  $\dot{x}_s$ . Similar to the full car model from Section 4.3.1 the sub-matrices  $A^*$ ,  $B^*$ ,  $H^*$  and  $T^*$  are used to construct the system matrices and output matrices used in the nonlinear coupled state space full car model.

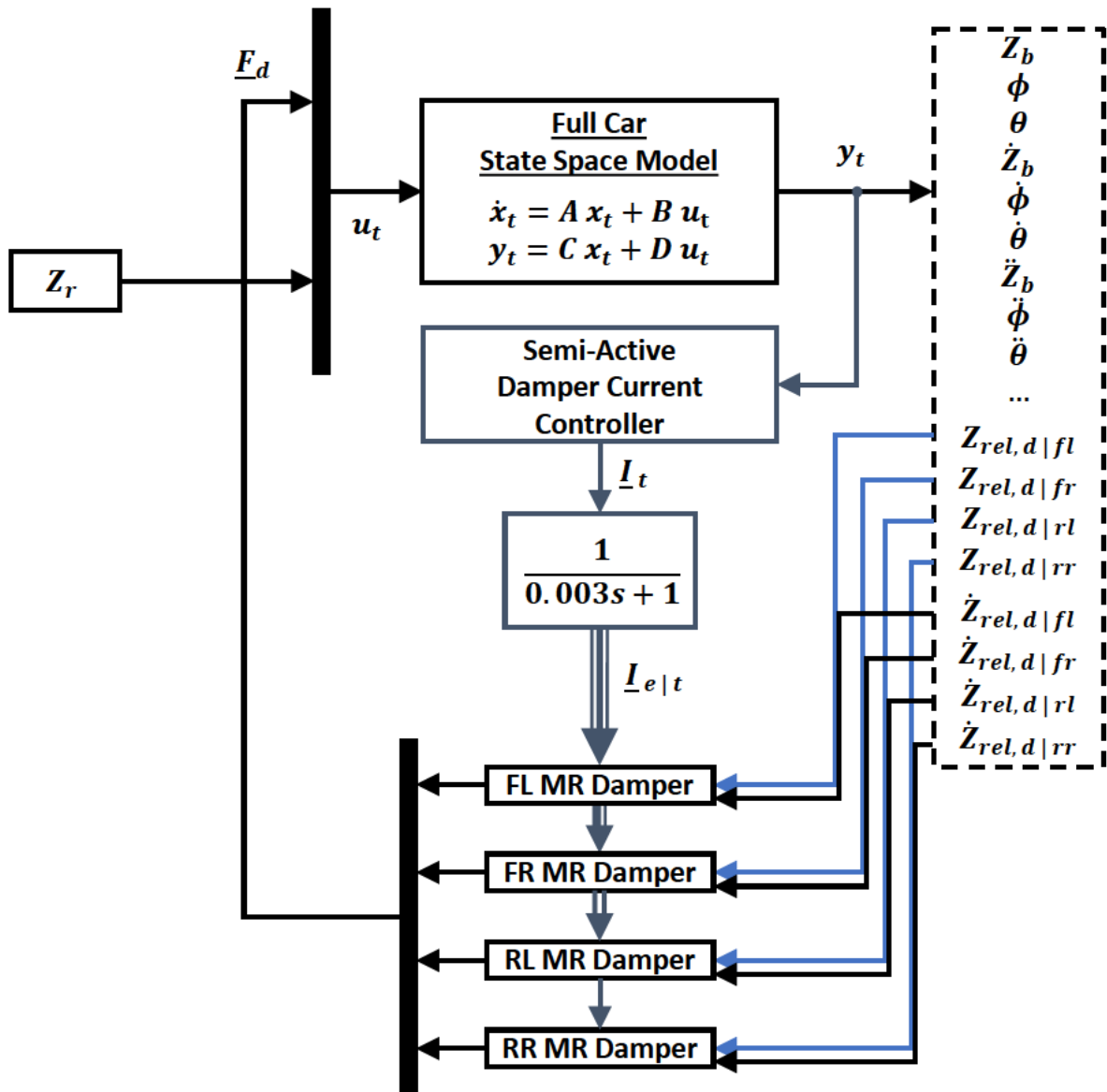


Fig. 4.5 Simulink Connection Diagram of the Full Car Model from Method 1

The separation of the wheel mass motion into its own disturbance matrix allows for the user to supply any data to represent the displacement, and velocity of the wheel masses. The wheel inputs should be function of the damping forces, the latter being variable as in this work or constant.

$$\begin{aligned}
A_b &= \begin{bmatrix} \mathbf{0}_{3 \times 3} & \mathbf{I}_{3 \times 3} \\ -\Theta_b^{-1} A^* & \mathbf{0}_{3 \times 3} \end{bmatrix} & B_b &= \begin{bmatrix} \mathbf{0}_{3 \times 4} \\ -\Theta_b^{-1} T_d \end{bmatrix} & \Gamma_b &= \begin{bmatrix} \mathbf{0}_{3 \times 4} & \mathbf{0}_{3 \times 4} \\ \Theta_b^{-1} B^* & \mathbf{0}_{3 \times 4} \end{bmatrix} \\
C_b &= \begin{bmatrix} \mathbf{I}_{3 \times 3} & \mathbf{0}_{3 \times 3} \\ \mathbf{0}_{3 \times 3} & \mathbf{I}_{3 \times 3} \\ -\Theta_b^{-1} A^* & \mathbf{0}_{3 \times 3} \\ \mathbf{0}_{4 \times 3} & \mathbf{0}_{4 \times 3} \\ \mathbf{0}_{4 \times 3} & \mathbf{0}_{4 \times 3} \\ T_d^T & \mathbf{0}_{4 \times 3} \\ \mathbf{0}_{4 \times 3} & T_d^T \end{bmatrix} & D_b &= \begin{bmatrix} \mathbf{0}_{3 \times 4} \\ \mathbf{0}_{3 \times 4} \\ -\Theta_b^{-1} T_d \\ \mathbf{0}_{4 \times 4} \\ \mathbf{0}_{4 \times 4} \\ \mathbf{0}_{4 \times 4} \\ \mathbf{0}_{4 \times 4} \end{bmatrix} & \Gamma_{b1} &= \begin{bmatrix} \mathbf{0}_{3 \times 4} & \mathbf{0}_{3 \times 4} \\ \mathbf{0}_{3 \times 4} & \mathbf{0}_{3 \times 4} \\ \Theta_b^{-1} B^* & \mathbf{0}_{3 \times 4} \\ \mathbf{I}_{4 \times 4} & \mathbf{0}_{4 \times 4} \\ \mathbf{0}_{4 \times 4} & \mathbf{I}_{4 \times 4} \\ -H_d & \mathbf{0}_{4 \times 4} \\ \mathbf{0}_{4 \times 4} & -H_d \end{bmatrix}
\end{aligned}$$

$$\dot{x}_{b,t} = A_b x_{b,t} + B_b u_t + \Gamma_b \omega_{b,t} \quad (4.27)$$

$$y_{b,t} = C_b x_{b,t} + D_b u_t + \Gamma_{b1} \omega_{b,t} \quad (4.28)$$

The output vector given in Equation 4.29 includes the values of the wheel mass displacements and velocities which are fed through the system rather than calculated internally. The calculations, that were present in the system described in Section 4.3.1, included in the output the calculation of the wheel mass vertical accelerations. However, for this particular model these calculations are now performed in the wheel mass system which is described in Equations 4.30 and 4.31 as it removes any additional components associated with the tyre, including the road/terrain height disturbances.

$$\begin{aligned}
y_b &= [Z_b, \phi, \theta, \dot{Z}_b, \dot{\phi}, \dot{\theta}, \ddot{Z}_b, \ddot{\phi}, \ddot{\theta}, \dots \\
&\quad Z_{w,fl}, Z_{w,fr}, Z_{w,rl}, Z_{w,rr}, \dot{Z}_{w,fl}, \dot{Z}_{w,fr}, \dot{Z}_{w,rl}, \dot{Z}_{w,rr}, \dots \\
&\quad Z_{rel,d:fl}, Z_{rel,d:fr}, Z_{rel,d:rl}, Z_{rel,d:rr}, \dots \\
&\quad \dot{Z}_{rel,d:fl}, \dot{Z}_{rel,d:fr}, \dot{Z}_{rel,d:rl}, \dot{Z}_{rel,d:rr}]^T
\end{aligned} \quad (4.29)$$

The wheel mass system described by Equations 4.30 and 4.31 calculates the response of each wheel as a result of the road/terrain disturbances and the effective change in the suspension

forces. the latter is a function of the angular and vertical motion of the vehicle body, which is connected to the vehicle body system described by State Space Equations 4.27 and 4.28.

$$A_w = \begin{bmatrix} \mathbf{0}_{4 \times 4} & \mathbf{I}_{4 \times 4} \\ -\Theta_w^{-1} [T^* + \underline{K}_t] & \mathbf{0}_{4 \times 4} \end{bmatrix} \quad B_w = \begin{bmatrix} \mathbf{0}_{4 \times 4} \\ \Theta_w^{-1} H_d \end{bmatrix} \quad \Gamma_w = \begin{bmatrix} \mathbf{0}_{4 \times 3} & \mathbf{0}_{4 \times 4} \\ \Theta_w^{-1} H^* & \Theta_w^{-1} \underline{K}_t \end{bmatrix}$$

$$\dot{x}_{w,t} = A_w x_{w,t} + B_w u_t + \Gamma_w \omega_{w,t} \quad (4.30)$$

$$y_{w,t} = C_w x_{w,t} + D_w u_t + \Gamma_{w1} \omega_{w,t} \quad (4.31)$$

The Simulink connection diagram, see Figure 4.6, shows how the interlinked systems share information and are coupled together to provide a full vehicle model that calculates the response of both the wheel masses and the vehicle body. The systems are connected through the use of the disturbance inputs  $\omega_{s,t}$  and  $\omega_{u,t}$ . The two disturbance inputs are introduced as separate input vectors as they represent the individual disturbances of each system. For the vehicle body system the disturbance inputs ( $\omega_{s,t}$ ) are the wheel mass displacements ( $\underline{Z}_w$ ) and velocities ( $\dot{\underline{Z}}_w$ ). The wheel mass system is influenced by the motion of the vehicle body, characterised by the vertical and angular displacements ( $[Z_b, \phi, \theta]^T$ ) which are used in the calculation of relative displacement of the suspension spring. The final four disturbance inputs, that make up the wheel system disturbance input vector ( $\omega_{u,t}$ ), are the road/terrain displacement values ( $\underline{Z}_r$ ) for each corner of the vehicle.

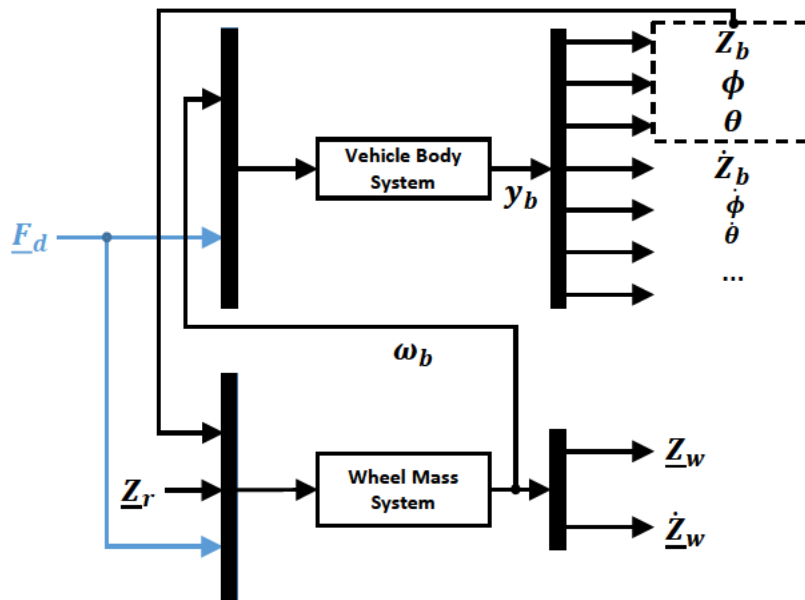


Fig. 4.6 Simulink Connection Diagram for Full Car Coupled State Space System

## 4.4 Modified Automotive Simulation Model (ASM) for Vehicle Dynamics Analysis

The Automotive Simulation Models (ASM) provided by dSPACE ([dSPACE GmbH 2020](#)) are a collection of Simulink libraries and models that are designed around the company's proprietary software to interface with real-time hardware such as the SCALEXIO real-time processing unit. The models include a 24 degrees of freedom vehicle dynamics model as explained in ([dSPACE GmbH 2020](#)). The degrees of freedom can be divided into the relevant aspects of the model with 13 associated with the drivetrain, three associated with the steering, six relating to the vehicle body motion and four associated with the vertical motion of the independent wheel masses.

A real-time capable model was chosen to closely resemble the behaviour of a real vehicle in the absence of physical testing. The real-time capabilities of the model highlight potential issues that could be present when implementing the controllers from Chapter 7 in real world testing. In addition, the real-time vehicle model could be used to reduce the computational resources of the simulation of the vehicle, freeing up more resources for the nonlinear controller.

The ASM Vehicle Dynamics model is split into 5 main subsections labelled as the Soft ECU (Electronic Control Unit), Engine, Drivetrain, Vehicle Dynamics and Environment, as seen in Figure 4.7.

**Soft ECU subsystem** Enables the user to perform software based control of the engine and drivetrain mimicking the behaviour of a real ECU when simulations are run offline. Additional elements may be added by the user when using other variants of the ASM vehicle models, such as the torque demand and modes used by Hybrid electric vehicles to monitor and control the charge of the battery including systems that use regenerative braking. The subsystem can be customised to meet the users needs, however for the purposes of this study the Soft ECU was left unchanged with the ECU communications with a delay of zero which is due to the control system

**Engine subsystem** This calculates the torque of the engine based on a lookup table representation model. This can be changed for other model types using the gasoline and diesel blockset libraries or replaced with electric motors for Hybrid or Full Electric Vehicle Modelling. The aspects of the engine subsystem result in a number of differences when compared to the quarter car and full car vehicle ride models from Sections 4.2 and 4.3. Firstly, since the engine lookup tables utilise nonlinear values the motion of the vehicle along the road/terrain is also nonlinear as the propulsion from the engine directly affects the drivetrain and thus the wheel and tyre

forces. In addition, the powertrain is not 100 percent efficient and therefore not all of the torque gets to the wheels. Finally, since the engine is not modelled in either the quarter car or full car vehicle ride models the vehicle can be simulated to have a constant velocity without any regard of the loss in velocity that a typical vehicle would encounter if making contact with an obstacle or moving up a slope.

This item has been removed due to 3rd Party Copyright. The unabridged version of the thesis can be found in the Lanchester Library, Coventry University.

Fig. 4.7 A Diagram Showing the Main Structure of the ASM Vehicle Dynamics Model ([dSPACE GmbH 2020](#))

**Drivetrain subsystem** Models the transfer of torque from the engine to the wheels and is capable of modelling Front Wheel Drive (FWD), Rear Wheel Drive (RWD) and All/Four Wheel Drive (AWD/4WD) drivetrains. The standard ASM model typically uses a rigid drivetrain

modelled using elastic elements while other variations are included with the software that allow for flexible drivetrains which dSPACE claims has 13 degrees of freedom (dSPACE GmbH 2020).

**Environment subsystem** Models the road and manoeuvre for the simulation which can be modified using the ModelDesk Software. The behaviour of the driver for both speed, longitudinal and lateral directions is modelled using a PI (Proportional-Integral) Controller which can be tuned to user specific gains for improved handling and control.

**Vehicle Dynamics subsystem** Describes the motion of the vehicle body and wheels with respect to the angular and linear forces present on the various masses and mass moments of inertia that compose the vehicle. The generalised mass matrix  $M$  is calculated at each time step to determine the motions of the vehicle modelled by the vehicle dynamics subsystem, which has 10 degrees of freedom. The motion of the masses and the vector of the generalised forces ( $Q$ ) acting on them are calculated at each timestep using Equations 4.32 and 4.33.

$$M \ddot{q} = Q \quad (4.32)$$

In addition to the vertical accelerations of the wheel masses, the accelerations of the vehicle in the x, y and z directions of the Vehicle Coordinate system are also considered ( $\dot{V}_x$ ,  $\dot{V}_y$  and  $\dot{V}_z$  respectively). Similarly the angular acceleration about each of these axes ( $\dot{\omega}_x$ ,  $\dot{\omega}_y$  and  $\dot{\omega}_z$ ) are used to populate the generalised motion vector  $\dot{q}$  (Equation 4.33). The longitudinal and lateral motions of the vehicle ( $\dot{V}_x$  and  $\dot{V}_y$ ) are not considered essential in the analysis of the suspension performance as part of this study, except in relation to the time delay between the start of the simulation and the onset of the bump. This can be also considered true when evaluating the rotational 'yawing' motion about the z axis of the vehicle ( $\dot{\omega}_z$ ).

The vertical acceleration in relation to the z axis ( $\dot{V}_z$ ) however, is identical to vertical 'heave' acceleration of the vehicle body ( $\ddot{Z}_b$ ) used in the previous formulations of the nonlinear full car model. Similarly, the angular rotations about the x and y axes ( $\dot{\omega}_x$  and  $\dot{\omega}_y$ ) are linked to the roll ( $\dot{\theta}$ ) and pitching ( $\dot{\phi}$ ) motion of the vehicle body.

$$\ddot{q} = \begin{bmatrix} \ddot{q}_1 \\ \ddot{q}_2 \\ \ddot{q}_3 \\ \ddot{q}_4 \\ \ddot{q}_5 \\ \ddot{q}_6 \\ \ddot{q}_7 \\ \ddot{q}_8 \\ \ddot{q}_9 \\ \ddot{q}_{10} \end{bmatrix} = \begin{bmatrix} \dot{V}_x \\ \dot{V}_y \\ \dot{V}_z \\ \dot{\omega}_x \\ \dot{\omega}_y \\ \dot{\omega}_z \\ \ddot{Z}_{w,fl} \\ \ddot{Z}_{w,fr} \\ \ddot{Z}_{w,rl} \\ \ddot{Z}_{w,rr} \end{bmatrix} \quad (4.33)$$

Figure 4.8 shows a simplified diagram of the high level elements used to calculate the vehicle motion which is linked with the drivetrain subsystem by the angular velocity of the four wheels ( $\Omega_{wi}$ ). The key elements for consideration in this study are the tyre model, the suspension kinematics, the suspension forces and the vehicle motion.

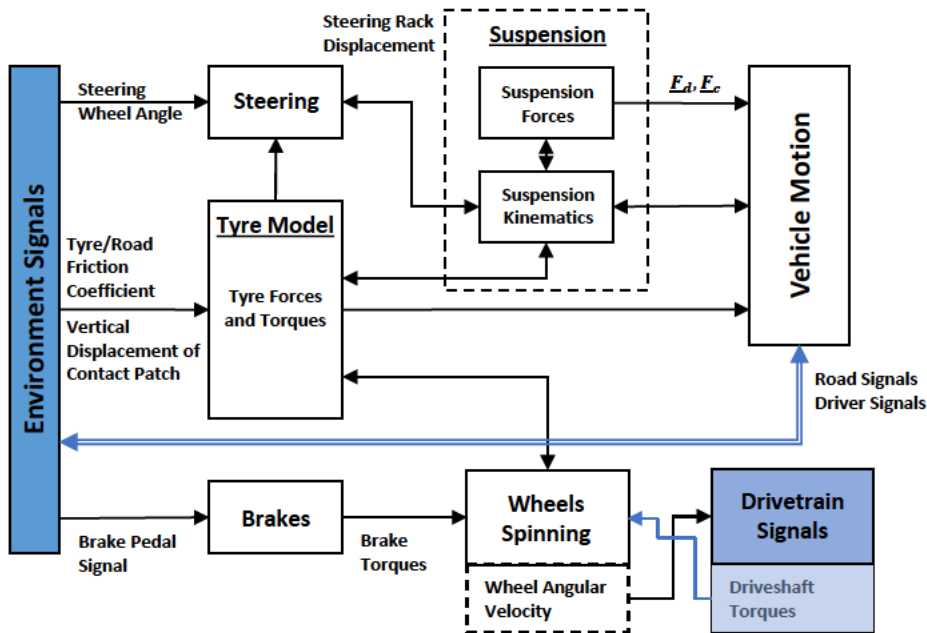


Fig. 4.8 A Simplified Diagram Showing the High Level Elements that form the Vehicle Dynamics Subsystem

Several modifications to the Vehicle Dynamics subsystem of the ASM Vehicle Model are needed to integrate the MR Damper models from Chapter 3 into the full car vehicle dynamics model. The response of the model is compared with that of the response of the standard ASM

Vehicle Dynamics model which uses the pre-programmed parameters included as part of the software package.

#### 4.4.1 Modifications to the ASM Vehicle Dynamics Model

The ASM Vehicle Dynamics model is one of the models available as part of the Automotive Simulation Models software package. This study utilises the 2016A release of the ASM vehicle dynamics model which is assumed to represent the digital clone of a mid-sized vehicle with its parameters derived from a real vehicle as stated in (Peperhowe and Schindler 2013). Additional limitations resulting from utilising the 2016A release also arise with the models limited to use with MATLAB 2015b. This results in some features not being supported by the ASM and MATLAB software which are available in later releases. The models rely on numerous feedback signals between the interconnected blocks of the ASM Simulink libraries which can pose additional challenges when modifying the models for the user's particular needs.

The standard ASM models typically uses a Simulink S-functions to determine the forces produced by the damper as part of the suspension system. This block can be parameterised by the ModelDesk software (also available in dSPACE) or replaced with an alternative block to convert the damper into an active damper. The limitation of the supplied block is that while the parameterised forces can be manipulated to reflect the forces of a particular damper, there is currently no method to include the hysteresis in the parameterisation process as the force values supplied through ModelDesk must be strictly monotonically increasing with respect to the damper piston velocity. The supplied block also cannot be guaranteed to include suitable parameterisation unlike the MR Damper models from Chapter 3, as the block is not a standard feature of the ASM Vehicle Dynamics model.

The first modification to the ASM Vehicle Dynamics model was the removal of the tyre damping to enable a comparison between the seven degrees of freedom model and the ASM model. Tyre damping was removed through a simple change to the parameter for radial damping of the tyre. The tyre model used in the ASM Vehicle Dynamics model uses a version of the TMEasy model from (Rill 2021) which includes additional damping elements in the longitudinal and lateral directions of the tyre. The tyre model is capable of calculating not only the tyre forces and torques but also the slip calculation in both the longitudinal and lateral directions. The damping along these directions were kept at the default values for the ASM model to ensure the motion of the vehicle was not significantly affected by the modifications to the radial tyre damping.

The TMEasy tyre model differs significantly from the spring tyre force used for the Quarter Car and Full Car models from Sections 4.2 and 4.3 with the transient motion of the rim being included as part of the calculations. Unlike the spring tyre model the TMEasy model can

modify the speed of the vehicle model when the vehicle approaches an obstacle as the change in the longitudinal and lateral force is the result of changes to the vertical force at the wheel centre and the slip in the specified direction. Such differences in the tyre and vehicle models lead to a slight phase shift of the acceleration values for the ASM Vehicle Model when compared to the 7DoF model (see Figure 4.9) as the ASM Vehicle decelerates when it encounters an obstacle. The spring tyre models velocity is fixed based on the road height data supplied as a disturbance.

A MATLAB function was constructed as part of the second modification in order to calculate the response of the MR Damper based on the modified Nonlinear Viscoelastic Plastic model (modNVEP) from Chapter 3. This function is utilised at each corner of the vehicle to represent the forces generated by the dampers and uses persistent variables to speed up the calculation of the damper forces at each time step. In addition, a second set of calculations were implemented to determine the gradient of the force-velocity curve at predetermined points along the curve. This calculation was required by the tyre model used in the ASM model to interact with some internal functions. While this fundamentally uses the same units as the gradient of the curve the associated ASM functions do not allow for gradients of less than or equal to zero.

The proposed solution for the calculation of this gradient was to utilise the gradients ( $C_{pr}$  and  $C_{po}$ ) used in the modified Nonlinear Hysteretic Biviscous model (modNonlinHBV) from Chapter 3 and implement the same conditional cases used in Equations 3.7 and 3.8 to determine whether the pre-yield or post-yield gradient should be used. The conditional cases from Equations 3.7 and 3.8 already utilise the appropriate gradients in order to calculate the forces produced by the damper. Removing the additional terms ( $F_y$ ,  $v(t)$ ,  $v_i$  and  $c_i$ ) from the cases and multiplying the gradients by 1000 produces the required gradients in N.s/m.

#### 4.4.2 Comparison of Standard ASM Model and Modified ASM models

A comparison of the standard ASM Vehicle Dynamics model and the modified models including the MR Damper based model is conducted to determine the discrepancy between the proposed the standard model. A step bump profile of magnitude 0.02 m identical to that seen later in Figure 8.1 was used to identify the response of the passive system models. The results of the comparison simulations can be seen in Figure 4.9, where the various models are used to generate the vertical 'heave' acceleration of the vehicle body.

Table 4.3 shows the parameters for the second set of ASM simulation parameters used in the simulations from Figure 4.9. The parameters for the first set are shown in Table 4.2 and are referred to as the standard ASM parameters. The built in ASM active suspension uses many of the same parameter values with the exception of the spring stiffness and the damping values.

The damping values are set to the default block parameters that use a linearised damping model which calculates the damping force based on the damper piston velocity and the control signal.

Table 4.3 ASM Vehicle Model Parameters - Using Built-In Active Suspension Block ([dSPACE GmbH 2020](#))

This item has been removed due to 3rd Party Copyright. The unabridged version of the thesis can be found in the Lanchester Library, Coventry University.

A single step input is suitable to excite both the primary and secondary ride frequencies of the vehicle which means that the dynamics of the model versions can be compared with one another. Figure 4.9 shows two clear spikes in the acceleration values for all the model types which correspond to the moment of contact with the step for the front and rear wheels. The front wheels make contact with the bump at 4.55 seconds while the rear contacts the step at 4.66 seconds.

Figure 4.9 shows that the removal of the tyre damping results in an increase of the vehicle body acceleration at the peak times of 4.55 and 4.66 seconds when compared to the standard ASM model. The phase of the secondary and tertiary oscillations for the modified model are also shifted as a result of the removal of the tyre damping as the tyre damping is no longer retarding the motion of the vehicle body.

The Active Suspension Forces blocks provided in the ASM Simulink Libraries and used to determine the forces for the built in Active Dampers at the front and rear shows significant differences in the response as the spring and damper forces for the suspension change in relation to the parameterisation of the Active Suspension blocks. The response shows a reduction in the positive vehicle body accelerations but larger spikes in the negative spike seen at 4.58 seconds. There is also a phase shift in the later oscillations that occur after 4.7 seconds.

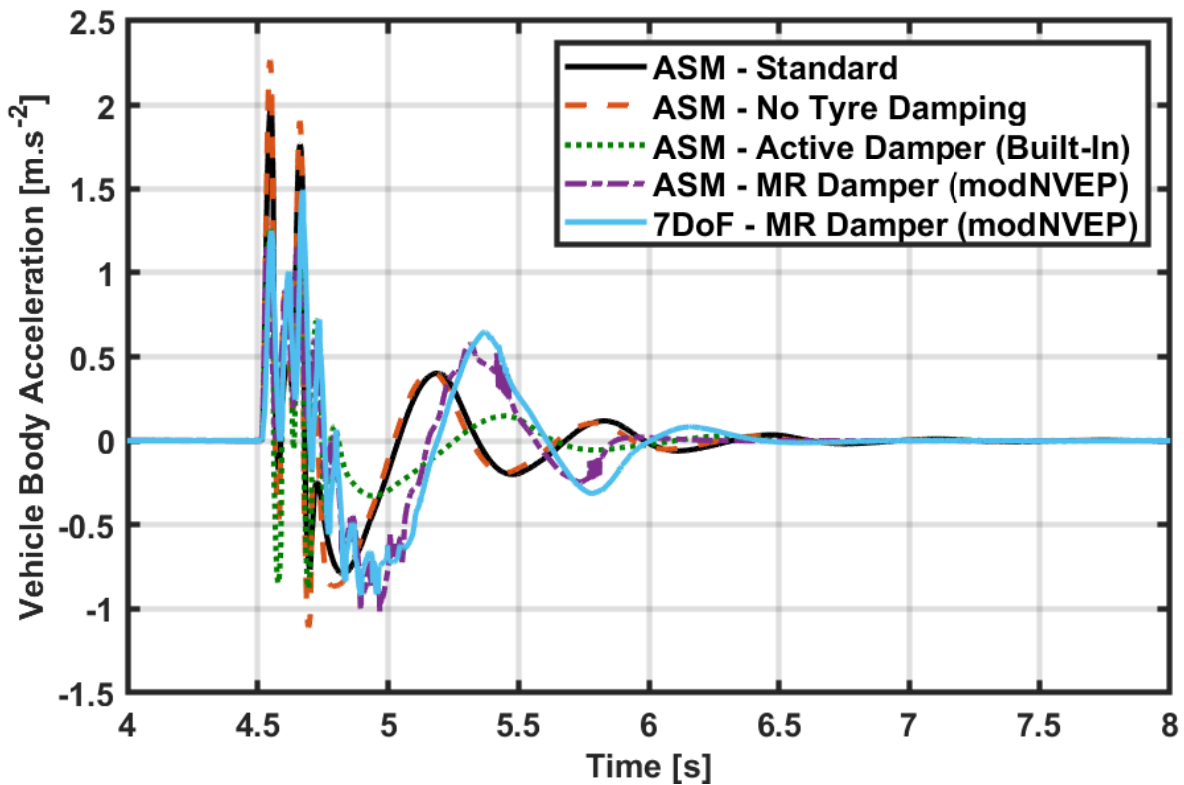


Fig. 4.9 The simulated response of the ASM and 7DoF vehicle models to the step bump road profile of height 0.02m at 90 km.h<sup>-1</sup> (25 m.s<sup>-1</sup>)

The introduction of the modified Nonlinear Viscoelastic Plastic (modNVEP) MR Damper model as part of the ASM shows a similar response to the active forces block with a similar phase shift after 4.7 seconds and similar magnitude during the spikes at 4.55 and 4.66 seconds. The magnitude of the low frequency oscillations seen in the standard ASM are comparable to the similar frequency oscillations seen in the MR Damper based suspension response with the negative peaks closer in magnitude than the positive peak values.

Oscillations of the vehicle body acceleration for the MR Damper version of the ASM vehicle seen at around 5.4 seconds and 5.8 seconds are the result of the implementation with the ASM Vehicle model. The oscillations occur when small displacements and small velocities are applied to the damper. These oscillations occur as the damper approaches zero velocity and the acceleration of the damper piston shifts between positive and negative at high frequency. The oscillations are visible in the body acceleration as the damper model produces forces that jump between the hysteresis values of the preyield region. This is a rare occurrence and typically only occurs when the damper model begins to transition outside of the frequency that it was parameterised at. This is less visible in the 7DoF model but occurs at a much lower magnitude.

Due to the constraints on physical testing this is assumed to be acceptable for the simulations in this thesis as the controller will minimise any oscillations that occur.

The simulated response of the full car model from Section 4.3.1 is also compared to the response of the similarly modified ASM model as well as to the original ASM model. Figure 4.9 shows that the response of the models are similar with the magnitude of the modified ASM and full car models remaining within  $0.06 \text{ m.s}^{-1}$  of each other at the second low frequency peak. The results from Figure 4.9 also show that while the response closely matches the modified ASM vehicle model, there are slight timing issues with the calculation of the peaks for the vehicle body acceleration. The differences likely occur as a result of the slight reduction in vehicle speed that the ASM model calculates in response to the bump onset. The latter is not considered by the seven degrees of freedom model from Section 4.3.1. However, the main response of the vehicle was captured by the seven degrees of freedom model. The resulting response shows that the model is suitable to model a real-vehicle with as it exhibits the same characteristic behaviour as the response given by the ASM model, assuming that the standard model provided is parameterised to reflect the digital clone mentioned in (Peperhowe and Schindler 2013).

## 4.5 Concluding Remarks

This chapter proposed two different formulations of a nonlinear quarter car model that utilises the MR Damper models from Chapter 3. These models are utilised later in Chapters 5 and 6 as part of the off-road quarter car model and are also used in the simulation and composition of the Quarter Car Nonlinear Model Predictive Controller (NMPC). The key novelty of the quarter car model proposed in Section 4.2.2 was the use of two state space models to calculate the response of the vehicle. As the quarter vehicle models rely on fundamentals derived from the literature, the response is assumed to reflect that seen from other quarter car vehicle models, this is later discussed in more detail as part of the simulation setup and studies from Chapter 8.

In addition to the quarter car vehicle models, two other formulations of a seven degrees of freedom vehicle model were proposed. These formulations are used for the simulation and composition of a Full Car NMPC strategy which is developed in Section 7.3. The vehicle model from Section 4.3.2 was also developed for the purpose of simulating the behaviour of a vehicle travelling on off-road soft soils using the further modifications stated in Section 5.6. The models integrate freely with the nonlinear MR Damper models from Chapter 3, potentially giving the user four different vehicle model responses. However, for the purposes of this study, the vehicle plant models selected was the modNVEP MR Damper model because of its ability to reproduce the force-velocity relationship curve as stated in Chapter 3.

Modifications to the Automotive Simulation Models for the integration of the nonlinear MR Damper models were also discussed in Sections 4.4.1 and 4.4.2. The changes to the vehicle response as a result of the modifications were highlighted in Section 4.4.2 while a comparison of the the response for the modified ASM model and the seven degrees of freedom Full Car Vehicle Model from Section 4.3.1 was performed. The modified ASM model is used in Chapter 8 as a means to verify the performance of the proposed NMPC strategy for full car semi-active MR Damper based suspension control.

# Chapter 5

## Tyre-Soil Interaction Modelling for Off-Road System Analysis

### 5.1 Introduction

This chapter introduces the tyre-soil interaction model used for the off-road simulation studies in Chapter 8, which is a modified version of the Bekakos model mentioned in Section 2.6.4. The equations and computational algorithm used in the calculation of the vertical and longitudinal tyre forces are described in Section 5.3. The sinkage of the tyre into the soil, as a result of the load applied at the wheel centre and the slip ratio of the tyre, are also introduced with the pressure-sinkage relationship explained in detail in Section 5.3.1.

Section 5.4 describes the process involved with parameterising the tyre-soil interaction model in preparation for the simulations in Chapter 8. Section 5.5 continues to develop the tyre-soil interaction model to allow for faster calculation of the response on a predetermined terrain type using the proposed pre-lookup method. This method, developed by the author, can determine the best estimate of the static sinkage from a lookup table describing the relationship between the vertical load force, the slip ratio values and the tyre sinkage. This method removes the need to run the bisection method online as the lookup table is populated with the static sinkage values from running the bisection method for multiple load force and slip ratio values to achieve a balancing load within a narrow tolerance of the load force applied.

Tyre-soil interaction models calculate the response of the tyre on flat terrain. Note that as a result of the tyre sinking into the soil, the wheel always traverses uphill. Section 5.6 proposes the use of coordinate transformations together with that of static friction to calculate the response of a tyre on a gentle sloped terrain. It assumes that the pressure distribution curve relationship with respect to the load force is not severely affected by the inclination.

This proposed method allows the user to estimate the effects of the incline for both uphill and downhill cases. It allows the user to recreate cases that reflect some of the conditions typically seen on off-road terrain.

Changes to the Quarter Car vehicle model from Chapter 4 are discussed in Section 5.7 to allow for the integration of tyre-soil interaction models. The chapter concludes with a summary of the key models and novelties introduced throughout this chapter and how they are utilised in the later sections of this thesis, including in the simulations conducted in Chapter 8.

## 5.2 Wheel Velocity and Slip Ratio

The wheel velocity and its tyre's slip ratio are interlinked. The latter is determined by the ratio of the longitudinal motion of the vehicle with respect to the rotation of the wheel. Since this value is required for the calculation of the tyre sinkage, a suitable calculation/estimation of the wheel velocity and the resulting slip ratio is required.

Equation 5.1 is used to calculate the longitudinal velocity of the vehicle with respect to the longitudinal force produced by the tyre soil interaction model discussed later in Section 5.3. The equation is a derivation of Newton's second law of motion for a change of momentum. It is rearranged to obtain the final velocity of the vehicle in response to the longitudinal force. This equation assumes that the mass of the vehicle is unchanging with the sum of the sprung mass and the unsprung mass equalling the total mass of the vehicle. The force from the tyre-soil interaction is also assumed to apply a constant longitudinal force between the fixed step simulation times. The time between fixed step intervals are given by the variable  $\Delta t$ .

$$V_x(t) = \left( \frac{F_x(t)}{m_s + m_{us}} \right) \Delta t + V_x(t-1) \quad (5.1)$$

Equation 5.1 assumes that the vehicle is at a known velocity, at time  $t = 0$ , to calculate all future velocities. The wheel tangential velocity at the wheel surface can also be determined by the angular velocity of the wheel ( $\omega$ ) and the unloaded radius of the tyre ( $R_u$ ). This results in the need to determine a value of the wheel angular velocity in order to determine the tangential velocity of the wheel ( $V_t$ ) seen in Equation 5.2.

$$V_t = \omega \cdot R_u \quad (5.2)$$

Both the tangential velocity at the wheel radius and the longitudinal velocity of the vehicle are needed to calculate the slip ratio of the tyre ( $sr$ ). Equation 5.3 shows how the slip ratio is calculated and relies on the angular velocity of the wheel. Due to this dependency on the

angular velocity, a known angular velocity profile must be supplied or a longitudinal controller must be used to ensure that the longitudinal velocity of the vehicle meets a desired velocity.

$$sr = \frac{\omega \cdot R_u - V_x}{\omega \cdot R_u} \quad (5.3)$$

For the simulations in Chapter 8, both methods of defining the angular velocity of the wheel are utilised to show how the system behaviour changes with respect to the slip ratio of the tyre. The Pre-Lookup Method proposed in Section 5.5 calculates the response of the tyre-soil model to discrete values of the slip ratio. This removes the need for Equations 5.1 to 5.3 in its formulation.

### Defining the Angular Velocity Profile

The angular velocity of the wheel is required in the calculation of the sinkage of the tyre into the soil and as a result needs to be defined for simulations of the vehicle on off-road soft soils. The three angular velocity profiles as shown in Figure 5.1 are used in the calculation of the wheel speed and slip ratio.

The velocities are used to represent the different aspects of driving that could occur during low velocity manoeuvres on off-road terrain. Angular Velocity Profile One seen in Figure 5.1 can be used to represent two scenarios and has a constant angular velocity of  $20.8325 \text{ rad}\cdot\text{s}^{-1}$  which is approximately equivalent to a desired velocity of  $30 \text{ km}\cdot\text{h}^{-1}$ . The first of the two scenarios this profile can be used for is when the initial velocity of the vehicle is zero. During this scenario the vehicle would respond to the angular velocity increase by the production of a sudden acceleration of the vehicle. The response would be similar to a step input response and is suitable for identifying the time dynamics of the system. The second scenario is where the initial velocity of the vehicle is close to a velocity of  $30 \text{ km}\cdot\text{h}^{-1}$ . Initial velocities greater than  $30 \text{ km}\cdot\text{h}^{-1}$  would result in some small deceleration of the vehicle while velocities lower than this threshold would likely result in some small acceleration of the vehicle until the equilibrium conditions are met. When the equilibrium velocity of approximately  $30 \text{ km}\cdot\text{h}^{-1}$  is set as the initial velocity the vehicle would continue to move at a constant velocity.

Angular Velocity Profile One could potentially be implemented as a real world test condition where the vehicle wheel speed is measured using wheel mounted encoders and wheel speed could be maintained by an electric motor control system to ensure that the angular velocity of the wheel is maintained throughout the test. However, it is acknowledged that the real world data would not be able to fully recreate the ideal angular velocity profile as mechanical limitations and controller performance would likely result in times when the angular velocity could not be kept constant the entire time.

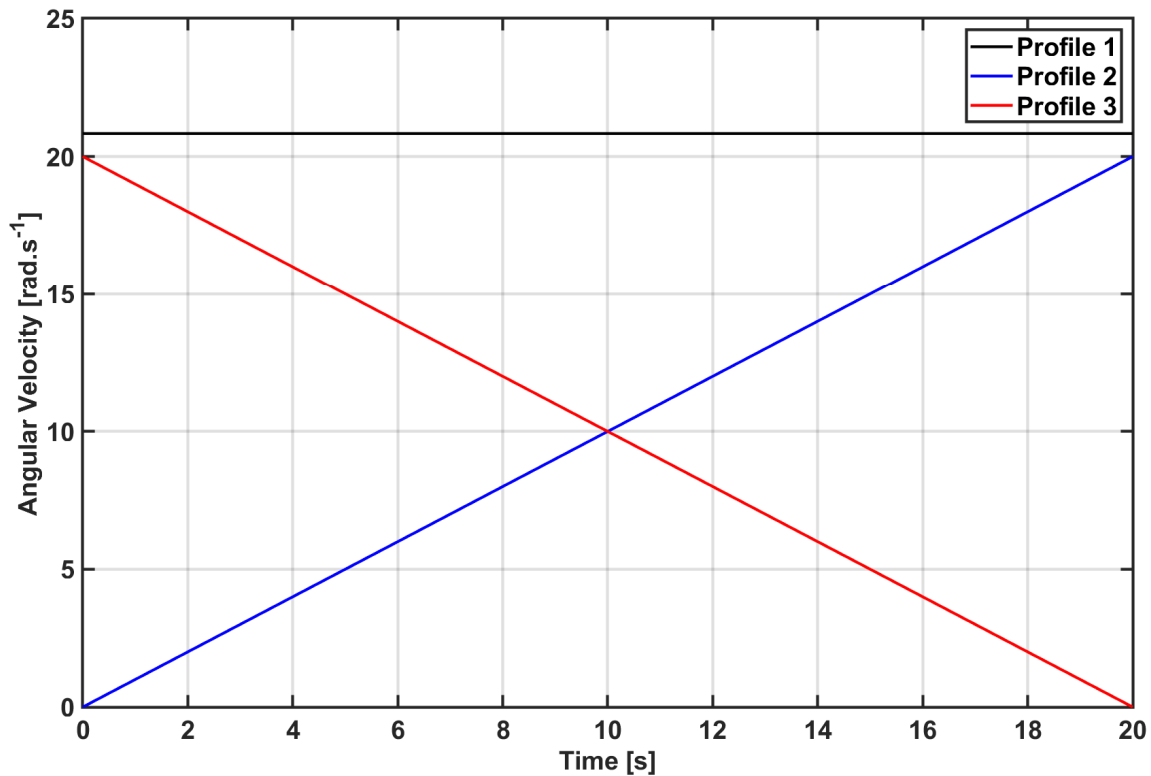


Fig. 5.1 The three angular velocity profiles using the predefined method.

Angular velocity profile two which is also shown in Figure 5.1 simulates a gradual acceleration of the angular velocity of the wheel to  $20 \text{ rad.s}^{-1}$  and focuses on the influence the lower slip ratio values have on the calculations and the sinkage of the tyre into the soil. Instead of the sudden acceleration which results in the rapid generation of longitudinal forces, the gentle slope ensures that the longitudinal forces are not of the same magnitude to identify the influence on the vertical response of the vehicle. Similar to the first angular velocity profile, controlled increases of the angular velocity can be performed using an electric motor control system for real world testing. However, due to the nonlinear nature of the system and the longitudinal relaxation length of the tyre, as the forces build up within the carcass achieving an exact match is unlikely, especially around an angular velocity of zero.

The final profile (Angular Velocity Profile Three) shown in Figure 5.1 indicates a gradual deceleration of the vehicle to  $0 \text{ km.h}^{-1}$ . This deceleration is necessary to identify the resulting impact of reducing the slip ratio has on the simulation of the vertical response of the vehicle. This gradual reduction of vehicle velocity can be achieved in reality through the use of electric motor control or through automated braking systems. However, the same issue as described for

angular velocity profile two still applies with the application to real world testing which makes an exact match to the profile unlikely. Absolute angular velocity measurements for the tyre outer surface are also likely to include both measurement noise and inaccuracies due to real world tyre deformation and residual loading of the soil, this further complicates the approach taken but this is acknowledged as part of the following simulation study.

### 5.3 Rigid Wheel Tyre-Soil Interaction Modelling

Rigid wheel tyre-soil interaction models were discussed in Section 2.6.4 as one of the many techniques used to model the behaviour of a tyre travelling across off-road terrain. The Bekakos model described in (Bekakos et al. 2016b) is a rigid wheel tyre-soil interaction model that calculates the response of the tyre on soft soils. It was chosen as the main baseline model used in this study, see Section 2.6.4. This rigid wheel model assumes that there is no deformation of the tyre as a result of the loads applied at the wheel centre. This results in the tyre sinking beneath the surface of the soil to balance the pressure of the vertical load. In addition, the model in (Bekakos et al. 2016b) assumes that the soil is not loaded beyond its bearing capacity. For more information on this topic, the reader should refer to (Clayton et al. 1995; Terzaghi et al. 1996).

Figure 5.2 shows an example diagram of a two dimensional rigid wheel model with two soil failure regions labelled zones A and B. These two zones are used to explain the differences in the pressure distribution curve as part of the tyre-soil interaction modelling process.

The two failure regions pressure-sinkage model used by the authors in (Bekakos et al. 2016b) are defined by the angle of maximum stress ( $\theta_M$ ) that is a function of the slip ratio of the tyre. The angle of maximum stress has been shown to lie somewhere between directly beneath the wheel and the entry angle ( $\theta_0$ ) and is often related to the slip ratio as seen in (Bekakos et al. 2016b; Senatore and Sandu 2011)(Equation 5.6). The changes made to the pressure distribution curve are calculated using one of the pressure-sinkage equations described in Section 5.3.1. The angles  $\theta_1$  and  $\theta_2$  shown in Figure 5.2 are used to represent the sweeping angle  $\theta$  which discretises the contact patch as it moves through zones A and B respectively.

The static sinkage of the tyre ( $z_{static}$ ) is the maximum vertical displacement the wheel moves as a result of the load present on the wheel centre when the wheel is stationary. The soil also undergoes mild spring rebound effects towards the rear exit angle ( $\theta_r$ ), which is heavily dependent on the soil type and conditions. An increase of the moisture in the soil has been seen to result in changes to the firmness and plasticity of the soil as explained in Wong's plastic theory and shear stress for dry sand and wet clay soils in (Wong 2009:31-45).

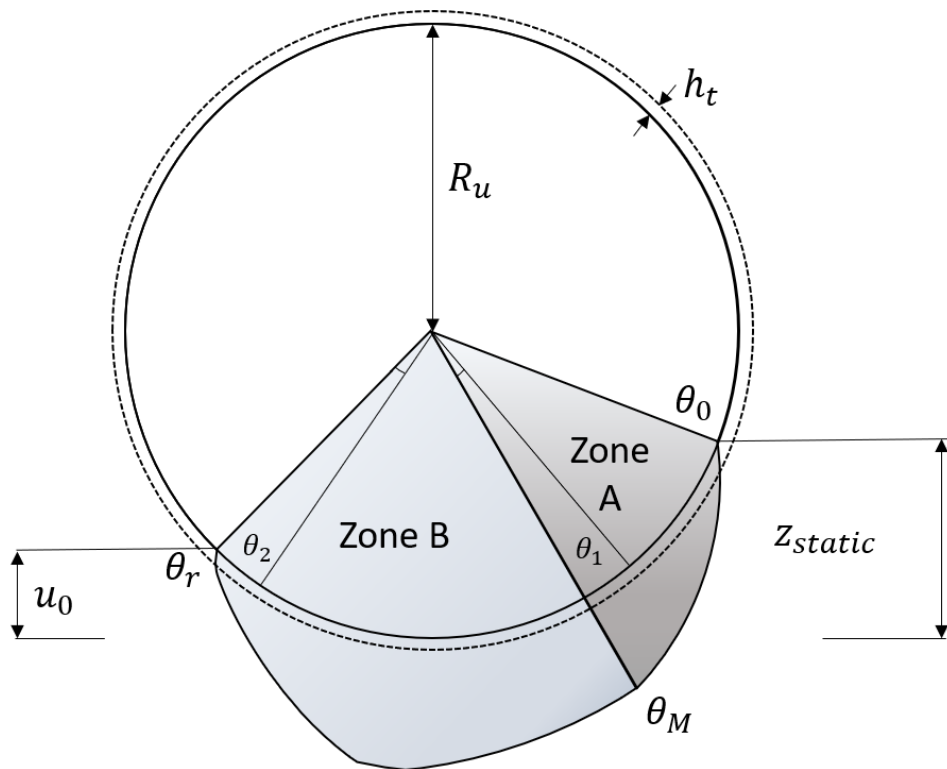


Fig. 5.2 Diagram of a Rigid Wheel Model

The rebounding effect is exaggerated and illustrated in Figure 5.2 with the increase in soil height after loading represented by  $u_0$ . Loading of the soil along the contact patch occurs nonlinearly, as the soil mounds up along the leading edge when the wheel is driven. This leads to increased resistance and a rut forming towards the trailing edge of the tyre contact patch as illustrated in (Wong 2009:41-42). The figure also illustrates the tyre tread height ( $h_t$ ) and the unloaded radius ( $R_u$ ) which influence the behaviour of the tyre sinkage based on the tread pattern and the surface area of the voids in the tread.

For the purposes of this research, it is considered that the main factor that influences the suspension is the vertical response of the wheel as a result of the changing sinkage of the tyre. Therefore, it is required to calculate the motion of the vehicle as a secondary value for the user to determine the slip ratio of the tyre and the resulting tyre sinkage into the soil. This work focuses on the response of the vehicle motion in the longitudinal direction. It is assumed that the lateral motion of the vehicle is not required to analyse the effect the tyre-soil interaction has on the suspension. Note that this model ignores the effects of bulldozing forces on the tyre response.

### 5.3.1 Pressure-Sinkage Relationship

The Pressure-Sinkage relationship is a widely discussed area of research with various equations proposed to predict how a tyre will sink into soft soils. The biggest influences on the vertical response of a tyre on off-road terrain are the vertical load applied to the wheel centre and the balancing reaction force which is a function of the tyre sinkage on off-road soft soils. The pressure applied across the contact patch area is one of the more complex relationships that influence the sinkage of the tyre into the soil. As mentioned in Section 2.6, the sinkage can often be calculated using the Bekker equation. The latter assumes that the sinkage of the tyre can be compared to that of a flat plate that applies a load to the soil.

The Bekakos model from (Bekakos et al. 2016b) utilises a version of the Load Sinkage Analysis (LSA) pressure sinkage model from (Lyasko 2010a). It calculates the parameters of the model from analytical expressions based on some simple hand measurements using the bevameter or penetrometer. However, when verifying the results from (Bekakos et al. 2016b), soil parameters, which would produce identical results to those seen in the paper, could not be obtained. Therefore, the main pressure-sinkage equation from (Bekakos et al. 2016b) could not be formally verified. However, based on the data presented, it follows the trends seen in both (Lyasko 2010a) and (Senatore and Sandu 2011). The lack of soil parameters in (Bekakos et al. 2016b) resulted in the need for an alternative pressure-sinkage equation to be substituted into the computation process.

The authors in (Bekakos et al. 2016b) highlight alternative calculations for the pressure-sinkage equation dating back to the original Bekker equation (Bekker 1962) recreated and rearranged here in Equation 5.4. This has been widely used and was modified using the methods in (Reece 1965; Wong and Reece 1967) to create the other alternative two failure region model seen in (Bekakos et al. 2016b; Senatore and Sandu 2011).

$$p = \left( \frac{k_c}{b} + k_\phi \right) \cdot z^n = (k_c + b k_\phi) \cdot \left( \frac{z}{b} \right)^n \quad (5.4)$$

Equation 5.4 uses the variables  $k_c$  and  $k_\phi$  to respectively represent the cohesive and frictional effects of the soil. These values are related to the plate dimensions with  $b$  which indicates the longer dimension of the bevameter plate used during physical parameterisation testing.

The updated version of the Bekker pressure-sinkage model from (Reece 1965) has been used in a number of studies, e.g. (Bekakos et al. 2016b; Senatore and Sandu 2011). It has been shown to more realistically reproduce the response of a soil to loading. However, there is a wide mix of notations used throughout the literature and published soil parameters have not been standardised. To account for this discrepancy the pressure-sinkage equation used in the modified model utilises the formulation first proposed in (Wong and Reece 1967), which has a

number of sources that state the parameters required for the simulation of a tyre over a number of different soil types.

$$p(\theta) = \begin{cases} (k_c + b k_\phi) \cdot \left(\frac{R_u}{b}\right)^n \cdot (\cos \theta - \cos \theta_0)^n & \theta_M \leq \theta_1 < \theta_0 \\ (k_c + b k_\phi) \cdot \left(\frac{R_u}{b}\right)^n \cdot \left[ \cos \left( \theta_0 - \left( \frac{\theta - \theta_r}{\theta_M - \theta_r} \right) (\theta_0 - \theta_M) \right) - \cos \theta_0 \right]^n & \theta_r \leq \theta_2 < \theta_M \end{cases} \quad (5.5)$$

The pressure-sinkage equation shown here as Equation 5.5 allows for the calculation of the pressure curve in relation to the area of contact with the soil for a rolling tyre. The plate dimension of the bevameter ( $b$ ), used in Equation 5.4, is replaced with the wheel width ( $b$ ) for all of the following calculations; including to calculate the pressure at small discrete angle increments for Equation 5.5. The angle of maximum stress is determined as a function of the slip ratio and the entry angle as seen in Equation 5.6, recreated here from (Senatore and Sandu 2011).

$$\theta_M = (c_1 + c_2 |sr|) \theta_0 \quad (5.6)$$

### 5.3.2 The Computational Algorithm

The computational algorithm of the off-road tyre-soil interaction model is illustrated in Figure 5.3. It shows the calculation process for the model and the various stages used to verify that the model balances the vertical load placed on the wheel at its centre. The model explains how the Bisection method is utilised to determine an accurate estimation of the static sinkage of the tyre ( $z_{static}$ ). Through various iterations, the vertical force at the wheel centre is compared to the reaction force produced by the soil in response to the pressure at the contact patch.

It is shown in Figure 5.3 that the model is capable of calculating the response for both treadless (slick) tyres and treaded tyres. Tyres with a tread pattern (treaded) can be expressed in terms of a void ratio to determine the ratio of the area covered by the tread pattern and the voids as a result of siping and other grooves that make up the tread pattern.

The pressure-sinkage of a treaded tyre would undoubtedly be different from that of a treadless tyre. The differences that result from the inclusion of the tread would generally alter the magnitude of the forces and sinkage, rather than the overall shape of the curve when used on the same soil (Bekakos et al. 2016b). The author acknowledges that the presence of tread would alter the vertical response of the tyre on the soil. However, the dynamic variation of the vertical response would be similar and many of the proposed changes in this chapter could be

This item has been removed due to 3rd Party Copyright. The unabridged version of the thesis can be found in the Lanchester Library, Coventry University.

Fig. 5.3 A Diagram illustrating the computational process used in the semi-analytical Bekakos model (Bekakos et al. 2016b)

applied to a treaded tyre, in the same way that they would for a treadless tyre. The treaded tyre response is calculated using the same approach as in (Bekakos et al. 2016b; Harnisch et al. 2005).

The reaction force of the soil can be directly related back to the choice of the value of the static sinkage as seen by substituting Equation 5.8 into Equation 5.7. An increase of sinkage increases the overall contact patch length of a stationary wheel. It results in the pressure supporting the wheel load to increase as the load is distributed over a larger area. When the values of the vertical force at the wheel centre and the reaction force balance, the wheel reaches an equilibrium position. This result in the sinkage changing only if the slip ratio or vertical load are altered. Note the soil type is assumed to remain fixed for each simulation due to the limitations of the tyre-soil interaction model.

$$F_z = 2R_u b \int_0^{\theta_0} p \cos(\theta) \cdot d\theta \quad (5.7)$$

$$\theta_0 = \arccos\left(1 - \frac{z_{static}}{R_u}\right) \quad (5.8)$$

When the tyre is stationary with relation to the terrain surface and there are no additional forces present, the conditions result in only the first line of Equation 5.5 needing to be used for the calculation of the pressure. Equation 5.7 can be used to calculate the static reaction force of the tyre on flat terrain as the pressure distribution is symmetrical with the entry and exit angles being equal which causes the maximum stress angle to lie directly beneath the wheel centre.

As the tyre begins to rotate or move, relative to the terrain surface, the slip ratio increases. This results in the need to calculate the pressure differently using the entirety of Equation 5.5. The calculation of tyre slip in the longitudinal direction for a given angular velocity of the wheel was discussed in more detail in Section 5.2.

The calculation of the reaction force of the soil cannot be performed in the same way as the stationary condition, as the shearing forces present from the frictional condition at the contact patch results in additional stresses in the soil. The shear stress is calculated using Equations 5.9 - 5.11 which are a combination of the approaches presented in (Janosi and Hanamoto 1961; Labuz and Zang 2012) and the Mohr-Coulomb failure criterion equation.

$$\tau_{max} = c + p(\theta) \tan \phi \quad (5.9)$$

$$\tau(\theta) = \tau_{max} \left( 1 - \exp \frac{-j_x}{k_x} \right) \quad (5.10)$$

$$j_x(\theta) = \int_{\theta_r}^{\theta_0} R_u [1 - (1 - sr) \cos(\theta)] d\theta \quad (5.11)$$

The shear stress values from the calculation of Equation 5.10 and the normal stress from the pressure on the soil calculated using Equation 5.5 are combined, as seen in Equation 5.12. The resulting value of Equation 5.12 calculates the soil reaction force in the upward direction of a rolling tyre to balance the vertical load at the wheel centre as seen in (Senatore and Sandu 2011).

$$W = R_u b \int_{\theta_r}^{\theta_0} [p(\theta) \cos(\theta) + \tau(\theta) \sin(\theta)] d\theta \quad (5.12)$$

The forward motion of the vehicle is determined by the longitudinal force, or drawbar pull ( $F_z$ ), that is generated at the tyre-soil interface. It is related to the vertical load and the slip ratio of the tyre. The longitudinal motion of the vehicle is required to calculate future values of the wheel velocity and the slip ratio which are discussed in Section 5.2. The longitudinal force of the tyre-soil interaction model from (Bekakos et al. 2016b) is calculated using Equation 5.13.

$$F_x = R_u b \int_{\theta_r}^{\theta_0} [\tau(\theta) \sin(\theta) - p(\theta) \cos(\theta)] d\theta \quad (5.13)$$

The longitudinal force and the motion of the vehicle is usually used to determine the tractive efficiency (Senatore and Sandu 2011). As the soil parameters are changed to represent the different soil types and the vertical load of the wheel changes, the tractive efficiency varies with the driving torque of the vehicle. However, as the focus of this thesis is on ride comfort, it focuses on the vertical response of the vehicle body. It is acknowledged that the torque demand increases from additional forces generated by active and semi-active suspension. The influence of the semi-active suspension and its control system on the torque demand for the vehicle to

move in the longitudinal and lateral directions is outside the scope of this thesis. However, this is an area that has been marked for future work which is briefly discussed in Section 9.2.

## 5.4 Tyre-Soil Interaction Model Parameterisation

In Section 2.6.5, parameters available for use with the chosen pressure-sinkage model were presented with the values selected from the available literature. This thesis uses the parameters for the three soils listed in Table 5.1. These are used in the simulations from Chapter 8 and in the parameterisation of the Pre-Lookup Method's lookup table. The soils are used to compute the difference in the wheel's response to the soil type has on the sinkage values and the indirect effects of the suspension.

Table 5.1 Soil Parameters for Tyre-Soil Interaction Modelling (Wong 2008; 2009)

| Soil Type                        | $n$ [-] | $k_c$<br>[ $kN/m^{n+1}$ ] | $k_\phi$<br>[ $kN/m^{n+2}$ ] | $c$ [ $kN/m^2$ ] | $\phi$ [deg] | $\rho$ [ $kg/m^3$ ] |
|----------------------------------|---------|---------------------------|------------------------------|------------------|--------------|---------------------|
| Soil 1:<br>Dry Sand              | 1.1     | 0.99                      | 1528.43                      | 1.04             | 28           | 2000                |
| Soil 2:<br>Upland Sandy<br>Loam  | 1.10    | 74.6                      | 2080                         | 3.3              | 33.7         | 1557                |
| Soil 3:<br>Rubicon Sandy<br>Loam | 0.66    | 6.9                       | 752                          | 3.7              | 29.8         | 1561                |

## 5.5 Pre-Lookup Method Development

The Pre-Lookup method proposed here is introduced as an alternative to running the bisection method at every time interval to determine the static sinkage of the tyre. The method utilises a lookup table that is populated with the values of the pre-calculated static sinkage. The lookup table output value is then fed into the tyre-soil interaction model in order to speed up the runtime calculations of the tyre forces in response to a change in the slip ratio or the vertical load at the wheel centre. The method can be used in conjunction with the bisection method to ensure that the static sinkage values in the lookup table correspond to the static sinkage calculated by the tyre-soil interaction model for each operating condition. The discrete values pre-calculated for the lookup table are determined through the offline testing explained in

Section 5.5.1. The benefits of this approach are compared to simply using lookup tables in place of the tyre-soil model equations, see Section 5.5.2.

### 5.5.1 Generating Lookup Tables for Tyre-Soil Interaction

The Pre-Lookup (P-LUT) Method utilises the model from Section 5.2 to calculate the static sinkage of the tyre that is required to obtain the balancing reaction force of the soil ( $W$ ). This particular study utilises the model from Section 5.3 to calculate the response of the tyre on the three different soils discussed in Section 5.4. However, the process could potentially be utilised for any of the tyre-soil interaction models that utilise the bisection method, or any other form of optimisation to determine the static/dynamic sinkage of the tyre into a particular soil.

It is important to note that the method assumes that the soil is homogeneous and that the lookup table is used for the same tyre-soil type as it was parameterised for. While it is possible to generate lookup tables for the forces generated by the tyre, there are a number of disadvantages to just using lookup tables for all of the tyre-soil interaction model outputs. The P-LUT method which utilises the tyre-soil interaction model for the calculation of the forces is compared to just using lookup tables in Section 5.5.2 to highlight the key differences between the two approaches.

The lookup table for the static sinkage used in the P-LUT method is generated using the same bisection method as used in the formulation of the tyre-soil interaction model. A lookup table of the static sinkage is generated by iterating through a range of slip ratios ( $sr$ ) with tested values in the range of -5 to 0.99 increasing in increments of 0.01. The vertical load ( $F_z$ ) was also tested at 4000 N, 5000 N and 6000 N. The bisection method minimises the error between the reaction force of the soil and the vertical load at the wheel centre. The error is reduced through every iteration of the bisection method until the error is found to be less than a tolerance chosen by the user.

Depending on whether the starting value of the static sinkage used for the bisection method was further away from the final value the method typically would take substantially longer to obtain the final value which would lie within the user tolerance range. A study into the time to calculate the final value was conducted versus the tolerance in the vertical load error, the results of which have been summarised by Table D.1 in Appendix D. The Error between the values of the vertical load and the reaction force of the soil are also shown a vertical load of 4000 N in Figure D.1 of Appendix D.

The values from both Table D.1 and Figure D.1 are performed from a minimal sinkage value of 1 mm as the starting condition, which is referred to as Cold Start point. Through the introduction of the P-LUT method, the time to reach the final condition is dependent on the tolerance chosen. However, most tests resulted in the P-LUT method converging within a single

iteration of 0.01 s. Differences from the single iteration conditions only occurred as a result of the lookup table having been generated for a wider tolerance than the tolerance allowed during simulation, resulting in the use of the Bisection method during runtime.

The tolerances investigated in both Table D.1 and Figure D.1 ranged between  $\pm 10$  N and  $\pm 0.001$  N. It can be seen that when the tolerances, seen in Figure D.1, reduce the convergence time increases which is a trade-off for the accuracy. The results from Figure D.1 show that tolerances of less than 0.1 N resulting in marginal improvements of accuracy for an increase of 0.1 s to the convergence time. Therefore, without the P-LUT method the bisection method would take between 16-25 times longer to converge. This highlights the additional benefit of using the P-LUT method where the lookup table values can be pre-populated with those of smaller tolerances resulting in improved accuracy without increasing the calculation time at runtime.

When performing the P-LUT method parameterisation for the simulations in Chapter 8 the number of data points that are used to generate the lookup tables are increased. Data points for vertical load on the wheel were taken across a wider region with the density of data samples increasing the closer the vertical load is to 0 N. The data can be grouped into the following vertical force lookup zone regions:

- lookupzone1 = [0.1:0.1:1];
- lookupzone2 = [2:1:10];
- lookupzone3 = [20:10:1000];
- lookupzone4 = [1050:50:7000];
- lookupzone5 = [7100:100:10000];

The lookup table is further configured to linearly extrapolate values outside of these values as it is unlikely such forces would occur under general operation. A small segment of these tested data points is used for the comparison with the Lookup Table Method in Section 5.5.2.

### 5.5.2 Lookup Table versus Pre-Lookup Method

The two approaches compared in this section are the Lookup Table (LUT) Method and the Pre-Lookup (P-LUT) method. The LUT method utilises two lookup tables to improve the speed of calculation for the tyre model outputs. The first lookup table relates the inputs for vertical force and slip to the longitudinal force, while the second lookup table gives the sinkage for the same inputs. The P-LUT method combines a lookup table that supplies the static sinkage

( $z_{static}$ ) to the tyre-soil interaction model which in turn calculates the longitudinal force of the tyre ( $F_x$ ) as shown in Figure 5.4.

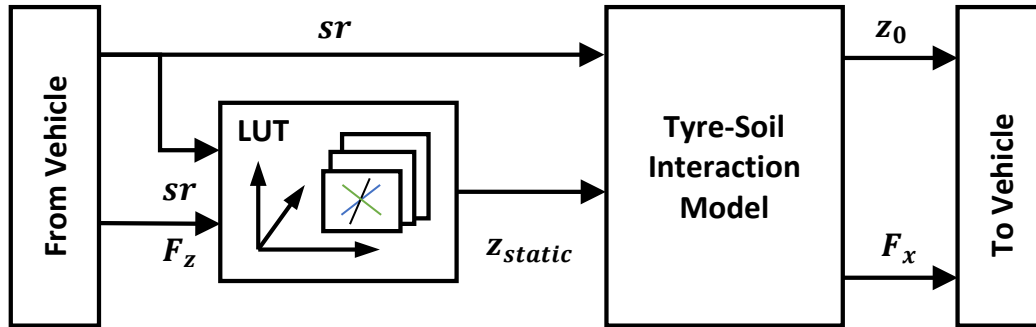


Fig. 5.4 A Simplified Block Diagram of the Pre-Lookup Method

The lookup table for the static sinkage uses a two dimensional lookup table with interpolation between known values of the sinkage. It calculates the static sinkage for any given slip ratio value or loading force within the range of loading conditions used to produce the lookup table. The P-LUT method has the added benefit of reducing the number of data points required to be stored in the available memory to calculate the tyre forces. However, for the LUT method to produce similar results, the number of data points necessary for the calculations are doubled. This is due to the additional points needed to determine the longitudinal force value. This would likely triple in the case of using an additional lookup table for the lateral forces produced by the tyre.

The P-LUT method has the advantage of calculating the response of the tyre using the tyre-soil interaction model, which allows for the dynamic adjustment of the output to the changing conditions rather than just utilising a static lookup table. The dynamic behaviour of the P-LUT method is particular suited to situations where the sinkage has been sampled at small intervals of the slip ratio and vertical force. However, this does not entirely remove the LUT method for consideration when operated at the discrete test points used in parameterisation which can be seen in more detail in Figure 5.5.

A sinusoidal slip ratio input between  $\pm 0.8$  was given to the lookup table for a vertical force of 5000N with a tolerance of  $\pm 0.001$  N, which resulted in the black points shown in Figure 5.5. Another sinusoidal input with the same amplitude as the lookup table method was used to represent the slip ratio for the P-LUT method resulting in the blue curve seen in Figure 5.5. It can be seen from Figure 5.5 that the curves for the pre-lookup and lookup table methods follow almost the same path. This confirms that the interpolation of the lookup table values closely matches the behaviour of the longitudinal force for a fixed vertical force.

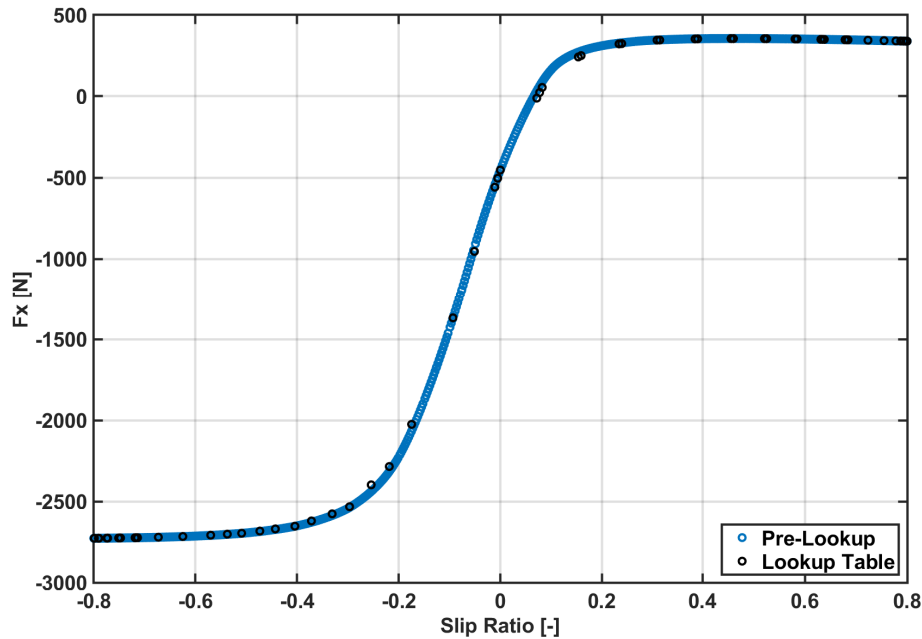


Fig. 5.5 A Comparison Between the Pre-Lookup Method and the Lookup Table Longitudinal Force versus Slip Ratio Curve for  $R_u = 0.4$  m,  $b = 0.2$  m and  $F_z = 5000$  N for Dry Sand (Soil 1).

A significant force difference is often visible between the positive and negative slip ratio values for off road tyre-soil interaction models as seen in Figure 5.5. This is due to the bulldozing effect of the tyre rotation and the build up of soil in front of the tyre due to the linear velocity of the tyre being at a lower velocity than that of the vehicle. The bulldozing effects of the tyre on the soil is more prevalent in the lateral dynamics of the tyre but in braking conditions such as those experienced during the negative slip the longitudinal displacement of the soil in relation to the tyre load applied to the soil results in the motion of the soil from underneath the tyre to be shifted to in front of the wheel. Similar behaviour can be seen in the results from (Bekakos et al. 2016b; Senatore and Sandu 2011) for the longitudinal force of the tyre even when pre-loading of the soil (multi-pass effects) are present.

Dynamic Loading simulations were also conducted to identify the transient effects relating to the change in vertical load applied to the tyre. The loading on the soil is directly related to the longitudinal force which is capable of being generated by the tyre-soil interaction. The loads on the soil were varied between 4000N and 6000N, which are within a reasonable range of typical loads. The results of the dynamic loading test, illustrated in Figure 5.6, reflect a similar friction curve to that seen in (Blundell and Harty 2014) for on-road cases when the slip angle changes with respect to the lateral direction. The key issue associated with the LUT method is highlighted in the response of the model. The discrepancy between the two methods

is pronounced and is partly due to the linear interpolation of the force  $F_x$  for the LUT method case. While other interpolation methods may lessen the degree of the difference between the LUT method and the P-LUT method, the main issue associated with the LUT method, in this case, is a lack of data points/operating conditions as part of parameterisation.

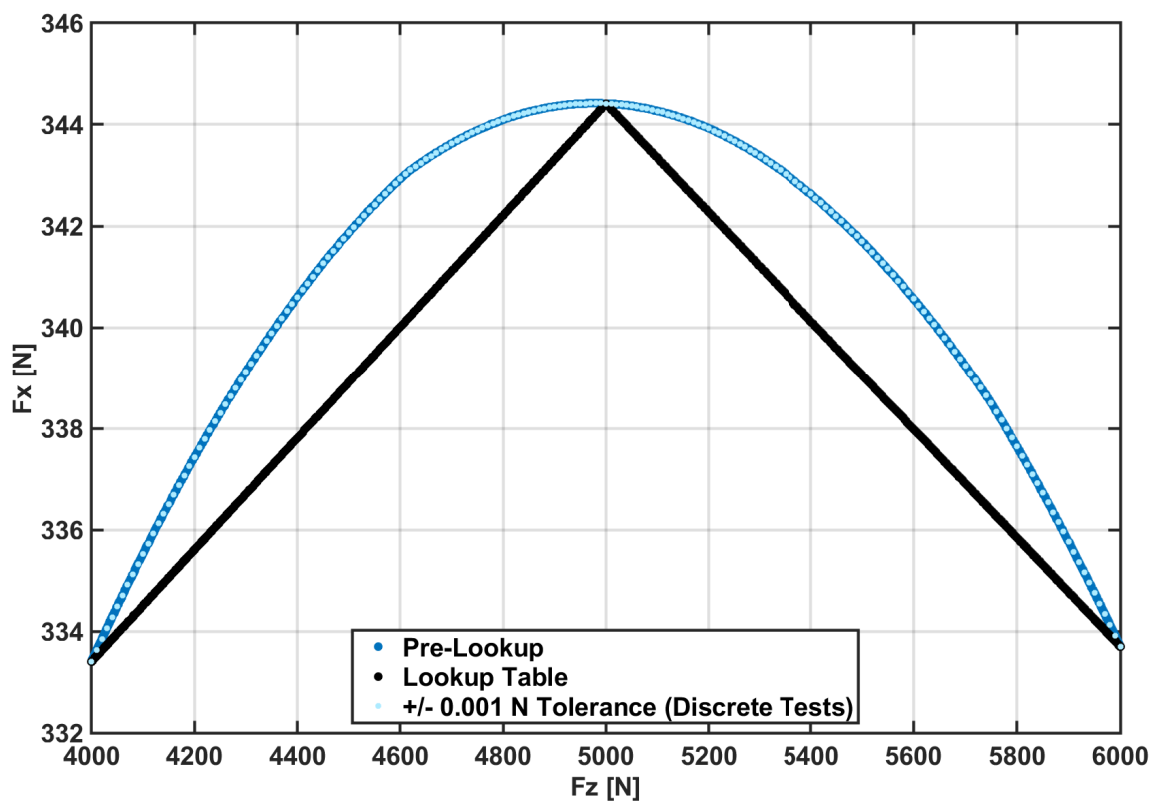


Fig. 5.6 A Comparison Between the Pre-Lookup Method and the Lookup Table Longitudinal Force versus Vertical Load at the Wheel Centre

The same information about the force at three operating conditions at 4000 N, 5000 N and 6000 N has been shared equally between both the P-LUT and LUT methods. However, since the forces of the tyre-soil interface are calculated by the tyre-soil interaction model, the P-LUT method is more flexible in the calculation of unknown conditions. The sinkage values in the lookup table, for the P-LUT method, include the data points for each slip ratio value tested. This results in a high resolution surface to be interpolated between each of the three loading conditions in the case of the P-LUT method. However, since the value of the longitudinal force is not corrected by the tyre-soil interaction model, when calculated as part of the LUT method, the model does not realise the curved shape during interpolation. This results in the need to use more data to interpolate the response of the tyre when utilising the LUT method. This means that, for the LUT method, the longitudinal force is considered to linearly increase

between these operating points resulting in the triangular shaped line seen in Figure 5.6. While it is possible to utilise other interpolation techniques, linear interpolation clearly shows how a lookup table parameterised with only 3 force conditions cannot replicate the curve effectively, resulting in lower estimations for the tractive force in the longitudinal direction.

## 5.6 Sloped Terrain Tyre-Soil Interaction Modelling

It was highlighted in Section 2.6.4 that the tyre-soil interaction models, currently used for determining the response of a tyre on soft soil, are limited to operate mostly on flat terrain using homogeneous soil. However, in reality this is rarely the case. This section proposes coordinate transformations to enable rigid wheel tyre-soil interaction models to calculate the response of a wheel on gently sloping terrain. The definition of gently sloping terrain in this study is assumed to be angles of less than  $10^\circ$  for both positive and negative inclines.

The primary assumption for this particular method is that the inclination of the slope does not alter the shape of the pressure-sinkage curve, but instead is rotated by the angle of inclination. The approach taken to calculate the response of the tyre on the sloping soil is that the tyre is assumed to behave similarly to a tyre on flat soil with reduced vertical load and increased longitudinal force to generate the required static friction to maintain the tyre's position and motion over the terrain.

To modify the tyre-soil interaction model for sloped terrain, the model is rotated to match the slope of the terrain. By rotating the model, the sinkage of the tyre into the soil remains perpendicular to the sloped surface of the soil. Consequently, all the forces on the wheel centre are split into their parallel ( $F_2$ ) and normal ( $F_1$ ) components with respect to the Sloped Terrain Reference Frame (STRF) seen in Figure 5.7.

Figure 5.7 shows the Ground Inertial Reference Frame (GIRF) defined by an arbitrary point along the terrain being traversed. The motion of the wheel along the ground progresses longitudinally with respect to the positive  $X_G$  direction. The terrain height increase/decrease therefore is calculated with reference to the normal to the  $X_G$  axis with positive values of  $Z_G$  determined as an increase above the  $X_G$  axis.

It can also be seen from Figure 5.7 that the force  $F_z$  normal to the  $X_G$  axis generated by the quarter car model acts parallel to the  $Z_G$  axis, as the model assumes that the quarter car is always in parallel alignment with the GIRF. In addition to the reaction force perpendicular to the slope ( $F_1$ ) there is also a component of the vertical load at the wheel centre which when converted to the STRF operates parallel with the slope ( $F_2$ ) and is calculated using Equation 5.15.

$$F_1 = \sin \theta \cdot \left( \frac{F_z}{\sin \phi} \right) \quad (5.14)$$

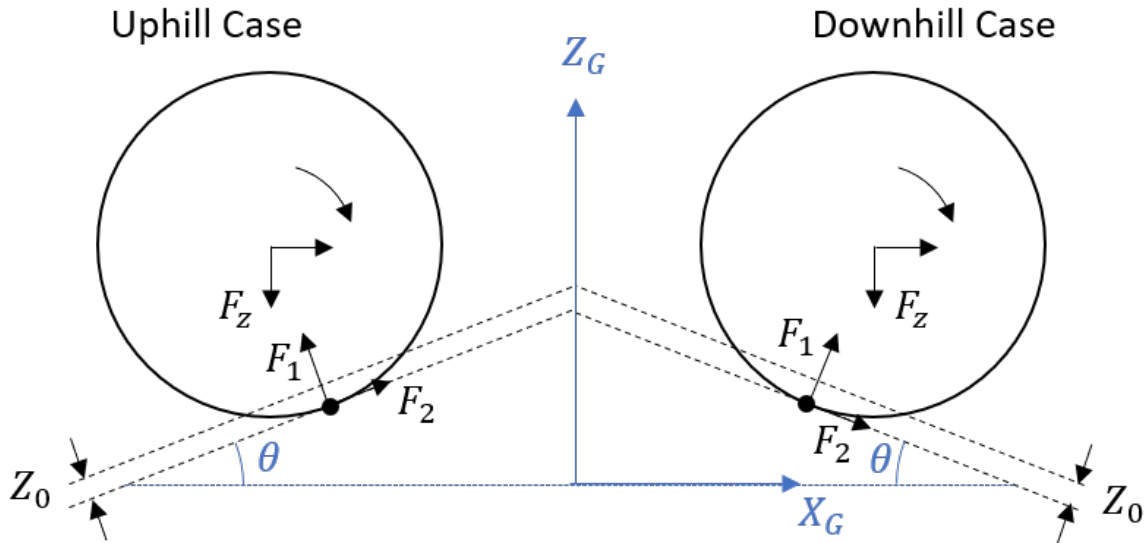


Fig. 5.7 A Diagram of the Sloped Terrain and the Reference Directions of the Sloped Terrain Modifications

$$F_2 = \sqrt{F_1^2 + F_z^2} \quad (5.15)$$

Equations 5.14 and 5.15 show how the force is divided into components in relation to the slope of the terrain. Equation 5.14 comprises of the angles for the slope inclination ( $\theta$ ) and the inverse slope inclination ( $\phi$ ). The uphill cases where  $\theta$  is positive the direction of  $F_1$  results in some resistance to the tyre's motion as it climbs the terrain slope. While in the downhill case the direction of  $F_1$  aids the motion of the tyre. On the other hand  $F_2$  has the opposite effect with positive inclinations resulting in an increase in the force parallel to the slope surface in the direction of travel, while negative inclinations oppose the direction of travel all while the force continues to be parallel to the terrain surface.

Equation 5.14 shares some similarities to the Equation 5.16 from (Ma et al. 2015). The load force acting on the ground ( $F_z$ ) is determined often by the mass of the object multiplied by the gravitational constant ( $g$ ). However, when on a sloped surface the force acting towards the centre of the earth is determined by the angle of the slope as some of the net force is counteracted by the friction force between the object and the slope.

$$F_z = m \cdot g \cdot \sin \theta \quad (5.16)$$

However, for the full vehicle model this assumption is not always valid due to the angular motion of the vehicle body. The force on a typical vehicle wheel centre is also not necessarily always vertical. Therefore, this method is a special case currently for simulation only. Future

testing using a specifically designed test rig would be necessary to analyse the response of a vehicle on gently sloped terrains to identify the influence of the suspension kinematics on the validity of the model and further verify the simulated response of the sloped terrain model proposed here.

The sloped terrain model is a newly proposed model that will require further testing to match the response of a real tyre on gently sloped terrains. Therefore, the influence of the proposed changes to the tyre-soil interaction model is analysed on the basis that the tyre would reflect similar behaviour to a wheel on a rigid slope with the exception of the additional motion resulting from the inclined sinkage. The sloped terrain model has been applied to the quarter car vehicle model to limit the inaccuracies which would be present by having multiple wheels in motion. Equation 5.17 calculates the vertical reaction force of the tyre-soil model with respect to the ERF. The longitudinal force acting parallel to the sloped surface ( $F_{x1}$ ) is transformed to calculate the component of the force which acts upwards as a result of climbing the incline.

$$W = \sqrt{F_2^2 - F_1^2} + F_{x1} \cdot \sin \theta \quad (5.17)$$

The longitudinal force of the model is calculated in a similar fashion with the horizontal component of the sloped longitudinal force calculated to be used in Equation 5.18. It can also be seen that the two cases for the longitudinal force are dependent on whether the slope is a positive or negative incline. For positive inclines the angle of the slope ( $\theta$ ) is considered to be greater than zero. A component of the vertical force acts against the motion of the wheel which is subtracted from the longitudinal force generated by the tyre-soil interaction model. The Mohr-Coulomb failure criterion equation (Equation 5.9) which is used in the tyre-soil interaction model, as part of the shear stress calculations and vertical reaction force of the soil, calculates the maximum shear strength of the soil. This value cannot be exceeded and as a result the force required to maintain the wheel's position on the slope must be accounted for, and subtracted from the available longitudinal force generated by the tyre, to ensure that the wheel's position is not affected by the slope.

$$F_x = \begin{cases} F_{x1} \cdot \cos(\theta) - F_1 & \text{if } \theta > 0 \\ F_{x1} \cdot \cos(-\theta) + F_1 & \text{if } \theta < 0 \end{cases} \quad (5.18)$$

Uphill Case:  $\theta > 0$  and  $\phi = 90^\circ - \theta$

$$Z_x = Z_0 \cos(\phi) \quad (5.19)$$

Downhill Case:  $\theta < 0$  and  $\phi = 90^\circ + \theta$

$$Z_x = -Z_0 \cos(\phi) \quad (5.20)$$

The sinkage into the soil also provides movement perpendicular to the soil's surface as part of the tyre-soil interaction model. When the sinkage is translated to the ERF, the sinkage does not act directly down. Instead the angle results in some of the sinkage contributing to the forward motion of the vehicle. To accommodate for this displacement ( $Z_x$ ), the derivative of the sinkage is used alongside Equation 5.1 to calculate the new equation for a change in velocity of the quarter car vehicle, see Equation 5.21.

$$V_x(t) = \left( \frac{F_x(t)}{m_s + m_{us}} \right) \Delta t + V_x(t-1) + \dot{Z}_x(t) \quad (5.21)$$

Figure 5.8 shows the calculated longitudinal force for each of the slope angles on Dry Sand. As expected, the  $\theta = -4^\circ$  case reaches the desired velocity faster than the other cases with a sharp decline in the force after 8 seconds. Meanwhile, the  $\theta = 4^\circ$  case does not manage to reach the desired velocity within the 20 seconds simulation duration. This is due to the incline which prevents sufficient force to be generated to maintain the position on the slope and accelerate the vehicle to the desired velocity.

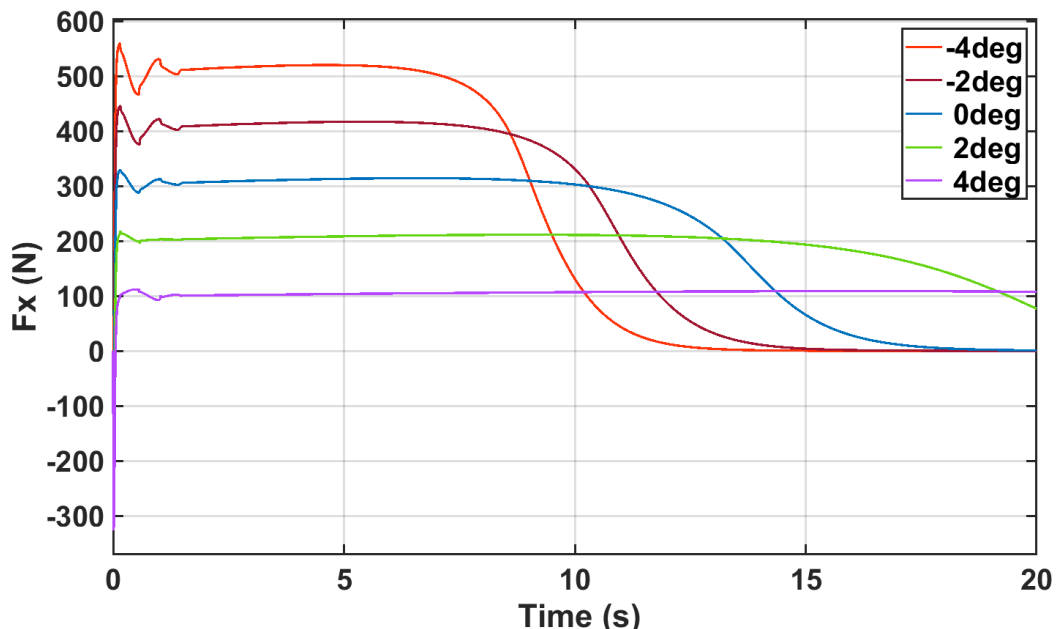


Fig. 5.8 Longitudinal Force ( $F_x$ ) with respect to time for multiple inclines of sloped Dry Sand terrain with a vertical load of 4000N

The desired velocity of  $30 \text{ km.h}^{-1}$  ( $8.333 \text{ m.s}^{-1}$ ) which was defined in Section 5.2 is equivalent to constant angular velocity of the wheel equal to 20.833 radians per second and the unloaded radius equal to 0.4 meters. This assumes that the tyre behaves as a perfect transfer of rotational motion to the terrain surface in order to move the wheel forwards. In reality the velocity plot from Figure 5.9 shows how the velocity of the wheel increases over time irrespective of the wheel rotating at a faster angular speed.

Figure 5.9 confirms that the vehicle reaches a higher maximum longitudinal velocity for the downhill cases than those seen in the uphill cases. This is consistent with the motion of a rigid wheel moving up a slope without the presence of sinkage as the forces on the wheel need to overcome the gravity in the uphill case, while the downhill case is working with gravity. The longitudinal velocity is linked to angle of inclination of the soil with the overall acceleration of the negative angle cases being higher than that of the flat terrain case.

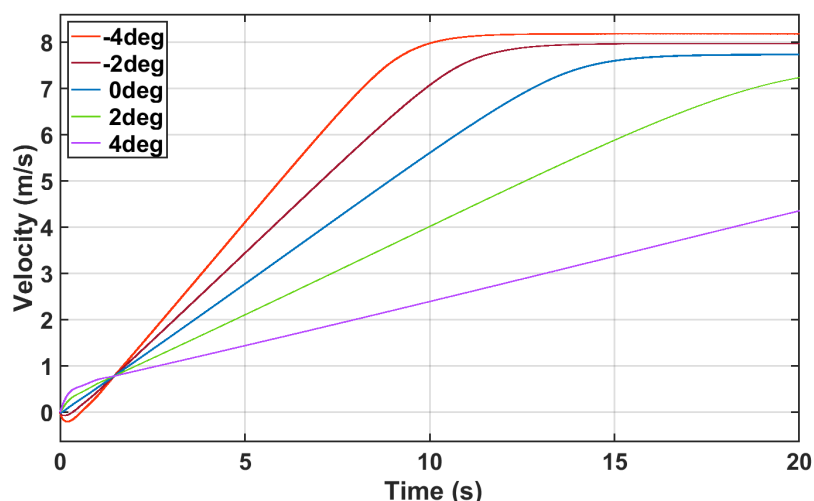


Fig. 5.9 Longitudinal Velocity for sloped Dry Sand with a vertical load of 4000N

Figure 5.10 shows how the slip ratio levels out during the later stages of the simulation. However, the final value changes between inclination angles. High negative inclinations lead to an almost zero slip condition where the tyre is more closely linked to a free-rolling wheel due to the slope effects. Larger positive inclinations lead to a plateau effect as seen in the  $\theta = 4^\circ$  case.

The plateau effect seen in Figure 5.10 highlights how for some soft soils the conditions do not allow for the tyre-soil interface to generate sufficient uphill thrust to reach the intended speed. The  $\theta = 4^\circ$  case shows that the value of the slip ratio is decreasing and that the longitudinal velocity seen in Figure 5.9 is increasing steadily. The over-rotation of the wheel at the start of the simulation, as a result of the fixed angular velocity, is undesirable as the soil

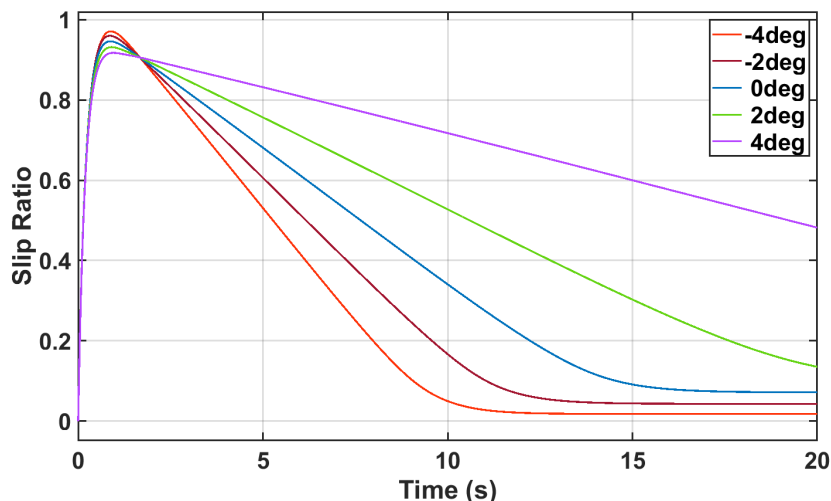


Fig. 5.10 Slip Ratio of Sloped Dry Sand cases with 4000N of vertical load at wheel centre

fails before sufficient longitudinal force can be generated for efficient motion of the wheel over the terrain.

## 5.7 Model Integration with Vehicle Models

This study focuses on the integration of the tyre-soil interaction model and sloped terrain method with the quarter car vehicle model from Section 4.2.2. Section 5.7.1 describes which modifications to the quarter car model are performed, with a summary of the overall changes made in this section and the rest of the chapter available in Section 5.8.

### 5.7.1 Quarter Car Off-Road Vehicle Model

The first step in modifying the quarter car vehicle model, for use on off-road soft soils, is the removal of the spring tyre model that was used in the equations of motion from Section 4.2.1 and 4.3.1. The variable  $W$  is introduced to represent the reaction force to the vertical load at the wheel centre, see Equation 5.22.

$$W = K_t \cdot (Z_{us} - Z_r) \quad (5.22)$$

The tyre force from the tyre-soil interaction model can be used to balance Equation 5.23 by eliminating the tyre spring coefficient terms used to calculate the motion of the unsprung mass. As the sprung mass equation of motion is not directly influenced by the tyre forces, there are no terms relating to the spring tyre model in Equations 4.2.1 and 4.2.2. Therefore the sprung

mass equation of motion remains unchanged for the quarter car off-road vehicle model shown in Equation 4.1. However, by substituting the variable  $W$  into the equation of motion for the unsprung mass (Equation 4.2), the resulting equation removes the tyre deflection in favour for the reaction force seen in Equation 5.23.

$$m_{us} \cdot \ddot{Z}_{us} = K_c \cdot (Z_s - Z_{us}) + F_d - W \quad (5.23)$$

Figure 5.11 shows how the reaction force is introduced into the free body diagram for the quarter car vehicle model. The displacement, velocity and acceleration of the unsprung mass use the same positive direction, as seen in Figure 4.1. However, they are heavily influenced by the tyre sinkage into the soil ( $z_0$ ) whether the vehicle is stationary or in motion. The increased load of the suspension, due to residual acceleration of the sprung mass, is considered to influence the behaviour of the tyre sinkage. This results in the tyre sinking more or less into the soil depending on the disturbances to the sprung mass from other external loads/forces. The same effect is predicted to occur when the use of semi-active and active suspension generates additional forces to stabilise the motion of the sprung mass and ensure that there is sufficient ground contact between the tyre and the soil.

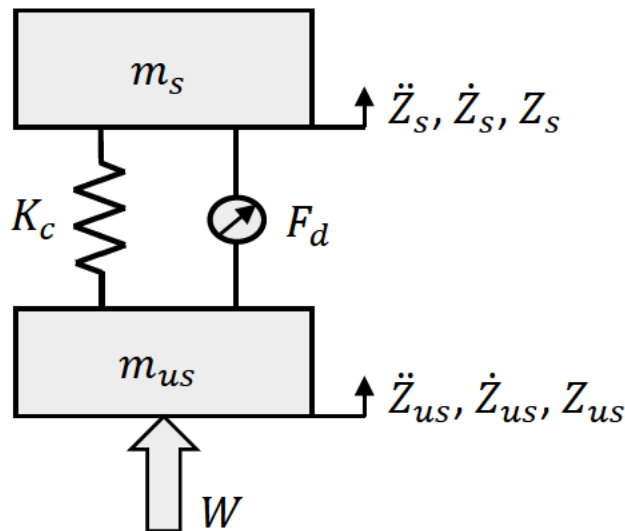


Fig. 5.11 Modified Quarter Car Vehicle Model for Off-Road

The tyre-soil interaction model is heavily influenced by the load at the wheel centre ( $F_z$ ) which is calculated by the sum of the spring and damping force in addition to the unsprung mass weight due to gravity. Under steady state equilibrium conditions the spring and damping forces balance the weight of the sprung mass. This results in the total load at the wheel centre

being the sum of the two masses multiplied by the gravitational constant ( $g = 9.81 \text{ m.s}^{-2}$ ). However, when there are disturbances in the system, an additional force to represent the force imbalance ( $F_i$ ) is required as shown in Equation 5.24.

$$F_z = K_c (Z_s - Z_{us}) + F_d + m_{us} g = F_i + (m_s + m_{us}) g \quad (5.24)$$

Figure 5.12 shows a diagram of the modified quarter car vehicle model which utilises the tyre-soil interaction model to determine the motion of the unsprung mass. Note that the motion of the unsprung mass is linked to the sinkage of the tyre into the soil. The unsprung mass displacement is equivalent to the sinkage of the tyre in addition to any subsequent change in the terrain height. However, large sudden variations of the terrain height can reduce the pressure on the surface of the soil to zero. This would result in the wheel rising above and losing contact with the soil surface. This particular scenario is undesirable. First, the tyre-soil interaction model equations would no longer be valid as there would be no pressure on the soil to determine a response. Second, the vehicle handling and stability would be severely impaired with the tyre's inability to generate any longitudinal or lateral forces, as the tyre is no longer producing normal and shear forces within the soil, leading to loss of control of the vehicle.

It can also be seen from Figure 5.12 that while the sprung mass system from Section 4.2.2 is present in the off-road quarter car model the unsprung mass system is not used. There are two reasons for this important change.

Firstly, for the modification of the unsprung mass system to be included in the off-road model Equations 4.27 and 4.28 must be adapted in such a way to reflect something similar to the state space system given by Equations 5.25 and 5.26. While on first glance the equations may seem to adequately model the motion of the unsprung mass, the unsprung mass displacement is not coupled to the tyre sinkage into the soil. In addition the reaction force of the tyre and soil would effectively balance out any other disturbances to the system from the terrain height since the tyre is considered rigid and non-deformable for the purposes of the tyre-soil interaction model.

$$\begin{aligned}
 A_u &= \begin{bmatrix} 0 & 1 \\ -\frac{K_c}{m_{us}} & 0 \end{bmatrix} & B_u &= \begin{bmatrix} 0 \\ 1 \\ \frac{1}{m_{us}} \end{bmatrix} & \Gamma_u &= \begin{bmatrix} 0 & 0 \\ \frac{K_c}{m_{us}} & -\frac{1}{m_{us}} \end{bmatrix} \\
 C_u &= \begin{bmatrix} 1 & 0 \\ 0 & 1 \\ \dots & \dots \\ -\frac{K_c}{m_{us}} & 0 \end{bmatrix} & D_u &= \begin{bmatrix} 0 \\ 0 \\ \dots \\ 1 \\ \frac{1}{m_{us}} \end{bmatrix} & \Gamma_{u1} &= \begin{bmatrix} 0 & 0 \\ 0 & 0 \\ \dots & \dots \\ \frac{K_c}{m_{us}} & -\frac{1}{m_{us}} \end{bmatrix}
 \end{aligned}$$



sinkage and the sprung mass system without further modification leads to inaccurate calculations of the system states. This is due to the shift in the system equilibrium point due to the inclusion of the tyre-soil interaction model.

To accommodate for the shift in the equilibrium point, the system must first be simulated using an expanded system block diagram shown in Figure 5.13 which is similar to the system model used in (Messner et al. 2021).

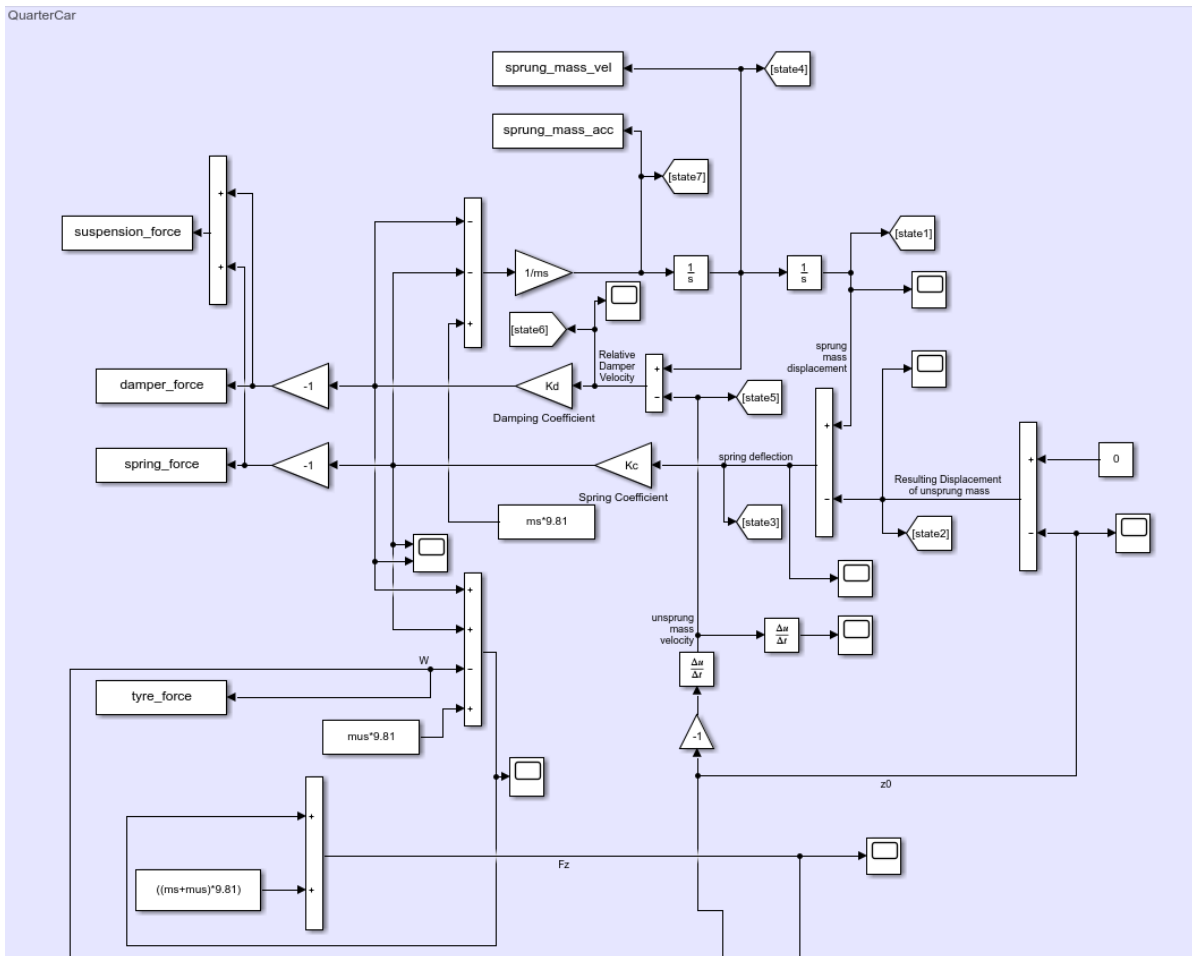


Fig. 5.13 Expanded Quarter Car System Block Diagram

As the system reaches the stable equilibrium condition, the simulation is stopped and the system states are obtained for the sprung mass and unsprung mass displacements. These equilibrium points are used later in Chapter 8 for the calculation of the off-road prediction horizon for the NMPC off-road controller.

## 5.8 Concluding Remarks

This chapter has addressed the need to obtain a tyre-soil interaction model to simulate the behaviour of a tyre on soft-soil. The model is aimed to provide an estimate of the behaviour of a quarter car vehicle travelling on off-road soft soils. The vehicle suspension and control techniques for off-road are discussed in more detail in Chapters 3 and 8 respectively.

A model based on (Bekakos et al. 2016b) was modified for integration with a quarter car vehicle model as part of Section 5.7. The proposed method pre-calculates the tyre static sinkage with respect to a range of operating conditions using a model adapted from (Wong and Reece 1967). Offline optimisation is performed using the bisection method to determine a value of the static sinkage which balances a small range of given vertical loads across a number of slip ratio values. The results of the optimisation process are stored in a lookup table in preparation for use during online simulations as part of a Pre-Lookup Method.

The proposed Pre-Lookup (P-LUT) method calculates the static sinkage through interpolation of the stored data in the lookup table. This reduces the calculation time during online simulations as the bisection optimisation process does not need to be performed at every time-step of the simulation. The sinkage value is necessary for the calculation of the tyre response and is given to the modified tyre-soil interaction for the calculation of the longitudinal force.

A comparison between the use of a lookup table to replace the tyre-soil interaction model and the proposed Pre-Lookup method was performed in Section 5.5.2. The results of the comparison show that the P-LUT method requires less data-points than the Lookup Table method, with the Pre-Lookup method resulting in improved accuracy over the Lookup Table method. The P-LUT method has the added benefit that it can be used in conjunction with the bisection method online. The latter is used if the interpolated values of the sinkage fail to produce a reaction force of the soil within the users tolerance of the vertical load placed at the wheel centre. This condition would rarely occur when the lookup table for the P-LUT method is used as shown in Figure 5.12. The P-LUT method is utilised in the simulation studies conducted in Section 8.5 to assess the performance of the proposed NMPC strategy that is introduced for off-road vehicle suspension control on soft soils.

The sloped terrain model is a newly proposed model that calculates the tyre response for gently sloping soft-soil terrain. The method utilises the modified tyre-soil interaction model described in Sections 5.3 and 5.4 to calculate the response of the tyre using loads that have been rotated into the Sloped Terrain Reference Frame (STRF), see Section 5.6. With the exception of the additional motion resulting from the inclined sinkage and the adjustments of the longitudinal force to account for the force needed to maintain the tyre position on the slope, the sloped terrain model shares the same fundamental behaviour than the tyre-soil interaction model.

Having established the appropriate means to model the interaction of the wheel with the soil, the next two chapters focus on the quarter car and full car semi-active suspension controllers. All the aforementioned models and controllers are then combined in Chapter 8 to evaluate the off road behaviour of the proposed NMPC.

# Chapter 6

## Nonlinear Quarter-Car Semi-Active Damper Controller Design

### 6.1 Introduction

This chapter introduces the quarter car semi-active damper controllers for the MR Damper based suspension. The controllers are used to manipulate the current supplied to the MR Damper models from Chapter 3. The MR damper models represent the behaviour of semi-active suspension fitted to the quarter car vehicle models from Chapter 4. The controllers are focused on reducing vertical accelerations of the sprung mass to improve vehicle ride comfort.

Section 6.3 describes and utilises a traditional PID controller to directly manipulate the current supplied to the damper in response to the acceleration of the sprung mass. The controller is then modified in Section 6.4 where an Adaptive PID controller, which adapts the controller gains with respect to the changing displacement and velocity of the damper, is proposed. The proposed Adaptive PID controller has been adapted from other application domains and industries (Sahputro et al. 2017) to the problem of controlling MR Damper based semi-active suspensions. The optimisation methods used to tune the PID and Adaptive PID controllers are described in detail with the gains for each controller assessed for their influence on the overall vehicle response.

The formulation of a Nonlinear Model Predictive Controller (NMPC), which utilises the Nonlinear MR Damper models from Chapter 3, is proposed in Section 6.6. The controller predicts the motion of the quarter car vehicle masses across a predefined horizon in order to perform optimisation methods to calculate the optimal current within a set of system constraints. The NMPC optimisation of the current supply is a novel approach to finding the optimal control output as previous work has focused predominantly on the optimisation of control forces as

discussed in Chapter 2. The controller weightings, applied to the NMPC cost function, are discussed in detail and the impact the controller weights have on the system response critically evaluated.

An alternative version of the NMPC strategy, which implements dual-rate sampling for the controller predictions, is then proposed. The dual-rate sampling reduces the number of optimisation variables used to determine the optimal controller output, thereby reducing the time spent minimising the controller cost function. The dual-rate controller is proposed with aims to address some of the issues related to future implementation of the NMPC strategy on hardware for physical real-time testing. The chapter concludes by explaining how the controllers are utilised in Chapter 8.

## 6.2 Constant Current Control

One simple method of controlling the damper is to set up a constant current supply for a particular scenario. This method ignores the MR Dampers dynamics with respect to current as the change in response is only influenced by the dampers velocity and displacement. Since the behaviour of the fluid doesn't change throughout this form of control it cannot be considered as a semi-active control strategy, but offers a insight into the behaviour of the system when the damper is set to an MRPassive - Soft or MRPassive - Hard configuration.

### 6.2.1 MRPassive - Hard

The MRPassive - Hard configuration of the damper is defined as the damper's behaviour when subjected to a maximum constant current of 1A. The damper's forces with respect to the displacement and velocity of the damper piston are at a maximum and result in a stiffer ride experience that is in most cases an undesirable condition as disturbance energy introduced in to the system is transferred more readily into the vehicle body. In addition the damper is limited to operate at this current for a maximum of 30 seconds as explained in the RD-8041 technical specifications ([Lord Corporation 2009](#)), which means that this configuration is unsuitable for long term use.

### 6.2.2 MRPassive - Soft

The MRPassive - Soft configuration of the damper is defined as the newtonian-fluid like behaviour of the damper when there is zero current supplied to the MR Damper. This behaviour is similar to a typical passive damper as the viscoelasticity of the MR Fluid does not change with respect to the loads applied to the damper. Unlike the MRPassive - Hard configuration

however, the soft configuration can operate indefinitely as the damper resides at a stable steady state. The MRPassive - Soft configuration offers the lowest damping the damper can provide and as such is often too soft to avoid conditions such as wheel hop during larger disturbances. The benefit of operating at this condition however, is that there is no additional energy needed to be injected into the system by the current controller. The reduced current is often optimal during stable steady state conditions where the damper is not required and the suspension springs maintain an equilibrium between the body and wheel masses. For the remainder of the tests conducted in this thesis the MRPassive - Soft condition will simply be referred to as MRPassive as seen in Figures 6.5 to 6.7.

### 6.3 PID Controller

The parallel form of the Proportional-Integral-Derivative (PID) Controller is a classical control technique that is used to control linear or linearisable systems. The processes involved with tuning the controller assumes that there are no disturbances present during the tuning process. However, in the case of semi-active suspension applications, MR Dampers reaction depends on the external road disturbances that impact the damper piston displacement and velocity. Further the damper responses are known to be nonlinear as shown in Chapter 3. These problems are generally overcome by linearising the suspension system response or optimising the controller gains for a known input disturbance as seen in (Altinoz and Yilmaz 2018). The controller uses the PID equation seen in Equation 2.1 from Section 2.5.1 with the sprung mass acceleration used as the Process Variable (PV) while the supply of damper current is the Manipulated Variable (MV).

The error signal ( $e$ ) is calculated, at each time step, by subtracting the measured PV value from the desired Set Point (SP). For the purposes of suspension control, the primary objective is to minimise the sprung mass vertical acceleration. Therefore the desired SP for the PID controller is zero meters per second squared.

Figure 6.1 shows how the PID controller is connected to the system plant model in Simulink with the chosen Nonlinear MR Damper model and the quarter car vehicle model described in Chapter 4. The Simulink model is run with a fixed step size of 0.001 s and utilises a continuous time model. The displacement and velocity of the damper model are provided as feedback signals for the MR Damper model. These feedback signals are delayed by 0.001 s to avoid the creation of algebraic loops. The PID controller block is also configured to saturate the current supplied to the MR Damper to between 0A and 1.1A which has been illustrated separately to the PID controller in Figure 6.1.

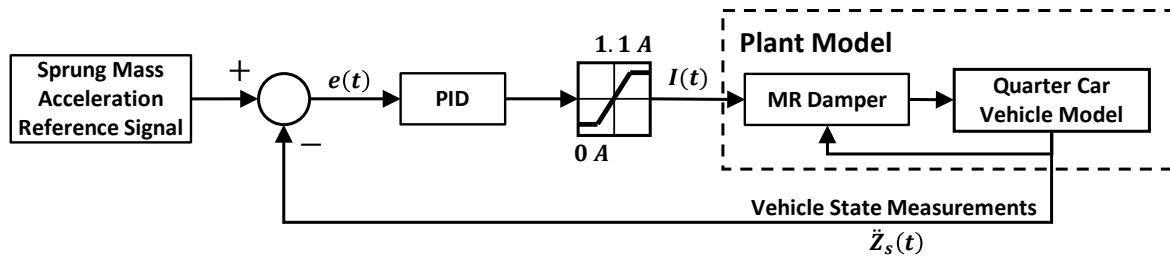


Fig. 6.1 A Simplified Block Diagram of the Quarter Car Vehicle PID Controller

### 6.3.1 Tuning of the PID Controller Gains

Tuning scalar values corresponding to the PID Controller gains  $K_P$ ,  $K_I$  and  $K_D$  can be challenging for the control of nonlinear systems. There is a range of tuning methods for PID tuning, each with advantages and drawbacks and dependent on the system being controlled. Among the methods more commonly used in the literature are the Ziegler-Nichols Step Response Tuning and Frequency Response Tuning Methods as explained in (Åström and Hägglund 1995). For the Frequency Response Tuning Method the tuning of the parameters are based around the ultimate gain ( $K_u$ ) and the period of oscillation of the system ( $T_u$ ). Other more complex methods of tuning the PID gains were discussed in more detail in Section 2.5.1 which are typically suited to offline optimisation, while some offer limited online optimisation such as gain scheduling.

In this study, the PID controller gains are determined using offline optimisation of the controller performance. To facilitate the offline tuning of the controller, it is advantageous to have an accurate model of the system being controlled. Once an acceptable baseline of the performance has been achieved on simulation, further tuning should be performed online to fine tune the controller performance. The simulated response of the quarter car vehicle model, from Section 4.2.2, for a particular set of controller gains is optimised over a limited time manoeuvre/simulation. The motion of the vehicle in response to a known disturbance is calculated and the influence of the controller outputs evaluated. The resulting motion is tuned through optimisation of the controller gains to determine the 'best' response across the entire simulation time.

The gains for the PID controller used here are determined through a simulation of three seconds, using a step bump disturbance identical to that seen in Figure 8.1. The controller gains are chosen to minimise the sprung mass acceleration, resulting from the bump disturbance, by satisfying a cost function comprising of the Key Performance Indicators for Ride Comfort that were proposed and described in detail in (Anderson and Harty 2010; Blundell and Harty 2014) and are recreated here as Equations 6.1 and 6.2.

$$KPI_1 = \left( 5 - \sqrt{\frac{\int_0^t (filt(\ddot{Z}_s))^2 dt}{t}} \right) \cdot 2 \quad (6.1)$$

Equation 6.1 refers to the motion of the body in the primary ride frequencies. The Key Performance Index  $KPI_1$  refers to the duration and magnitude of accelerations of the sprung mass in the primary ride frequencies of between 0 Hz and 3 Hz. The value of  $t$  refers to the duration of the oscillations within the frequency band, while the *filt* term refers to the filtering process performed on the sprung mass acceleration in heave ( $\ddot{Z}_s$ ). The sprung mass accelerations are filtered using a low-pass, four pole, Butterworth filter with a cutoff frequency of 3 Hz and a sampling frequency of 1000 Hz. The Butterworth filter is used here to ensure a smooth transition between the low frequency pass-band and the stop-band with maximal flatness in both the pass-band and stop-band.

The value  $dt$  refers to the sampling time of the data which for the purposes of this study is 0.001 seconds. Integrating the square of the filtered acceleration ensures equal influence for both positive and negative acceleration values.  $KPI_1$  is linked to the severe discomfort threshold experienced by a passenger in the 1-2 Hz range in relation to the ISO 2631 standard, with an RMS value of 5 m/s<sup>2</sup> equating to severe discomfort for one hour of exposure.

$$KPI_2 = \left( 3 - \sqrt{\frac{\int_0^t (filt(\ddot{Z}_s))^2 dt}{t}} \right) \cdot \frac{10}{3} \quad (6.2)$$

The process for calculating the Key Performance Index  $KPI_2$  is similar to Equation 6.1, referring to the duration and magnitude of accelerations of the sprung mass in the secondary ride frequencies between 3 Hz and 20 Hz. For the second KPI, the sprung mass accelerations are filtered using a high-pass Butterworth filter with a lower cut-off frequency of 3 Hz and the same sampling frequency of 1000 Hz. Both filters utilise zero phase shifting through the use of the MATLAB *filtfilt* function, which performs filtering in both the forward and backward directions.

Both equations calculate a Key Performance Index value in the range 0 to 10. The value 10 results in a very comfortable ride and improved ride comfort and 0 results in 'severe discomfort' and potentially damaging accelerations for the passengers, should these accelerations be prolonged. These values correspond to the ISO 2631 standard discomfort boundary as stated in (Anderson and Harty 2010; Blundell and Harty 2014). the adoption of these criteria enable to quantify the ride comfort. The values from Equations 6.1 and 6.2 are used in Chapter 8 to analyse the performance of the controller and assess the performance for the full car semi-active suspension controllers from Chapter 7.

The cost function shown in Equation 6.3 uses the KPI equations to calculate the controller performance for each set of controller gains.  $KPI_1$  and  $KPI_2$  are assumed to be in the range 0 to 10 for any given set of sprung mass acceleration values. The larger values of  $KPI_1$  and  $KPI_2$ , the smaller the values of the cost function.

The cost function is minimised using the *fmincon* command in MATLAB which uses the Interior Point Optimisation Method by default (The Mathworks Inc. 2021). Note that the values of  $K_P$ ,  $K_I$  and  $K_D$  are not included in the main cost function equation except on the left hand side. This shows, that the cost function value is influenced by the choice of parameters but not used directly in the equation. Instead, during each of the three second simulations the controller gains, provided by the solver, have a lasting impact on the response of the sprung mass acceleration ( $\ddot{Z}_s$ ) and are considered to remain constant for the length of each simulation. The resulting value of the sprung mass acceleration is then filtered and used in line with the conditions stated by the KPI in Equations 6.1 and 6.2 which indirectly influences the value of the cost function.

$$J(K_P, K_I, K_D) = \arg \min \left( (10 - KPI_1(\ddot{Z}_s)) + (10 - KPI_2(\ddot{Z}_s)) \right) \quad (6.3)$$

To evaluate the choice of controller gains a PID tuning application was created that performs the same three second simulation as used by the controller gains optimisation process. The passive response of the vehicle is calculated and the acceleration of the sprung mass is produced in the plot area shown in Figure E.1 of Appendix E. Meanwhile, the various sliders are also included to allow for the modification of the controller gains. The effect of any change in parameter values is simulated and their impact illustrated in an interactive plot.

The PID response to manual changes of the controller gains are illustrated using the PID tuning application shown in Appendix E. Table 6.1 summarises the influence of an increase of each of the controller gains with respect to observable changes in the sprung mass acceleration, rise time, settling time and Maximum Amplitude.

Increasing the proportional gain led the controller to act more aggressively but induced additional oscillations in the sprung mass accelerations with the control current varying largely between fixed step times as shown in Figure E.2. An increase of the integral gain reduced the unsprung mass accelerations error signal while offering the most desirable response for the current supply as the controller was only active during the disturbance rather being increasingly large. The derivative gain when increased results in a reduction of the oscillatory behaviour introduced by an increase of the integral gain. However, when increased on its own the system becomes increasingly oscillatory with rapid fluctuations in the damper current value given as the control output.

Table 6.1 Influence of Controller Gains on System Response

|   |  | $K_P$         | $K_I$                | $K_D$                |
|---|--|---------------|----------------------|----------------------|
| 1 | Rise Time<br>(Sprung Mass Displacement)  | Increase      | No Change            | Increase             |
| 2 | Settling Time<br>(Sprung Mass Displacement)  | Decrease      | Increase             | Increase             |
| 3 | Maximum Amplitude<br>(Sprung Mass Displacement)                                      | Decrease      | No Change            | Decrease             |
| 4 | Absement of Suspension<br>(Integral of Suspension Displacement with Respect to Time) | Decrease to 0 | Increase away from 0 | Decrease away from 0 |
| 5 | Positive Maximum Amplitude<br>(Sprung Mass Acceleration)                             | Increase      | No Change            | Increase             |
| 6 | Negative Maximum Amplitude<br>(Sprung Mass Acceleration)                             | Increase      | No Change            | Increase             |
| 7 | Integral of Control Action<br>(Current Supply to MR Damper)                          | Decrease      | Increase             | Increase             |
| 8 | Integral of Absolute Difference of Control Action                                    | Increase      | Increase             | Increase             |

## 6.4 Adaptive PID

The issues related to the use of linear controller gains to control a nonlinear system lead to varying results which heavily rely on the quality of the controller gain tuning achieved. An adaptive PID controller is proposed to overcome the issues related to the PID controller tuning process for a system with disturbances present and the changing nonlinear behaviour of the MR Damper models.

The proposed Adaptive PID controller relates the PID controller gains to key variables responsible for nonlinearity in the response of the system to a control input. Prior versions of an adaptive PID controller with dynamic gains typically involves gain scheduling or online optimisation of the controller gains in addition to other approaches that utilise online recursive least squares in addition to pole placement as seen in (Sahputro et al. 2017). However, this study proposes the use of the absolute displacement and absolute velocity of the damper piston, which are key influencing factors of the nonlinearity within the damper, to formulate the controller gains.

The proportional, integral and derivative gains of the Adaptive PID controller are each converted into functions which give a scalar values for each of the controller gains based on the sum of the controller gain components seen in Equations 6.4 to 6.6. By introducing nonlinearity of the controller gains, which is related to the displacement and the velocity of the damper piston, the fitting of the gain values are not generally limited to any specific scenario/manoeuvre but to the general motion of the sprung and unsprung masses.

$$K_P = P_1 + P_2 |(Z_s - Z_{us})'| + P_3 |(\dot{Z}_s - \dot{Z}_{us})'| \quad (6.4)$$

$$K_I = I_1 + I_2 |(Z_s - Z_{us})'| + I_3 |(\dot{Z}_s - \dot{Z}_{us})'| \quad (6.5)$$

$$K_D = D_1 + D_2 |(Z_s - Z_{us})'| + D_3 |(\dot{Z}_s - \dot{Z}_{us})'| \quad (6.6)$$

The adaptive gains  $K_P$ ,  $K_I$ , and  $K_D$  can potentially increase/decrease as a result of the tuning of the individual Adaptive PID controller gain components. In the current formulation of the adaptive gains, it is possible to utilise negative components. However, this is not advisable as there is the high probability that the absolute displacement or absolute velocity of the damper could potentially result in the adaptive gains for particular conditions becoming negative.

Even if in the case of the adaptive proportional gain, calculation the gain component  $P_1$  were to remain much greater than zero, the values of the gain components  $P_2$  and  $P_3$  would need to be much smaller in magnitude if both components were negative in values to ensure that the overall adaptive proportional gain remains positive. The same situation applies to the other components for  $K_I$  and  $K_D$ .

The block diagram in Figure 6.2 shows a simplified version of the Adaptive PID controller for the quarter car control of the MR Damper electrical current supply. Figure 6.2 illustrates the feedback loops for only one of the three adaptive gain. Note that similar loops exist as part of the feedback to the controller for the other two adaptive gains.

### 6.4.1 Tuning of the Adaptive PID Controller Gains

Tuning of the Adaptive PID is performed using a similar method to that used previously in Section 6.3.1. The main difference is the additional optimisation variables introduced into the controller optimisation process as a result of the various gain components that are specific to the Adaptive PID controller. The cost function for the Adaptive PID controller is therefore modified to that seen in Equation 6.7.

$$\begin{aligned} & J(P_1, P_2, P_3, I_1, I_2, I_3, D_1, D_2, D_3) \\ & = \arg \min \left( (10 - KPI_1 (\ddot{Z}_s)) + (10 - KPI_2 (\ddot{Z}_s)) + w_i \left( \frac{\sum_0^t I}{t} \right)' \right) \end{aligned} \quad (6.7)$$

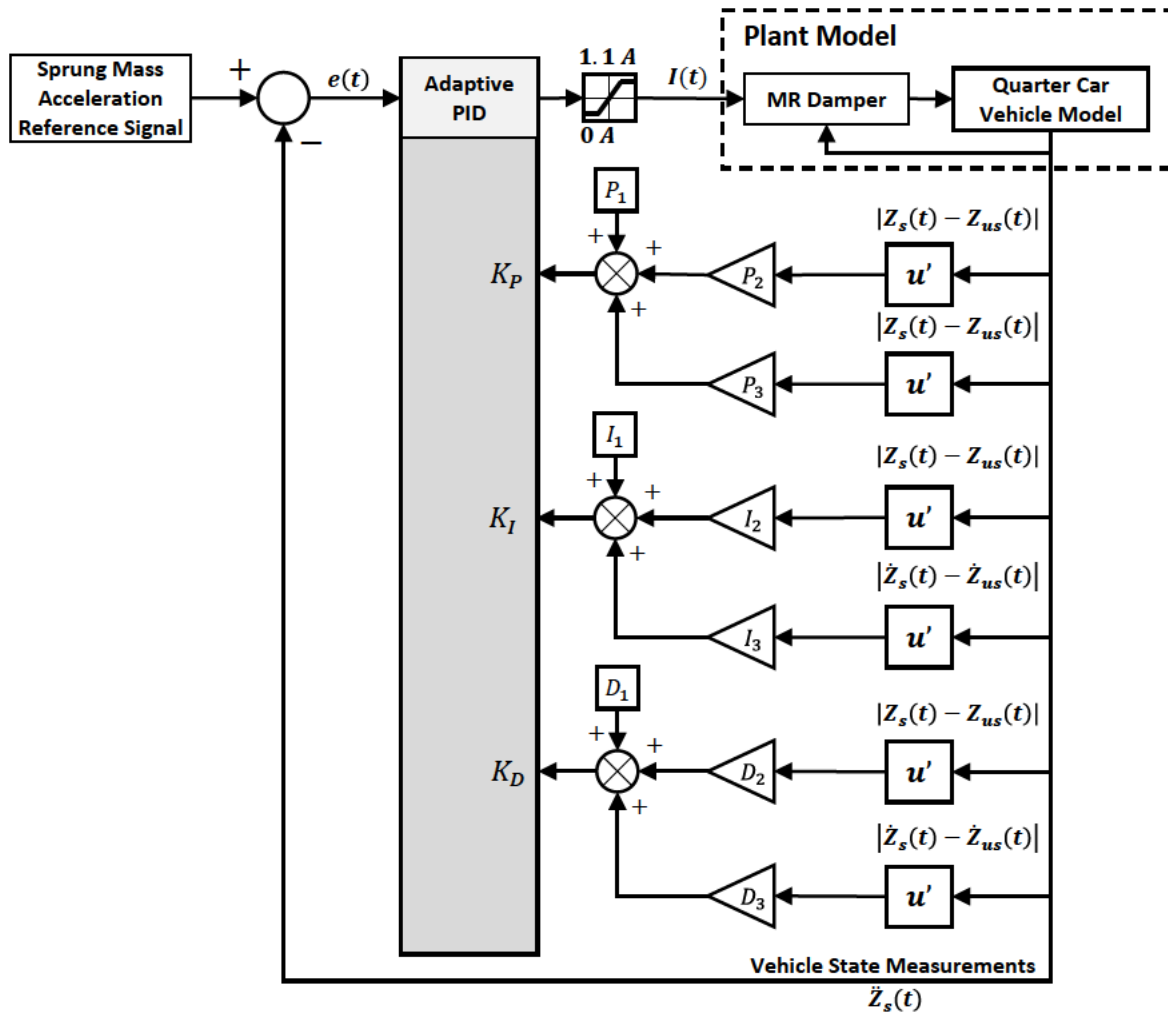


Fig. 6.2 A Simplified Block Diagram for the Quarter Car Vehicle Adaptive PID Controller

The Adaptive PID controller cost function focuses on meeting three objectives when the controller gains are chosen. Firstly  $KPI_1$  is utilised to maximise the ride comfort in the primary ride frequencies through the minimisation of the sprung mass acceleration. The next objective utilises  $KPI_2$  for the secondary ride frequencies of the wheel which is also attributed to the sprung mass acceleration and is in partial competition with the first objective. The final objective is the minimisation of the normalised weighted sum of the control action, which in the case described is the current supplied to the MR Damper. The final objective is important to avoid excessively large control actions that exceed the saturated range of between 0 A and 1.1 A. This term also improves the overall energy efficiency of the controller since the weightings can be configured to achieve a solution with minimal control actions.

To ensure that the adaptive controller gains for this study remain greater than zero the components were each given a lower bound constraint of zero. This forces the adaptive

controller gains to be greater than zero for any value of the displacement or velocity of the damper. Similar to the PID tuning process the impact each controller gain has on the system response was evaluated using the extended version of the PID tuning application seen in Figure E.3 of Appendix E.

The Adaptive PID controller's performance is compared to the PID from Section 6.3 to identify the overall benefits of the controller. This comparison is performed later in Section 8.4 highlighting how the controller gains change with respect to the relative suspension motion. The Adaptive PID is also compared to the quarter car NMPC strategy in Chapter 8 to determine the most efficient controller for quarter car semi-active MR damper based suspension control.

## 6.5 Standard MPC

While the Nonlinear MPC strategy proposed in Section 6.6 is similar to standard MPC in many ways there are a number of differences that make it different from other approaches. Before these differences can be explained an introduction into how a standard MPC is formulated is necessary.

In a standard MPC for semi-active suspension there are three horizons that are of importance when determining the control action. Firstly, the control horizon determines the number and time intervals between control actions with control actions typically held constant between the time intervals. Secondly, the prediction horizon which is how far into the future a suitable vehicle model is used to predict the system states and outputs. The third of the horizons that are a part of standard MPC is the preview horizon. The preview horizon is typically only utilised when preview information is supplied to the controller from sensors on the vehicle. Like with the control horizon the preview horizon works at set time intervals and is limited in the overall length as the accuracy of the information collected deteriorates with increased distance beyond the sensor's optimal working range. Figure 6.3 shows a diagram illustrating the three horizons and the states of the system as they converge to the desired trajectory.

Each of the three horizons influence the speed and accuracy of the controller as shorter time intervals between control, prediction and preview information updates lead to a slower control system with increased accuracy. Theoretically, while the controller would perform better given the time, the limitations of the physical hardware for real world testing and use mean that the overall response of this controller is far from ideal.

Standard MPC also relies more on a linearised model of the plant system being controlled in order to determine the working area of the actuator and allow for constraining functions to force the solution to lie within the feasible area. However, linearising the plant model leads to model-plant mismatch which must be compensated by the controller to avoid divergence from the

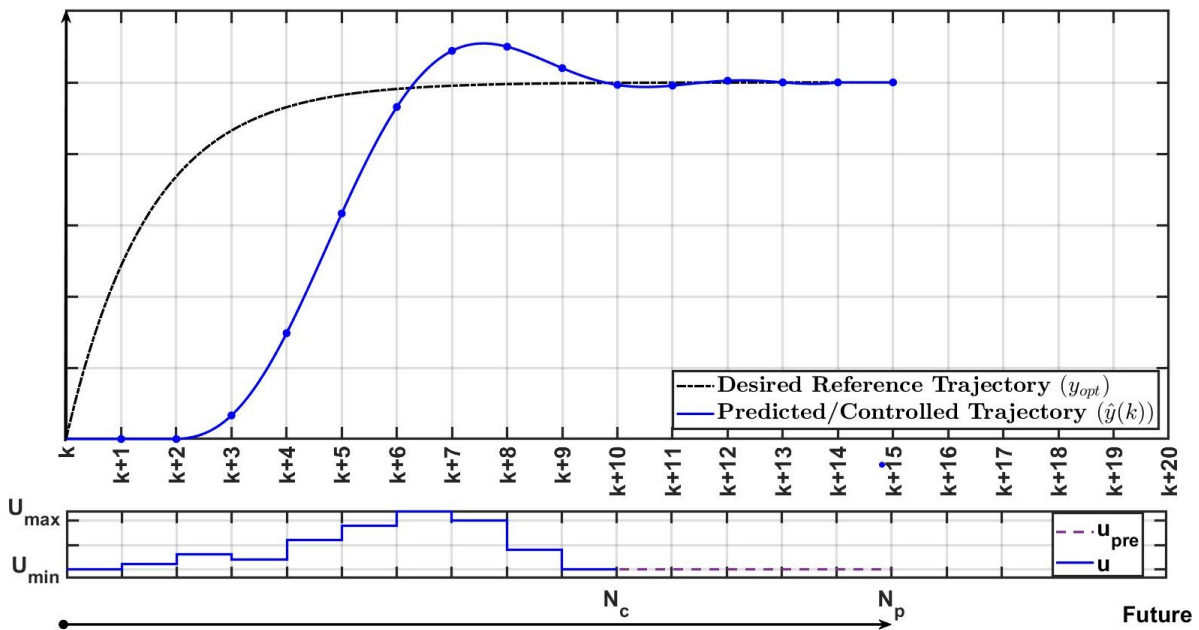


Fig. 6.3 A Diagram showing the three horizons of a standard model predictive controller

desired trajectory. Linearising based on the current for the nonlinear damper models discussed in Chapter 3, would be suitable in most cases where the damper current has a fairly linear relationship. However, the data collected during experimental testing shows nonlinearities that closely resembles that of a nonlinear first order system similar to that seen in (Strecker et al. 2015). In addition, the system shows nonlinearity with the current across various frequency values which result in the system deviating from the first order system representation as the frequency changes. The resulting changes make a linearised MPC strategy less than ideal and requires further development of the damper models in Chapter 3 with respect to multi-frequency responses.

## 6.6 Nonlinear MPC

This section proposes a Nonlinear Model Predictive Controller (NMPC) that optimises the value of the current supplied to the nonlinear MR damper models from Chapter 3. The controller utilises the dynamic behaviour of the nonlinear damper within the controller's formulation. It computes the optimal damper current by minimising a cost function exploiting the sprung mass acceleration of the quarter car vehicle model.

Unlike the controllers in Sections 6.3 and 6.4 the controller operates in discrete time with the controller outputs fed to the continuous time MR Damper and quarter car vehicle models that

form the plant system. The system shown in Figure 6.4 explains the process of implementing the NMPC controller within the continuous time system. The controller represented in Figure 6.4 consists of the components required for hardware implementation of the controller with the controller programmed onto a microprocessor ( $\mu P$ ) to perform the NMPC optimisation process and synchronisation maintained using the system clock signal.

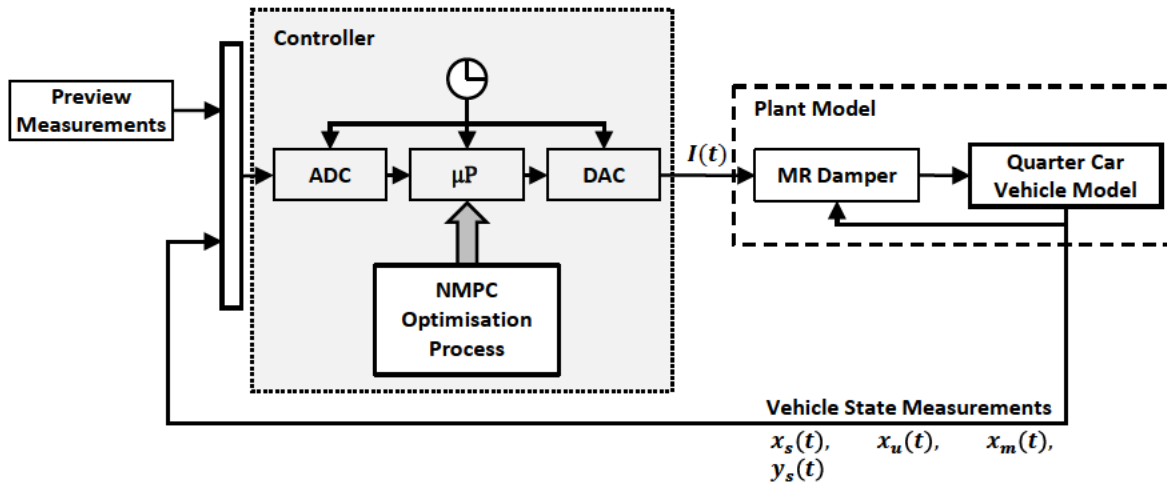


Fig. 6.4 An example showing the NMPC as part of the MR Damper based Semi-Active suspension system for quarter car suspension control

The controller samples the behaviour of the continuous-time system at discrete time intervals using an Analogue-to-Digital Converter (ADC). The ADC gives the controller model the required sample data about the system states and the necessary information to predict the future response of the system along the prediction horizon. This is achieved by utilising the measurements from a preview sensor providing the road/terrain height profile ahead of the vehicle. The authors from (Göhrle et al. 2015) explain how the road height profile can be estimated from camera measurements between "4 m and 18 m in front of the front axle" (Göhrle et al. 2015) which corresponds to a theoretical maximum preview time of 0.72 seconds when the vehicle is travelling at a velocity of  $90 \text{ km.h}^{-1}$  ( $25 \text{ m.s}^{-1}$ ).

For the NMPC controllers formulated in this study it is assumed that the sensor supplies a true representation of the road/terrain height profile to the controller. However, the author acknowledges that the real signal will include noise and error in the height measurements which increase as the vehicle speed and preview length is increased. Sensing and signal processing methods are beyond the scope of this study but are mentioned briefly in Chapter 2.

To generate a preview signal the road profile calculated by Equation 8.1 in Chapter 8 is fed to the controller in advance of the values being fed to the vehicle plant model used to generate the vehicle system outputs. The number of data points between the road profile identified by

the sensor and the moment the plant model is provided with the same profile data is configured as the preview length which is specified in each simulation case.

The discrete time controller output is supplied to a Digital-to-Analogue Converter (DAC) to generate a signal that is usable in continuous time. The DAC performs the Zero-Order Hold (ZOH) method on the output current as the microprocessor calculates the output current values at defined intervals rather than at every time period. The ZOH output of the controller output current ( $I$ ) is calculated using Equation 6.8 for each time step where  $T_s$  is the sampling time of the controller.

$$I(t) = I(k \cdot T_s) \quad \forall t \in [k \cdot T_s, (k+1) \cdot T_s] \quad (6.8)$$

The controller output, that has been held using the ZOH method, is then supplied to the transfer function representing the current lag effect. The latter calculates the effective current ( $I_{e|k}$ ) and then supplies it to the MR Damper model. The feedback signals of the suspension deflection and velocity are provided to the MR Damper model as part of the plant model. They are used to calculate the force of the damper. The road disturbance is fed to the quarter car vehicle model as part of the system inputs to calculate the new response of the vehicle.

### 6.6.1 Defining the Quadratic Problem (QP)

The Nonlinear Model Predictive Controller (NMPC) is defined using the vehicle model from Section 4.2.2. The model's state space systems are converted from continuous time to discrete time via the ZOH method. However, while other discretisation schemes are available to convert from continuous time to discrete time such as First-Order Hold (FOH), and least squares methods offered by the *c2d* command in MATLAB (The MathWorks Inc. 2021) the ZOH method was found to offer the best reproduction of the continuous time states in discrete time. In addition, to the ZOH method being the default option of the *c2d* command a number of other studies utilise this method including (Gohrle et al. 2014).

A sample time ( $T_s$ ) of 0.001 seconds is used to reflect the sampling time of the INSTRON tensile testing machine used for collecting the physical MR Damper test data, see Chapter 3. As the vehicle model from Section 4.2.2 consists of two separate state space models, the controller uses two sets of discrete state space matrices to describe the motion of the quarter car vehicle.

The first set of equations are used to describe the motion of the vehicle body with the states being updated at the next time step by Equation 6.9. In addition, the system output vector ( $y_s$ ) from the sprung mass system calculated using Equation 6.10 is identical to that presented in Section 4.2.2.  $y_{s|k}$  represents the system output vector's value at time  $t = kT_s$ . The other key differences in the notation is the use of the subscript  $d$  to represent the discrete matrix versions

of the  $A_s$ ,  $B_s$ ,  $C_s$  and  $D_s$  matrices. The subscripts for  $\Gamma_d$  and  $\Gamma_{d1}$  are also used to represent the discrete versions of  $\Gamma_s$  and  $\Gamma_{s1}$  respectively.

$$x_{s|k+1} = A_d x_{s|k} + B_d u_k + \Gamma_d \omega_{s|k} \quad (6.9)$$

$$y_{s|k} = C_d x_{s|k} + D_d u_k + \Gamma_{d1} \omega_{s|k} \quad (6.10)$$

The second discrete state space system used to describe the motion of the unsprung mass and update the unsprung mass system states for the next time step are given by Equations 6.11 and 6.12. Once again the system inputs and outputs mirror those of their continuous time counterparts shown in Section 4.2.2. The unsprung mass discrete matrices are identifiable by the additional 1 in the subscript. The exceptions being the discrete versions of  $\Gamma_u$  and  $\Gamma_{u1}$  represented by  $\Gamma_k$  and  $\Gamma_{k1}$  respectively.

$$x_{u|k+1} = A_{d1} x_{u|k} + B_{d1} u_k + \Gamma_k \omega_{u|k} \quad (6.11)$$

$$y_{u|k} = C_{d1} x_{u|k} + D_{d1} u_k + \Gamma_{k1} \omega_{u|k} \quad (6.12)$$

In addition to the two discrete systems for the vehicle model, the transfer function used to represent the time lag for the MR Damper's response to the current supply must also be represented within the controller. To accommodate this a separate discrete state space model is used to determine the response of the effective current of the damper. This system is easily obtainable using MATLAB to perform state space conversion and continuous to discrete conversion of the transfer function shown in Figure 4.2 during the simulation initialisation phase. The system matrices of the resulting time-invariant discrete state space model are given by the matrix variables  $A_m$ ,  $B_m$ ,  $C_m$  and  $D_m$ . They are used both within and outside of the proposed NMPC strategy.

The proposed vehicle model from Section 4.2.2 combined with the time lag effect of the MR Damper responding to the current supplied is not compatible with standard quadratic problem solvers. This is a result of the coupling of the two system as the unsprung mass states must be passed between the two systems before the calculation of the next set of sprung mass states. Therefore, a new computational algorithm which is specifically suited to the coupled system is proposed.

### The Computational Algorithm

The computational algorithm proposed here begins by assuming that the system states for both the sprung and unsprung mass systems are known or are equal to zero at the initial

condition. The algorithm uses this knowledge to determine the shared outputs of both systems and predefine them for the initial condition. The procedure of calculating the future vehicle dynamic response values then follows the process shown in Figure 6.5 where the values at the initial time step are used to obtain the values at the next.

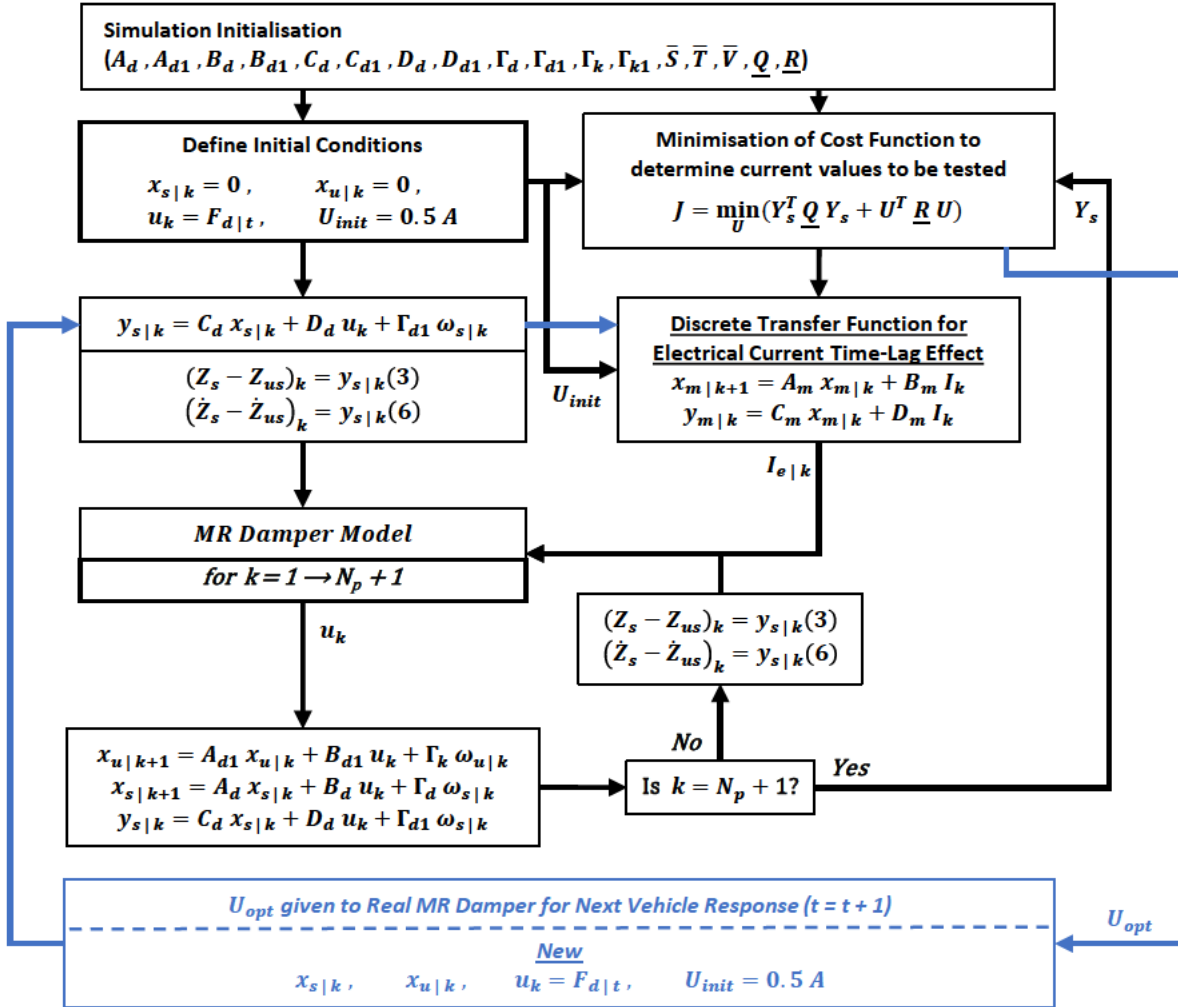


Fig. 6.5 A Process Flow Chart Detailing the Proposed Computational Algorithm

The optimisation of the current supply is performed using *fmincon* at every fixed step time interval. *fmincon* minimises the cost function to determine the optimal current. The cost function, defined by Equation 6.20, relies on an iterative cycle which determines the response of the vehicle to a given vector of current values provided by the solver.

The beginning of the iterative cycle uses the same discrete system matrices at each iteration and every time step. The calculations performed within the controller can be accelerated by utilising persistent variables. The values which are held as persistent variables are cleared and redefined whenever there is a change to the system matrices, which is generally performed

during the simulation initialisation phase. It can be seen in Figure 6.5 that once the system matrices have been defined and the initial condition provided, the response at the current time step is calculated to determine the displacement and velocity of the MR damper at one sample time ahead.

The discrete state space system shown in Equations 6.13 and 6.14 is used to represent the transfer function for the current time-lag effect introduced previously in Figure 4.2. The discrete transfer function state space model is used in conjunction with the vector of current values provided by the solver to determine the current to be supplied to the damper at each sample time of the prediction horizon. This limits the current supplied to the damper for predictions to the effective current ( $I_{e|k}$ ) as an output of the model which in turn is then fed to the MR Damper model at the specified sample time to calculate the damping force.

$$x_{m|k+1} = A_m x_{m|k} + B_m I_k \quad (6.13)$$

$$y_{m|k} = C_m x_{m|k} + D_m I_k \quad (6.14)$$

The damping force calculated using the damper model is then used as part of the calculation for the future unsprung mass states, using the  $k^{th}$  values of the sprung and unsprung mass states to advance the predictions of the system states ahead by one sample time. The output vector is then calculated using the current sample time's system states. The new output vector is then used to calculate both the displacement and velocity of the damper for the next time step. It is important to note that the MR Damper response used in the controller prediction model is not always represented by the modNVEP model, this can be changed based on the user's own judgement. However, unless otherwise stated, this study utilises the modNVEP model for the damping force predictions due to the accurate reproduction of the MR Damper response combine with its selection to represent the response of the damper as part of the vehicle plant model.

Once the iterative cycle is complete and the process loop shown in Figure 6.5 has reached enough calculated values of the future states and outputs to match the prediction horizon length ( $N_p$ ), the value of the cost function ( $J$ ) is determined. Finally, the optimisation solver chooses a new set of current values ( $U$ ) for evaluation of the cost function. To speed up the optimisation process at each time step, the number of iterations for evaluating the cost function using a new current control vector is limited to 35. The limitation on the number of the iterations were decided after observations of the results shown in Figure F.1 of Appendix F and other similar occurrences revealed that the solver converges to a near optimal solution after 35 iterations.

The cost function used in the optimisation process is derived from a typical quadratic program given in the form shown in Equation 6.15 where  $Q$  is the weight matrix associated

with the system outputs  $y_i$  and  $R$  is the weight matrix associated with the control variable  $u_i$ . Using the computational algorithm from Figure 6.4, the output values of the discrete time vehicle model are calculated from the current sample time ( $kT_s$ ) to the end of the prediction horizon ( $[k + N_p]T_s$ ).

$$J = \arg \min_{u_i} \left( \sum_{i=k}^{N_p} (y_i^T Q y_i + u_i^T R u_i) \right) \quad (6.15)$$

s.t.

$$u_{\min} \leq u_i \leq u_{\max}$$

The cost function in Equation 6.15 is subject to the upper and lower bounds for the control variable ( $u_i$ ), namely  $u_{\min} = 0$  A and  $u_{\max} = 1.1$  A. This differs from other studies which apply limits to the damper force or displacement to ensure that the controller does not exceed the physical limits of the damper. The physical limits of the suspension in terms of maximum suspension travel were not applied directly to the controller solver as weightings could be applied to the suspension deflection in order to achieve a similar result. The potential implications of this being that there could be opportunities where the rattlespace is exceeded and the suspension reaches the end of its travel making contact with the rubber bump stops. However, any cases where this occurs would be minimised since the control action would be chosen in order to return the suspension to a zero deflection state in order to reduce the overall cost incurred as part of the cost function in Equation 6.15.

In addition, the controller predictions are based on a theoretical maximum damping force of 8896 N which equates to the maximum tensile strength of the damper, as stated in (Lord Corporation 2009) and is enforced through saturation of the damper force resulting in any predictions that values which are infeasible due to excessive force automatically producing large cost function values.

The sum of the weighted outputs and inputs is calculated using matrix multiplication for speed and repeatability. The outputs for future sample times are collected to form the vector of system outputs across the entire prediction horizon ( $Y_s$ ). Similarly, the control inputs are rearranged into vector form to give the vector of control variables ( $U$ ). The forward expansion of the state space model across the prediction horizon using Equations 6.9 to 6.14 is performed to allow for the calculation of future sample time responses using the states from the current time step.

Equation 6.16 is used to represent the calculation of the system outputs vector. The matrix equation used to produce the result which is reliant on the  $k^{th}$  sample of  $x_s$  and the pre-calculated

values for the unsprung mass system states is given in vector form as  $\Omega$ . The disturbance input vector  $\Omega$  is constructed using the disturbance inputs ( $\omega_s$ ) for the sprung mass system seen in Equations 6.10 and 6.11. They are arranged vertically and consist of the values from samples  $k$  to  $(k + N_p)$ .

$$Y_s = \begin{bmatrix} y_{s|k} \\ y_{s|k+1} \\ y_{s|k+2} \\ \vdots \\ y_{s|k+N_p} \end{bmatrix} = [\bar{S}x_{s|k} + \bar{T}U + \bar{V}\Omega] \quad (6.16)$$

The matrix equation also uses the matrices  $\bar{S}$ ,  $\bar{T}$  and  $\bar{V}$  which are the result of the simplified version of the expanded state space forward expansion. The  $\bar{S}$  matrix is constructed using the product of the discrete system matrix  $A_d$  and output matrix  $C_d$ , as shown in Equation 6.17. This results in  $\bar{S} \in \mathbb{R}^{7N_p \times 2}$ . The matrices  $C_d$ ,  $A_d$ ,  $B_d$  and  $D_d$  are also used to produce the larger matrix  $\bar{T}$  as shown in Equation 6.18, resulting in  $\bar{T} \in \mathbb{R}^{7N_p \times N_p}$ .

$$\bar{S} = \begin{bmatrix} C_d \\ C_d \cdot A_d \\ \vdots \\ C_d \cdot A_d^{N-1} \end{bmatrix} \quad (6.17)$$

$$\bar{T} = \begin{bmatrix} D_d & 0 & \dots\dots\dots & 0 \\ C_d \cdot B_d & D_d & 0 & \dots & 0 \\ C_d \cdot A_d \cdot B_d & C_d \cdot B_d & \ddots & 0 & 0 \\ \vdots & \vdots & & \ddots & 0 \\ C_d \cdot A_d^{N-2} \cdot B_d & C_d \cdot A_d^{N-3} \cdot B_d & \dots\dots\dots & D_d \end{bmatrix} \quad (6.18)$$

The  $\bar{V}$  matrix used in conjunction with the disturbance input vector is similarly constructed to the  $\bar{T}$  matrix with the most notable changes being the use of  $\Gamma_{d1}$  along the primary diagonal instead of the  $D_d$  seen in Equation 6.18. The other change when comparing  $\bar{V}$  with  $\bar{T}$  is the use of  $\Gamma_d$  in the lower triangle rather than  $B_d$ . The remaining components of the two matrices remain the same with the upper triangles of the matrix occupied by zeros.

$$\bar{V} = \begin{bmatrix} \Gamma_{d1} & 0 & \dots\dots\dots & 0 \\ C_d \cdot \Gamma_d & \Gamma_{d1} & 0 & \dots & 0 \\ C_d \cdot A_d \cdot \Gamma_d & C_d \cdot \Gamma_d & \ddots & 0 & 0 \\ \vdots & \vdots & & \ddots & 0 \\ C_d \cdot A_d^{N-2} \cdot \Gamma_d & C_d \cdot A_d^{N-3} \cdot \Gamma_d & \dots\dots\dots & \Gamma_{d1} \end{bmatrix} \quad (6.19)$$

As the system output vector ( $Y_s$ ) can vary greatly with respect to the magnitudes of the various output values, especially the unsprung mass velocity ( $\dot{Z}_{us}$ ), the values of the outputs must first be normalised. By normalising the values of the output values the weightings applied to each of the values have more of a balanced impact on the value of the overall cost function and also ensure that the output values are of similar magnitude to the controller output.

The normalisation scheme proposed in this study involves the use of the passive response of the MR Damper vehicle model to obtain a suitable maximum and minimum for each of the output values ( $y_s$ ) which are then mapped to values between -1 and 1. It was decided that due to the potential impact the current supplied to the damper would have on the magnitude of each of the output signals, the absolute maximum values of the passive response outputs are doubled and used as maximum and minimum with opposing signs.

By doubling the maximum values for each of the passive response output signals and using these values as the maximum and minimum of the normalised range, an increase of any particular output signal more than twice the size of the passive equivalent receives greater penalisation than a signal within the normalised range.

The cost function shown in Equation 6.20 relates to the modified quadratic problem where  $\underline{Q}$  is a diagonal matrix with the weightings repeated for all discrete sample times that form the prediction horizon. Similarly,  $\underline{R}$  is a diagonal matrix for the weightings applied to the control variable as a means to minimise the control action while maintaining the system performance.

$$J = \arg \min_U \left( [\bar{S}x_{s|k} + \bar{T}U + \bar{V}\Omega]^T \underline{Q} [\bar{S}x_{s|k} + \bar{T}U + \bar{V}\Omega] + U^T \underline{R}U \right) \quad (6.20)$$

s.t.

$$U_{\min} \leq U \leq U_{\max}$$

The matrix equation from Equation 6.16 is used in place of the vector of system outputs ( $Y_s$ ), resulting in the removal of the sum operation seen in Equation 6.15. The values provided by the matrix equation shown in square brackets are normalised using the proposed normalisation scheme. The limitations on the controller current supply on the damper continue to be reflected

here by the lower bound constraint ( $U_{\min}$ ) of 0 A and upper bound constraint ( $U_{\max}$ ) of 1.1 A. There are no limitations on the rate of change of the current supply assuming that the change imposed by the controller is instantaneous. Additionally, suspension deflection limits are implied through the application of sufficient weightings on the suspension deflection to avoid reaching the bump stops.

### 6.6.2 Controller Output Sampling Time

The controller output sampling time has a large effect on the time the controller has available to determine a solution. The MR Damper cannot instantaneously respond to a current supplied and reach its steady state. However, the time between controller outputs can be used to manipulate the effective current of the damper. This is typically faster than waiting for the damper to reach steady state for a previous control input before a new control output is supplied. An example of this is when the damper current suddenly increases to a value of 1.1 A before needing to reduce to 0.2 A during the next controller output. Waiting for the damper to reach steady state to generate a new control action may reduce the ability of the controller to act on the latest inputs and associated predictions, which could potentially reduce the performance of the overall system.

The behaviour of the damper's response to current is delayed due to the time required to generate the resulting magnetic field and the magnetic particles within the fluid to align with the magnetic field. Such a delay is negligible and does not occur for the response of the MR fluid to compression as a result of the damper piston velocity. This is due to the fluid being already pre-loaded to avoid cavitation. This results in a complex problem to model at larger sample times as the damper's changing response to current and the velocity of the piston both require sufficiently fast sampling.

#### Dual-rate sampling for controller prediction horizon

An alternative to using optimisation to determine new current values at every millisecond sample time is through the use of the transfer function which was introduced into the plant model for addressing the current lag effect. As mentioned previously, the controller behaviour already includes this within the predictions as part of the computational algorithm seen in Figure 6.5. The current supplied to the damper can therefore remain constant for longer time periods. The change in the behaviour of the damper is approximated by using a low pass filter, implemented as a transfer function which accommodates for the fast control actions used for millisecond adjustments to the damper behaviour in response to current. The resulting system therefore employs a form of dual rate sampling for controller predictions.

In the cases where dual rate sampling is used, the controller actively calculates the response of the system using the current held between the sample time intervals of 0.01 seconds. The output from the DAC and the ADC shown in Figure 6.4 are synchronised to the 0.01 second interval using the ZOH method. The cost function still performs predictions based on intervals of 0.001 seconds to match the plant model.

The optimisation variables from the *fmincon* solver are then passed to the cost function which copy the same control action for 10 samples through the *repelem* command. This results in the control algorithm being kept constant for 0.01s. The sample time of the controller, with respect to the cost function, can potentially be varied by the user to reduce the number of optimisation variables while continuing to predict the behaviour of the damper for every millisecond.

This method is computationally more efficient than keeping the sampling for the prediction model at 0.001s. Increasing the sampling time, reduces the prediction horizon and associated number of function calls to the model used within MPC time. The accompanying reduction in the number of optimisation variables reduces the number of operations required by the solver to obtain a solution. Note that there are several alternative methods to achieve this behavioural characteristic, including utilising the ZOH method for the state space discretisation at alternative sampling times. However, the latter was not selected as keeping the damping force constant for the lower sampling rate would result in large model to plant mismatch. The latter would lead to worse MPC performance.

### Dual-Rate Sampling Comparison Simulations Setup

A comparison between the controller response using the 0.001 s intervals and the 0.010 s sampling intervals with the NonlinHBV model for damper force predictions was performed, see Figure 6.6. The simulation was performed using the step bump profile shown later in Figure 8.1 from Chapter 8 with a height of 0.02 m and utilised the quarter car vehicle parameters from Table 4.1. Both controllers were given the same preview length (0.1 seconds) to ensure that a direct comparison could be performed. While the controllers have the same preview length the number of prediction steps differ between the two approaches with the standard millisecond controller using  $N_p = 100$  and the dual-rate sampled controller using  $N_p = 10$ .

The results show that the controller sampled at 0.010 s is capable of minimising both the sprung mass displacement ( $Z_s$ ) and vertical acceleration ( $\ddot{Z}_s$ ) much faster than the 0.001 s case. However, while the controller sampled at 0.001 s also results in reductions in the displacement and accelerations of the sprung mass when compared to the MRPassive case (see Figure 6.6) the settling times of the two systems are considerably different.

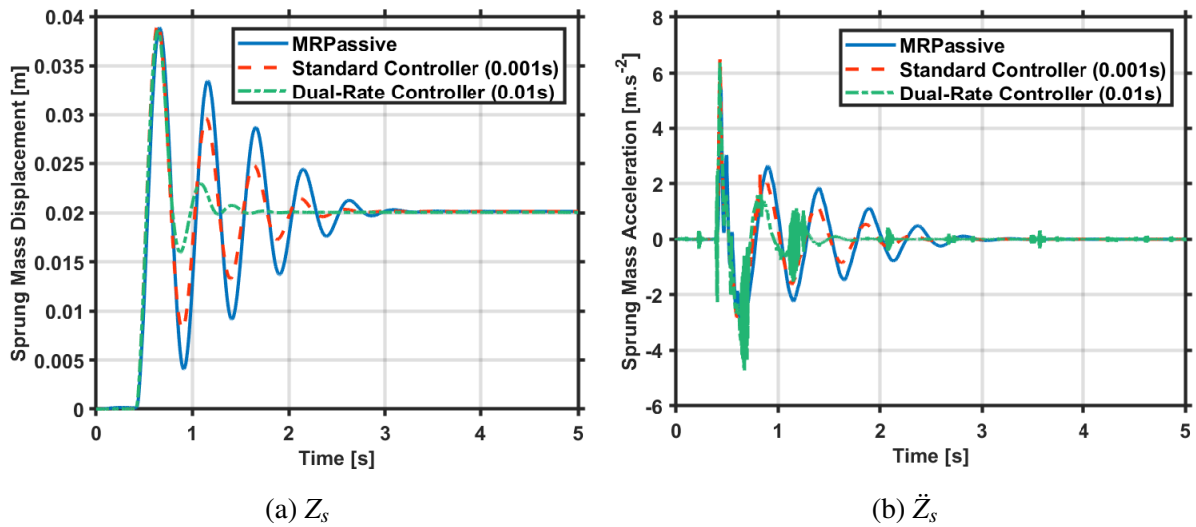


Fig. 6.6 Quarter Car Controlled Response over time for the two sampling time methods with a preview length of 0.1 seconds

The settling time of the Standard millisecond sampled controller is measured to be 2.404 seconds, while the Dual-Rate sampled controller measures 1.479 seconds, in comparison to the much slower MRPassive case with a settling time of 2.891 seconds. While the cost functions of both controllers are weighted identically the controller sampled at 0.01 s is unable to apply the same number of control actions. The differences between the controller's performance highlight how effective the dual-rate sampling method is at constraining the control action to find a suitable solution.

This limitation on the controller sampled at 0.01 s has the advantage to reduce the number of choices available to the solver. Which eliminates some regions with local minima that are less than optimal and typically speeds up the calculation time. However, through the exclusion of part of the solution space, this approach could in some cases remove the global minima from the region of feasible values, and may prevent the controller from reaching the global optimum, as the constant current between the samples could make it impossible to achieve an optimal solution.

The use of dual-rate sampled control using the NMPC strategy has the benefits of being faster, in addition to it providing the controller with the time required to find a solution. The method compromises on the optimality of the final solution to provide a solution that is capable of being implemented on real-time hardware for future testing. The controller with a sampling time of 0.001s is an ideal case solution, if tuned accordingly, but it is computationally expensive and slow to calculate for the longer preview lengths needed for greater performance.

The trade off between performance and time to obtain a solution is illustrated in Figure 6.7. The NMPC sampled at 0.001 s requires 500 preview steps to exploit terrain height prediction 0.5s in advance. It was simulated over several days to obtain 3 seconds worth of response data. This is much slower than real-time using a typical desktop computer. Therefore, implementation on an ECU is expected to result in even an slower computational time, thus making it unfeasible to use large preview times and large control horizons with the 0.001 second interval controller. It is important to note that Figure 6.7 uses parameters that differ from elsewhere in this study and have been provided in the figure caption for your reference.

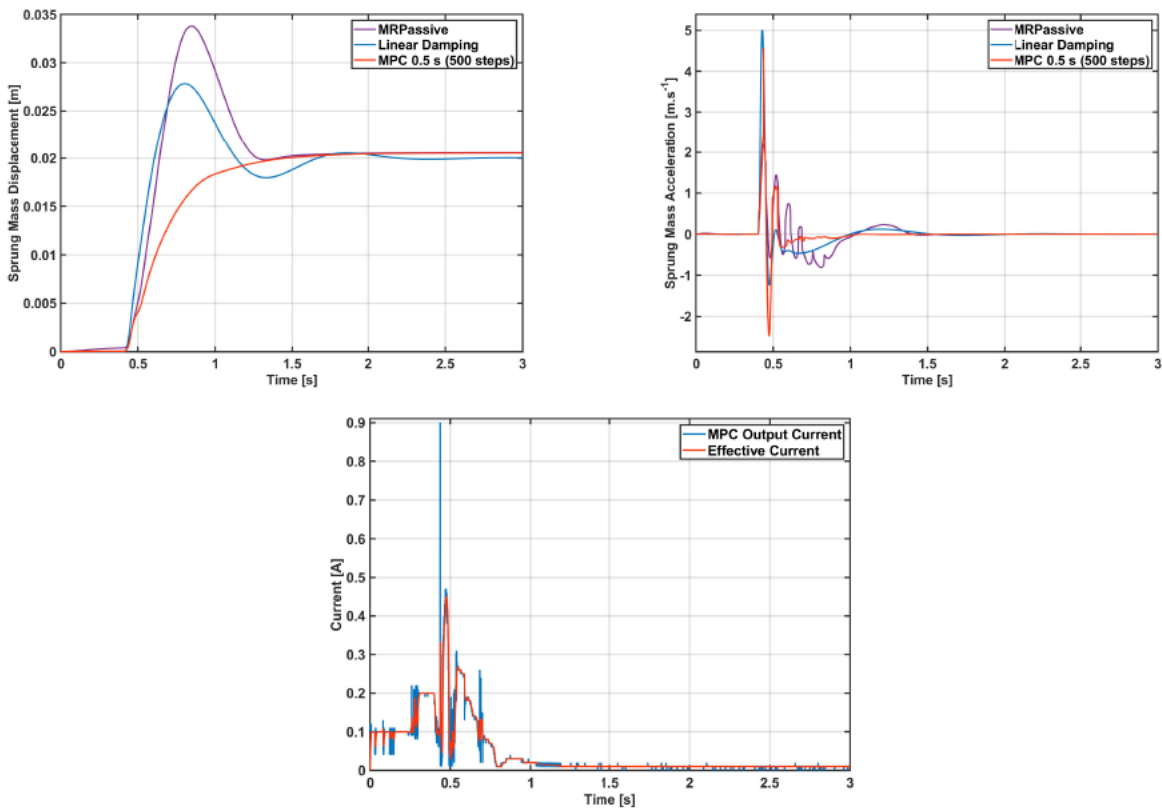


Fig. 6.7 Nonlinear Model Predictive Controller with Prediction/Preview Horizon of 500 steps (0.5 seconds),  $m_s = 500$  [kg],  $m_{us} = 50$  [kg],  $K_c = 21300$  [N/m],  $K_t = 270000$  [N/m], Vehicle Velocity =  $90 \text{ km.h}^{-1}$  ( $25 \text{ m.s}^{-1}$ ),  $Q = [0,0,0,0,0,0,1000]$ ,  $R = 0.1$

### 6.6.3 Controller Tuning and Horizon Lengths

The NMPC controller must be tuned correctly to obtain optimal results for each scenario however, certain considerations remain constant throughout whichever scenario is being simulated. Among the important considerations is the balance between performance and calculation time. A controller which can accurately determine the optimal control action but takes a significant

amount of time to perform the calculation is likely to miss the window of applying that control action. Similarly, a controller that is fast to calculate a response may not reach an optimal value and lead to degraded performance.

Section 6.6.2 highlighted the influence of the controller sample time on system performance with the ten millisecond controller calculating a response that while sub-optimal could potentially be feasible using existing hardware for real world applications. However, there are several other alternative methods that can be applied to speed up the controller's calculation time which have varying results on overall controller performance.

Among these strategies the simplest method is reducing the maximum number of iterations the solver can perform before ceasing the optimisation process. By limiting the iterations a sub-optimal solution can be achieved which is close to the ideal solution. However, the lower the number of iterations the less likely the controller is going to converge to an acceptable solution, therefore iterations must also be balanced with the number of control variables to ensure that there is enough iterations per variable to achieve convergence. For the simulations conducted in this study the number of iterations were limited to either 35 or 100 except for those cases where it is expressly stated.

The number of control variables that the solver attempts to optimise in order to minimise the cost function is closely linked to the control horizon as mentioned in Section 6.5. The control horizon can be modified through both the sampling time which is discussed in Section 6.6.2 and the number of control actions calculated per sample time. Reducing the control horizon reduces the number of control variables the solver must optimise, but it also influences the controller performance as it can lead the control actions to become more aggressive. The resulting trade-off balances the need for a reduced calculation time with the energy efficiency of the control actions. Energy efficient control actions in the case of semi-active suspension are when the damper current is minimised so that a supply of current is only applied at low magnitude and/or short intervals to minimise the energy used to maintain the higher damping conditions.

During cases where the prediction horizon is greater than ten control variables it was determined that the control horizon would be limited to ten control variables to ensure that calculation speed is maintained over larger prediction horizons. In comparison, the results from Figure 6.7 took several days to achieve a prediction and control horizon of 500 steps using the millisecond controller which is not feasible for real world applications. Additionally, the MR Damper is assumed to be in the MRPassive state, to ensure that future predictions beyond the control horizon remain accurate enough that the control variables minimise the sprung mass accelerations over the entire prediction horizon. The utilisation of the MRPassive state for control actions beyond the control horizon is similar in principal to the approach illustrated

back in Figure 6.3 which shows the minimum control input used beyond the control horizon as part of the Standard MPC approach.

The preview horizon length in this thesis is considered to be of the same length as the number and quantity of prediction steps to allow for an accurate prediction of the vehicle states including the MR Damper velocity calculations for each millisecond. However in a real world test condition sensor data could be delayed or lost on the internal communications network of the vehicle this study focuses on the performance of the controllers under ideal conditions.

Figure 6.8 shows an example comparison between two identical simulation conditions with only the prediction horizon changing in length. The parameters for the simulation are given in Tables 4.1 and 8.1.

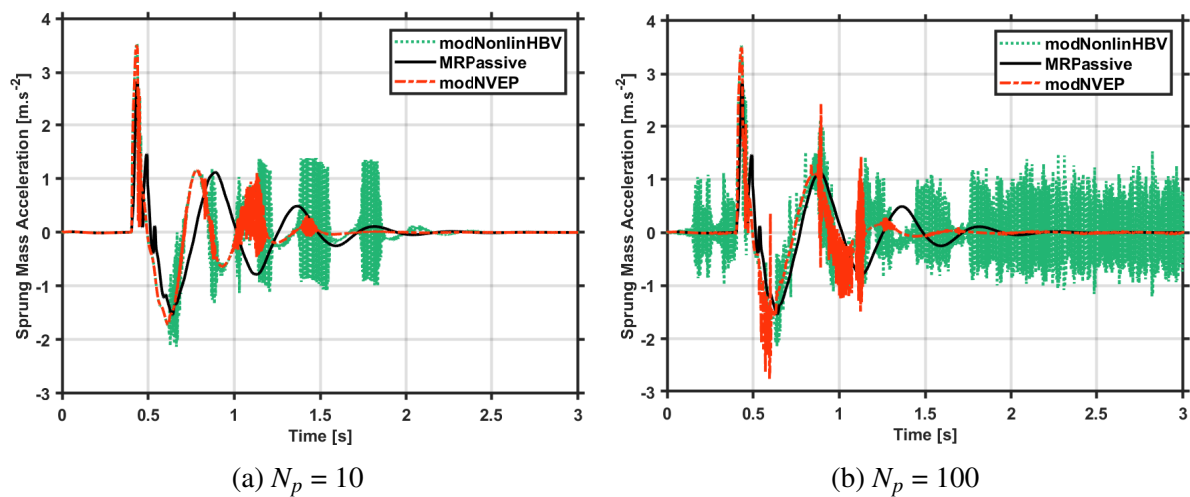


Fig. 6.8 A Comparison between the NMPC Controller for bump step of height 0.02 m travelling at a velocity of  $90 \text{ km.h}^{-1}$ .

The clear difference seen in the Figures 6.8a and 6.8b is the oscillatory behaviour that occurs after 1.5 seconds which is more aggressive on Figure 6.8b due to the longer prediction horizon. It is important to note that this is the result of too much control action as the controller must constantly correct itself. Whereas in Figure 6.8a the oscillations die out after the two second mark. Figure 6.8 highlights how the weightings must be adjusted to accommodate and gives a brief insight into the complexity of finding the optimal weighting for a given prediction horizon. Further investigation into the impact of the prediction horizon length on the controller performance is performed in Section 8.4 of Chapter 8.

#### 6.6.4 Adapting the Controllers for Off-Road Use

There are some necessary changes that the Quarter Car Nonlinear Model Predictive Controller (NMPC) must have in order to operate effectively during the off-road simulations.

The necessary changes to the vehicle model for off-road simulations on soft-soil were described in depth in Chapter 5. There are additional changes that need to be made to the predictive model used in the NMPC controller to account for the changes in the wheel motion as a result of the tyre sinkage. The changes to the controller utilise the lookup table from the P-LUT method described in Chapter 5. This is used to predict the soil sinkage and apply it to the discrete vehicle model to determine the prediction horizon for the current time step. It is acknowledged that the current tyre-soil interaction models do not fully characterise the behaviour of the tyre sinkage. However, the proposed P-LUT table offers the best approximation of the soil sinkage for future predictions as the output is derived directly from the tyre-soil model. It is expected that future improvements in tyre-soil interaction models and computational power available on vehicles will improve the accuracy of the tyre sinkage predictions on various terrain types, including soft-soils.

As the wheel is assumed to be rigid, any sinkage of the tyre results in an equal motion of the wheel hub. The P-LUT method's lookup table for the static sinkage values offers the best estimation of the motion for the unsprung mass. The unsprung mass state space system was removed in Section 5.7.1 as the motion of the unsprung mass was limited to the sinkage value and small disturbances only. Another approach which was based on the residual motion of the sprung mass was introduced as the residual motion of the masses are already considered for the calculation of the tyre-soil model. The important aspect to consider is the motion of the sprung mass which increases or decreases the load at the wheel centre and results in problems with the ride comfort of the vehicle.

The lookup table which is used for the static sinkage computation requires the slip ratio to calculate the output value. The slip ratio can be assumed to remain constant between control actions and therefore can be sampled and held inside the controller at every fixed step of the simulation. Alternatively the calculation of the the tyre-soil interaction model, can be performed within the controller to anticipate the future slip ratio value.

This study focuses on the constant slip ratio approach, primarily due to the issues surrounding the prediction of the driver's intention to accelerate and brake in relation to the desired speed which would be required for accurate prediction of future slip ratio values.

As mentioned in Section 5.7.1 the calculations of the quarter car vehicle model used in the generation of the controller in Section 6.6 typically assumes the vehicle to operate around an equilibrium point with a value of zero for the displacement of the sprung and unsprung masses. However, the effects of the tyre sinkage cause the equilibrium point to shift downwards to accommodate for the vertical load balancing at the tyre-soil interface.

To ensure correct calculation of the controller predictions of the acceleration response the points must be re-centred to accommodate for this change. The correction values which are

calculated from the equilibrium points of the passive vehicle for a constant slip ratio value of 0.2, are applied to the values entering the controller. The slip ratio value was chosen to reflect the point on the longitudinal force curve (see Figure 5.5) where maximum traction is achieved and would reflect a stable reference point for the tyre-soil interaction model for any given model. The current sprung mass displacement correction ( $Z_{s|corr}$ ) and the current unsprung mass displacement correction ( $Z_{us|corr}$ ) are applied using Equations 6.21 and 6.22.

$$Z_s = Z_s - Z_{s|corr} \quad (6.21)$$

$$Z_{us} = Z_{us} - Z_{us|corr} \quad (6.22)$$

Additional calculations are necessary within the controller iteration process to enable the calculation of the unsprung mass displacement as a result of the tyre sinkage. The vertical force is calculated similar to Equation 5.23 with the force of the spring and damper calculated for the current timestep. The vertical force ( $F_z$ ) is then utilised for the calculation of the tyre-sinkage ( $z_0$ ) using the slip ratio value of the current timestep ( $sr$ ) as shown in Equation 6.23.

$$z_0 = \text{interp2}(F_{z|lut}, sr_{lut}, Z_{0|lut}, F_z, sr) \quad (6.23)$$

Equation 6.23 utilises the MATLAB *interp2* command to interpolate the lookup table from the P-LUT method at the query points of the vertical force and slip ratio values. The variables  $F_{z|lut}$  and  $sr_{lut}$  correspond to the range of vertical loads and range of slip ratios respectively defining the sample ranges of the interpolation.

$$y_{s|k} = C_d x_{s|k} + D_d u_k \quad (6.24)$$

$$y_{s|k}(1) = y_{s|k}(1) - Z_{s|corr} \quad (6.25)$$

$$y_{s|k}(2) = y_{s|k}(2) - Z_{us|corr} \quad (6.26)$$

$$y_{s|k}(3) = y_{s|k}(1) - y_{s|k}(2) \quad (6.27)$$

Equations 6.24 and 6.27 integrate the corrections for the sprung mass displacement and unsprung mass displacement to ensure that the values between each timestep incorporate the shift in equilibrium. The performance of the controller after the proposed changes are made to the controller are shown in Section 8.5.

## 6.7 Concluding Remarks

This chapter has presented three different controllers for the manipulation of the current supplied to a semi-active quarter car MR Damper suspension system. The first was a PID controller which is used to compare and identify the performance of the other two controllers during the simulation studies in Chapter 8.

The second was an Adaptive PID controller. It proposes a formulation which is unlike the linear PID, due to its ability to take into account some of the plant nonlinearities, through the adaptation of its gains. The formulation introduced in this chapter is a novel approach to controlling the semi-active suspension using the normalised suspension deflection and velocity to calculate the controller gain totals. The approach to modify the controller gains online is not a new concept, but mapping the change in controller gains to the relative motion of the suspension offers the ability to have larger control actions when the suspension is under the most motion.

The third controller introduced in this chapter was a Nonlinear Model Predictive Controller (NMPC) this model utilises a model of the plant to effectively predict the behaviour of the quarter car vehicle model from Section 4.2.2. The MPC's ability to exploit knowledge of the terrain ahead and predict the likely behaviour of the vehicle to a set of predicted control actions should make it the best in terms of performance for changing conditions.

The NMPC controller was also modified using the proposed changes in Section ?? for use on off-road soft soils through the removal of the unsprung mass equation of motion in favour for a lookup table of the tyre sinkage generated using the method described in Section??. As the tyre is considered to be a rigid wheel the resulting motion of the unsprung mass is therefore equal to the tyre sinkage when no other disturbances are present.

Each of the controllers presented in this chapter are compared in terms of their performance, to a given disturbance in Chapter 8 as part of the simulation studies.

# Chapter 7

## Nonlinear Full Car Semi-Active Damper Controller Design

### 7.1 Introduction

This chapter proposes three controllers for the control of semi-active MR Damper based full car suspension systems. Through the introduction of the other corners of the vehicle, Section 7.2.1 introduces a similar PID controller to that seen in Section 6.2. It minimises the vertical 'heave' acceleration by supplying the same current values to each of the four corners of the vehicle to improve vehicle ride comfort. This approach is limited to the minimisation of the heave acceleration only and as such is used as an example of a single objective controller for comparison with the other controllers presented in Section 8.4.

Section 7.2.2 further adapts the PID controller to utilise a form of adaptive cascade control, whereby the controllers associated with each corner of the vehicle utilise the Adaptive PID controller introduced in Section 6.3. The gains of the controller change with respect to the displacement and velocity of the dampers. This should lead to improved tracking performance compared to controllers with fixed gains which will be confirmed when the adaptive cascade PID controller is compared to the response of the PID controller in Section 8.4.

Section 7.3 introduces a full car version of the NMPC from Section 6.4 where the controller matrices are modified to account for the four corners of the vehicle and relate the motion of the vehicle body back to its centre of mass. Section 7.3.1 re-explores the concept of dual-rate sampling of the full car NMPC strategy to identify whether the introduction of the other dynamics associated with the full car model influence the performance of the dual-rate sampled controller. Section 7.4 summarises the key impact of this work in terms of control for on road suspension control and how it fits into the rest of the work conducted in this study.

## 7.2 PID and Adaptive Cascade PID Controllers

This section introduces the PID and Adaptive Cascade PID controllers for full car semi-active suspension control. The controllers are configured to minimise the vertical heave of the vehicle body as the primary objective in the controller optimisation process.

### 7.2.1 Full Car PID Controller

The PID controller from Section 6.2 is re-purposed for full car vehicle suspension control by applying the same control output for each of the four corners of the vehicle. This is performed by calculating the error between the vehicle body vertical 'heave' acceleration ( $\ddot{Z}_b$ ) and the vehicle body heave acceleration reference signal ( $\ddot{Z}_{b,ref}$ ).

Similar to the previous PID controller, for the quarter car vehicle model, the controller can be simulated as a continuous time controller within Simulink. In addition, the PID controller continues to only consider the vertical acceleration of the vehicle body and does not consider the pitch or roll directly within the error signal ( $e(t)$ ) to the PID controller.

Figure 7.1 shows a block diagram with simplified connections between the vehicle model and the PID controller. As there is no physical vehicle being used as part of the simulations in Chapter 8, the measured signals are supplied by the full car vehicle model and the modNVEP model for the MR Damper force calculations. Similarly to the quarter car PID block diagram

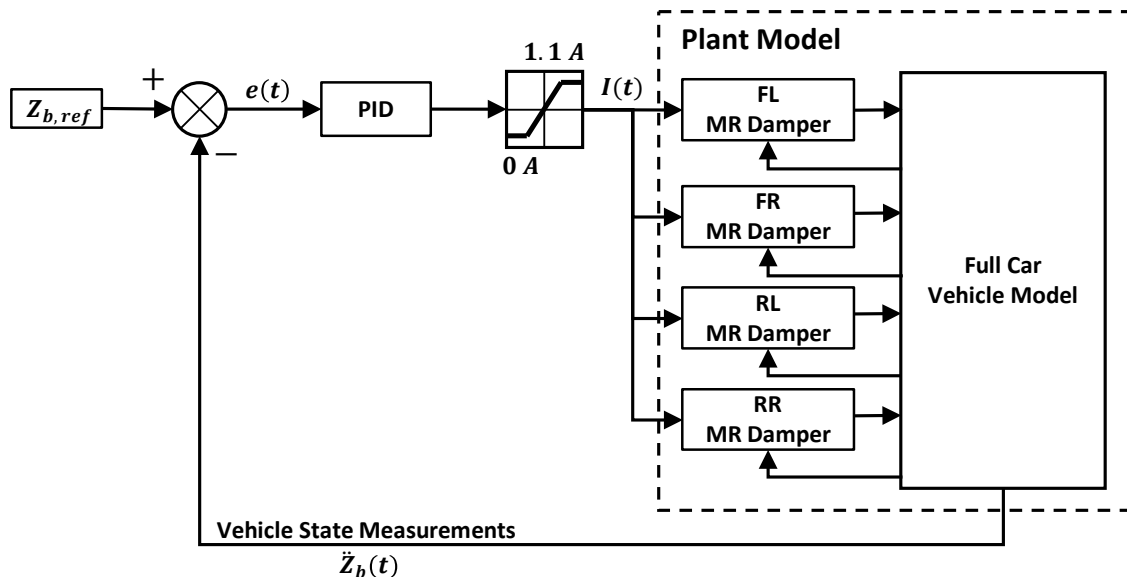


Fig. 7.1 A Block Diagram of the Full Car PID Controller

from Figure 6.1 the MR Dampers are supplied the relative displacement of the damper ( $Z_{rel,d}$ )

and the relative velocity of the damper ( $\dot{Z}_{rel,d}$ ). The controller is tuned using the method described later in Section 7.2.3 which is similar in comparison to the tuning method used earlier in Section 6.2.1 to tune the quarter car PID controller.

## 7.2.2 Adaptive Cascade PID Controller

The Adaptive Cascade PID Controller is a modified version of a typical cascade PID controller. The adaptive nature of the controller relates to the changing values of the proportional, integral and derivative gains with respect to the relative displacement and velocity of the MR Damper piston which was presented in Section 6.3 for use with the quarter car vehicle model.

The Adaptive Cascade PID Controller only uses the Adaptive PID controller from Section 6.3 in the inner control loop that is concerned with the roll acceleration of the vehicle as the final current is supplied to the MR Damper after this stage. Each adaptive PID controller, associated with one of the corners of the vehicle, considers the relative displacement and velocity of its respective corner.

Figure 7.2 shows a simplified block diagram of the three control loops that compose the Adaptive Cascade PID Controller. The inner loop is concerned with the roll acceleration and is given a set-point from the PID controllers for the pitch control for the front and the rear of the vehicle. The error between the roll acceleration set point passed down from the pitch controller and the roll acceleration measured signal is calculated depending on the corner being specified with the direction of the rotation considered as part of the error calculations for each side of the vehicle. The roll rotation clockwise around the x axis is considered positive. It results in positive downward pressure on the right hand side of the vehicle. The error signals for each of the four corners must therefore consider the direction of this pressure when calculating the response to oppose this motion.

From a corner by corner representation of the angular accelerations for pitch and roll, positive downward pressure on the respective corner/side is considered to be the positive direction. This results in the summation of the signals for each corner having different signs to calculate the error signal supplied to the Adaptive PID controllers. For example the pitch motion results in positive downward pressure on the front two corners of the vehicle. The calculation of the error for the front set-point should have a negative sign for the pitch acceleration of the vehicle body. The rear corners of the vehicle should have a positive sign to determine the error for the rear set-point.

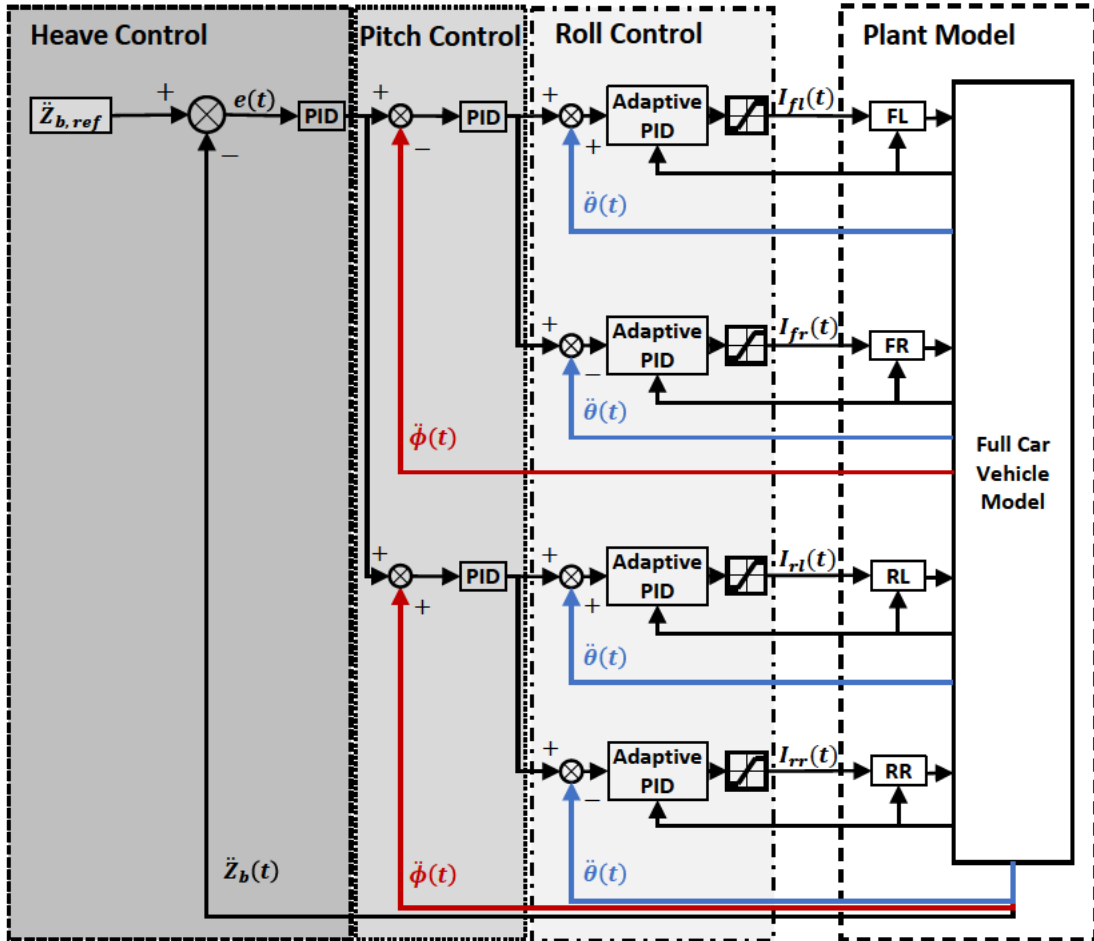


Fig. 7.2 A Simplified Block Diagram of the Adaptive Cascade PID Controller

### 7.2.3 PID and Adaptive Cascade PID Tuning

The tuning process for the PID controller is similar to the procedure used in Section 6.2.1. Equation 6.4 is reused and optimised to obtain the gain values for the controller. However, instead of using the response of the sprung mass acceleration, the vertical heave acceleration of the vehicle body is used in its place. The vertical heave acceleration is filtered according to the process described in Section 6.2.1. This tuning process ignores the angular motion of the vehicle body for the full car model and as such the controller is designed to meet the demands of a single objective.

The angular motion of the vehicle is therefore only impacted indirectly through the controller outputs at each corner and the respective damper displacements and velocities. The corners with larger displacements and velocities would result in larger forces in line with the modNVEP

damper model as described in Chapter 3 which would be amplified by the current from the PID controller. The disparity between the velocities at each corner would therefore result in some corners generating larger forces than others.

The Adaptive Cascade PID controller is tuned in a similar process to that described in Section 6.3.1 with some alterations. Similarly to the full car PID tuning process the sprung mass acceleration in Equation 6.8 is replaced by the vertical heave acceleration of the vehicle body for the full car. The approach taken in controller tuning of the Adaptive Cascade controller assumes that the controller tuning for one particular corner should also be identical to the other corners. This method ignores the differences between the corners in terms of response as this is considered by the normalised suspension deflection and normalised relative velocity of each corner.

It is also considered that the tuning of the controller for the outer loop heave acceleration should be tuned to the same gains obtained from the full car PID tuning. This avoids a situation whereby the controller gains of the heave and pitch controllers would settle around one while the adaptive PID controllers of the inner roll control loop would be much larger in magnitude. Pre-defining the controller gains for the heave acceleration led to lower controller gains at the lower levels which is increasingly important for the adaptive PID controllers where the values of the suspension deflection and relative velocity gain components can cause the gain totals to increase substantially.

Other approaches to tuning the Adaptive Cascade PID controller could be utilised in the future to explore how the controller gains for each control loop can be tuned more effectively to minimise their respective loop to achieve a much greater effect. However, the current controller tuning is considered adequate to provide a comparison with the full car NMPC described in Section 7.3.

## 7.3 Nonlinear MPC

This section identifies the process for formulating the Nonlinear Model Predictive Controller (NMPC) for a full car. It is an extension of the theory used in Section 6.4. The introduction of more actuators into the system increase the number of possibilities to reduce the accelerations of the vehicle body. However the control problem becomes more complex.

The controller developed in Section 6.4 cannot be wholly applied to the full car vehicle model as the quarter masses used in the quarter car vehicle model would change with respect to the motion of the centre of gravity and the angular motion of the vehicle body mass, which is not modelled by the quarter car vehicle model.

The controller from (Gohrle et al. 2013) provides the control of the actuator displacement or control force instead of the control current for the MR Damper. This approach is common in the literature, however, some studies control the current, see Section 2.4.1. The following process uses the nonlinear damper models and the transfer function for the current time lag to predict the forces of the damper. It allows for the minimisation of the control current for each corner of the vehicle at each time step.

Control of the suspension is once again performed by a simulated microprocessor at discrete intervals similar to that seen in Figure 6.3. It uses an Analogue to Digital Converter (ADC) and a Digital to Analogue Converter (DAC) with a fixed sampling rate. The Zero-Order Hold method is performed by the DAC to convert the discrete time control signal to continuous time using Equation 7.1

$$\underline{I}(t) = \underline{I}(k \cdot T_s) = \begin{bmatrix} I_{fl}(k \cdot T_s) \\ I_{fr}(k \cdot T_s) \\ I_{rl}(k \cdot T_s) \\ I_{rr}(k \cdot T_s) \end{bmatrix} \quad \forall t \in [k \cdot T_s, (k+1) \cdot T_s] \quad (7.1)$$

When the ZOH method is applied to the full car model, the four corners are independently held between the discrete intervals to form the vector  $\underline{I}_k$ . The control output is then fed into the transfer function to simulate the current lag effect at each fixed-step time interval to calculate the effective current ( $\underline{I}_{e|k}$ ) supplied to each of the four MR Dampers.

### 7.3.1 Defining the Quadratic Problem (QP)

The quadratic problem for the full car NMPC strategy shares a number of similarities to the one defined in Section 6.4.1. The key differences between the two include three additional control inputs per discrete sample time. In addition, the discrete vehicle model used by the controller is instead represented by the coupled full car vehicle model presented in Section 4.3.2.

To define the quadratic problem, the nonlinear full car model from Section 4.3.2 is discretised via the ZOH method. The discrete system matrices for the coupled state space systems of the quarter car model introduced the use of the matrices  $A_d$ ,  $B_d$ ,  $C_d$ ,  $D_d$ ,  $\Gamma_d$  and  $\Gamma_{d1}$ , see Section 6.4.1. This section reuses the same notation to represent the discretised versions of the vehicle body system matrices from Section 4.3.2. The discrete state space system for the vehicle body system of the coupled full car model from Section 4.3.2 is given by the Equations 7.2 and 7.3.

$$x_{b|k+1} = A_d x_{b|k} + B_d u_k + \Gamma_d \omega_{b|k} \quad (7.2)$$

$$y_{b|k} = C_d x_{b|k} + D_d u_k + \Gamma_{d1} \omega_{b|k} \quad (7.3)$$

The resulting system has 6 states ( $x_{b|k}$ ), 4 control inputs ( $u_k$ ) and an additional 8 disturbance inputs ( $\omega_{b|k}$ ). These inputs and states corresponds to the discrete versions of the system inputs previously described in Section 4.3.2. The system matrix notation of  $A_{d1}$ ,  $B_{d1}$ ,  $C_{d1}$ ,  $D_{d1}$ ,  $\Gamma_k$  and  $\Gamma_{k1}$  is also reused to represent the discrete versions of the matrices for the wheel mass system from Section 4.3.2.

### The Computational Algorithm

The computational algorithm is similar to the version introduced for the quarter car NMPC controller from Section 6.4. The development of the coupled state space systems from Section 4.3.2 results in a particular order of calculations shown in Figure 7.3.

The simulation initialisation phase pre-defines the controller matrices for  $\bar{S}$ ,  $\bar{T}$  and  $\bar{V}$  while also configuring the weighting matrices  $\underline{Q}$  and  $\underline{R}$ . The formation of the controller and weighting matrices are the same with respect to their construction using the discrete system matrices. However, the discrete system for the full car model has additional inputs and outputs and system states in line with the description of the system given in Section 4.3.2.

The damping force that is used to calculate the future predictions of the vehicle response is derived from the MR Damper models described in Chapter 3. This approach is similar to that described in Section 6.4.1 but is repeated four times using the respective displacements and velocities for the respective corners to calculate the damper forces.

The conditional loop used in the algorithm determines whether the entire prediction horizon's responses have been determined. The prediction horizon is considered equal to the control horizon. This results in a control action applied at every discrete sampling time, followed by the filtering from the transfer function used to represent the current lag effect seen in the damper responses from (Strecker et al. 2015).

The *fmincon* function is used to optimise the values for the current over the prediction horizon. The algorithm is limited to a maximum of 35 iterations to ensure that the calculation time is sufficient to produce a reasonable answer this is identical to the approach used for the quarter car NMPC controller. The optimal current at each time is then rounded to the nearest two decimal places of precision to ensure that the values are not needlessly small.

### 7.3.2 Controller Sample Time

The impact of the chosen sampling time was investigated to ensure that holding samples for the controller current for 0.01 s intervals would lead to improved/reduced performance when compared to the option of applying the control actions every 0.001 s and relying on the damper current lag effect to filter the effective current.

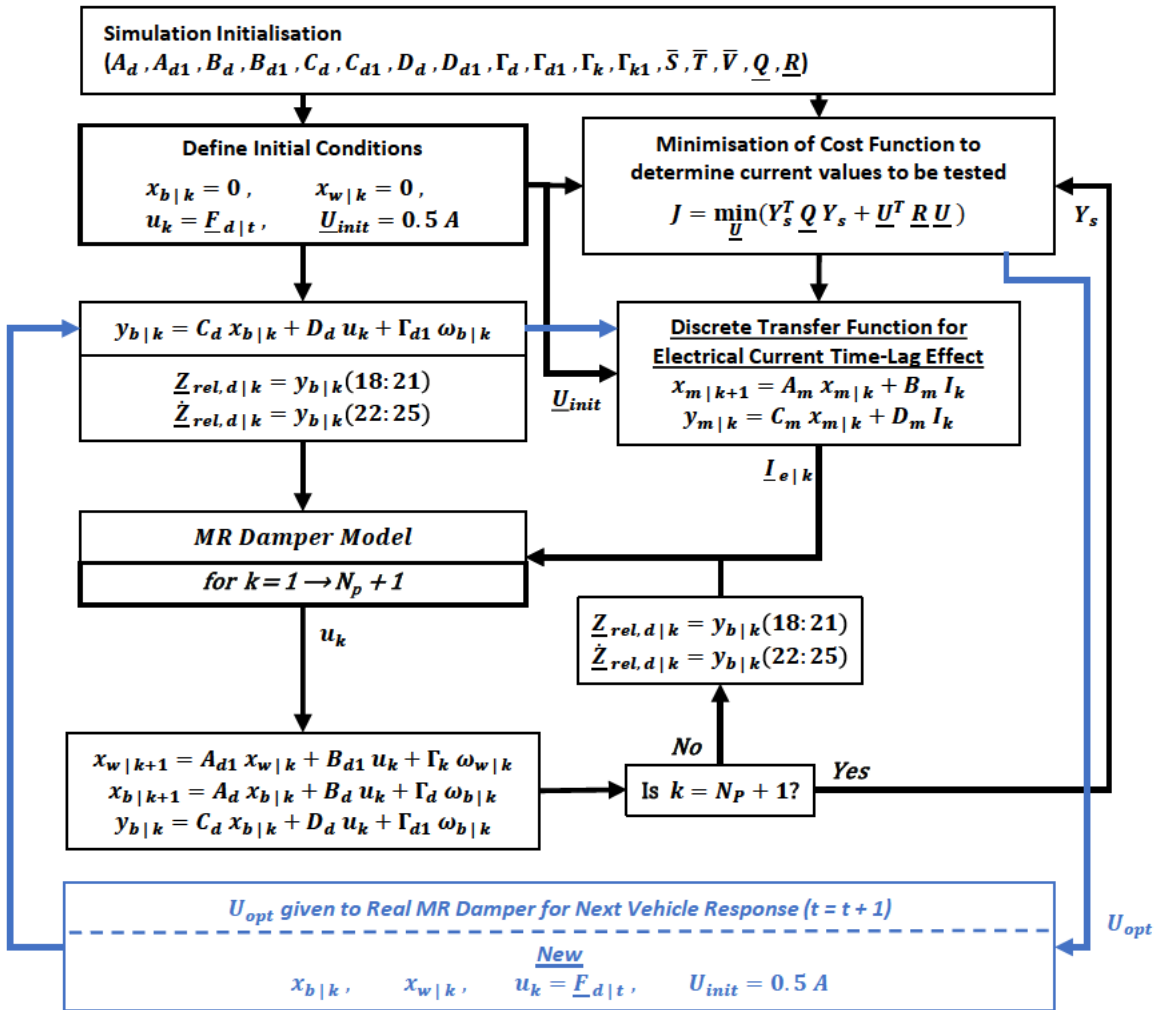


Fig. 7.3 The Full Car NMPC Algorithm

The controller effectiveness of the quarter car response seen in Figure 6.7 is improved when the controller current was held for 0.001 s intervals. However, while this is true for the quarter car response this resulted in an increased calculation time for long prediction horizons. This time would increase with the complexity of the system and the full car response would take much longer to acquire this result due to the increased number of actuators in the system. The use of 0.001 s intervals also relies on a minimum prediction horizon for the control to begin to operate as the optimum performance of the controller would often be considered to be the minimum current, especially for significantly shorter prediction horizons.

Additionally, while the controller is most effective when operated at 0.001 s intervals, it is assumed that the controller is able to compute the control action within this short time interval. This is not possible in practice with the current automotive electronic control unit (ECU) processing power.

It was noted in Section 6.6.2 that the damper current determined by the controller when operated at 0.001 s for the quarter car model is often held for 0.01 s or more. This led to the conclusion that sampling the controller at 0.01 s interval allows the time of calculation to be 10 times longer and also reduces the number of calculations required. A similar dual-rate sampling approach for full car control is explored here.

### Dual-rate sampling

The process of utilising dual-rate sampling was discussed in detail in Section 6.6.2 for the quarter car controllers. A similar approach to that described is employed here to determine the impact a dual-rate sampling approach has on the vehicle response. The simulation setup is described as follows:

- Vehicle Model from Chapter 4 is parameterised using the values from Table 4.3.
- Define Road Height Profile for Desired Vehicle Speed of  $90 \text{ km.h}^{-1}$  and Bump Height of 0.02 m using Equation 8.1 from Chapter 8.
- Controller Tuning Weight Parameters are defined as  
 $Q = \text{zeros}(25,1)$ ;  $Q(7) = 1000$ ;  
 $R = \text{diag}([1, 1, 1, 1])$ ;
- Limit Maximum Number of Solver Iterations to 35
- Set  $N_p = 30$  for 0.001 second controller
- Set  $N_p = 3$  for 0.01 second controller
- Run Simulation

The vehicle body mass, vertical displacement in response to the 0.02 m bump is shown in Figure 7.4 where the bump profiles have been included for reference. Figure 7.4 shows the moment of impact with the bump for both the front ( $Z_{r,f}$ ) and rear ( $Z_{r,r}$ ) axles. Short prediction horizons and the small number of control variables ensures that the simulation speed is improved, however the quality of the solution varies as a result of the controller iteration limit.

Figure 7.4 shows that the controller operating using the millisecond intervals method has a larger peak vehicle body displacement than both the passive (MRPassive) and the dual-rate sampled controller. The reduction after the peak however shows that while the controller is configured to minimise the heave acceleration as a result of the chosen weightings the controller does not automatically attempt to minimise the vehicle body displacement.

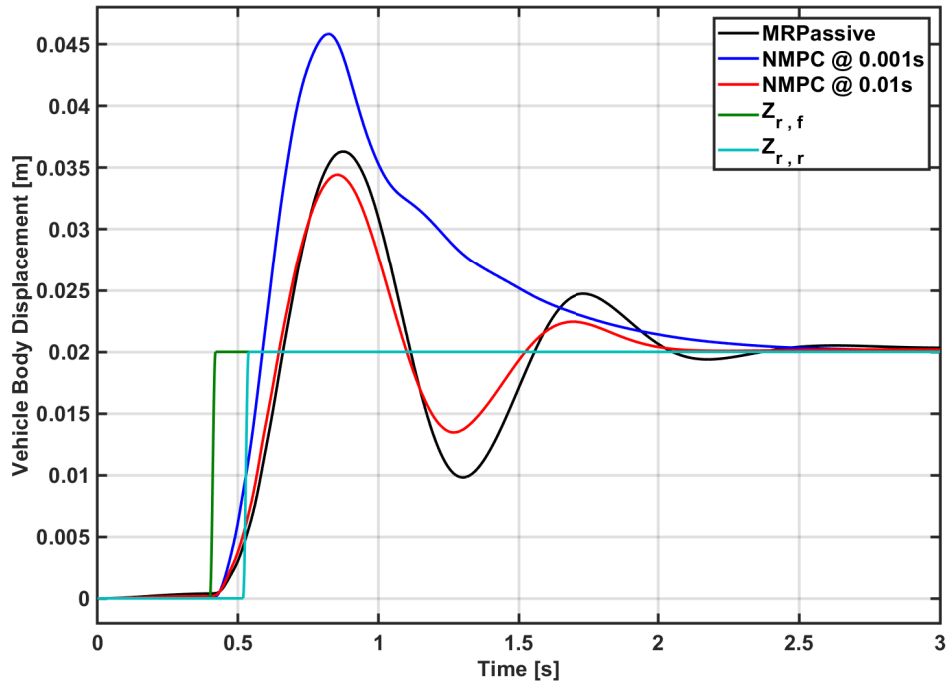


Fig. 7.4 Vehicle Body Mass Displacement over time for the two sampling time methods with a preview length of 0.030 seconds

It is also important to note that while these approaches use the same limit of 35 iterations to ensure a faster calculation. It is likely that the millisecond sampled controller is likely much further away from the optimum point after 35 iterations since the number of control variables is higher in the millisecond controller case. 35 iterations were chosen as the limit for the algorithm to converge to a reasonable solution based on the short prediction horizons and the required accuracy of the comparison test. However, even with the limitations imposed this would not be feasible for real-time implementation.

Further comparison between the controllers shows that the dual-rate sampled controller is the best in terms of minimising the vehicle body displacement. In terms of heave acceleration of the vehicle body mass seen in Figure 7.5, the dual-rate NMPC is slightly better than the passive system and the NMPC sampled at 0.001 s is the most aggressive, resulting in significantly lower acceleration after only 0.5 s. The moment the wheels on each axle hit the bump can be clearly seen in each of the cases as two distinct peaks in the acceleration values. The first peak in the acceleration values is seen at 0.45 seconds which signifies that the front wheels have made contact with the step bump's surface. The rear wheels follow with contact starting at 0.55 seconds, the time between the two induces the oscillatory motion of both the primary and

secondary ride frequencies which are damped out by the MR Damper controllers within two seconds.

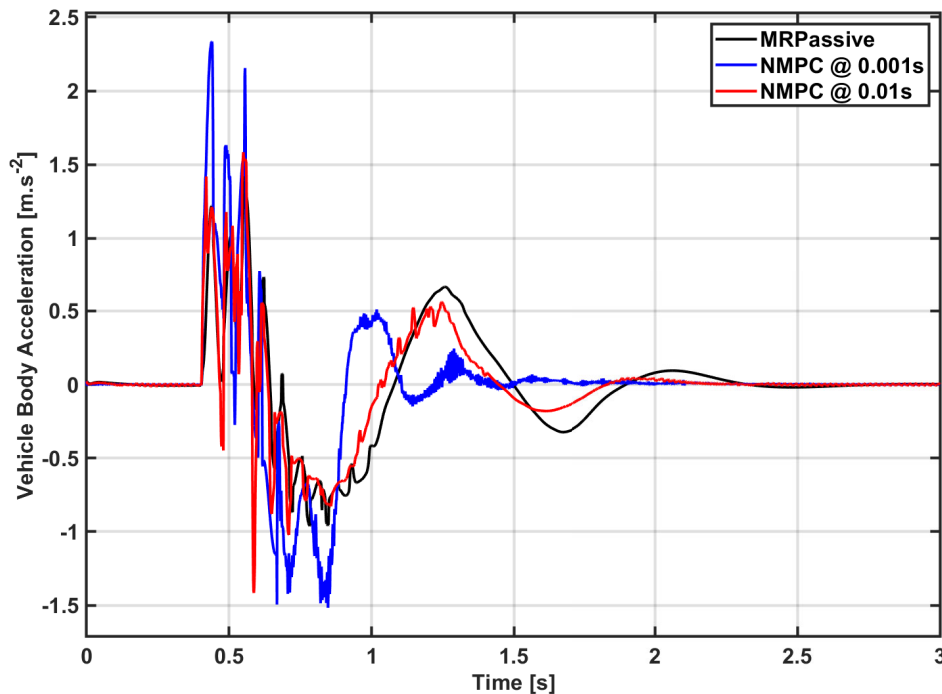


Fig. 7.5 Vehicle Body Vertical 'Heave' Acceleration for two sampling time methods with a preview length of 0.030 seconds

From a feasibility standpoint for implementation onto real-time hardware, the dual-rate sampled controller offers acceptable performance for a system limited by the speed of calculation and as such is considered better suited for the control of real-time semi-active suspensions. The millisecond controller while currently infeasible, in terms of real-world applications, could potentially be implemented in the future as the technology used in vehicular computer systems improves.

Further tests were carried out to identify the impact of the controllers on the pitch response of the vehicle, using the parameters listed in Table 8.2. The tests conducted use the same number of prediction steps for both controllers leading to a larger preview horizon for the Dual-rate controller.

Figure 7.6 shows the pitch response of the vehicle on contact with the bump, the high frequency oscillations seen in the data are damped out more quickly by the dual-rate controller as indicated by the NMPC @ 0.01 s. The pitch rate acceleration on the controlled cases shows higher spikes in the magnitude of the oscillations, which indicate that the controllers are

increasing the stiffness of the MR Dampers, in response to the vertical acceleration with no regard to the pitch being sacrificed.

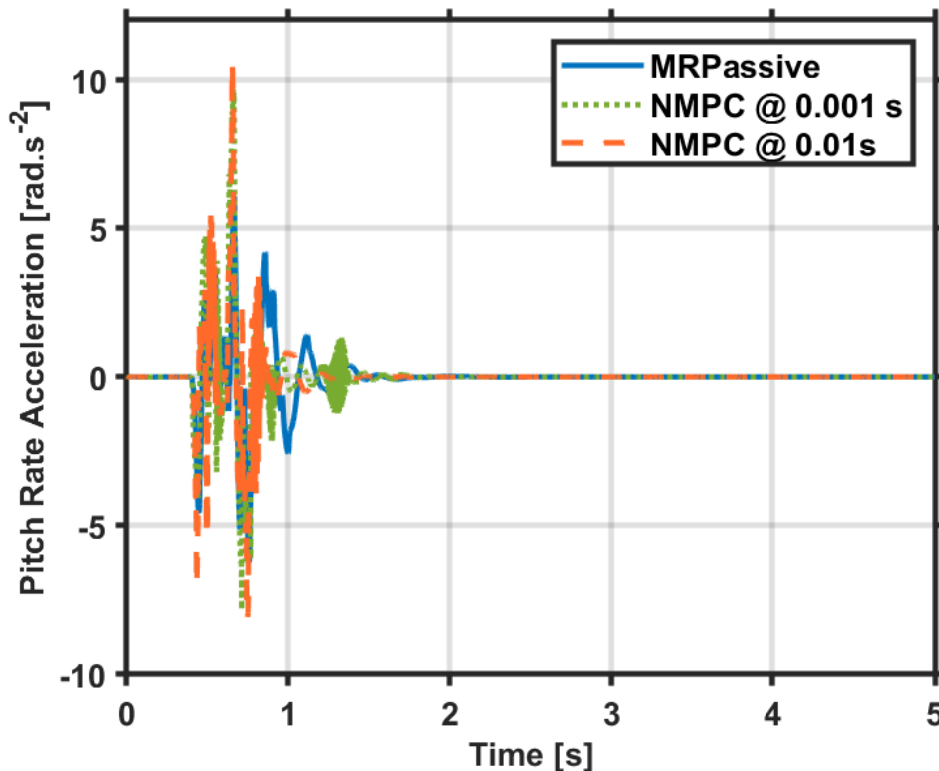


Fig. 7.6 Pitch Response of Full Car Model to Bump 0.02 m at 30 mph in comparison to the Dual-rate sampled controller

The vehicle simulated in Figure 7.6 is based on the parameters for the ASM Vehicle Dynamics model given in Table 4.2 with the parameters indicating that the load of the vehicle mass is not distributed 50/50 between the front and the rear axles of the vehicle. The controller formulations discussed thus-far can easily be configured using the variables  $H_c$  and  $H_d$  in addition to the track width, and wheelbase length which are explained in more detail in Chapter 4. The prediction horizon and sampling time is covered in more detail in Chapter 8.

## 7.4 Concluding Remarks

This chapter has proposed three controllers for controlling the current supply to a full car MR Damper based suspension system. The system utilised four MR Dampers with one located at each corner of the vehicle. The first of the three controllers introduced is the full car PID controller that utilised a single PID controller to manipulate the current of all four dampers

using the same control signal. The tuning method of the full car PID as described in Section 7.2.3 was similar in comparison to the approach taken in Section 6.2.1.

Building on the proposed Adaptive PID controller Section 7.2.2 proposed the Adaptive Cascade PID controller that utilised cascade control and a mixture of Adaptive PID and linear PID controllers to control three loops. The three control loops were configured to minimise the heave, pitch and roll accelerations of the vehicle body, with the primary objective equating to the reduction of the vertical heave acceleration of the vehicle body for improved ride comfort.

The Adaptive Cascade PID controller was tuned to minimise the heave acceleration using a mixture of the approaches used for the tuning of the full car PID and adaptive PID controller from Section 6.3.1. This tuning approach led to acceptable results for comparison with the NMPC controller. However there is the possibility of achieving improved performance through utilising other tuning methods. Candidate methods are identified in Section ?? and form part of the recommended future work.

The third controller developed in this chapter was a full car version of the NMPC strategy proposed in Section 6.4. The revised NMPC controller for full car MR Damper based suspension control was assessed for the feasibility of utilising dual-rate sampling. This approach was able to reduce computational times and allow for reduced number of optimisation variables to accommodate longer preview length. For a fixed preview length of 0.03 seconds both the millisecond interval and dual-rate sampled controllers were compared to each other. The results shown that both approaches led to a reduction in the heave acceleration of the vehicle body and that the millisecond response is infeasible with respect to real-time hardware implementation due to the short sampling time, the system settled within 1.8 seconds when compared to the dual-rate sampled controller which settled in under 2 seconds.

The controllers proposed in this chapter are utilised in the simulation studies conducted in Chapter 8 and are compared with each other to determine the most efficient controller for full car semi-active MR Damper based suspension control.



# Chapter 8

## Simulation and Discussion of Results

### 8.1 Introduction

This chapter describes the main simulation studies conducted to assess the performance and energy efficiency of the proposed NMPC control strategy and identify whether it is suitable for future development and implementation onto real-time hardware. The simulation studies present the responses for the quarter car and full car models and the improvements to ride comfort of a vehicle through the implementation of MR Damper based semi-active suspension used in conjunction with the NMPC strategies proposed in Chapters 6 and 7. The procedure used to setup the simulations is discussed in Section 8.2 with the common parameters used throughout the various simulations explained in detail.

The first simulation study (Section 8.3) investigates controller performance when the NMPC strategy utilises the various damper models discussed in Chapter 3. Section 8.3.1 shows the results for the quarter car response and identifies how the different damper models influence the performance of the suspension system through the reduction of the sprung mass acceleration. This section also compares how the different NMPC strategies compare to the PID and Adaptive PID controller responses. The simulation study critically analyses the frequency response of the systems through a range of test scenarios. Section 8.3.2 performs a similar analysis but instead focuses on the response of the full car ride model and the Modified ASM model.

Section 8.3.2 looks into the reduction of the vehicle body accelerations in the heave, pitch and roll directions for the full car vehicle model. Both sections (8.3.1 and 8.3.2) utilise the Key Performance Indices introduced in Section ?? to identify whether there is an acceptable level of improvement for the ride comfort in both the Primary and Secondary Ride Frequency Ranges. Section 8.3.3 combines the findings for both vehicle models (quarter car and full car) to evaluate the damper model best suited for use in conjunction with the NMPC strategy. The

section also assesses the advantages and disadvantages of the use of each damper model in the formulation of the NMPC strategies.

The second simulation study (Section 8.4) focuses on the preview length of the NMPC strategy and identifies the optimum preview length of the controller in relation to improvements in the vehicle body accelerations and controller activity. Section 8.4.1 investigates how preview and prediction horizon length influence the response of the quarter car vehicle model when controlling the MR Damper suspension using the best MR Damper and NMPC strategy formulation from Section 8.3.3 for quarter car control. Section 8.4.2 then continues to perform a similar assessment on the differences of the full car response to a change in the preview and prediction horizon lengths. Both Sections (8.4.1 and 8.4.2) identify the performance benefits of the control methods when evaluating the reduction of the vehicle body accelerations in relation to the secondary objective of minimising the control action for improved energy efficiency of the NMPC strategy. Section 8.4.3 then continues to summarise the findings of the simulation study to identify the optimum prediction and preview horizons for the two vehicle models.

The final simulation study (Section 8.5) identifies how the quarter car vehicle response changes with respect to the different off-road soils introduced in Chapter 5. Simulations on each of the soils are used to identify how a NMPC strategy for on-road is not necessarily optimum for off-road soft soils and how the NMPC strategy proposed in Section 6.6.4 improves the ride comfort of the vehicle. The simulation study further identifies if the sloped terrain model has an effect on the suspension response and the vertical dynamics of the quarter car model.

## 8.2 Simulation Study Setup

The simulation studies conducted in this chapter investigate the influence of the controllers for different aspects of the vehicle dynamics. While control of the system is primarily focused on the proposed NMPC strategy the studies also perform comparisons with the PID and Adaptive PID controllers to show how the performance is improved/reduced in relation to the baseline controllers. Table 8.1 provides the parameters used for the quarter car vehicle model which are used in all cases except where specifically stated. Similarly, the parameters shown in Table 8.2 are used for the full car vehicle model simulations.

Two vehicle disturbances are considered for the on-road simulations to assess the performance of the NMPC controllers. The step bump profile has a height equal to 0.02m and the step starts at 0.4 seconds as shown in Figure 8.1. This was constructed using the Equation 8.1 which is based on the equations presented in (Blundell and Harty 2014:265) with the rise time of the supplied step height profile sampled at millisecond intervals. The time for the bump to begin ( $t_b$ ) is used to define the onset of the bump for the quarter car or the front wheels of

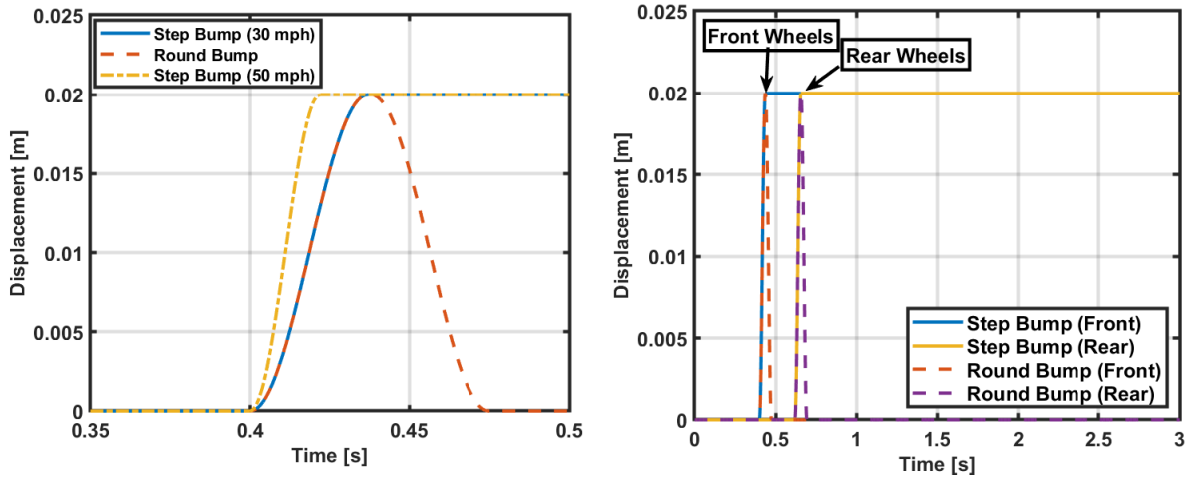


Fig. 8.1 The bump road profile height displacements used in this thesis for the quarter car (left) and full car (right) models.

the vehicle in the case of the full car model. The time for the bump to reach the maximum amplitude ( $A$ ) is given by the chosen time variable ( $t_e$ ) for a vehicle travelling at  $90 \text{ km.h}^{-1}$  ( $25 \text{ m.s}^{-1}$ ) this equates to 0.02 seconds while for a vehicle travelling at 30 mph ( $13.4112 \text{ m.s}^{-1}$ ) the time is increased to 0.037 seconds as illustrated in Figure 8.1.

$$Z_r = \begin{cases} 0 & \text{if } t < t_b \\ \frac{A}{2} \cdot \left( 1 - \cos \left( \pi \cdot \left[ \frac{t-t_b}{t_e} \right] \right) \right) & \text{if } t_b \geq t > (t + t_e) \\ A & \text{if } t \geq t_e \end{cases} \quad (8.1)$$

The time between the front wheels and the rear wheels hitting the bump profiles for the full car vehicle model is determined based on the vehicle's current velocity and the vehicle's wheelbase. The appropriate delay for the rear wheels is applied using the transport delay block for the rear two wheels. In the subsequent tests the simulations are assumed to occur on a road profile with no difference between the left and right hand sides of the vehicle.

Simulations using the round bump utilise a similar delay with the profile constructed using Equation 8.1. Since the road profile for the bump is a mirror image the profile is the result of the subtraction of two separate profiles. Profile 1 is the standard bump profile with the bump starting at 0.4 seconds, while the second profile is a profile where the bump starts at 0.438, the resulting subtraction leading to the profile seen in Figure 8.1.

The simulations in the following simulation studies use parameters which mirror those found in Tables 4.1 to 4.3 from Chapter 4 for the quarter car and full car models. However,

the majority of the following simulation studies in Sections 8.3 and 8.4 utilise the common parameters in Tables 8.1 and 8.2 except where explicitly stated. The values for the linear damping results are also provided in Tables 8.1 and 8.2 which refer to the linear damping of the damper when there is no current supplied to the MR Damper.

Table 8.1 Quarter Car Model Parameters

| Vehicle Parameter | Value  | Units   |
|-------------------|--|---------|
| $m_s$             | 561  | [kg]    |
| $m_{us}$          | 35   | [kg]    |
| $K_c$             | 130000   | [N/m]   |
| $K_t$             | 270000   | [N/m]   |
| $K_d$             | 3035   | [N.s/m] |
| $Q$               | [5, 0.0001, 1, 5, 0.0001, 0.0001, 10] <sup>T</sup> | [-]     |
| $R$               | 0.01   | [-]     |

Table 8.2 Full Car Model Parameters

| Vehicle Parameter | Value                                  | Units                |
|-------------------|--|----------------------|
| $M_b$             | 1880                                   | [kg]                 |
| $J_\phi$          | 680                                    | [kg.m <sup>2</sup> ] |
| $J_\theta$        | 2100                                   | [kg.m <sup>2</sup> ] |
| $\Theta_w$        | $diag([35, 35, 32, 32])$               | [kg]                 |
| $\underline{K}_c$ | $diag([130, 130, 123, 123])$           | [kN/m]               |
| $\underline{K}_t$ | $270000 \cdot \mathbf{I}_{4 \times 4}$ | [N/m]                |
| $\underline{K}_d$ | $3035 \cdot \mathbf{I}_{4 \times 4}$   | [N.s/m]              |

### 8.3 Simulation Study 1: The Influence of Damper Model on Controller Performance

This simulation study identifies the effect the MR Damper model has on the prediction of the vehicle's response as part of the NMPC strategy calculations and the performance of the system as a result of that choice. This simulation study highlights how the overall effective performance of four different controllers changes as a result of the differences in damper model selection. The primary objective of the controllers is the reduction of the vertical 'heave' acceleration for either the sprung mass (quarter car cases) or the vehicle body mass (full car cases).

This simulation study is divided into three sections. The first examines the influence on the quarter car vehicle model from Section 4.2.1 representing a single corner of the vehicle.

The second section of this simulation study evaluates the performance of the controller for the full car vehicle model from Section 4.3.1. The simulation study then compares the responses seen in both the quarter car and the full car model controllers. It aims to first identify if the controller performs better or worse in relation to the accuracy of the MR Damper model and second to determine whether the current supplied to the MR Damper is kept to a minimum whilst still achieving good performance.

### 8.3.1 Quarter Car Control

The four Nonlinear Damper models, chosen to be used for this set of simulation studies, are the Nonlinear Hysteretic Biviscous Model (NonlinHBV), the modified Nonlinear Hysteretic Biviscous Model (modNonlinHBV), the Nonlinear Viscoelastic Plastic Model (NVEP) and the modified Nonlinear Viscoelastic Plastic Model (modNVEP). This section highlights the differences in the responses and chosen control action for the formulations of the Nonlinear Model Predictive Controllers (NMPC). The resulting performance of each controller formulation is evaluated using the efficiency of the control action in relation to the overall reduction in sprung mass acceleration.

#### Test 1: 0.02 m Bump Step 30 mph

The response of the quarter car vehicle model for both the MRPassive and controlled cases are shown in Figure 8.2. As part of the first test the Prediction Length ( $N_p$ ) and controller weightings were maintained with a constant Prediction horizon of 10 steps ahead ( $N_p = 10$ ) with one millisecond between intervals. The test was conducted at a forward velocity of 30 mph ( $13.411 \text{ m.s}^{-1}$ ) with a simulation step size of 0.001 seconds.

The data in Figure 8.2a shows the sprung mass displacement for the first test over time, with the start of the step bump occurring at 0.4 seconds as seen previously in Figure 8.1. Prior to the bump a small displacement is visible as the vehicle model approaches the equilibrium point at its steady-state. The MRPassive and Linear Damping cases show a larger variation even though they both represent the same damper condition of 0 A of current. The resulting differences are due to the limits of the damper force and the change in the gradient of the force-velocity curve for the MRPassive case. A larger settling time in the linear damping case is the result to reduced damping for the low velocity cases with values oscillating around the zero mark. In addition, due to the residual force of the damper due to the force offset in the MRPassive case which is represented by the modNVEP model there is a higher magnitude of the oscillations but a shorter settling time.

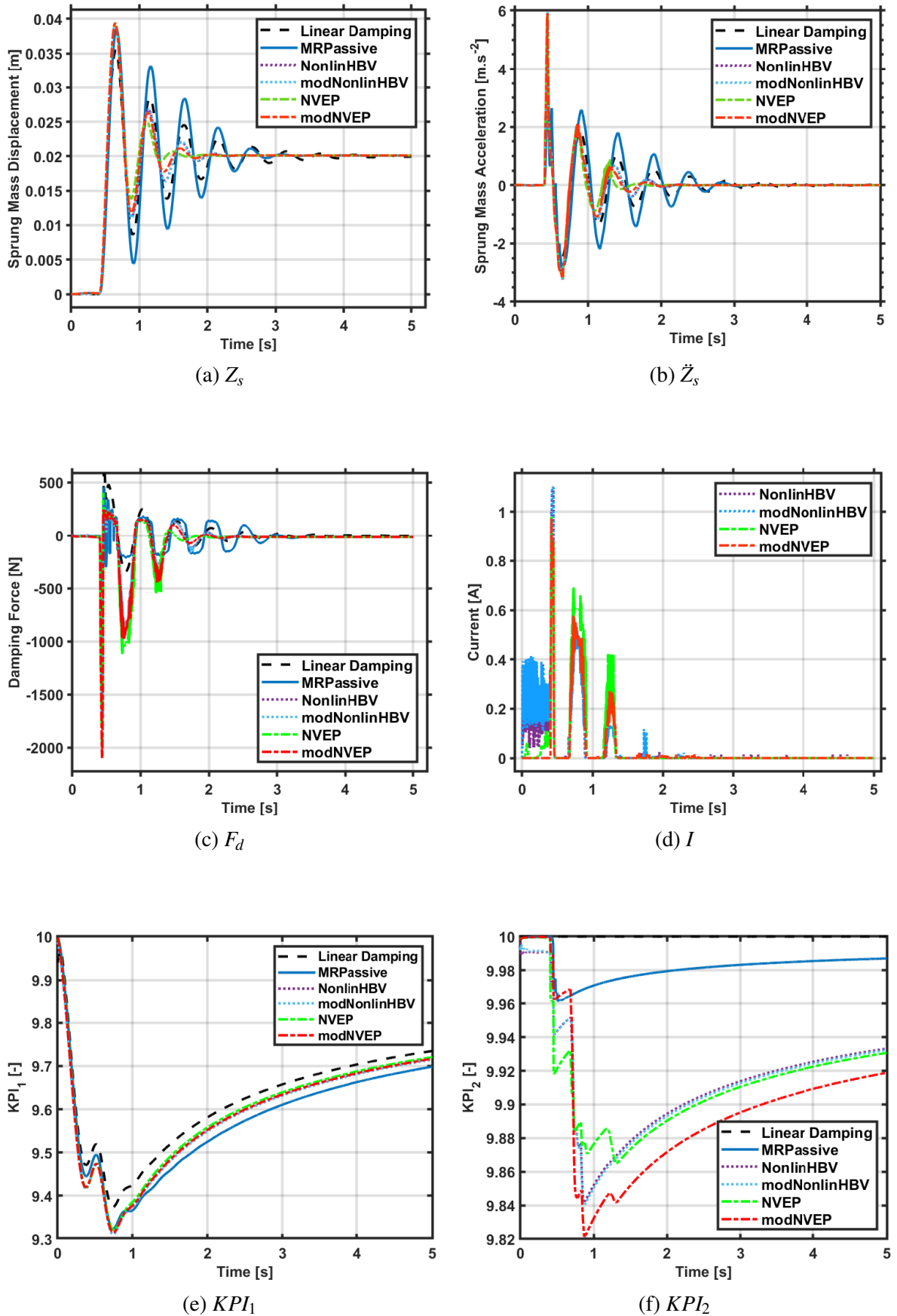


Fig. 8.2 Results of the MR Damper NMPC controllers for 30 mph

Table 8.3 shows the settling time for each of the cases, with the shortest settling time being the NVEP model which is not necessarily the best result when comparing the overall response of the system. The sprung mass displacement for the NonlinHBV and modNonlinHBV cases are fairly similar in their response with the response overlapping one another as seen in Figure 8.2a. In comparison there are some clear differences in the response of the NVEP and modNVEP controlled cases, with the settling times differing considerably.

Table 8.3 Settling Time of Sprung Mass Displacement for Quarter Car Vehicle Model During Test 1

| Case           | Settling Time [s] | Case         | Settling Time [s] |
|----------------|-------------------|--------------|-------------------|
| Linear Damping | 3.696             | modNonlinHBV | 1.939             |
| MRPassive      | 2.725             | NVEP         | 1.556             |
| NonlinHBV      | 1.937             | modNVEP      | 1.839             |

The changes in the response can be attributed to the sensitivity of the controller weighting for each model, while the weightings were kept constant for all the controlled cases in test 1 the differences in the predicted responses result in a different optimal solution. In addition, the simulation weightings are applied to both the system output and the control action which result in differences in the magnitude of the control action, and therefore a different response of the system as a whole.

Figure 8.2b shows the sprung mass acceleration of the quarter car vehicle model, there are similarities to the displacement but it more clearly shows the phase shift, that occurs during the secondary and tertiary oscillations of the controlled cases. The phase shift is more noticeable in the NVEP case where the results of the sprung mass acceleration have a shift of approximately 0.109 seconds leading the MRPassive case at the third peak. The sprung mass acceleration of the controlled cases also changes in magnitude during the first initial peak for all the controlled cases. The peak magnitude varies from case to case but it the common trend is an increase of approximately  $1 \text{ m.s}^{-2}$  due to the stiffness of the damper and the higher damping forces seen in Figure 8.2c.

After the initial peak acceleration of the sprung mass as the tyre makes contact with the bump the acceleration values die down considerably faster than the MRPassive case. Instead the acceleration values continue to follow the Linear Damping case until around one second with the behaviour of each case diverging from the common trajectory. The similarities between the NonlinHBV and modNonlinHBV cases are mirrored in the acceleration data as seen previously with the displacement of the sprung mass. However, in the case of the NVEP and modNVEP the trajectories diverge with the acceleration reducing more in the case of the NVEP model.

Figure 8.2c shows the damping force of the MR Damper models in response to the velocity and current changes. The force of the damper changes with respect to the current supplied to the MR Damper with the exception of the Linear Damping and MRPassive cases which have zero Amps of current. The Linear Damping case continues to oscillate about zero Newtons of force beyond three seconds which is considerably longer than the MRPassive case. In addition, the magnitude of the forces are larger for the NVEP and modNVEP cases.

The damping force of the NonlinHBV and modNonlinHBV controlled cases seen in Figure 8.2c have a magnitude of force of -1821.25 N in comparison to the NVEP and modNVEP cases with a maximum force of -2097.93 N. The differences in the force magnitude is linked to the current supplied to the damper ( $I$ ) based on the current determined by the solver. The current values shown in Figure 8.2d highlight the main differences in the current supplied to the damper for each case with the NonlinHBV and modNonlinHBV cases having the highest maximum current of 1.1 Amps.

The MR Damper current values in Figure 8.2d for the cases show peaks at intervals that coincide with the peaks in the oscillations of the sprung mass acceleration seen in Figure 8.2b. The current for the unmodified cases is generally higher as a result of the mismatch between the MR Damper model predictions and that of the modNVEP plant model. The increased inaccuracies lead to the damper current to be higher than necessary to reduce the magnitude of the sprung mass acceleration leading to an increase in the amount of energy consumed to maintain the MR Damper at the higher current value.

The energy consumed by the MR Damper ( $E$ ) to perform the required control action can be estimated using Equation 8.2. The Voltage of the MR Damper ( $V$ ) in a real world scenario would be a Pulse-Width-Modulated (PWM) signal to ensure that the correct control action is applied, however for the purposes of the following simulations the voltage can be assumed to be constant at 12 Volts which coincides with the Voltage given in the technical specifications of the MR Damper seen in (Lord Corporation 2009).

$$E(t) = \int_0^t V(t) \cdot I(t) \cdot dt \quad (8.2)$$

Table 8.10 shows the energy consumed in each of the controlled cases for test 1. The highest consuming controlled case in is the modNonlinHBV model which can be partly attributed to the weightings of the controller cost function. Since each case was conducted using the same weightings there is the possibility that there could be more optimally suited weightings for each controller type to improve the energy efficiency through the reduction of the energy consumed.

The modNVEP controller type case shows the least amount of energy consumed in relation to the chosen weightings which were determined through manual tuning and the minimum

Table 8.4 A table highlighting the energy consumed by the MR Damper assuming a constant control voltage of 12 Volts, 30 mph

| Controller Type | Energy Consumed [J] | Controller Type | Energy Consumed [J] |
|-----------------|---------------------|-----------------|---------------------|
| NonlinHBV       | 17.3483             | NVEP            | 6.3807              |
| modNonlinHBV    | 19.8534             | modNVEP         | 4.4823              |

amount of time required to determine the necessary weightings. While the system performance of the modNVEP case is not as ideal as the NVEP controlled case as indicated by the settling time of the sprung mass displacement and the reduction of the sprung mass acceleration, the resulting energy consumed makes the modNVEP control strategy more balanced controller in terms of control action to performance. The Key Performance Indices in Figures 8.2e and 8.2f show the change in the KPI values calculated using Equations 6.1 and 6.2 from Chapter 6.

The KPI values shown in Figure 8.2e refer to the ride comfort in the primary ride frequencies as explained previously in Chapter 6. The maximum value of this indicator is limited to 10 while the minimum is zero, as the value decreases the ride comfort of the vehicle is reduced. The highest overall out of the cases tested is the Linear Damping case which consistently scores higher than the other cases. However, the linear damping case does not consider the hysteresis in the system and therefore attention must be paid more to the MRPassive case. The MRPassive case scores high in comparison to the controlled cases until 0.645 seconds, after which the trend switches with the MRPassive generally performing the worst.

The accumulative nature of the integral term of the KPI value leads to the final value being the generally accepted as the average KPI value across the entire five seconds. The final values of the controlled cases resulted in an increase of between 0.017 and 0.022 for  $KPI_1$  while  $KPI_2$  decreases significantly. The subsequent decrease of the  $KPI_2$  values seen in Figure 8.2f which are linked to the secondary ride frequency comfort are the result of the increased stiffness of the damper to minimise the sprung mass acceleration. As mentioned previously in Chapter 2 the trade-off between the ride and handling is dependant on the level of damping and this in turn is linked to changes in the primary and secondary ride characteristics of the vehicle.

### Test 2: 0.02 m Bump Step 50 mph

The response of the quarter car vehicle model at a velocity of 50 mph ( $22.352 \text{ m.s}^{-1}$ ) for both passive and controlled cases are shown in Figure 8.3. The prediction horizon is consistent with the first test ( $N_p = 10$ ) an almost identical response can be seen which mirrors that of the 30 mph case from test 1 with the exception of minor phase shifting. In addition, the current is only marginally different from the 30 mph case, which has the overall effect of improving the efficiency of the controlled cases at 50 mph as seen by the energy consumed shown in Table 8.5

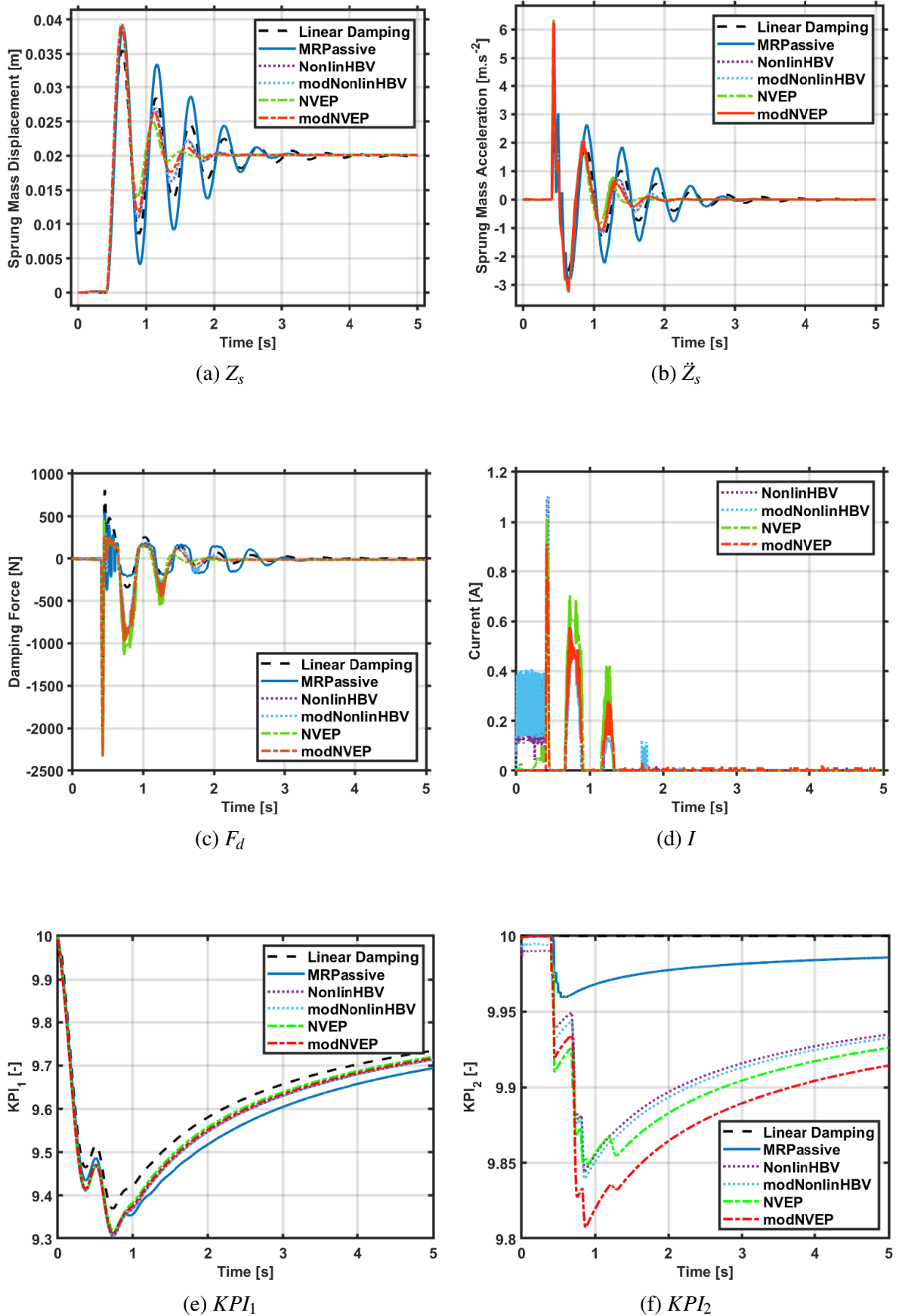


Fig. 8.3 Results of the MR Damper NMPC controllers for 50 mph

Table 8.5 A table highlighting the energy consumed by the MR Damper assuming a constant control voltage of 12 Volts, 50 mph

| Controller Type | Energy Consumed [J] | Controller Type | Energy Consumed [J] |
|-----------------|---------------------|-----------------|---------------------|
| NonlinHBV       | 17.2621             | NVEP            | 6.1251              |
| modNonlinHBV    | 18.9920             | modNVEP         | 4.1571              |

**Test 3: 0.02 m Round Bump 30mph**

The responses of a quarter car vehicle model to a round bump of 0.02 m in height for both passive and controlled cases are shown in Figure 8.4. The bump profile as seen in Figure 8.1 produces a sprung mass displacement (Figure 8.4a) that is significantly larger than the step bump case as the wheel position is displaced vertically before returning to zero. The low frequency oscillations seen in the sprung mass displacement reduce to zero quicker than the step bump case due to the wheel rebounding along the opposite side of the bump.

The high frequency spikes seen after two seconds are attributed to the aggressiveness of the control action in minimising the sprung mass acceleration. The control actions can be clearly seen in Figure 8.4d with some highly oscillatory behaviour in the case of the NonlinHBV and modNonlinHBV cases. Regardless of this the sprung mass displacement can be seen to settle rather quickly to within 2% of its final value.

Table 8.6 Settling Time of Sprung Mass Displacement for Quarter Car Vehicle Model During Test 3

| Case           | Settling Time [s] | Case         | Settling Time [s] |
|----------------|-------------------|--------------|-------------------|
| Linear Damping | 3.836             | modNonlinHBV | 1.306             |
| MRPassive      | 2.075             | NVEP         | 1.293             |
| NonlinHBV      | 1.311             | modNVEP      | 1.284             |

In contradiction to the previous two tests the KPI values that relate to the ride comfort within the primary and secondary ride frequencies show a significant difference in their shape with minimum  $KPI_1$  value equal to approximately 9.77 in comparisons to the 9.3 minimum seen in both tests 1 and 2. In addition, the energy consumed by the MR Damper to minimise is considerably higher, indicating potentially wasted energy through over-actuation of the MR Dampers. However, similar to the previous case the improvement of the  $KPI_1$  value still results in a reduction of the other KPI value ( $KPI_2$ ).

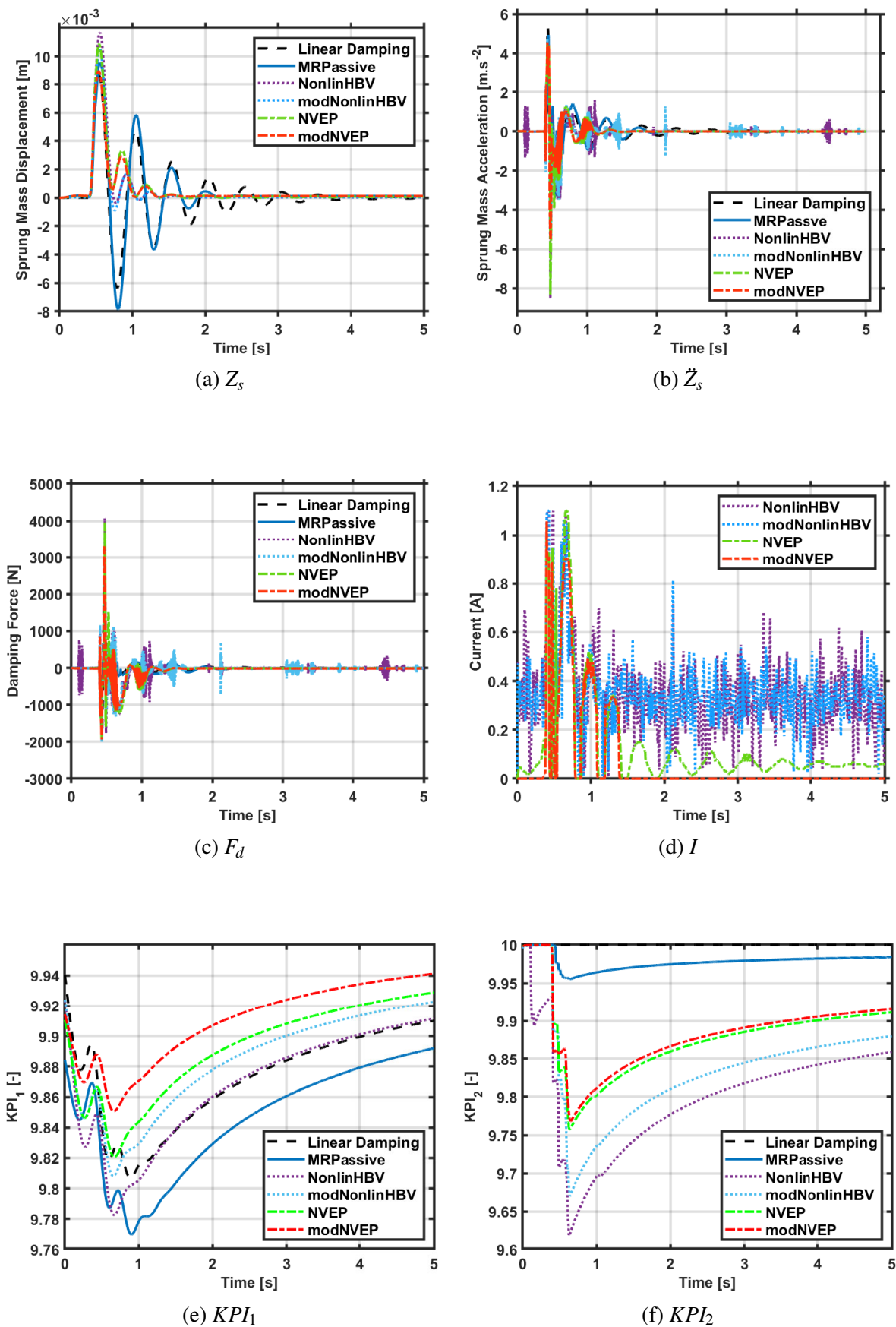


Fig. 8.4 Results of the MR Damper NMPC controllers for 30 mph round bump disturbance.

Table 8.7 A table highlighting the energy consumed by the MR Damper assuming a constant control voltage of 12 Volts, 30 mph round bump

| Controller Type | Energy Consumed [J] | Controller Type | Energy Consumed [J] |
|-----------------|---------------------|-----------------|---------------------|
| NonlinHBV       | 20.0230             | NVEP            | 7.5014              |
| modNonlinHBV    | 21.0335             | modNVEP         | 4.3908              |

Table 8.8 Quarter Car Key Performance Index Values for the Different Damper Models used in the Formulation of the NMPC Controller

| Model Type     | $KPI_1$ | $KPI_2$ |
|----------------|---------|---------|
| Linear Damping | 9.9101  | 10.0000 |
| MRPassive      | 9.8920  | 9.9840  |
| NonlinHBV      | 9.9116  | 9.8590  |
| modNonlinHBV   | 9.9227  | 9.8798  |
| NVEP           | 9.9289  | 9.9113  |
| modNVEP        | 9.9412  | 9.9156  |

The final KPI values for the uncontrolled and NMPC controlled cases are as seen in Table 8.8, in addition to the frequency response of the system obtained through the fast fourier transform as shown in Figure 8.5. The result of the fast fourier transform shows the results of the uncontrolled MRPassive case and the controlled modNVEP case. The peaks of the frequencies within the primary ride and secondary ride frequencies of the vehicle can be clearly seen from in the case of the MRPassive response. While, the response of the modNVEP model reduces the Magnitude by 0.1 for the primary ride and smooths the peak of the secondary frequency over the neighbouring frequencies.

### 8.3.2 Full Car Control

The influence of the MR Damper model chosen in the controller formulation of the Nonlinear Model Predictive Controller for the minimisation of the vehicle body accelerations is further investigated for the full car vehicle model from Section 4.3.1. The controller for the full car can be configured to minimise not only the vertical 'heave' acceleration of the vehicle body but also the angular acceleration in the pitch and roll directions. This section identifies how the MR Damper model, chosen for the four corners of the full car vehicle model used as part of the controller, has an impact on the vertical heave of the vehicle body and the overall response of the vehicle.

Figure 8.6 shows the vertical heave acceleration response of the seven degrees of freedom full car model with respect to the varying controller types. The vertical heave acceleration

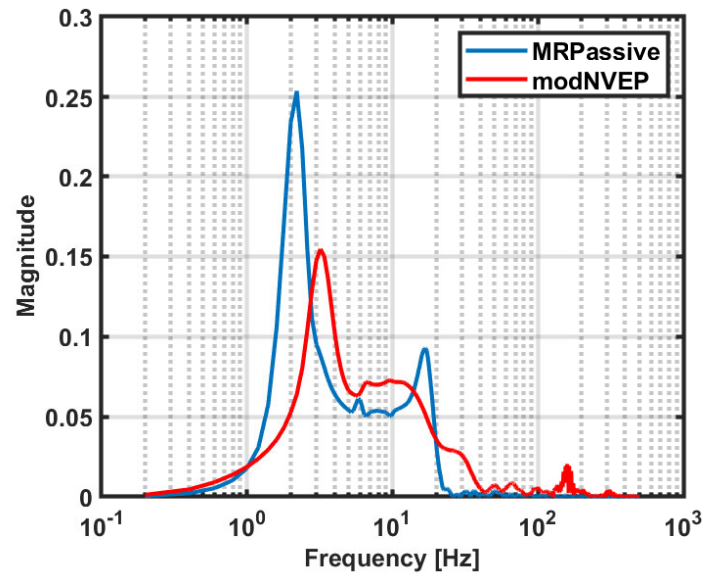


Fig. 8.5 Frequency Response of the modNVEP controlled case in comparison with the MRPassive case.

of the different models are similar to one another in respect to the overall pattern of the oscillations. Larger deviations are seen in the smoothness of the curve for the NonlinHBV and modNonlinHBV models with a larger fluctuation in the response between the models seen at 1.7 seconds. The modNVEP model shows the smoothest response with the smallest magnitude out of all the responses during the second trough at 1.4 seconds. This can be partly attributed to the closeness of the controller model to the plant system model but would likely be similar for the the response of a real MR Damper due to the accuracy of the model seen in the force-velocity curves in Appendix C.

The acceleration values when filtered and input into Equations 6.2 and 6.3 as per the method described in Section 6.2.1 result in the values seen in Table 8.3. As can be seen from the values the passive response of the damper offers the highest  $KPI_2$  value in the table as the damper naturally dampens out the high frequency oscillations from the wheel. This effect comes at the cost of the value of  $KPI_1$  being the lowest as more low frequency oscillations are transmit to the vehicle body when using passive suspension.

The controllers attempt to achieve the best case scenario whereby both values of the Key Performance Indices are equal to 10, a condition which can be attributed to maximum comfort for the passengers. The controllers with the modified model perform better than the controller with the original models, resulting in increasing the values of  $KPI_2$ . However, when basing the judgement on the value of  $KPI_1$  alone the response of the NonlinHBV model controller outperformed the other NMPC controllers. Whether this is particularly attributed to the short

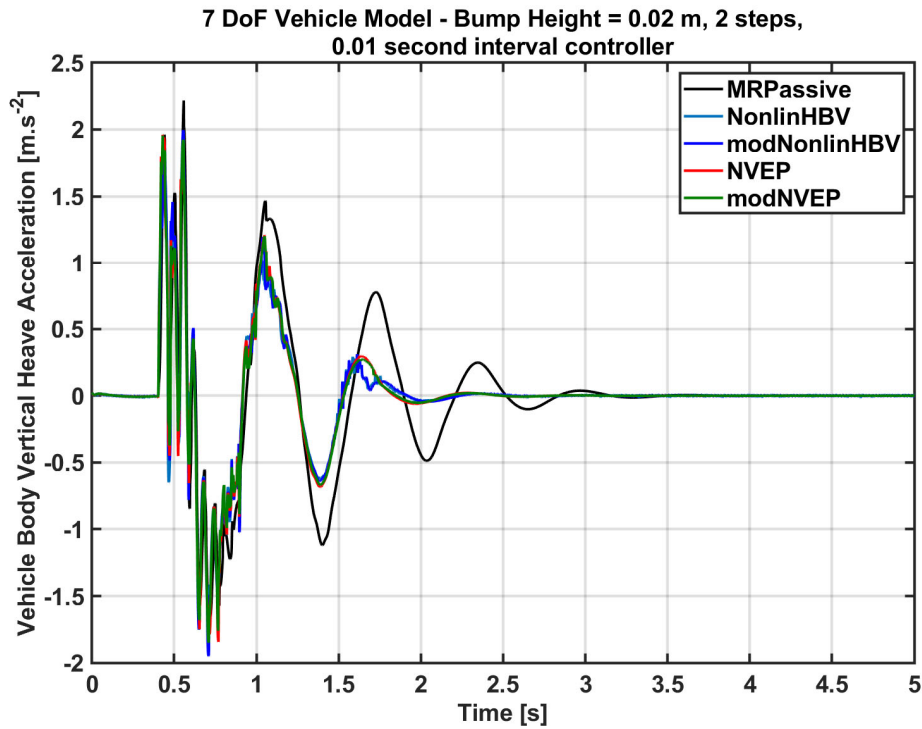


Fig. 8.6 Full Car Vehicle Response to step bump input

2 steps of preview information available to the dual-rate controllers and the controller being overactive in minimising the low frequency oscillations this is still unclear.

The controllers are ranked from worse to the best based on the sum of the two Key Performance Indices as they are considered equally important such that: Passive (19.2518), NVEP (19.3464), modNonlinHBV (19.3482), NonlinHBV (19.3512), and modNVEP (19.3583).

Table 8.9 Full Car Key Performance Index Values for the Different Damper Models used in the Formulation of the NMPC Controller

| Model Type   | $KPI_1$ | $KPI_2$ |
|--------------|---------|---------|
| Passive      | 9.5468  | 9.7050  |
| NonlinHBV    | 9.6720  | 9.6792  |
| modNonlinHBV | 9.6675  | 9.6807  |
| NVEP         | 9.6594  | 9.6870  |
| modNVEP      | 9.6647  | 9.6936  |

However, the controller performance is not solely assessed using the vertical heave acceleration alone. The controllers can be seen to reduce the vehicle body vertical displacement in Figure 8.5. The modNVEP controller performs particularly well at reducing the overall

variation of the vehicle body mass displacement from the new equilibrium point of the system (0.02 meters). All the controllers successfully dampen the oscillations out within 1.5 seconds of the disturbance with the passive response continuing until 3 seconds after the disturbance.

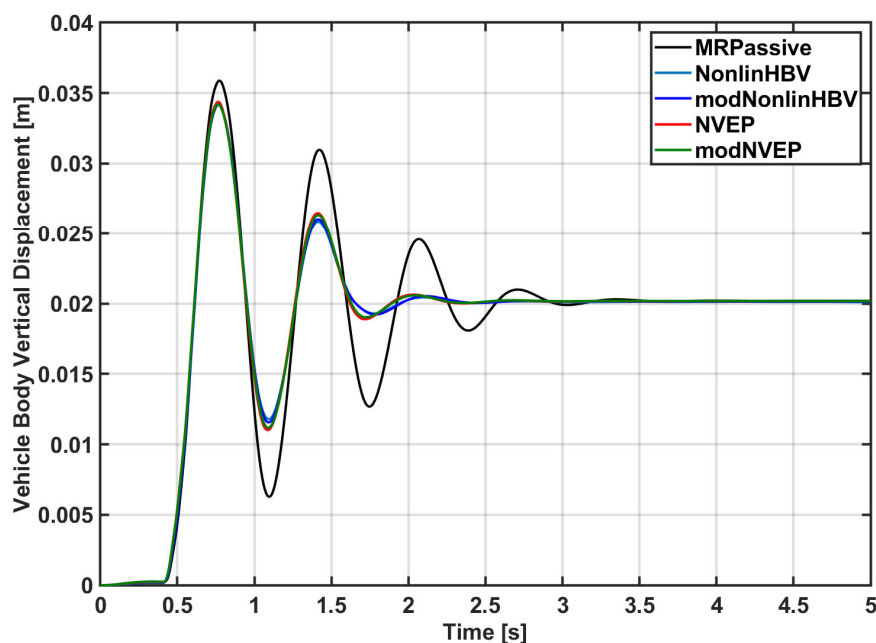


Fig. 8.7 Full Car Vehicle Response to step bump input

The frequency response of the full car system shows the peak for the MRPassive case in line with the Primary Ride Frequencies of between 0 Hz and 3 Hz. The secondary ride frequencies for the full car model do not get as excited as was the case for the quarter car model.

The modNVEP model also shows a reduction in the overall current supplied to the corners of the vehicle, see Figure 8.6. The smoothness of the response to the current supplied also highlights how the model mismatch of the NonlinHBV and modNonlinHBV models is responsible for the spikes in the supply of current in those cases.

From the evidence presented in Figures 8.2 - 8.10 and Table 8.3, the best controller for both quarter car and full car cases is the NMPC strategy that utilises the modified Nonlinear Viscoelastic Plastic (modNVEP) model. The controller is able to minimise the acceleration of the vehicle body mass and the displacements of the sprung and vehicle body masses with the least current supplied over the duration of the simulations.

The modNVEP Nonlinear Model Predictive controller (NMPC) is used in all subsequent comparisons of the controller response and is modified according to the changes presented earlier in Section 6.6.3 for the off-road simulation study conducted later in Section 8.5.

In order to verify whether the response of the NMPC strategy would minimise the acceleration of a more detailed full car model, the modified Automotive Simulation Model (ASM) for

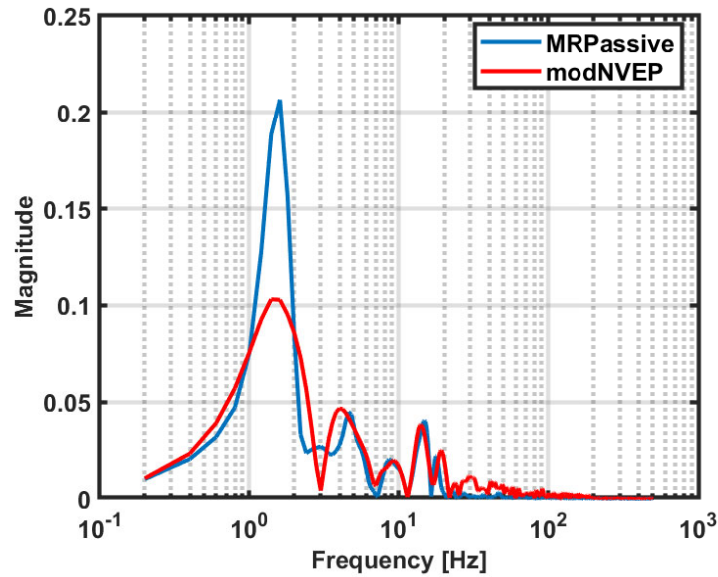


Fig. 8.8 Frequency Response of the Full Car Vehicle Model as a result of a step bump

Vehicle Dynamics Analysis as described in Section 4.4 was tested under similar conditions. Figure 8.10 shows the vertical acceleration of the vehicle body mass for the passive MR Damper suspension and semi-active MR Damper suspension ASM models. The disturbance to the vehicle is the same as that shown in Figure 8.1 with the exception that the bump is configured to start at 4.513 seconds. This additional time is used to compensate for the initialisation of the vehicle model and enable the vehicle to reach a steady velocity of  $90 \text{ km.h}^{-1}$  ( $25 \text{ m.s}^{-1}$ ). This time also allows for any residual accelerations to be eliminated to ensure for a fair comparison of the response of the vehicle.

The response of the vehicle seen in Figure 8.10 shows how the NMPC controller using the millisecond sampling approach and 5 prediction steps ahead of the vehicle results in the reduction of the acceleration of the vehicle body. The response of the NMPC controlled ASM model allowed the disturbance to be damped out within 1.5 seconds which corresponds to what was seen for the seven degrees of freedom full car model. The passive response continues to oscillate for a further 0.5 seconds after the NMPC controlled system has settled.

The current supplied to the dampers at each corner of the ASM vehicle model is shown in Figure 8.11 for the same test. The current supplied to the damper changed by the controller at every millisecond with the values of the current becoming more oscillatory once the vehicle has settled. This oscillatory behaviour can be attributed to the tuning of the controller weights, which is not optimally calculated and instead was decided to be a large value for the weighting applied to the acceleration of the vehicle body ( $Q(7,7) = 1000$ ). This large weighting in addition to the lower weighting of  $\underline{R}$  ( $\underline{R} = \text{diag}(1, N_p, N_p)$ ) for the control output is the main

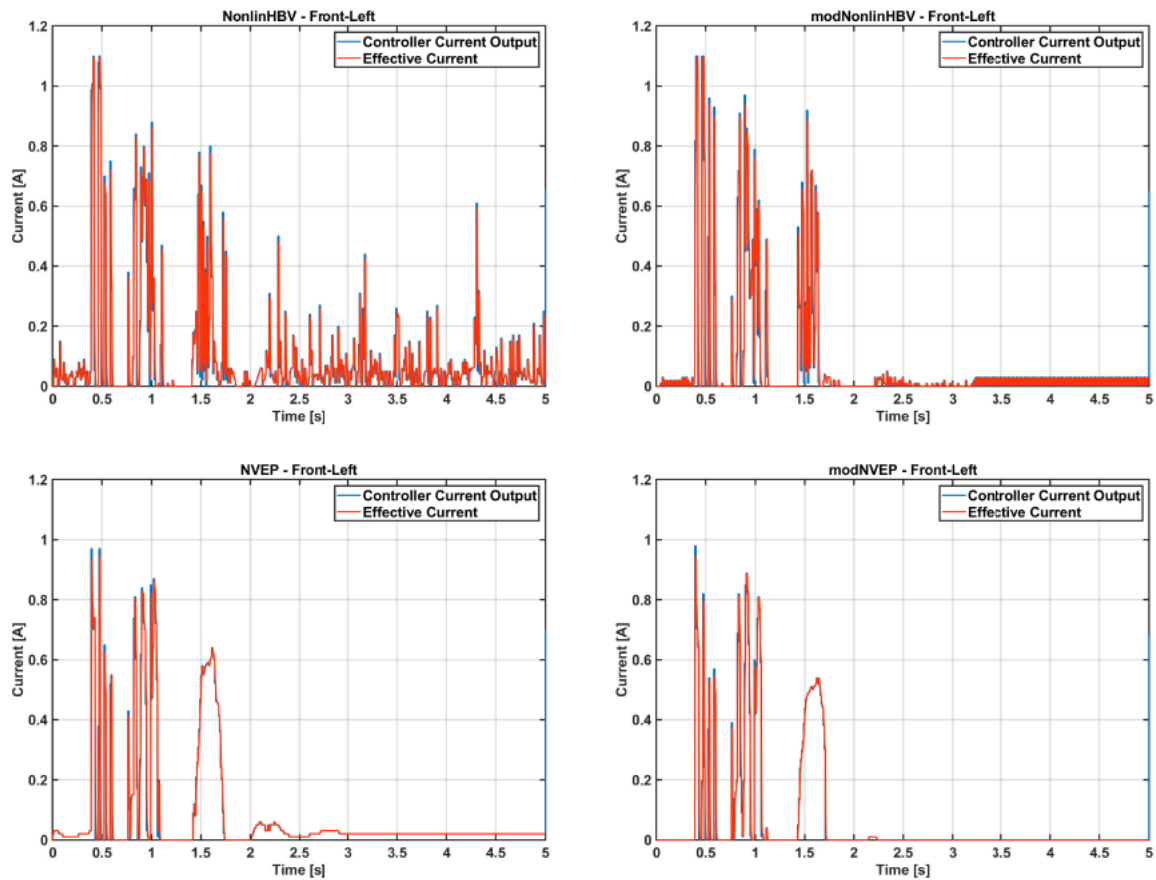


Fig. 8.9 Damper Current Supply for step bump input using NMPC strategy controllers

cause of the oscillation and the small increases in the acceleration that are present in Figure 8.10.

To improve the response of the controller in future tests the weights should be optimised to minimise the introduction of acceleration into the system through overactive behaviour.

### 8.3.3 Overall Findings for Simulation Study 1

The simulation results show that the modNVEP model used in conjunction with the NMPC controller offers the best performance in regard to the reduction of the vertical body accelerations. The simulation study finds that the modNVEP controller cases offer an all round benefit to the improvement of ride comfort and stability.

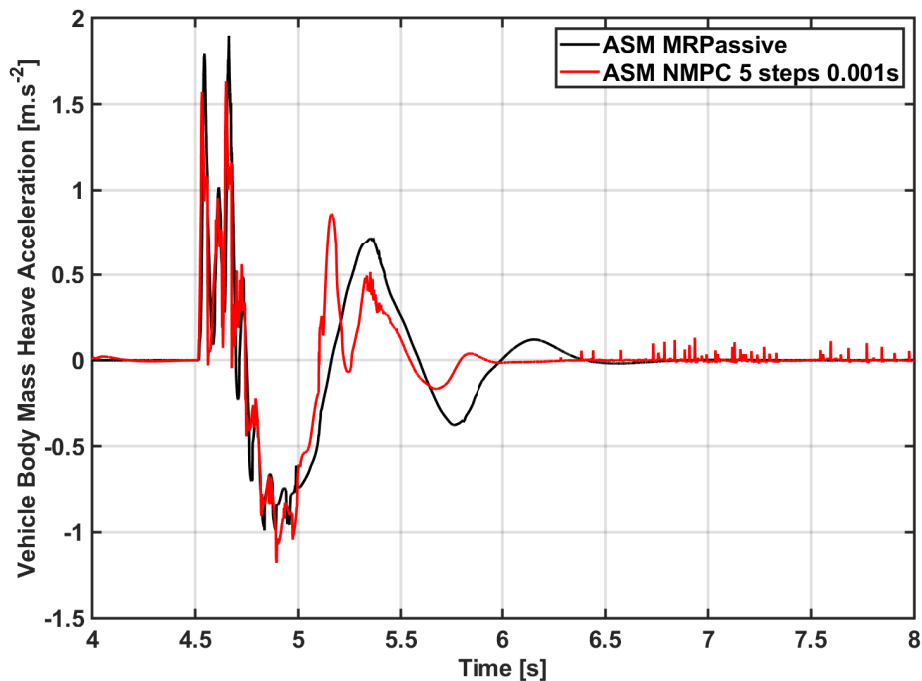


Fig. 8.10 Comparison between the passive ASM model and the ASM model with NMPC controller using the millisecond interval sampling

## 8.4 Simulation Study 2: The Influence of Preview Length on Controller Performance

This subsection critically evaluates the influence of the preview length on the controller's performance. Particular attention will be given to the impact, on the controller performance, of the number of optimisation variables and the preview horizon. The impact of dual-rate sampling has already been assessed in Sections ?? and 7.3.1. The simulations in this study employ the dual-rate sampling method to improve the controller response and see a more noticeable impact from an increase of the number of steps ahead of the vehicle.

The rationale to change the prediction horizon is that the longer the horizon, the better the controller performance should be. The cost of this improve performance is an increase in required computational power due to the increased number of optimisation variables considered. The aim of this study is to identify a suitable trade off.

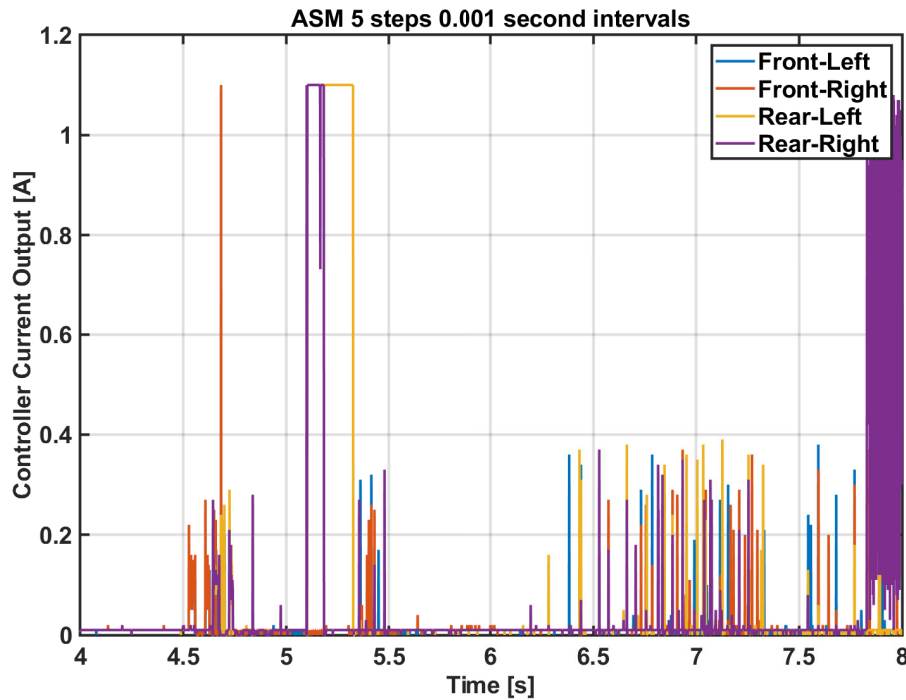


Fig. 8.11 NMPC Controller output for ASM Vehicle model test to step bump

### 8.4.1 Quarter Car Preview Length Testing

The preview length of the control system determines the control actions possible through insight into the future behaviour of the system. The preview length can be adjusted to accommodate for the differences in the system responsiveness and can aid the calculation of the system states.

The tests conducted on the quarter car vehicle model highlight the need for preview information ahead of the vehicle in order to anticipate unexpected scenarios such as a pothole or speed bump. The tests conducted in the following simulations show that it is necessary for adequate preview information to be collected.

Figure 8.12 shows the response of the quarter car vehicle model when controlled by a system supplied with/without preview information. The response shown produces unnecessary oscillations after the disturbance has settled since the controller can only operate re-actively instead of pro-actively in the case of the controller with preview supplied. The magnitude of the first peak in the acceleration of the sprung mass is considerably smaller for the preview case as the controller does not overshoot the optimum trajectory.

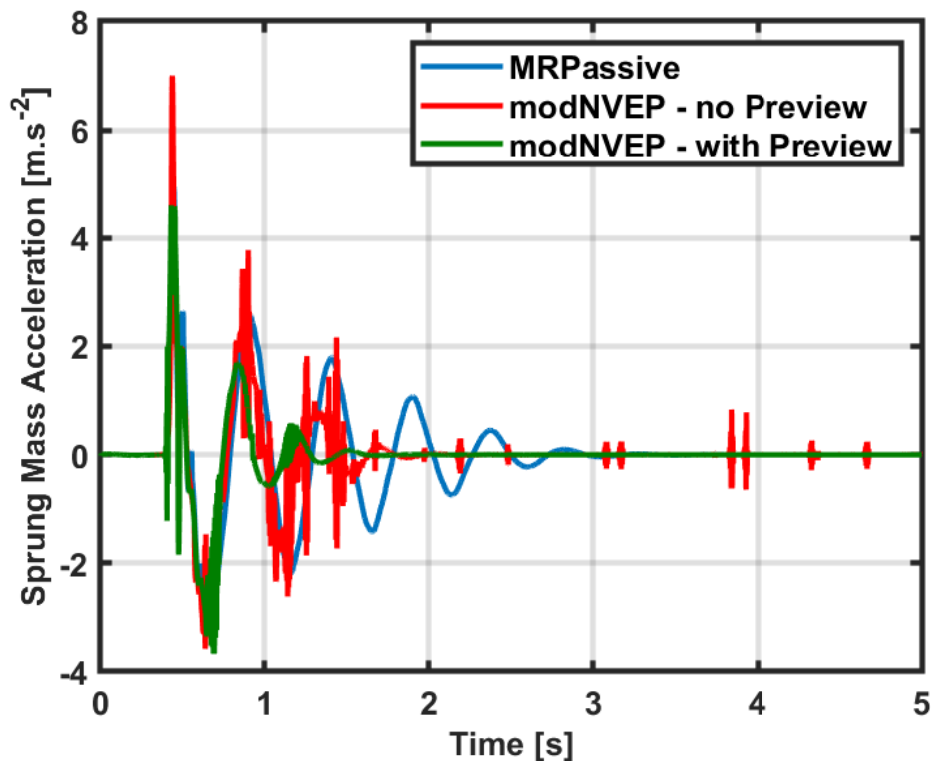


Fig. 8.12 A Comparison between the quarter car response for a preview controller and a controller without preview supplied

### 8.4.2 Full Car Preview Length Testing

The study analyses the response of the full car model from Chapter 4 when controlled using the Nonlinear Model Predictive Controller (NMPC) from Chapter 7. This controller is configured to use the modNVEP MR Damper which was determined in Section 8.3 to be the model that offered the best results when used with the NMPC strategy.

Figure 8.11 shows the vehicle body displacement response of the passive vehicle to the bump in comparison to the full car NMPC strategy responses for four different prediction horizons. The preview information supplied to the controllers is a direct match to the profile seen in Figure 8.1 with 0.01 second of time subtracted from the bump profile for every preview step added. This results in the furthest prediction steps into the future responding to the bump sooner.

From Figure 8.13 it is clear that the influence the prediction/preview distance has on the controller performance is substantial. The settling time of the NMPC with just two steps of 0.01 seconds is 1.5 seconds while an increase in preview length of an additional 0.01 second results in a settling time of 0.9 second. Further reductions in the settling time of the sprung mass are seen as the controller prediction/preview distance continue to be increased.

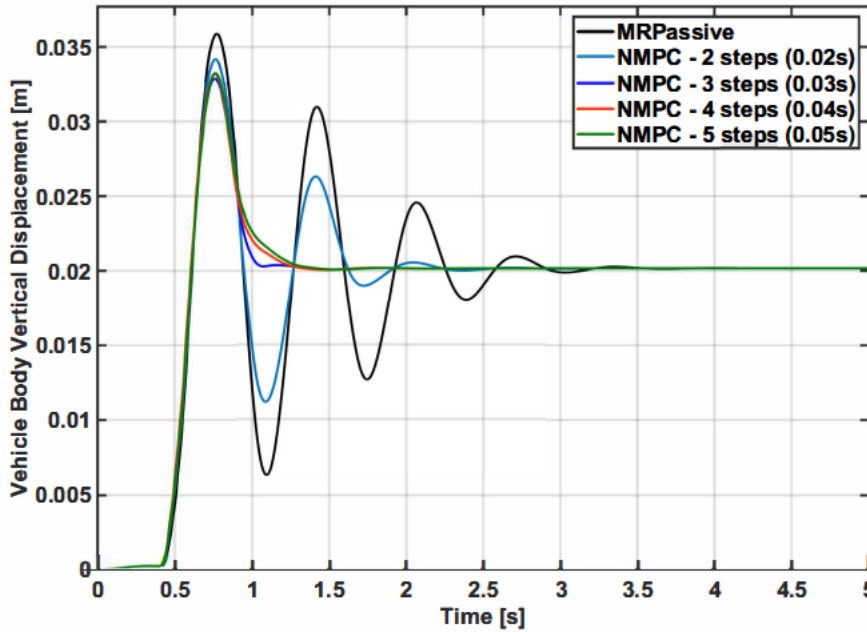


Fig. 8.13 Vehicle Body Vertical Displacement for Different Preview Lengths of the NMPC 10 millisecond Interval Controller

The controller's impact on the vertical heave acceleration is also compared. The results are similar to that of the displacement as shown in Figure 8.13. In addition, the increase of the preview length reduces the peaks in the acceleration.

The impact of the controller preview length is assessed using the Key Performance Indices shown in Table 8.10. The accelerations are filtered in line with the approach described in Section 6.2.1 and then fed into Equations 6.2 and 6.3 to give the values seen in Table 8.10.

Table 8.10 A Comparison between the Prediction/Preview Length and the Key Performance Index Values

| Preview Length in steps | $KPI_1$ | $KPI_2$ |
|-------------------------|---------|---------|
| Passive                 | 9.5468  | 9.7050  |
| $N_p = 2$               | 9.6647  | 9.6936  |
| $N_p = 3$               | 9.7472  | 9.6981  |
| $N_p = 4$               | 9.7490  | 9.6847  |
| $N_p = 5$               | 9.7519  | 9.6875  |

The values in Table 8.10 show a strong relationship between an increase in the controller preview length and the resulting Key Performance Index values. When analysing the response of only the low frequency responses ( $KPI_1$ ) the optimal value of those tested is five prediction steps ahead of the vehicle spaced 0.01 seconds apart.

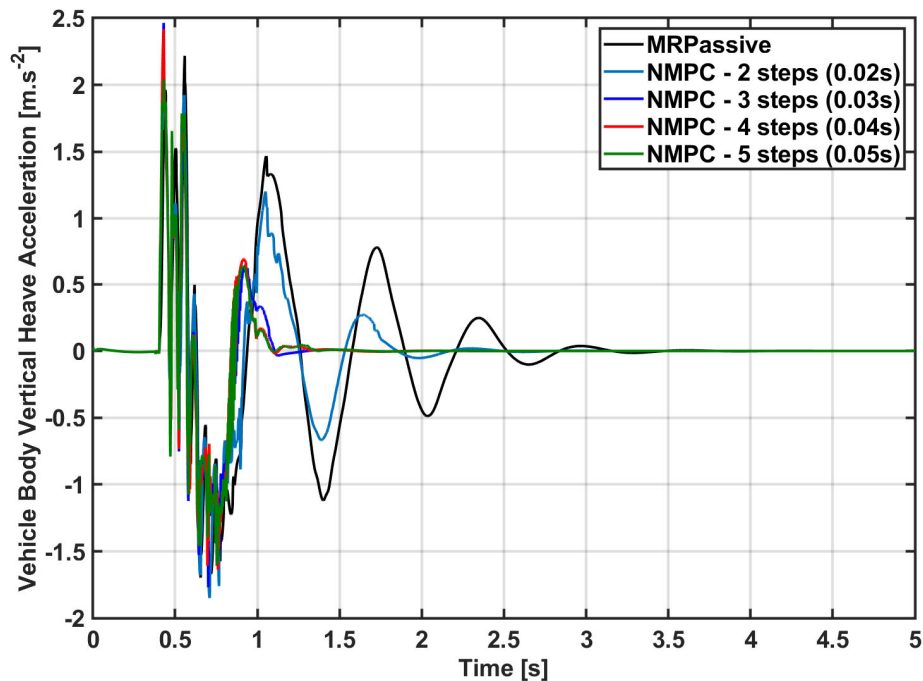


Fig. 8.14 Vehicle Body Heave Acceleration for Different Prediction/Preview Lengths measured in steps of 0.01 seconds using the Dual-Rate Sampling Method

The high frequency response on the other hand shows an optimum of 3 prediction steps ahead of the vehicle. The combined response of the controller response is listed in order of worst to best as follows; Passive (19.2518), Two Preview Steps (19.3583), Four Preview Steps (19.4337), Five Preview Steps (19.4397), and Three Preview Steps (19.4453).

### 8.4.3 Optimum Preview Horizon for NMPC

The optimum preview horizon for the NMPC strategy is an ambiguous question with it determined by both the tuning and the quality of the preview information. In addition to this the velocity of the vehicle has a large impact on the performance of the suspension when it encounters an obstacle.

## 8.5 Simulation Study 3: The Influence of Tyre Model for Off-Road Controller Performance

This study researches how the soil type used in conjunction with the off-road tyre-soil interaction model influences the behaviour of the controller. It goes further to discuss how future

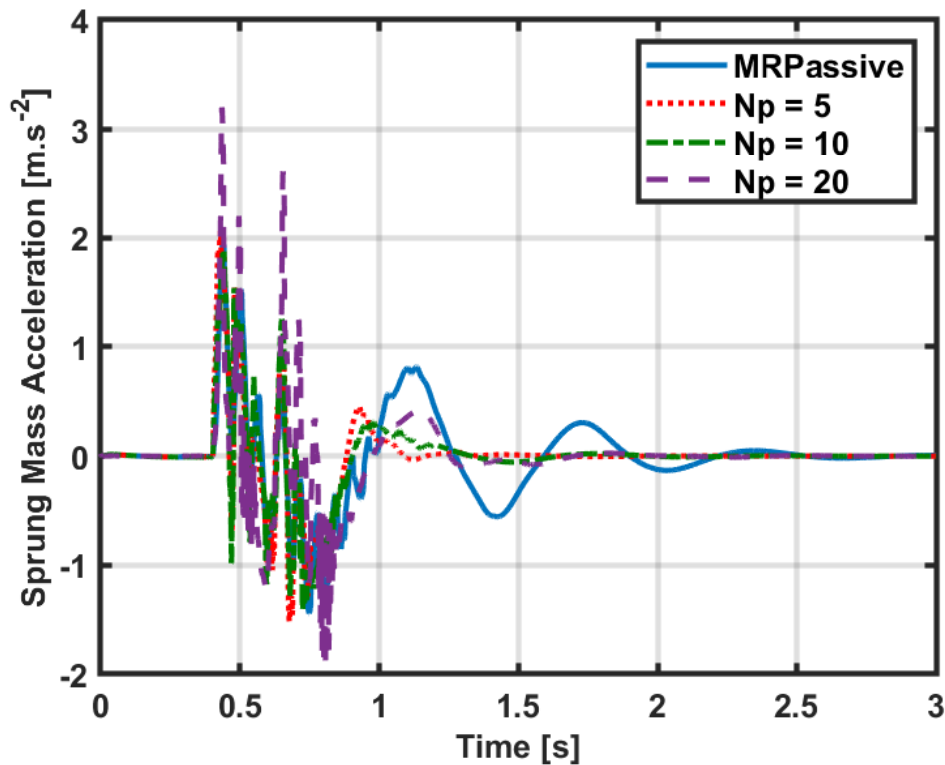


Fig. 8.15 A Comparison between the full car responses of the modNVEP controlled cases for a bump at 30 mph.

developments made to the accuracy of tyre-soil interaction models could potentially improve the performance of the controller discussed in Section ??.

Figure 8.17 shows the response of the quarter car off-road model with NMPC controller on the soft-soil with no additional disturbances. The vehicle in motion leads to changes in the slip ratio and associated sinkage value. This motion results in the high frequency oscillations seen in the acceleration of the sprung mass.

While the NMPC controller does try to minimise the sprung mass acceleration in the initial two seconds of the simulation the resulting motion of the sprung mass becomes oscillatory with the controller unable to correct the issue. The acceleration values for Soil 2 (not displayed here) were identical in comparison to the sprung mass acceleration.

The differences in the two responses can only be distinguished when looking at the unsprung mass displacement shown in Figure 8.17. The oscillations in the unsprung mass displacement are softened by the actions of the controller.

Figures 8.18 and 8.19 show the current of both soil cases and the sprung mass displacements. The response shows some additional reduction in the sprung mass response when compared to the passive response but the oscillatory behaviour of the response is not ideal.

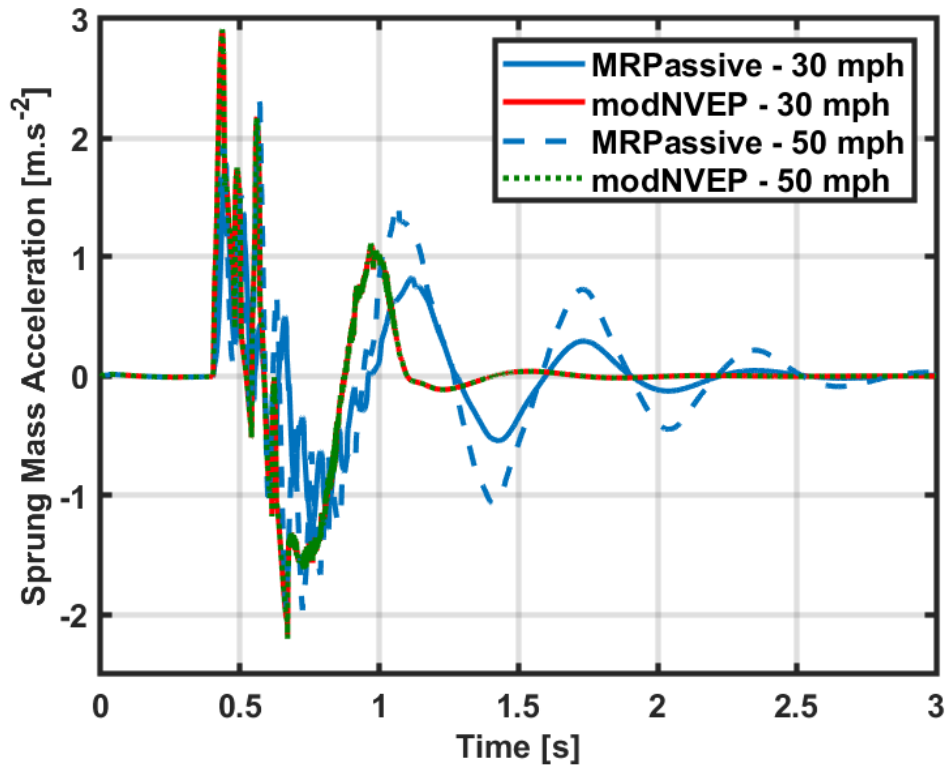


Fig. 8.16 A comparison between the velocity of the vehicle and the sprung mass acceleration for both uncontrolled and modNVEP controlled cases.

Further work into the tuning of the controller is required to achieve improvements which could include increasing the controller prediction horizon further so it can see more of the response or utilising the millisecond control method.

## 8.6 Concluding Remarks

This chapter identified the performance improvements of utilising the Nonlinear Model Predictive Controller for on-road and off-road suspension control.

It was determined that the modified Nonlinear Viscoelastic Plastic model offered the most improvement of the vertical acceleration and utilised the least amount of current to do so as shown in Section 8.3.

The modNVEP NMPC controller was then used to identify the performance improvements of increasing the preview distance for the controller which highlighted that the performance for low frequency damping is improved with increased preview distance as shown in Section 8.4.

The results on the performance of the NMPC controller for off-road control shown in Section 8.5 highlight that the controller while capable of dealing with the low frequency

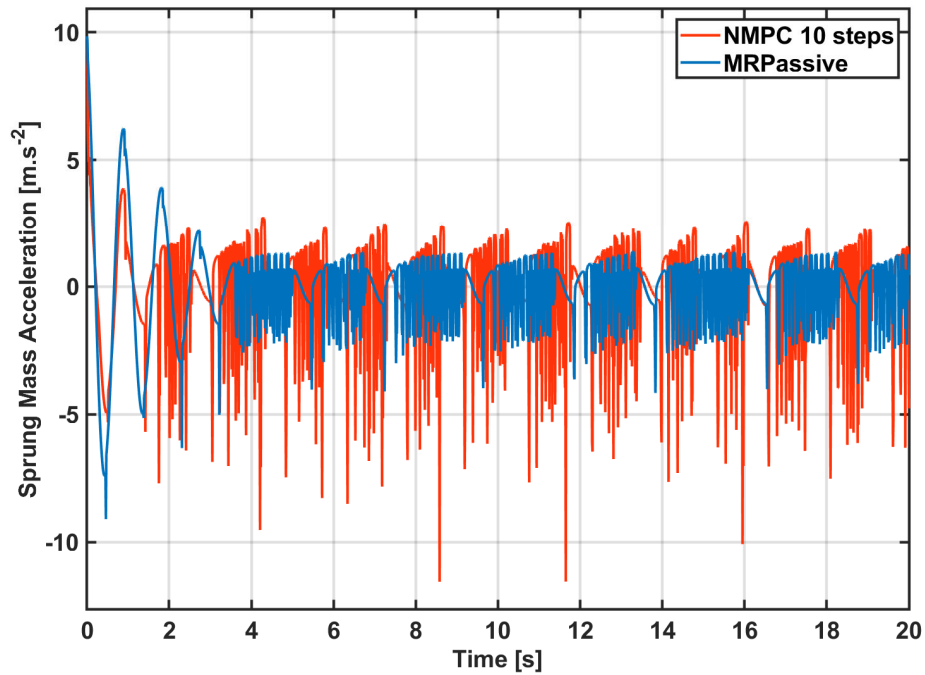


Fig. 8.17 Sprung Mass Acceleration of Quarter Car Vehicle on off-road Dry Sand with NMPC dual-rate sampled controller using 10 steps of preview

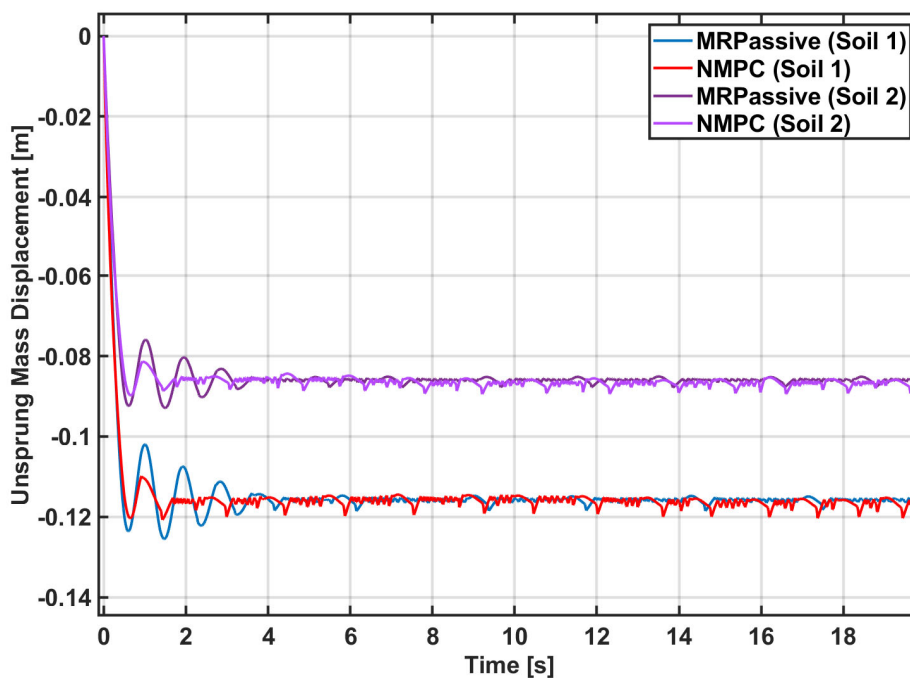


Fig. 8.18 Passive and semi-active responses for the unsprung mass displacement on Dry Sand (Soil 1) and Upland Sandy Loam (Soil 2)

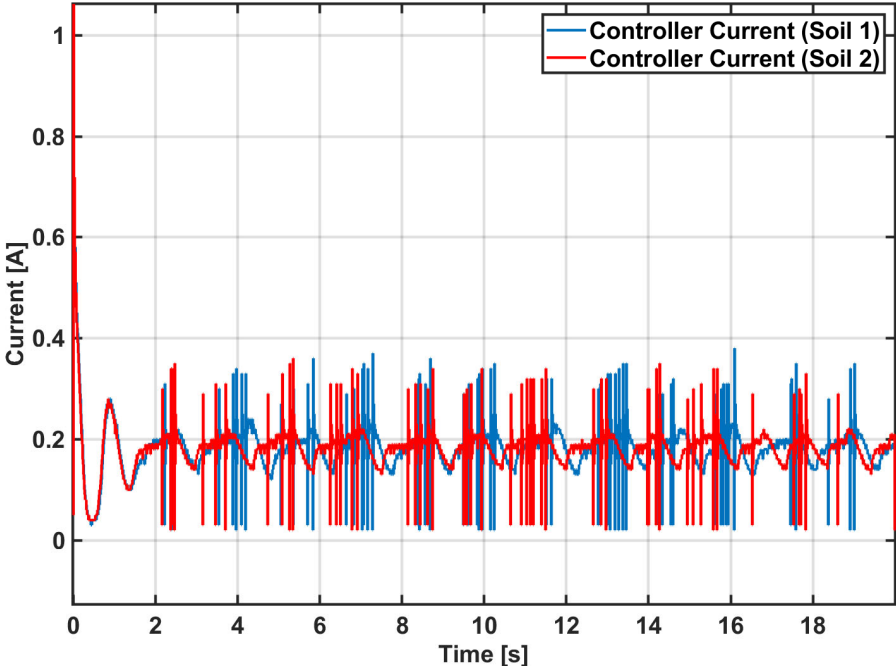


Fig. 8.19 The output current of the NMPC current using 10 steps of preview on Dry Sand (Soil 1) and Upland Sandy Loam (Soil 2)

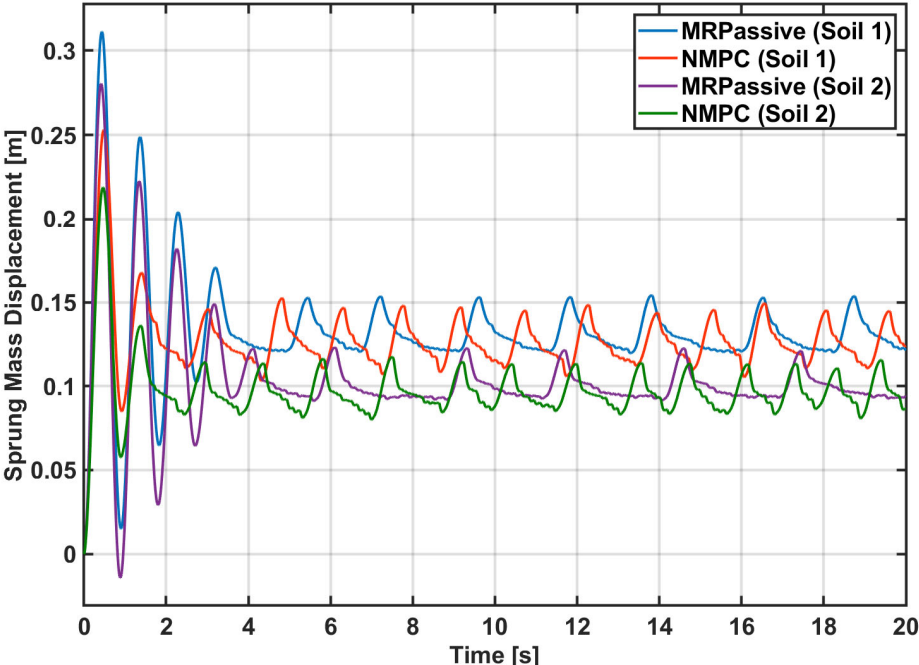


Fig. 8.20 The Sprung Mass Displacement of the NMPC and Passive responses on Dry Sand (Soil 1) and Upland Sandy Loam (Soil 2)

oscillations could not account for the high frequency disturbances present. As a result further testing and tuning of the NMPC off-road controller is needed for improvements to the sprung mass acceleration to become more visible. This will be recommended for future research along with the full physical validation testing needed to confirm the overall validity of the tyre model.

# Chapter 9

## Conclusions

This chapter presents the main contributions of this research and highlights how they enable to answer the research questions to meet the project objectives. Overall conclusions are then drawn based on the methods, algorithms and results presented in the previous chapters and finally areas of further work are identified.

### 9.1 Conclusions

The problem addressed in this thesis is that of designing a controller for off-road vehicle applications. The aim of these controllers is to improve ride comfort for both on-road and off-road terrains by reducing vertical accelerations of the sprung mass. The specific hardware considered are semi-active suspensions using Magnetorheological Dampers (MR Dampers) to adjust the suspension damping.

The literature review has identified the need for more accurate suspension control for off-road vehicles. It has identified semi-active suspension exploiting MR dampers as a suitable alternative to simple passive systems or more complex and expensive active suspensions. The review has also identified two candidate control strategies, namely adaptive cascade PID and model based predictive control.

The development of adaptive and model based controller requires appropriate models to simulate the vehicle in an off road environment. The focus of this work was on ride comfort, therefore models affecting the vertical acceleration of the vehicle were considered. These included tyre-soil, tyre, damper as well as other subsystems within a vehicle suspension systems.

Key to the simulation of the semi active suspension was the accuracy of the MR damper model and its ability to be used within the predictive model exploited by the model predictive control scheme investigated. The Nonlinear Hysteretic Biviscous (NonlinHBV) and Nonlinear

Viscoelastic Plastic (NVEP) models were identified as being the most suitable. However, parameterisation of the model from experimental data highlighted model mismatch due to non-zero mean at the origin of the force/velocity data and lack of symmetry about the origin.

Two improvements to the existing Nonlinear Hysteretic Biviscous (NonlinHBV) and Nonlinear Viscoelastic Plastic (NVEP) models were made and are referred to as the modified Nonlinear Hysteretic Biviscous model (modNonlinHBV) and the modified Nonlinear Viscoelastic Plastic model (modNVEP). The modified formulation introduces two shifting parameters to account for the non symmetrical and non zero mean around the origin of the force and velocity data. In both cases, the modified models reduce by a factor of 2 the Root Mean Squared Error Force Values, with values around 6 N, for each of the damper models. The modNVEP model was slightly better and therefore selected to represent the true response of the damper in the plant model. Look up tables were then used to enable the model use for frequencies where no data were available but within the range of operating frequencies measured. Two other modifications were made to model the dynamic response of the MR damper to changes in current. A lag was introduced modelled as a first order transfer function with a time constant of 0.003s. This lag enabled to model the time it take for the physical damper to react.

The first research question was: How can simpler, yet more accurate semi-active MR Damper based suspension systems be modelled using nonlinear modelling and system identification techniques?

The successful modelling of the MR damper provides a positive answer to this first research question. Significant accuracy gains were made at the cost of only two additional parameters. Whilst the proposed models were not simpler, they were still low order models perfectly suited to real time implementation.

To answer the other research questions the full systems, including models and controllers had to be simulated.

Original implementations of nonlinear vertical vehicle dynamics models were realised in Simulink using first principle modelling. A key novelty is the formulation of a coupled state space model between the sprung mass and the unsprung mass. This formulation enables the integration between the vehicle suspension system and different tyre models. This approach enabled the combination of the tyre soil model with its novel pre-lookup method to the vehicle semi active suspension system for quarter car as well as full car models.

The practical implementation of the tyre soil model using pre-lookup table reduced the need to call the bisection method, resulting in significant computational time savings whilst at the same time improving the accuracy of the model. This is considered a significant practical contribution that can be used with any of the tyre-soil interaction models using the bisection method.

The models developed were exploited by the controllers developed in this work which led to a further two contributions. The first contribution in terms of control is the formulation and method implemented to solve the NMPC control problem for an MR damper based semi active suspension.

NMPC are particularly computer intensive. The proposed use of dual-rate sampling, with the NMPC sampled 10 times slower than the plant, has been shown to be particularly effective in reducing computational time. It has also enabled to extend the preview horizon.

The second control contribution is the development of a cascade scheme exploiting the capabilities of an adaptive PID, which gains are calculated by functions that depend on sprung mass acceleration or the vertical heave acceleration of the vehicle body depending on the number of degrees of freedom of the vehicle model. This enables the PID gains to automatically adapt the dynamic response of the vehicle.

The comparison between the adaptive PID and NMPC has enabled to answer the following research question. How does a non linear predictive control approach compared to reactive and adaptive controllers? It was found that, if the computational time is not considered NMPC can offer significant advantages compared to adaptive PID. However, this advantage reduces as the controller sampling time increases and the prediction horizon and associated preview length reduces.

## 9.2 Recommendations for Future Work

During the course of this research programme a number of avenues of further work were identified. These avenues are categorised in terms of modelling, control, and tuning.

Particular focus was given to modelling the tyre-soil interface for the purpose of control system design. The proposed approach to separate the state space model to enable the connection of various tyre models was successful. However, further improvements are required to enable these models to be fully connected with full car as well as half car and quarter car representations.

For the future development of tyre-soil interaction models the method of integration with vehicle models needs to be addressed by improving the tools and software needed to integrate with them. The Automotive Simulation Models by dSPACE ([dSPACE GmbH 2020](#)) offer a range of functionality for on-road applications. However, the introduction of tyre-soil interaction modelling and in particular the sinkage of the tyre into the soil is needed for improved control system development.

System identification, model parameterisation and validation against measured data is key to the overall performance of the system modelled. Such model validation and verification should be applied to the proposed slope terrain model.

There is a range of parameters and associated assumptions, that have been used in tyre-soil model. Some improvement in terms of standardisation of tyre-soil model parameters and associated notations would be beneficial to the research community.

Several MR damper models were modified and critically evaluated. However, it would be useful to extend this critical evaluation to the modified Bouc Wen model, especially for use with the NMPC.

To improve the applicability of the work it would be useful to further develop the off-road tyre-soil interaction for of a full car model.

The pre-lookup method was shown to be very effective in speeding up online simulation. The next stage is to extend this approach to account for dynamic sinkage for slip-sinkage effects.

Several control strategies were proposed with NMPC being the most complex and adaptive PID offering a computationally efficient alternative against fixed gain PID control. Further tuning of the controller would however be beneficial to maximise the benefits of each scheme.

# **Appendices**



# Appendix A

## Model Fitting Application

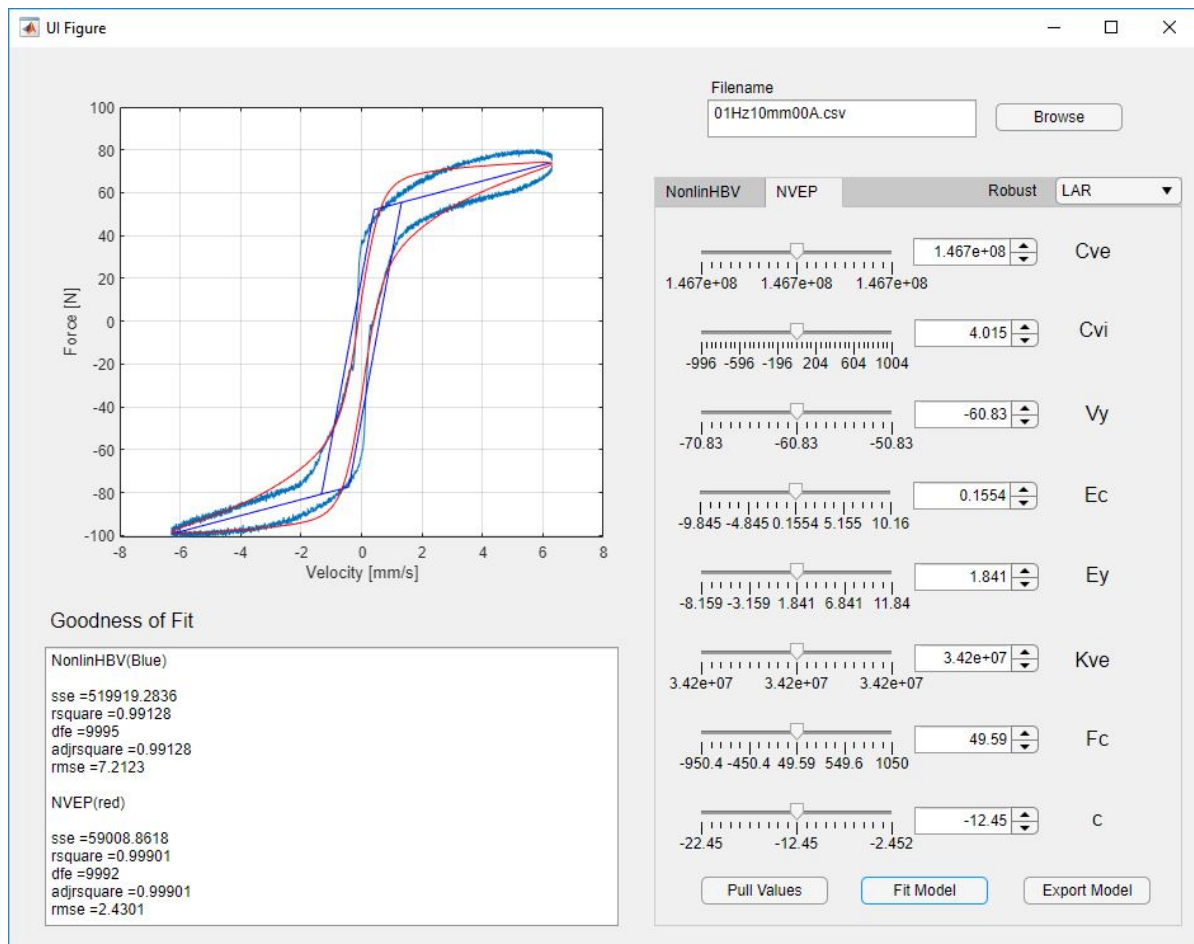


Fig. A.1 Model Fitting Application Example

The Model Fitting Application is a Graphical User Interface (GUI) that can be used to pull the force-Velocity curve data from a pre-prepared .csv file.

The Tool can be used to fit a multitude of damper models including the Nonlinear Hysteretic Biviscous Model, Modified Nonlinear Hysteretic Biviscous Model, Nonlinear Viscoelastic Plastic Model, and Modified Nonlinear Viscoelastic Plastic Model.

Table A.1 Available Robust Methods for use with Nonlinear Least Squares for Parameter Fitting

| Available Robust Method | Description  |
|-------------------------|--|
| LAR                     | Least Absolute Residuals<br>The method uses the procedure stated in ( <a href="#">Encyclopedia of Mathematics 2021</a> )           |
| Bisquare                | Bisquare Weights<br>A method of weighting the residuals of a function as per the procedure stated in ( <a href="#">NIST 2021</a> ) |

# **Appendix B**

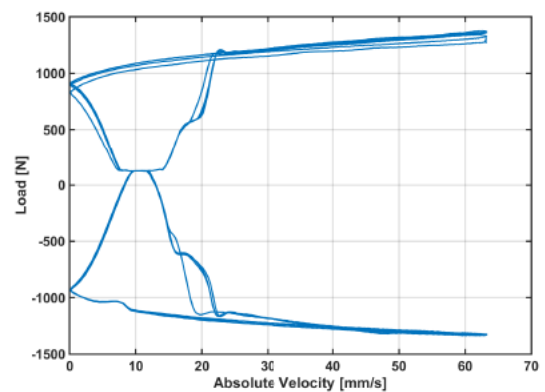
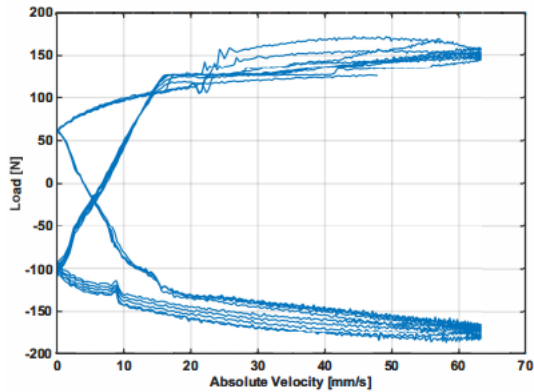
## **MR Damper Vehicle Model Damping Tech Sheet**

*MR Damper Test Case Analysis of Damping*

|  |        |
|--|--------|
| Sprung Mass Critical Damping [kg.s <sup>-1</sup> ]   | 6283.7 |
| Unsprung Mass Critical Damping [kg.s <sup>-1</sup> ] | 7632.8 |

| <u>0 A</u>                     |                       | <u>1.1 A</u>                   |                       |
|--------------------------------|-----------------------|--------------------------------|-----------------------|
| Knee Speed                     | 16 mm.s <sup>-1</sup> | Knee Speed                     | 22 mm.s <sup>-1</sup> |
| Low Speed Compression Damping  | 1400                  | Low Speed Compression Damping  | 83540                 |
| Low Speed Rebound Damping      | 1100                  | Low Speed Rebound Damping      | 89000                 |
| High Speed Compression Damping | 1003                  | High Speed Compression Damping | 4385                  |
| High Speed Rebound Damping     | 833.7                 | High Speed Rebound Damping     | 3765                  |

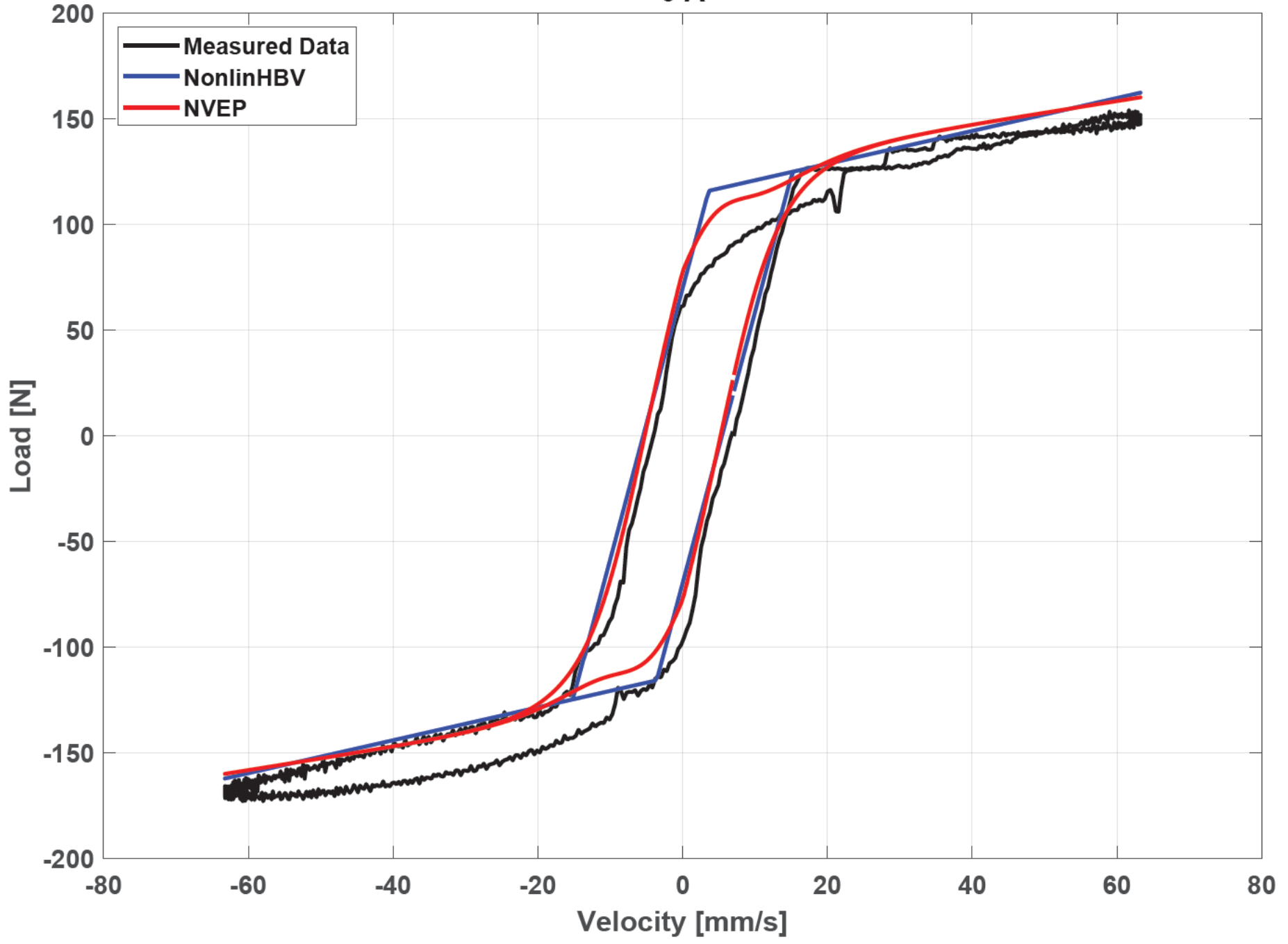
| <u>0 A</u>                 |                | <u>1.1 A</u>               |                |
|----------------------------|----------------|----------------------------|----------------|
| N at 5 mm.s <sup>-1</sup>  |                | N at 5 mm.s <sup>-1</sup>  |                |
| Compression                | -25.87, 82.9   | Compression                | -462.4, 997.8  |
| Rebound                    | -15.68, -120.1 | Rebound                    | 508.9, -1034.0 |
| N at 50 mm.s <sup>-1</sup> |                | N at 50 mm.s <sup>-1</sup> |                |
| Compression                | 157.5          | Compression                | 1290.0         |
| Rebound                    | -164.5, -169.9 | Rebound                    | -1290.0        |



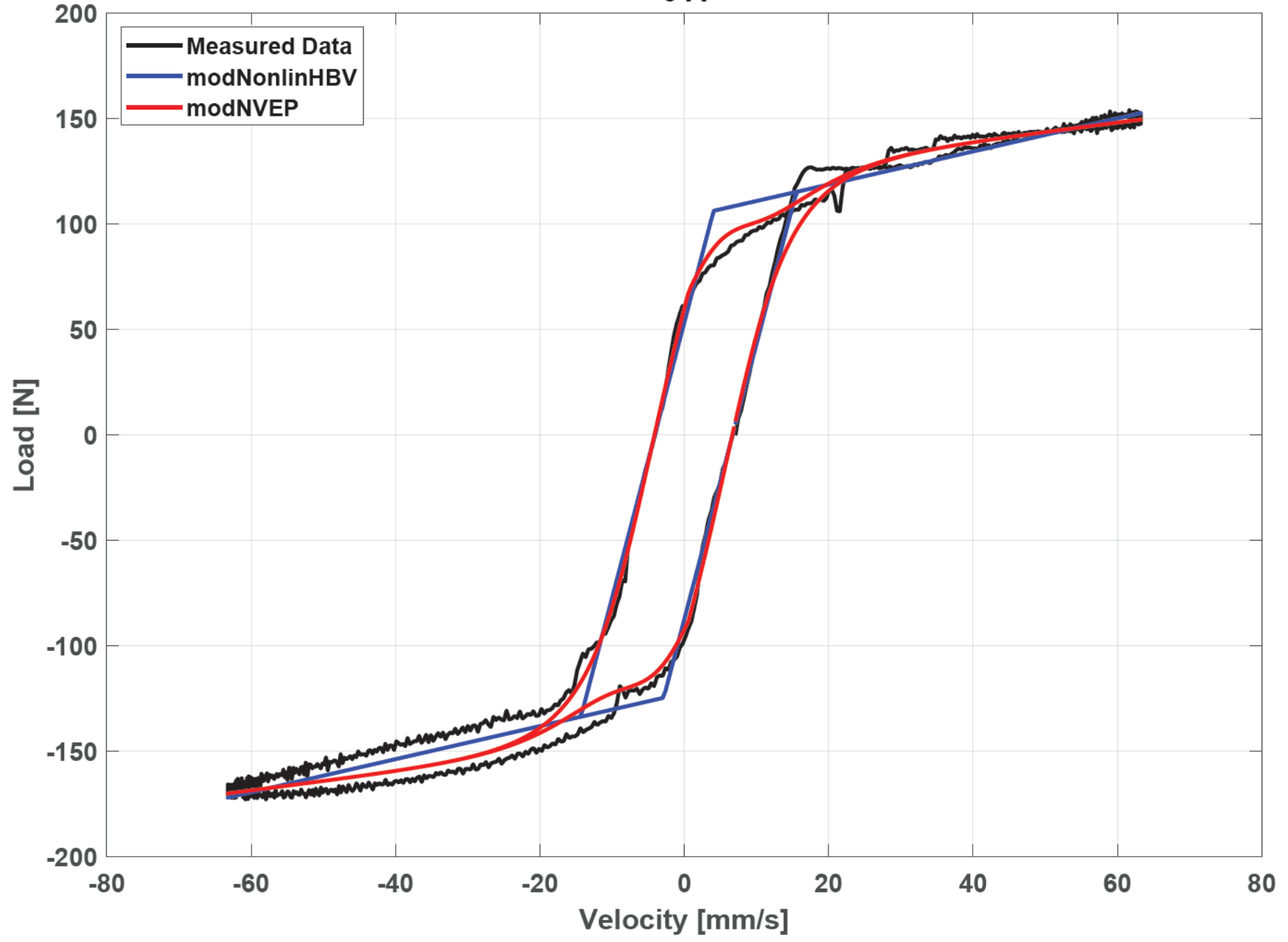
# **Appendix C**

## **MR Damper Model Fitting All Cases**

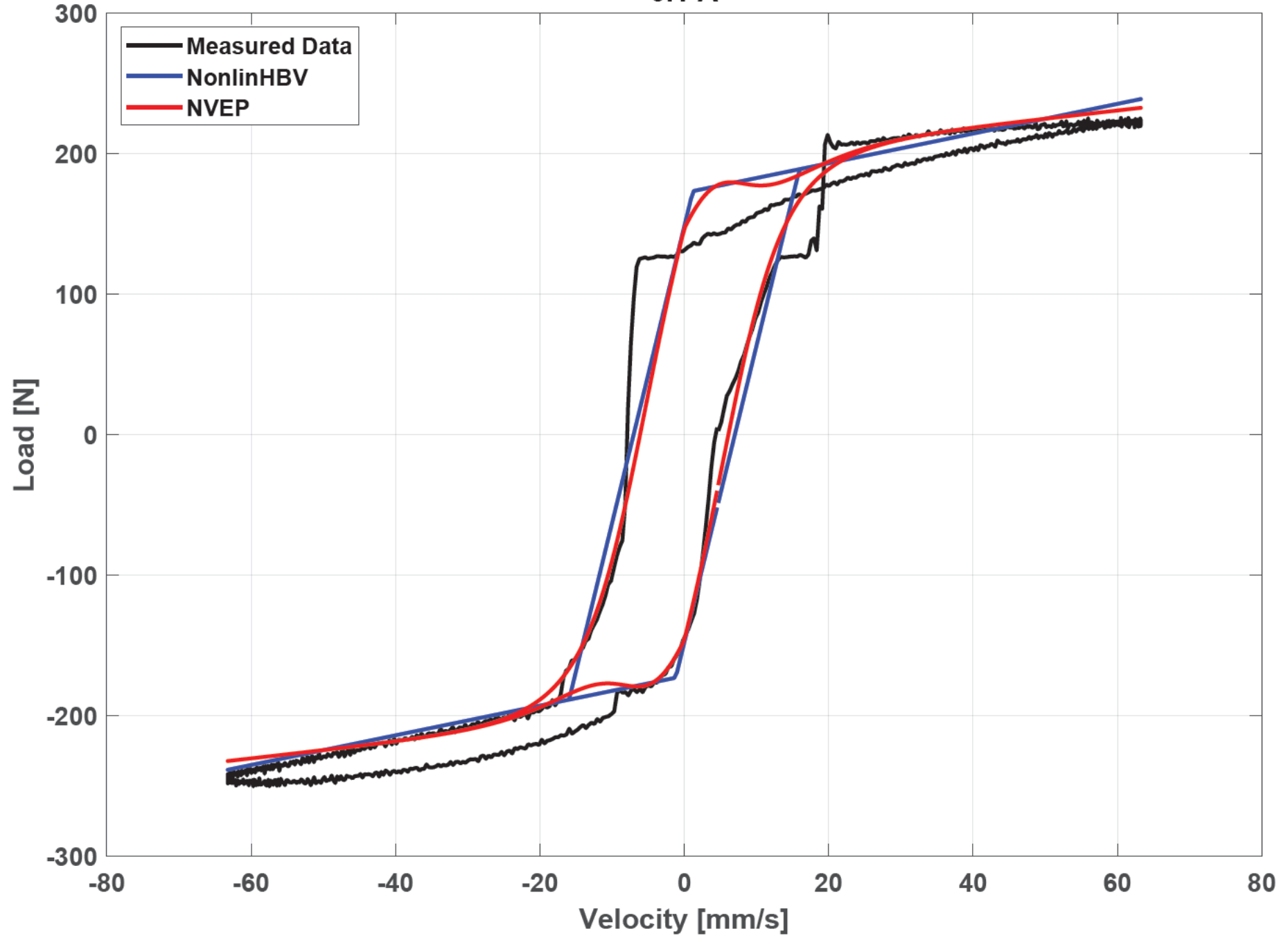
0 A



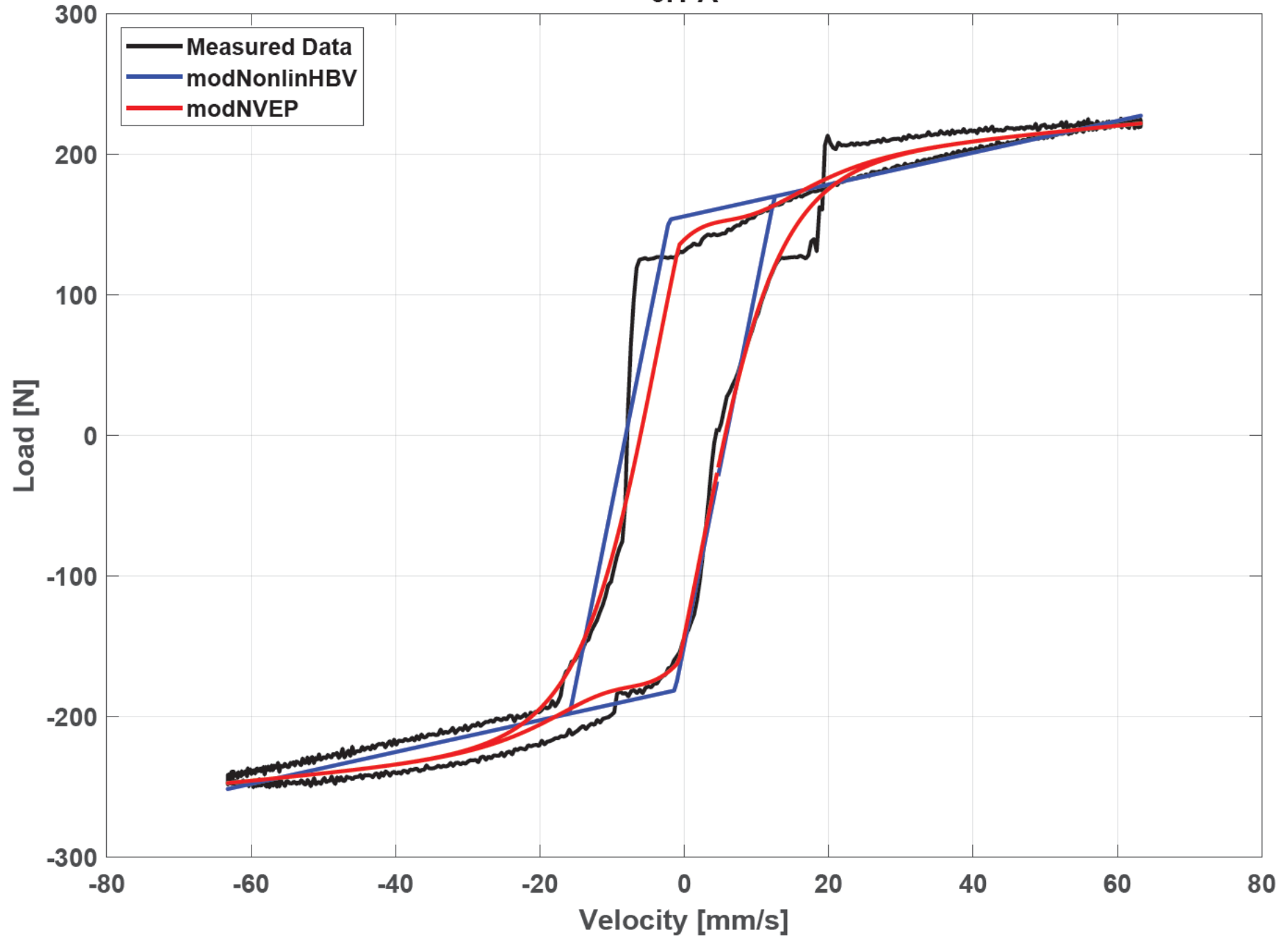
0 A



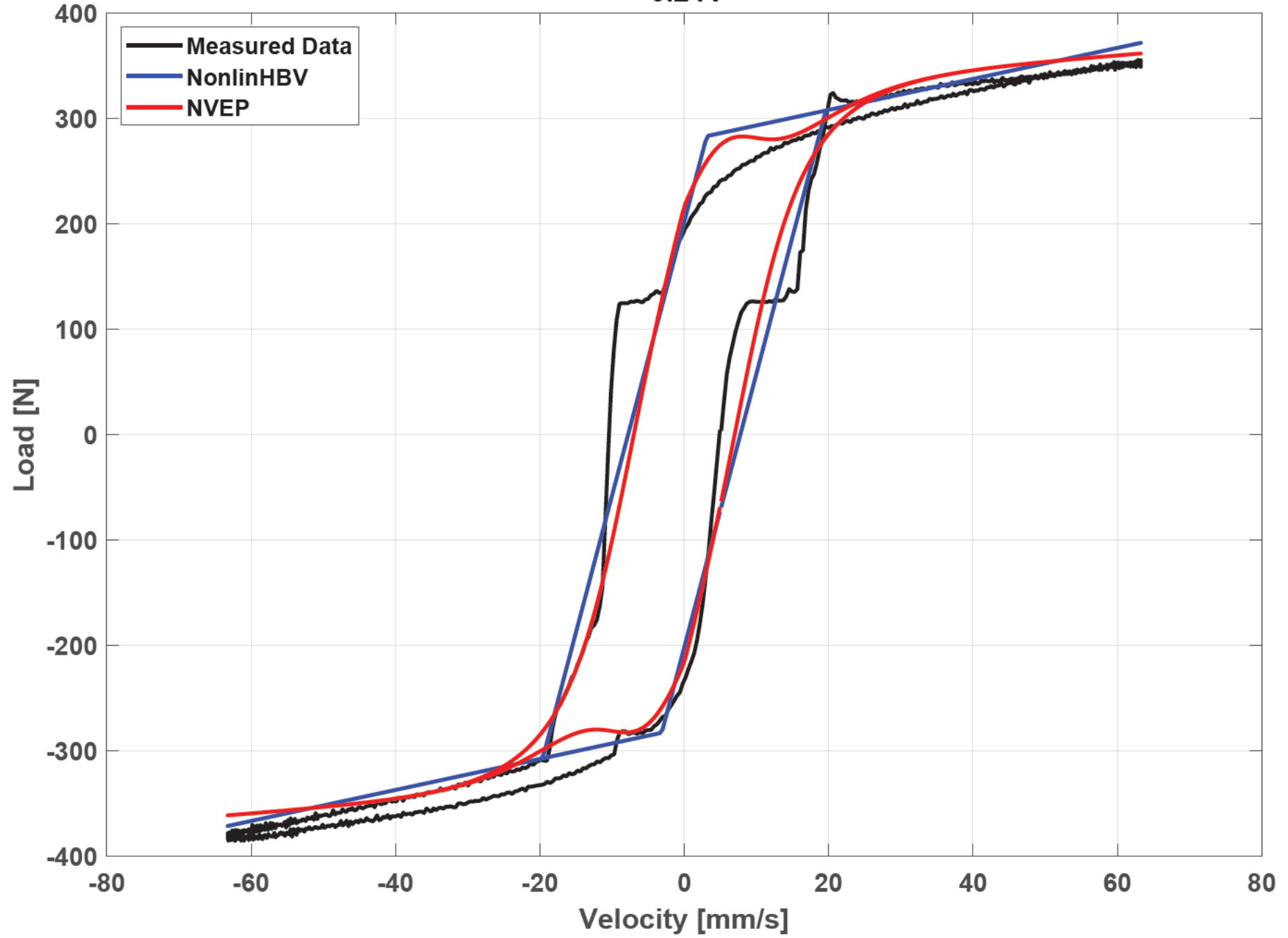
0.1 A



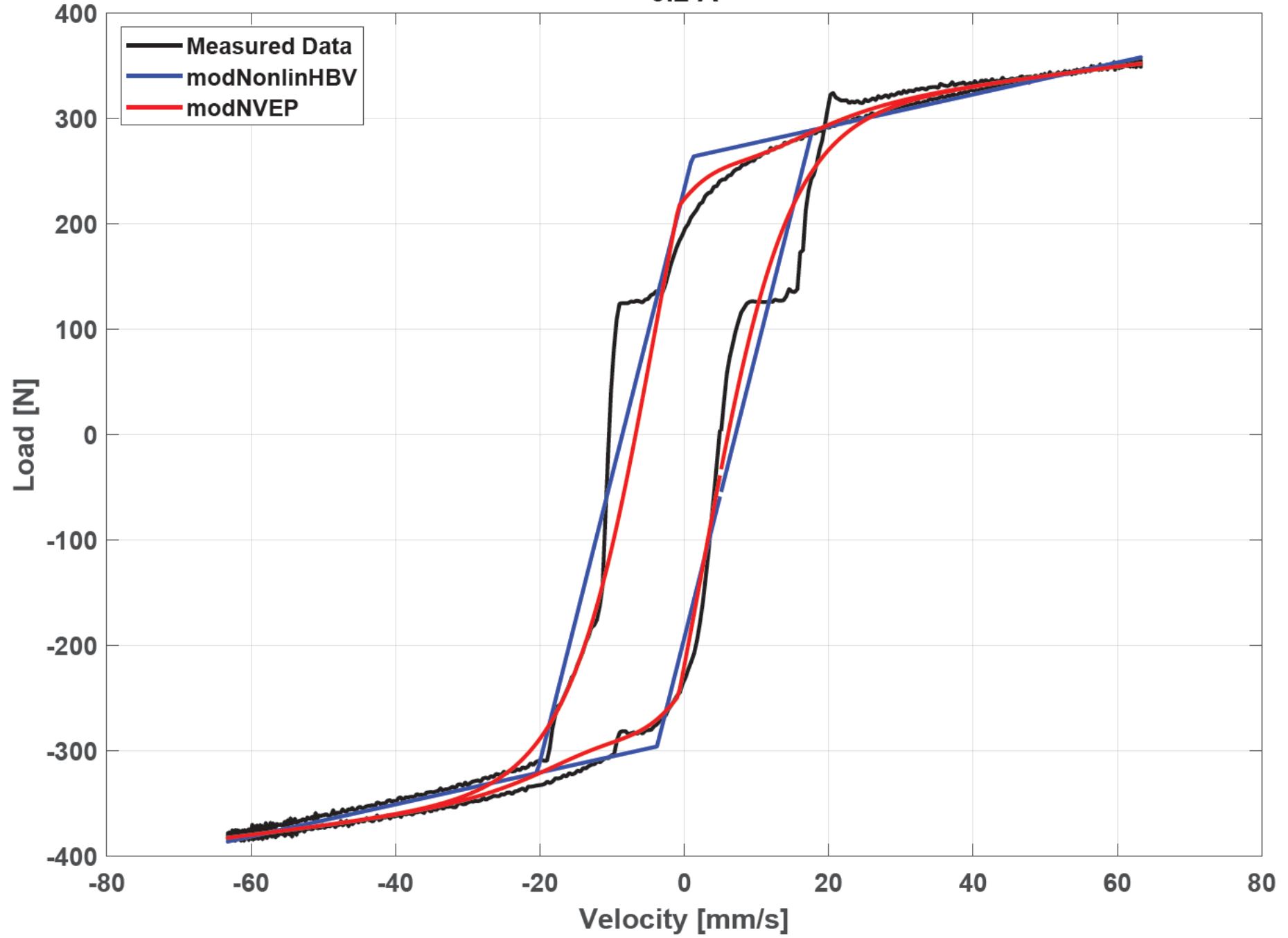
0.1 A



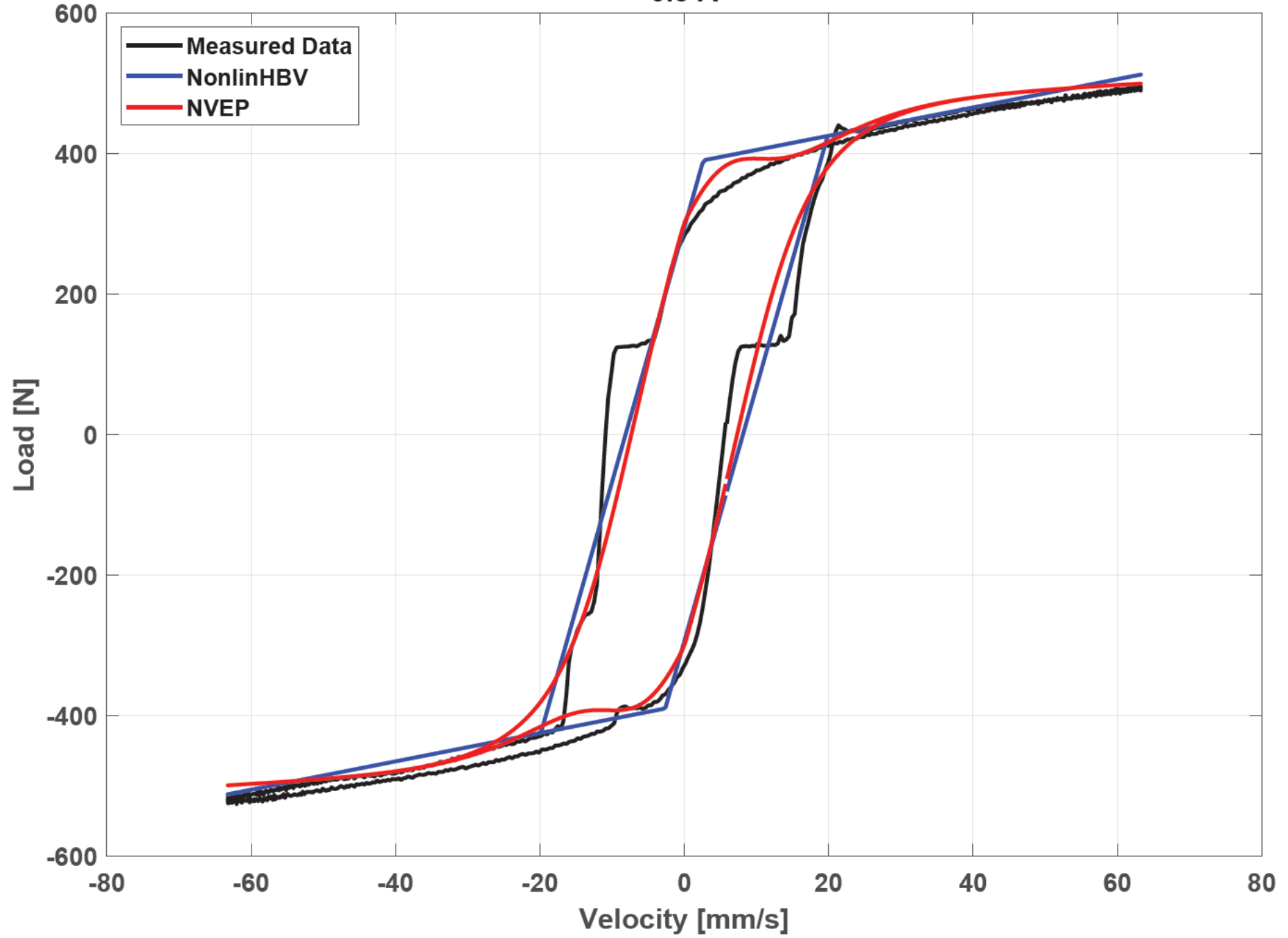
0.2 A



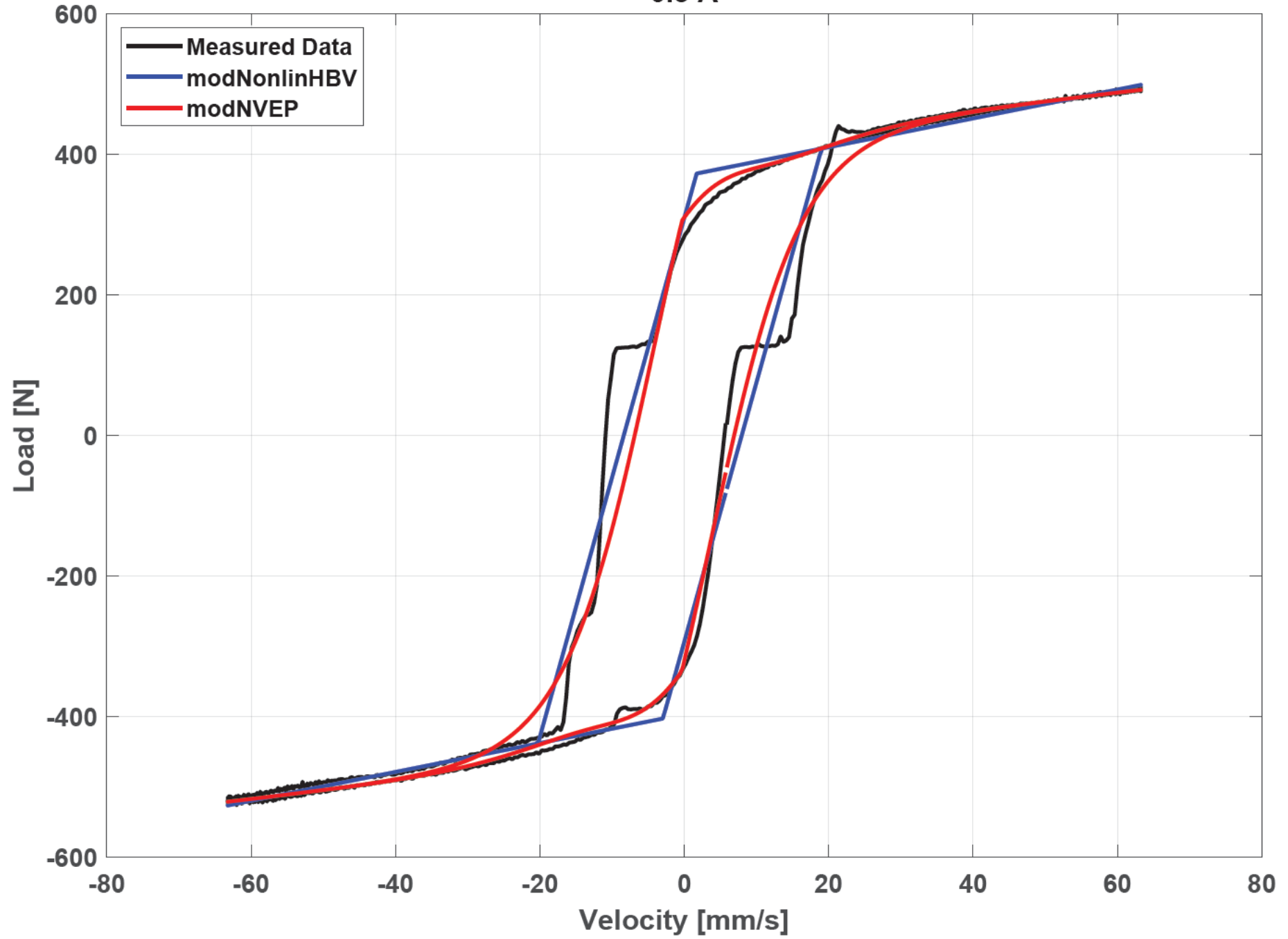
0.2 A



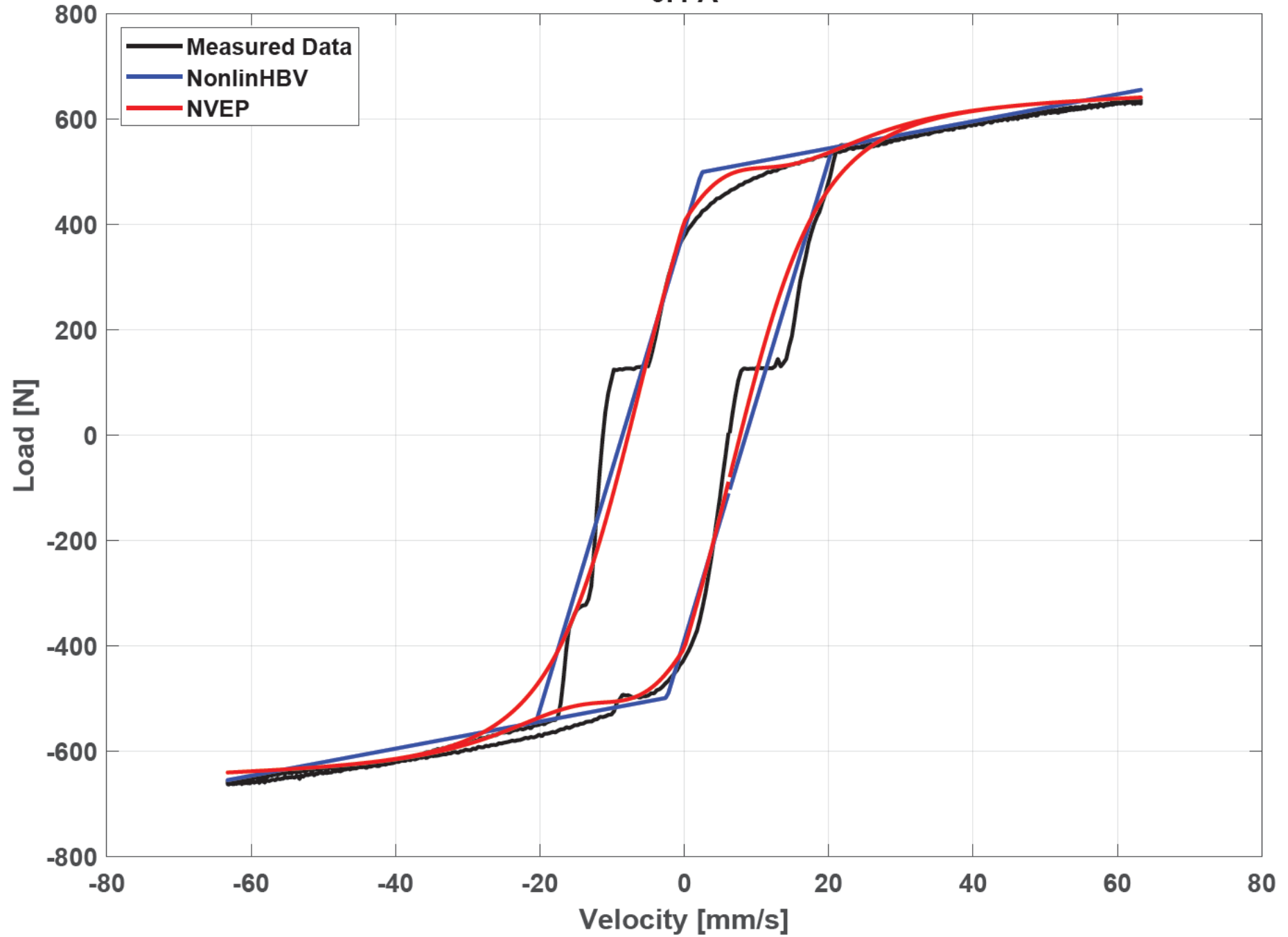
0.3 A



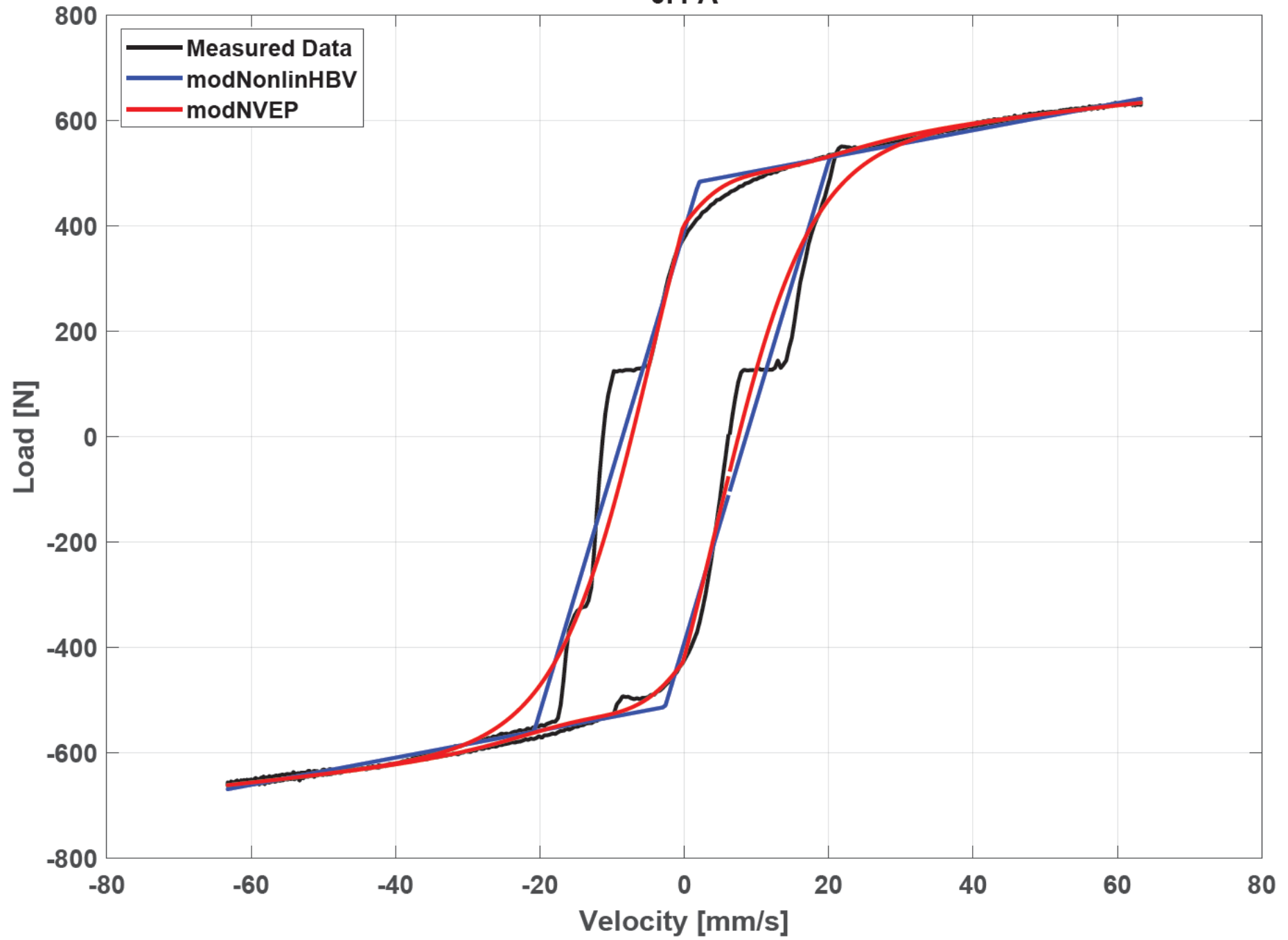
0.3 A



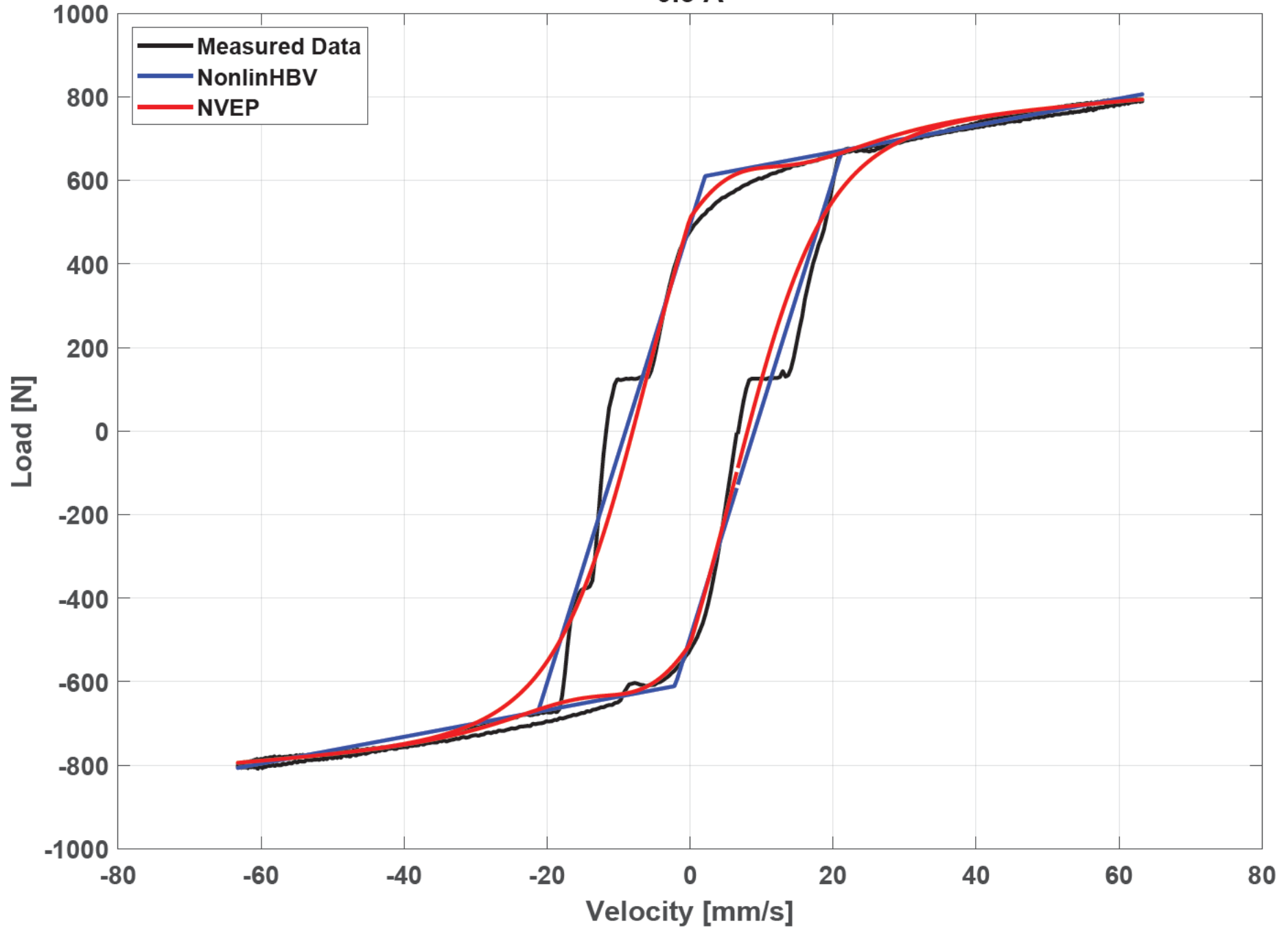
0.4 A



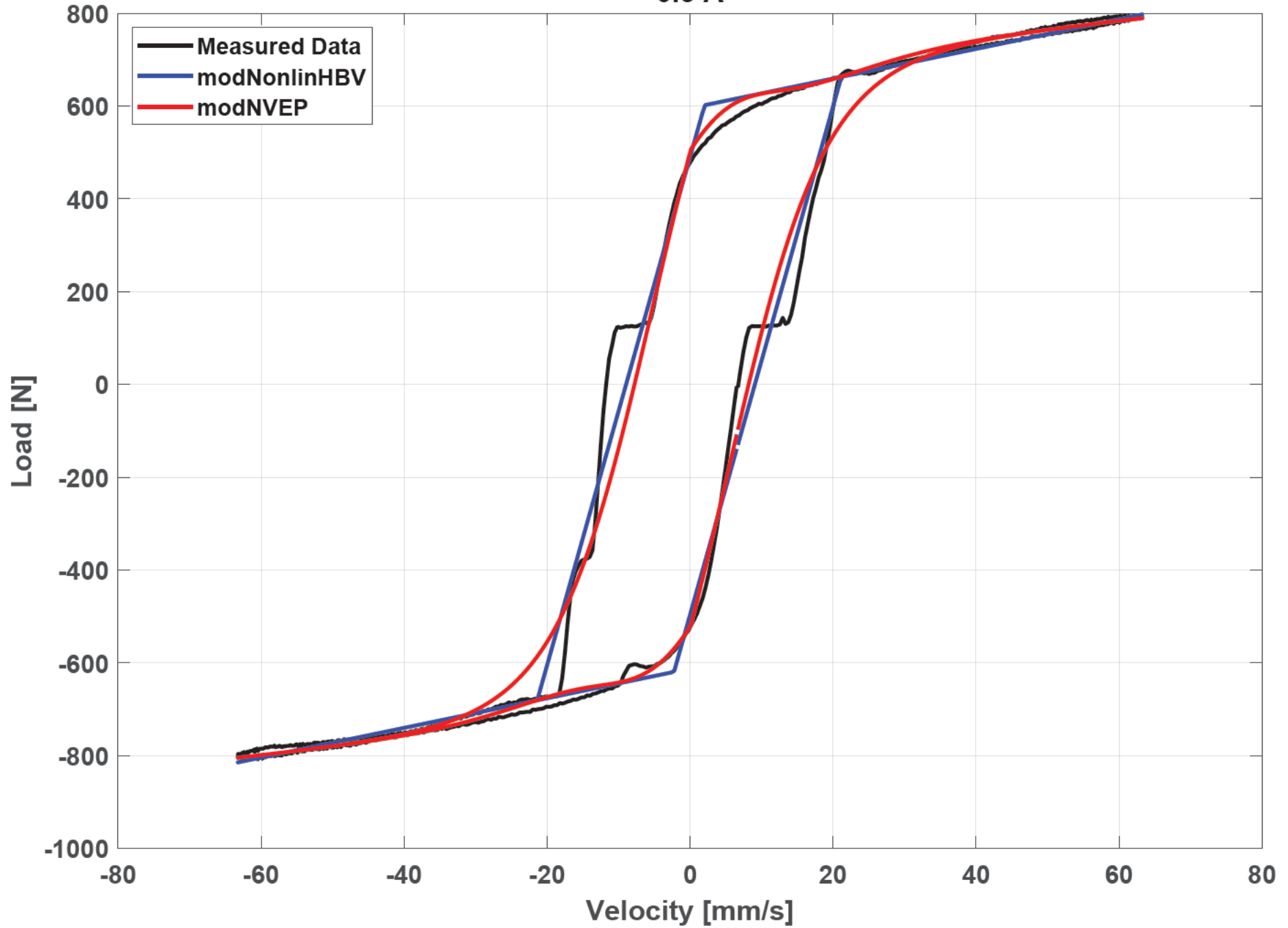
0.4 A



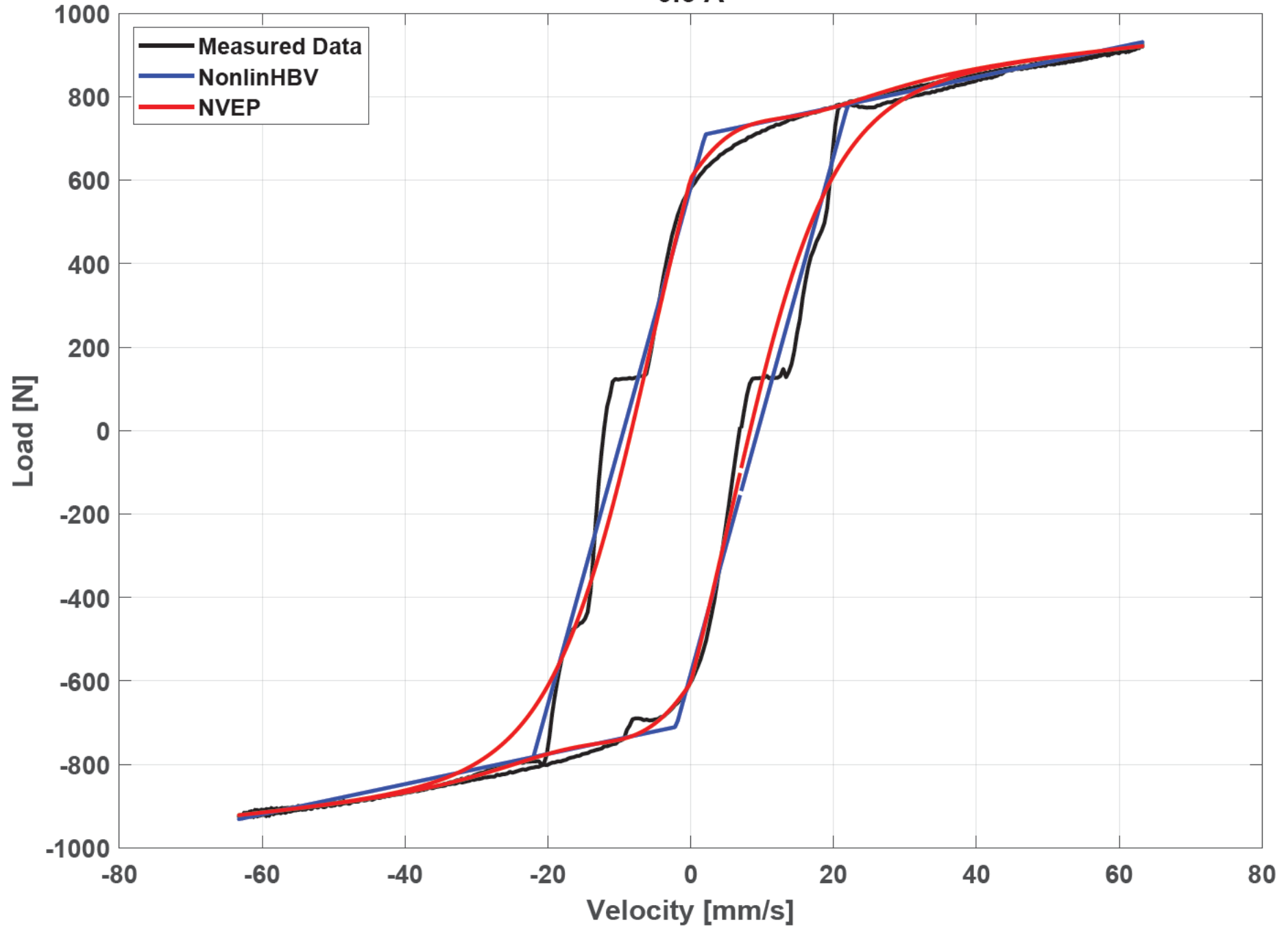
0.5 A



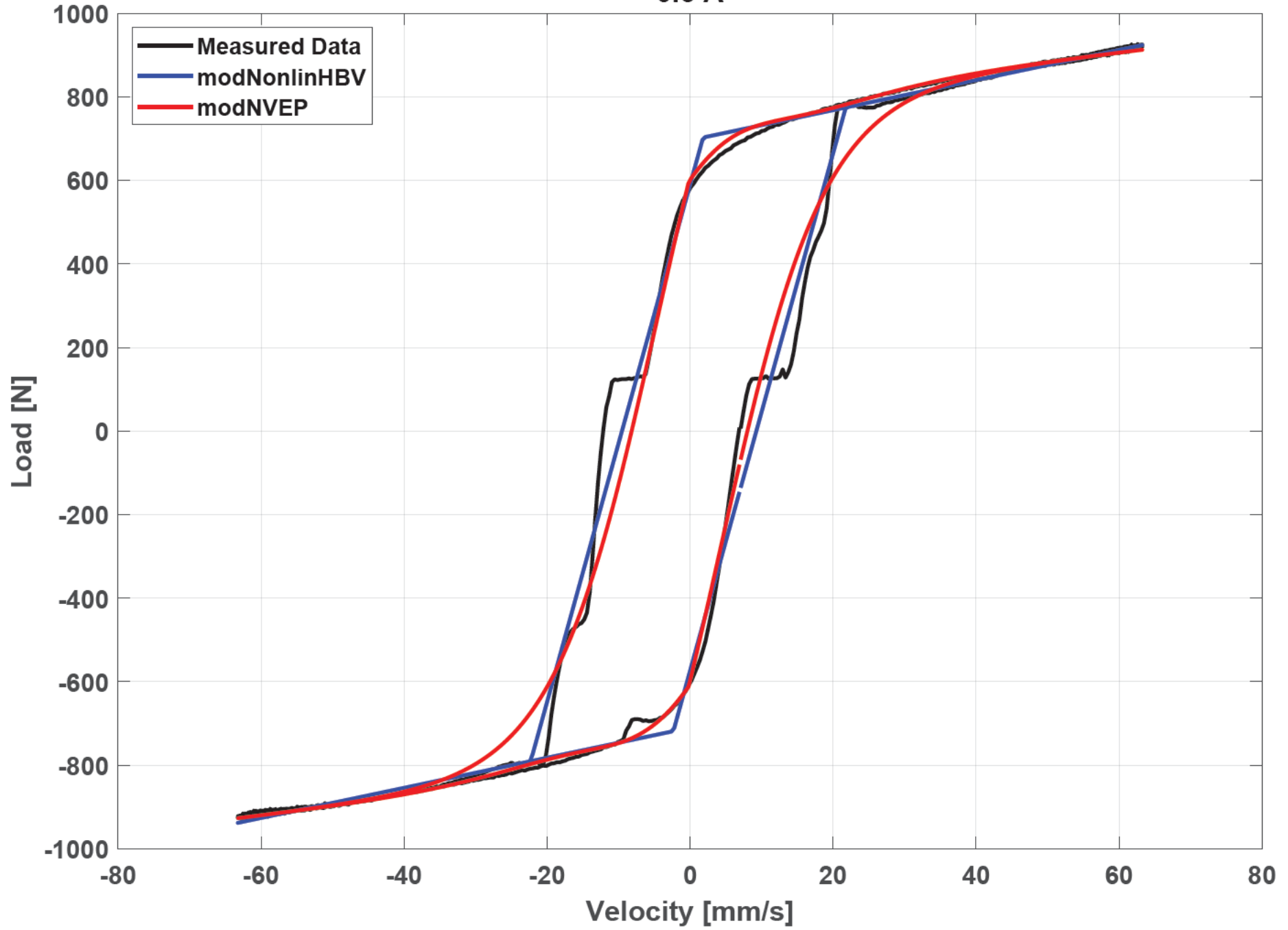
0.5 A



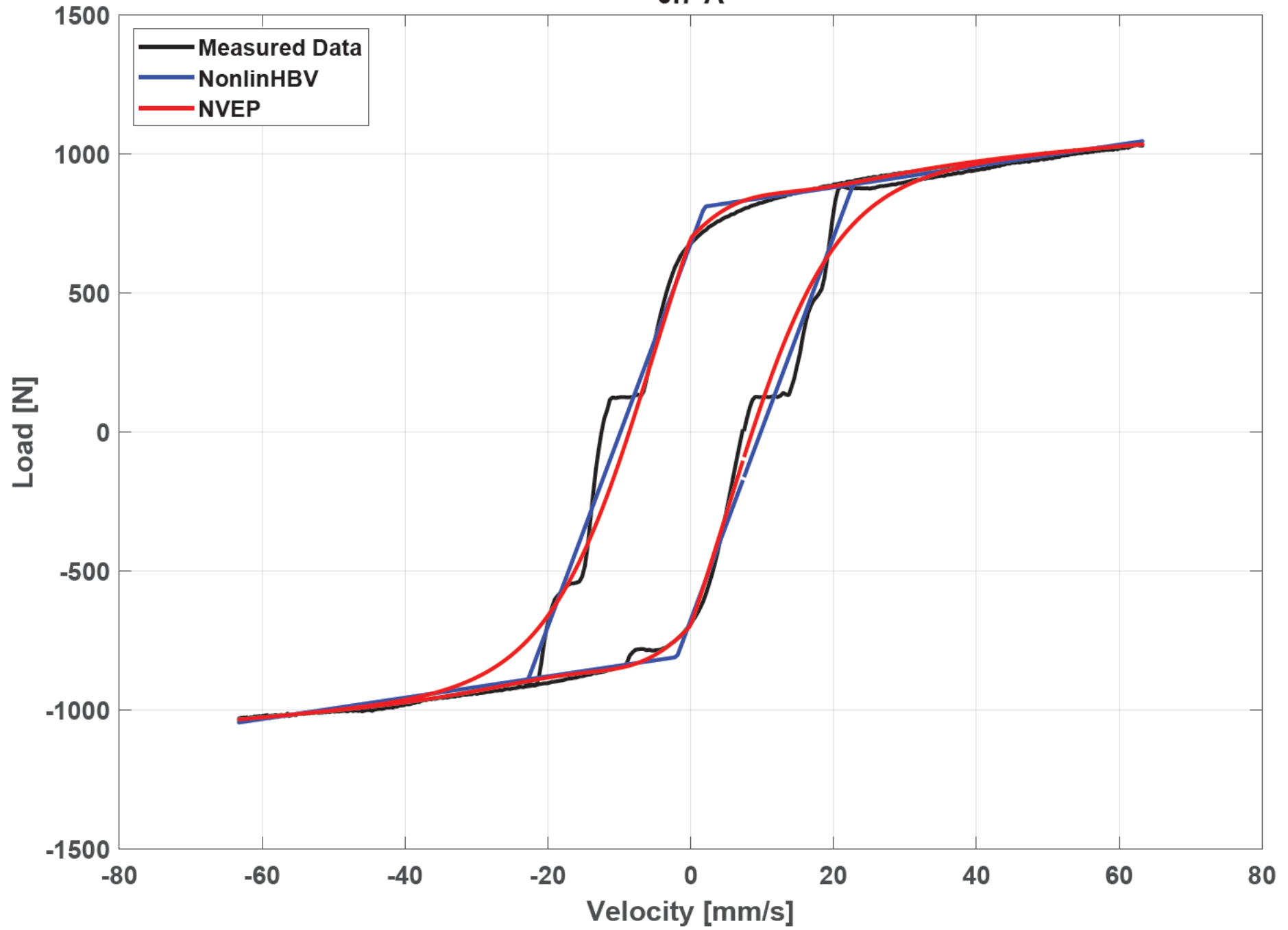
0.6 A



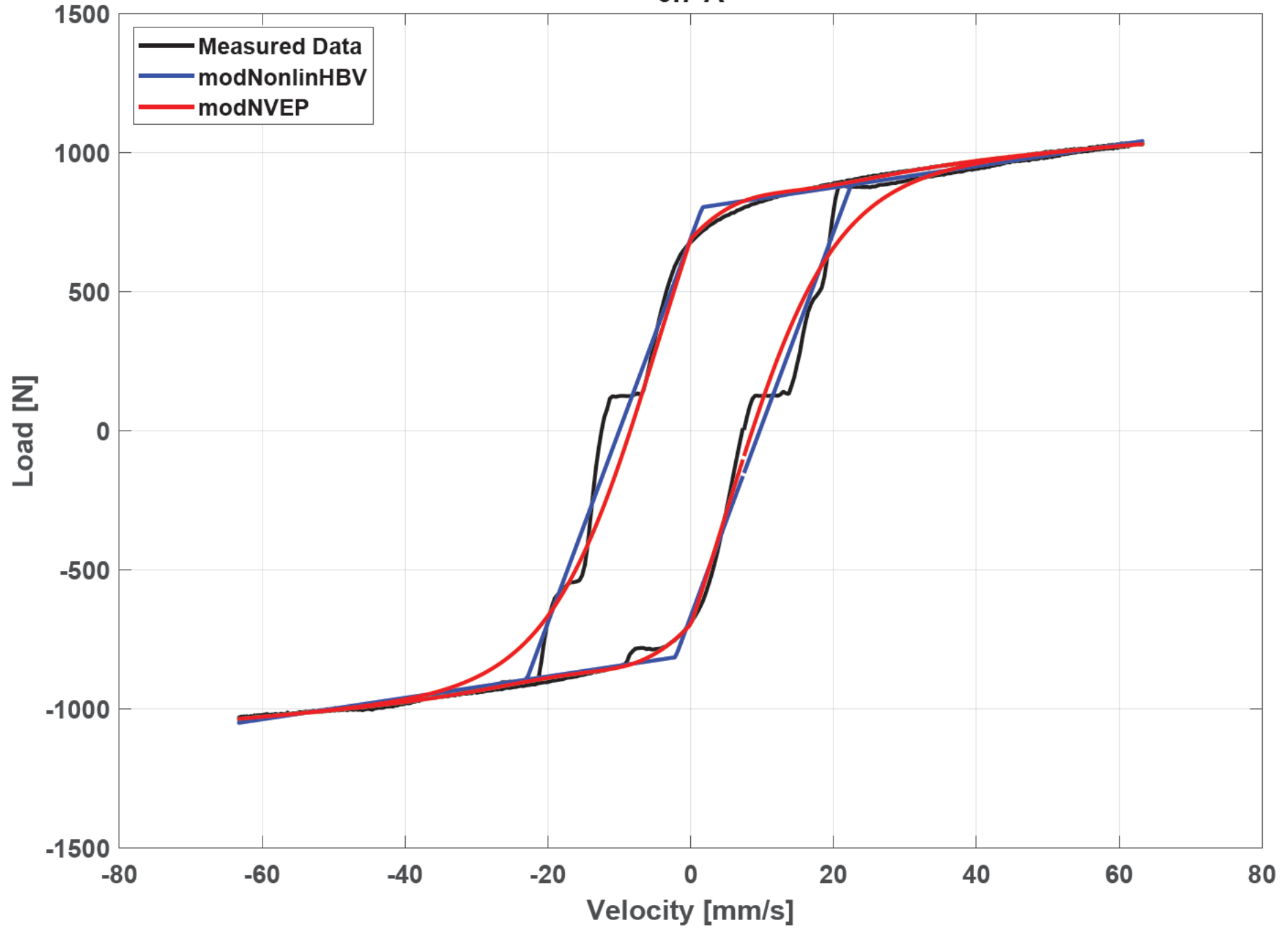
0.6 A



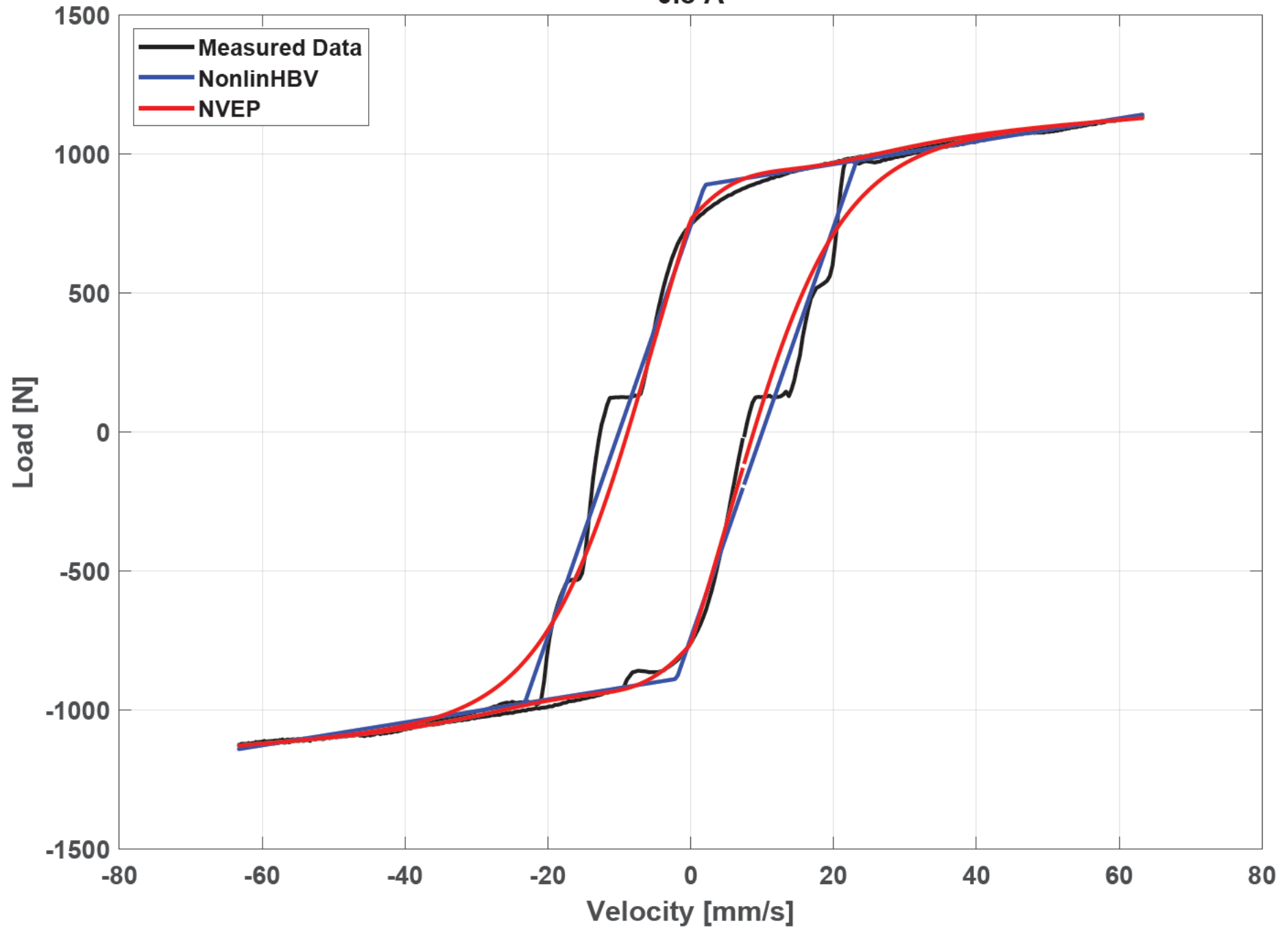
0.7 A



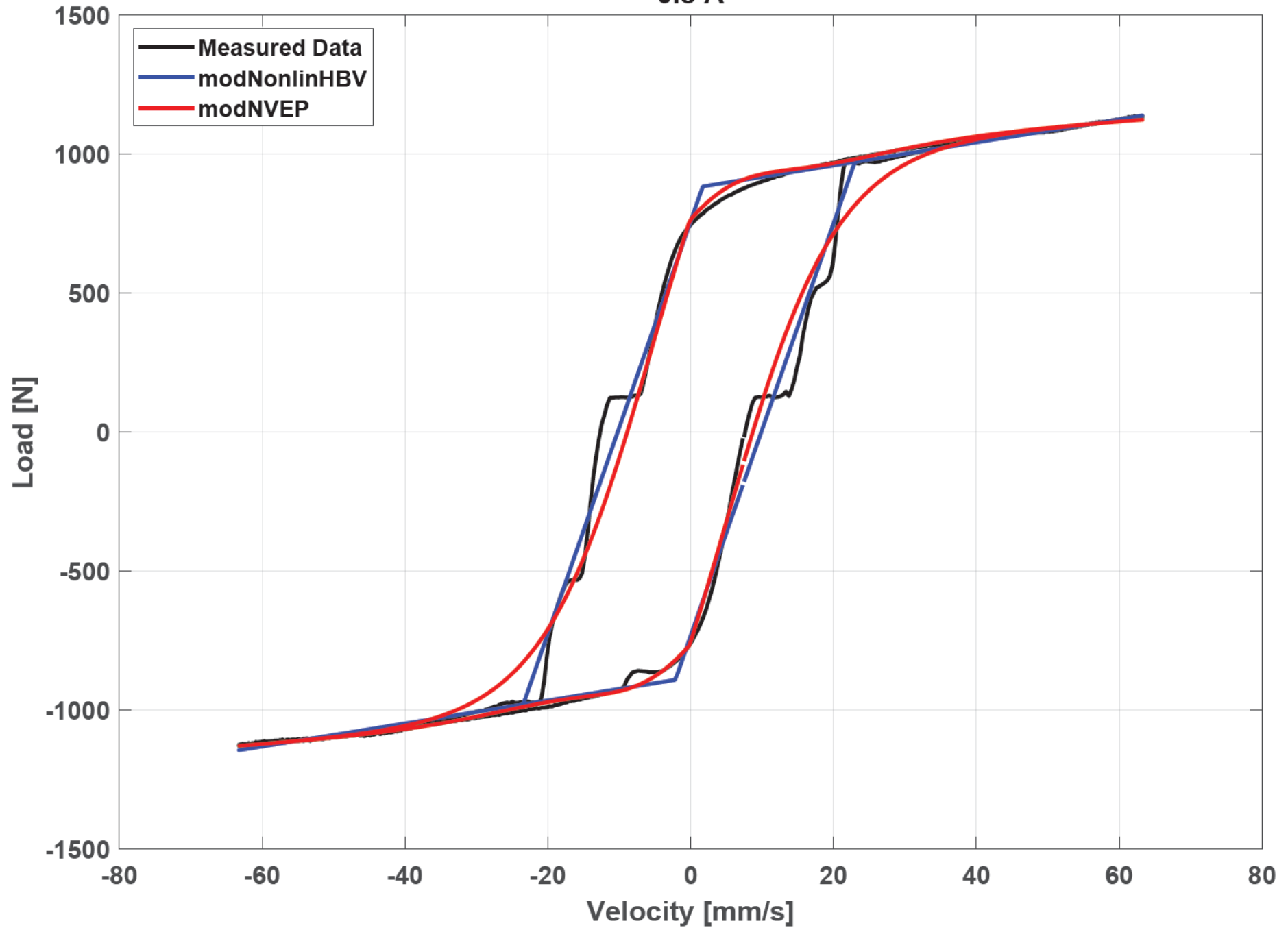
0.7 A



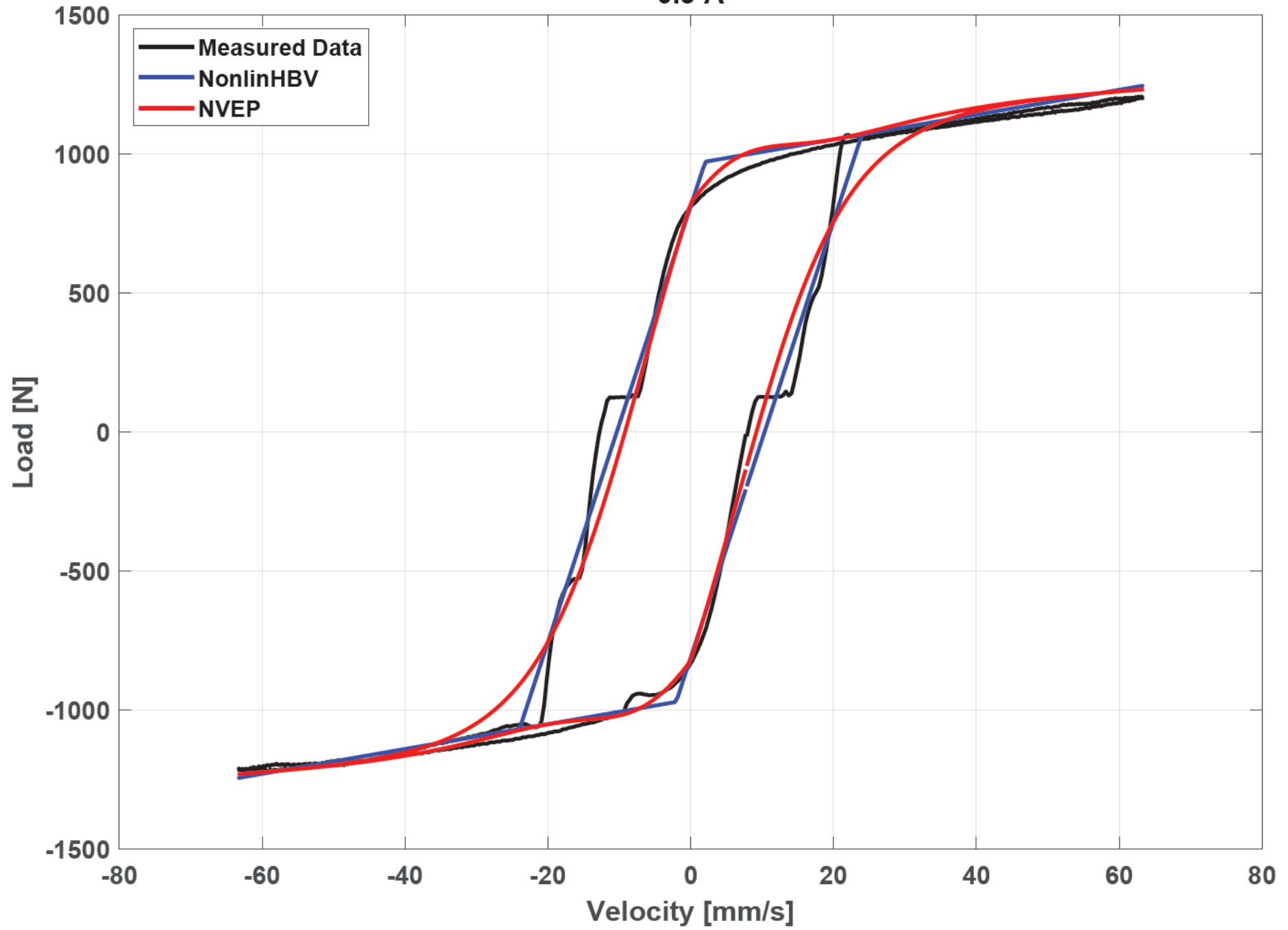
0.8 A



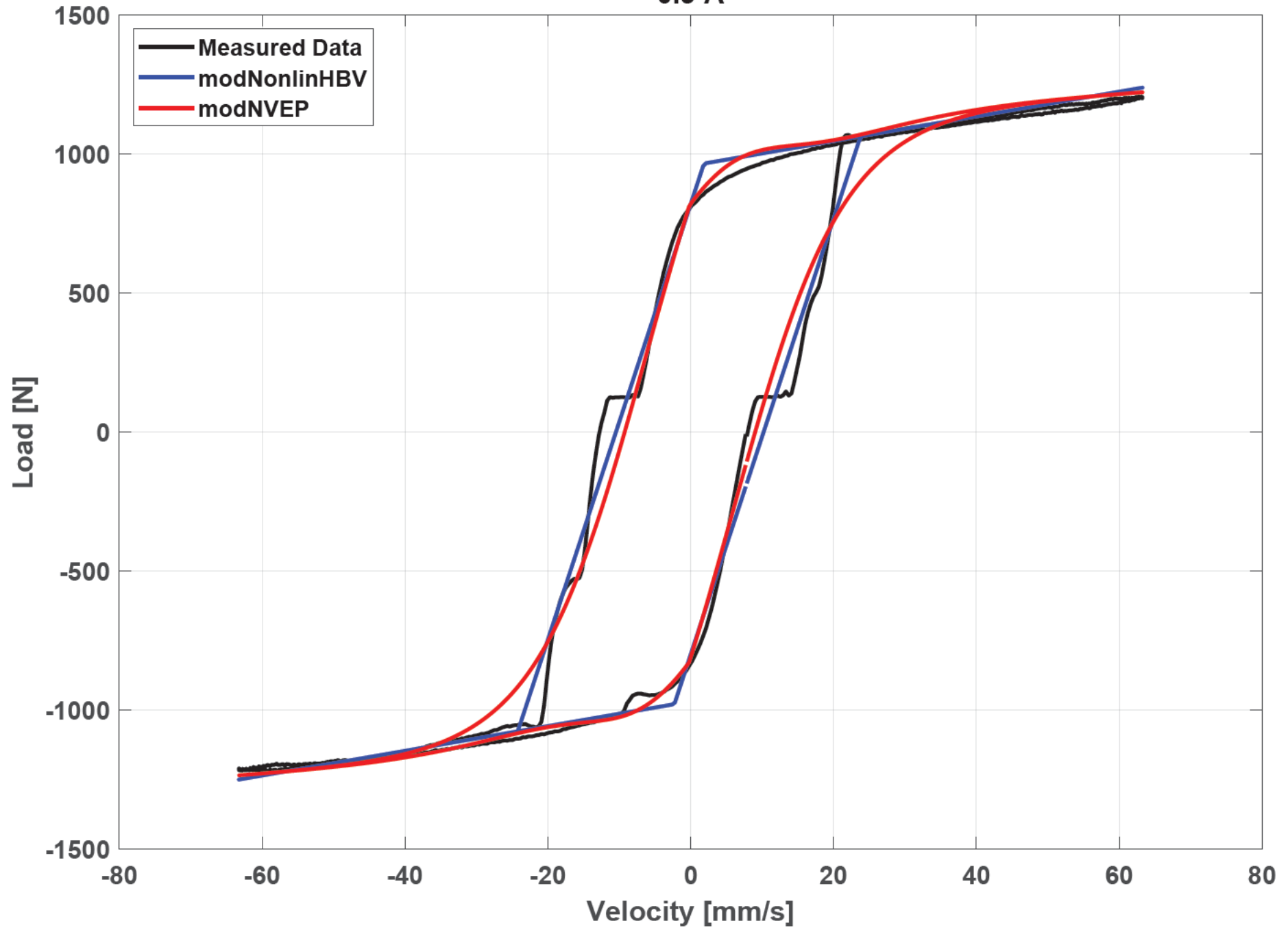
0.8 A



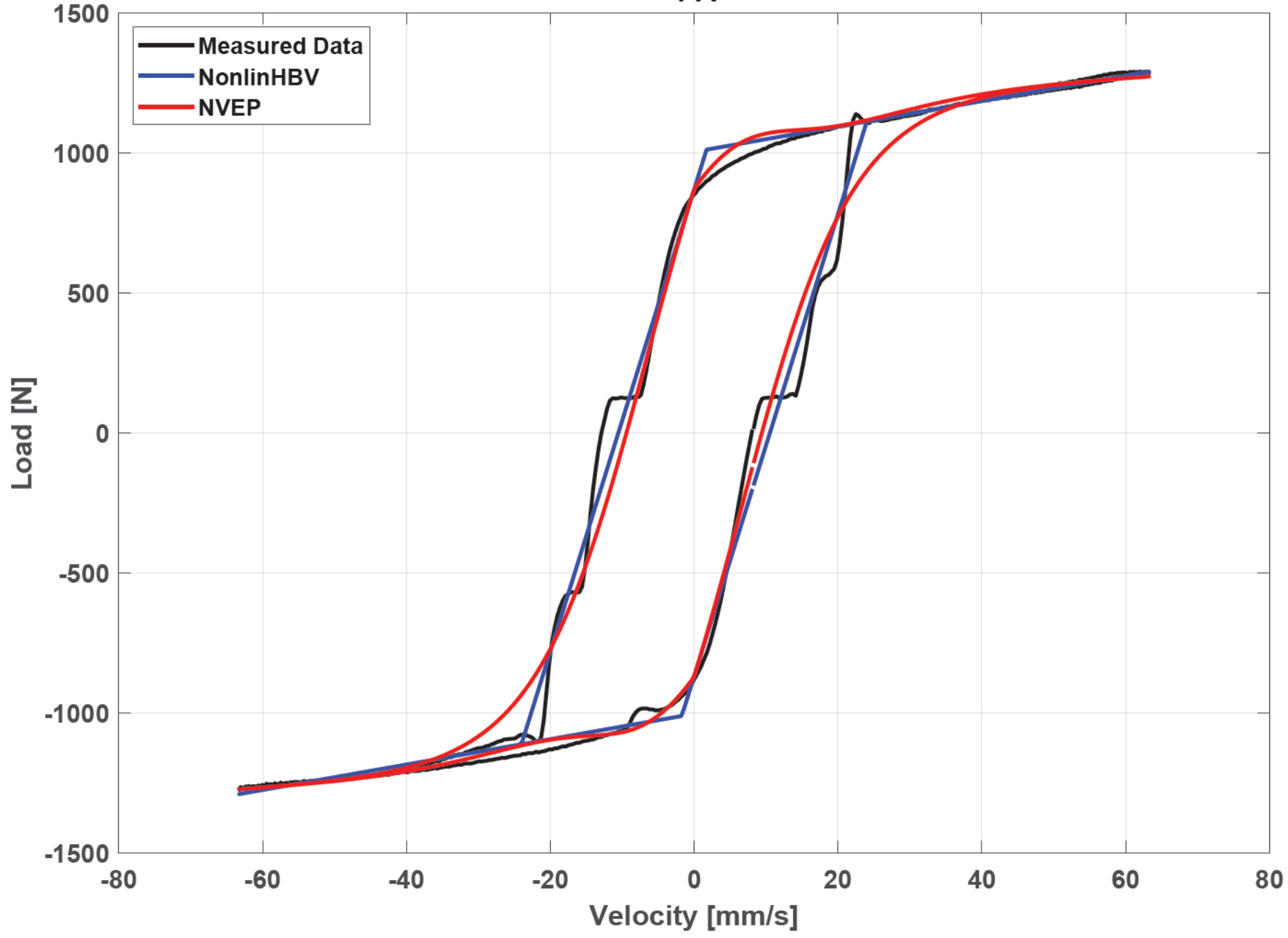
0.9 A



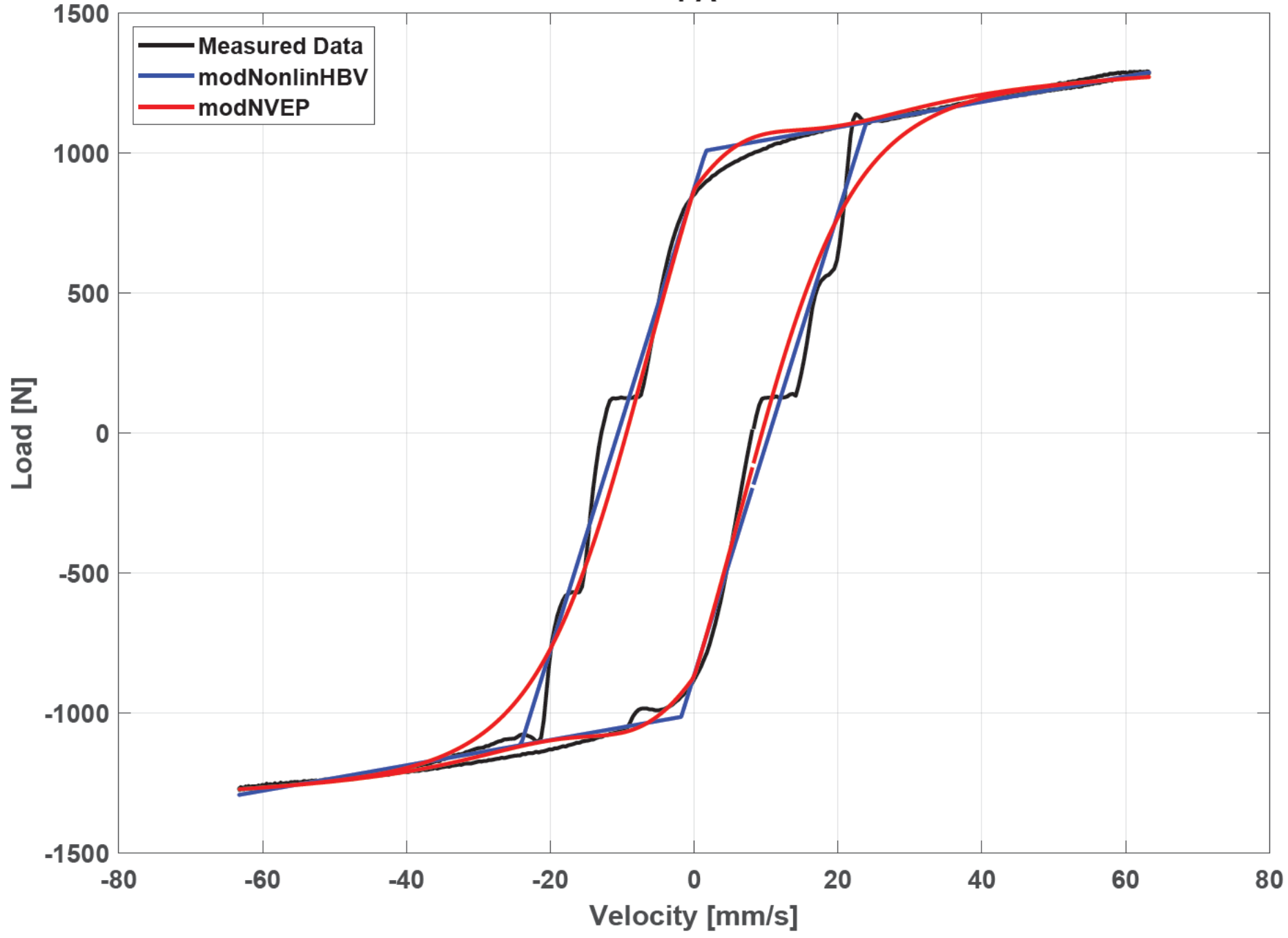
0.9 A



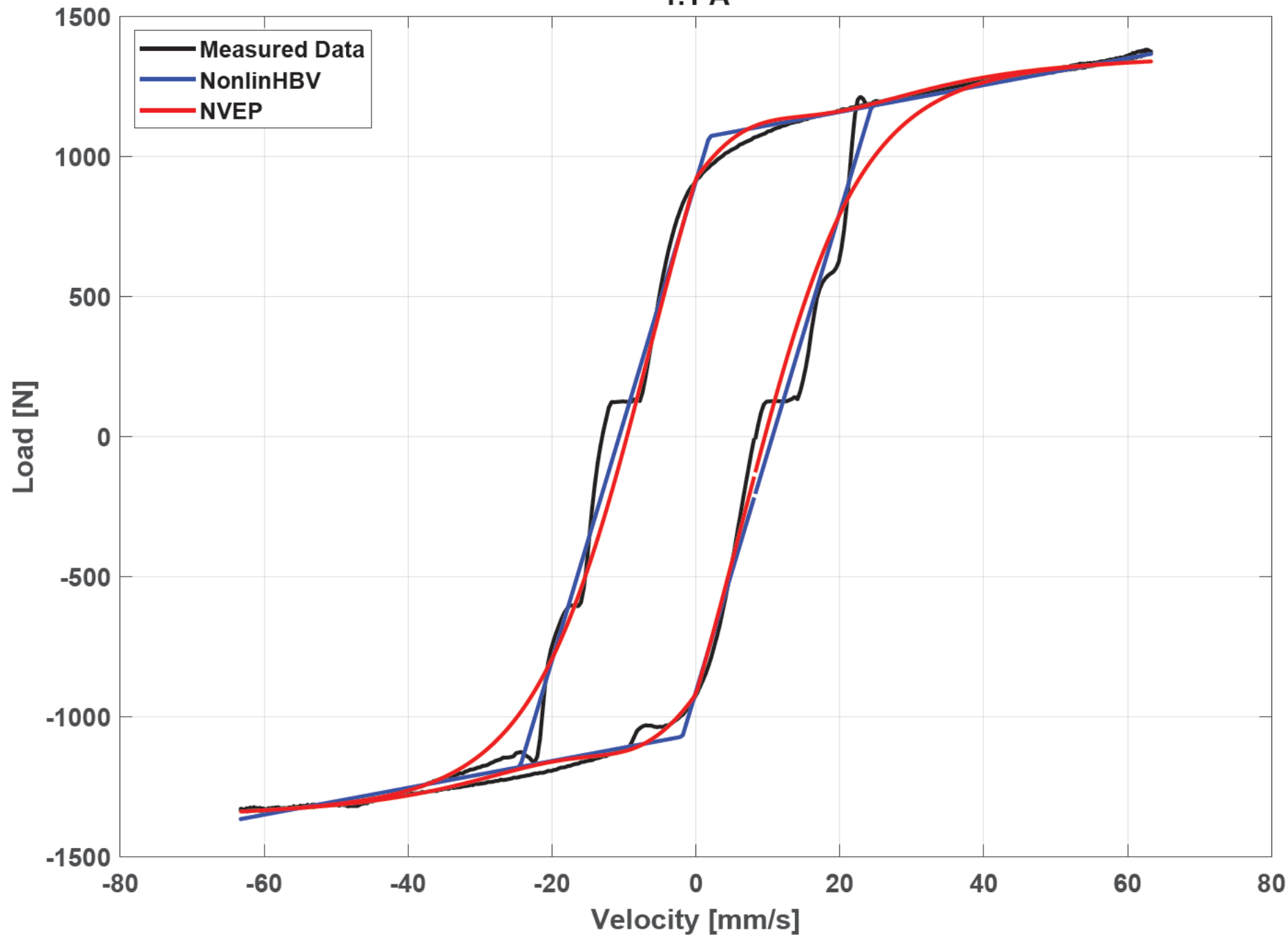
1 A



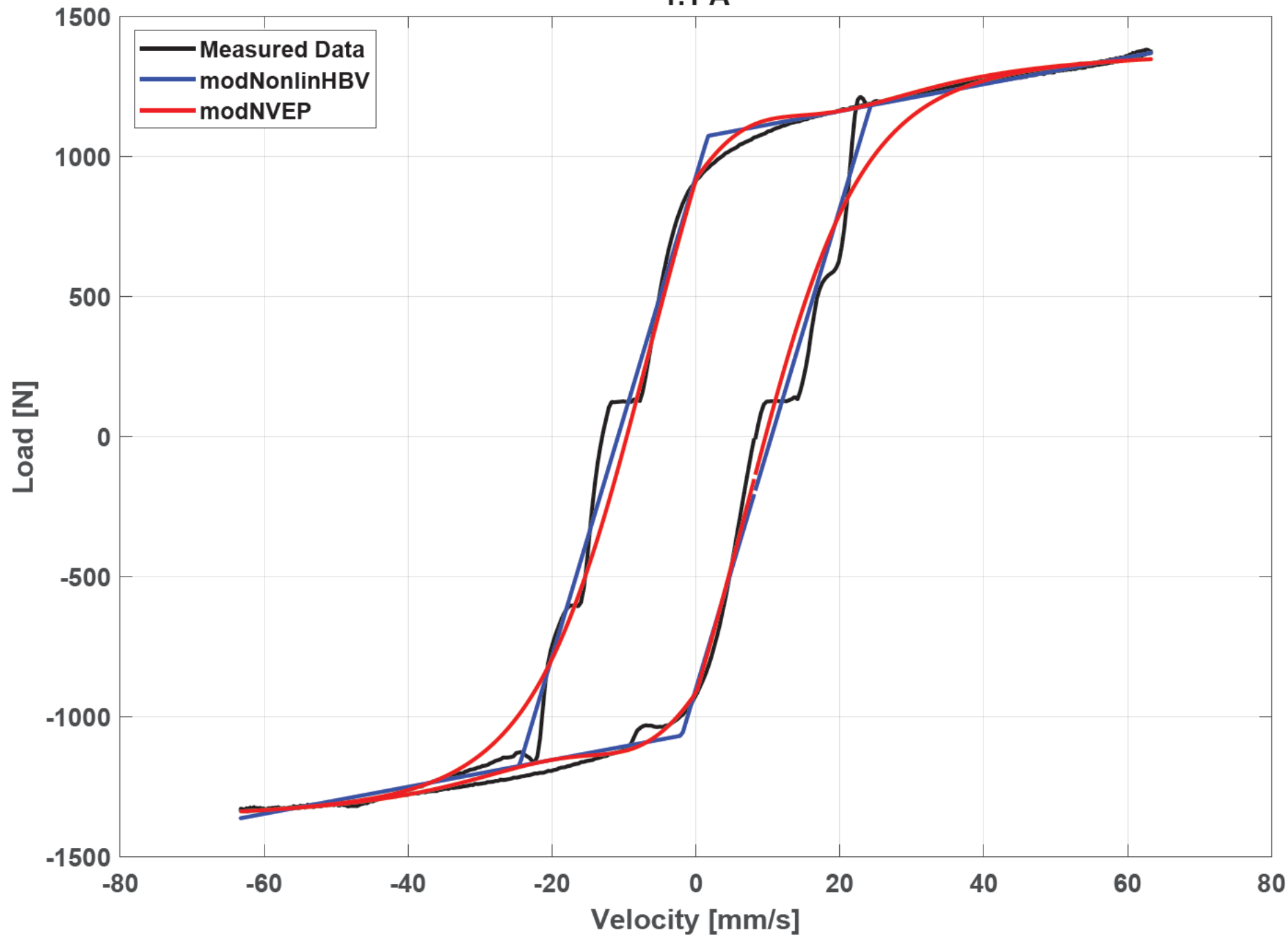
1 A



1.1 A



1.1 A





# Appendix D

## Convergence Time vs Tolerance

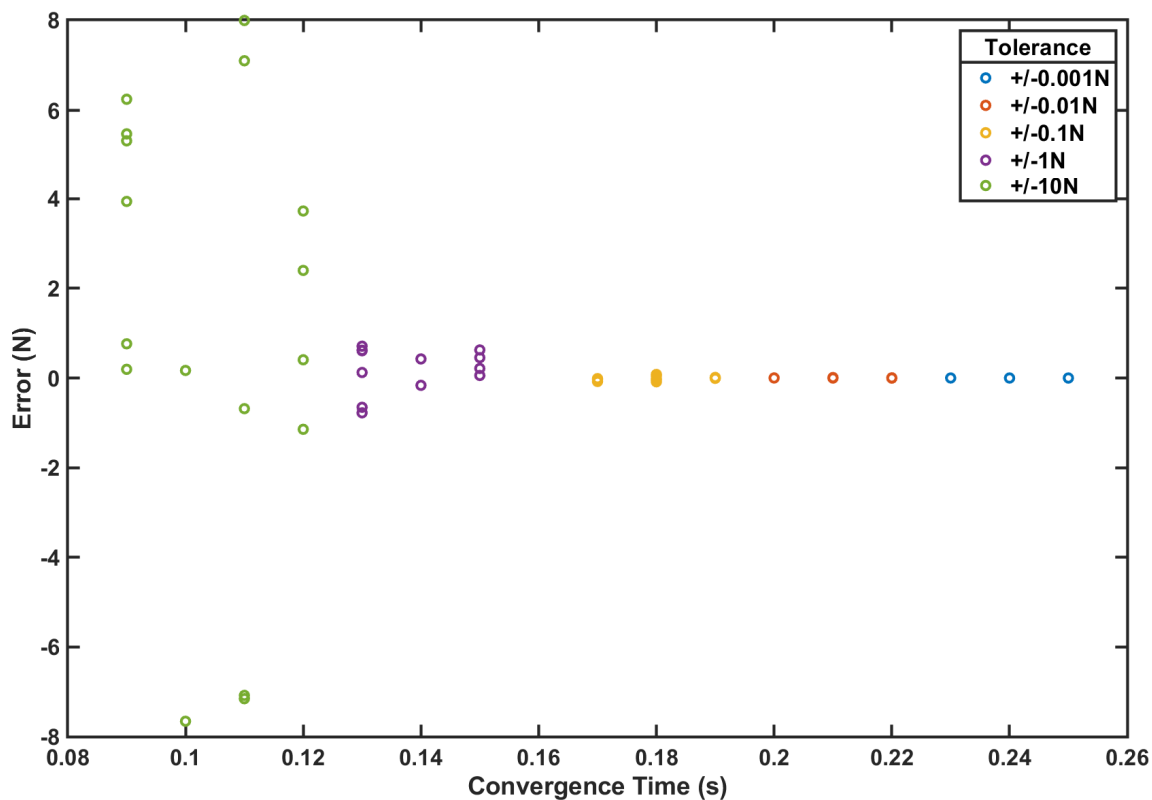


Fig. D.1 A graph showing the Error and Convergence Time of Discrete Tests at 4000 N (Cold Start) for different tolerance values

Table D.1 Bisection Method Convergence Times in seconds for Cold Start Tests

| Load [N]                             |           | 4000 |      |      |      |      | 5000 |      |      |      |      | 6000 |      |      |      |      |
|--------------------------------------|-----------|------|------|------|------|------|------|------|------|------|------|------|------|------|------|------|
| Tolerance [ $\pm N$ ]                |           | 1000 | 100  | 10   | 1    | 0.1  | 1000 | 100  | 10   | 1    | 0.1  | 1000 | 100  | 10   | 1    | 0.1  |
| Soil 1<br>(Dry Sand)                 | Treaded   | 0.25 | 0.22 | 0.19 | 0.15 | 0.12 | 0.25 | 0.22 | 0.19 | 0.15 | 0.12 | 0.25 | 0.22 | 0.19 | 0.16 | 0.12 |
|                                      | Treadless | 0.25 | 0.22 | 0.19 | 0.15 | 0.12 | 0.25 | 0.22 | 0.19 | 0.15 | 0.12 | 0.25 | 0.22 | 0.19 | 0.16 | 0.12 |
| Soil 2<br>(Upland<br>Sandy<br>Loam)  | Treaded   | 0.26 | 0.23 | 0.19 | 0.16 | 0.13 | 0.26 | 0.22 | 0.19 | 0.16 | 0.13 | 0.26 | 0.23 | 0.19 | 0.16 | 0.13 |
|                                      | Treadless | 0.26 | 0.22 | 0.19 | 0.16 | 0.12 | 0.26 | 0.22 | 0.19 | 0.16 | 0.13 | 0.26 | 0.22 | 0.19 | 0.16 | 0.13 |
| Soil 3<br>(Rubicon<br>Sandy<br>Loam) | Treaded   | 0.26 | 0.22 | 0.19 | 0.16 | 0.12 | 0.26 | 0.22 | 0.19 | 0.16 | 0.12 | 0.26 | 0.22 | 0.19 | 0.16 | 0.12 |
|                                      | Treadless | 0.26 | 0.22 | 0.19 | 0.16 | 0.12 | 0.26 | 0.22 | 0.19 | 0.16 | 0.12 | 0.26 | 0.22 | 0.19 | 0.16 | 0.13 |

# **Appendix E**

## **PID Tuning Application**

The PID Tuning Application uses the Matlab Application Toolbox to produce and tune the response of a PID Controller for use with MR Damper suspension. The Application is designed for ease of use to allow for manual tuning to improve the performance.

Table E.1 Adaptive PID Controller Gain Component Influence on System Response

- (1) Rise Time (Sprung Mass Displacement),  
 (2) Settling Time (Sprung Mass Displacement),  
 (3) Maximum Amplitude (Sprung Mass Displacement),  
 (4) Absentment of Suspension (Integral of Suspension Displacement with Respect to Time),  
 (5) Maximum Positive Amplitude (Sprung Mass Acceleration),  
 (6) Maximum Negative Amplitude (Sprung Mass Acceleration),  
 (7) Integral of Control Action (Current Supply to MR Damper),  
 (8) Integral of the Absolute Difference of Control Action

| Gain  | 1 | 2 | 3 | 4       | 5 | 6 | 7 | 8 |
|---|---|---|---|---------|---|---|---|---|
| $P_1$<br>(Static Proportional Gain Component)               | ↓ | ↑ | ↑ | 0<br>↑+ | ↑ | ↓ | ↑ | ↑ |
| $P_2$<br>(Dynamic Proportional Gain Displacement Component) | ↓ | - | - | 0<br>↑+ | ↓ | - | ↓ | ↓ |
| $P_3$<br>(Dynamic Proportional Gain Velocity Component)     | ↓ | ↑ | ↑ | 0<br>↑+ | ↓ | - | ↑ | ↑ |
| $I_1$<br>(Static Integral Gain Component)                   | ↑ | ↓ | - | 0<br>↓- | - | - | ↓ | - |
| $I_2$<br>(Dynamic Integral Gain Displacement Component)     | - | ↓ | - | 0<br>↓- | - | - | ↓ | - |
| $I_3$<br>(Dynamic Integral Gain Velocity Component)         | ↓ | ↓ | - | 0<br>↑+ | ↓ | ↑ | ↓ | ↓ |
| $D_1$<br>(Static Derivative Gain Component)                 | ↓ | ↑ | ↑ | 0<br>↑+ | ↑ | ↓ | ↑ | ↑ |
| $D_2$<br>(Dynamic Derivative Gain Displacement Component)   | ↓ | ↓ | ↑ | ↑+<br>0 | ↑ | ↑ | ↑ | ↑ |
| $D_3$<br>(Dynamic Derivative Gain Velocity Component)       | ↓ | ↑ | ↑ | 0<br>↑+ | ↑ | ↓ | ↑ | ↑ |

↑ Increase    ↓ Decrease    - No Change    0<sup>↑+</sup> Increase away from zero  
 0<sup>↑+</sup> Increase towards zero    0<sup>↓-</sup> Decrease away from zero

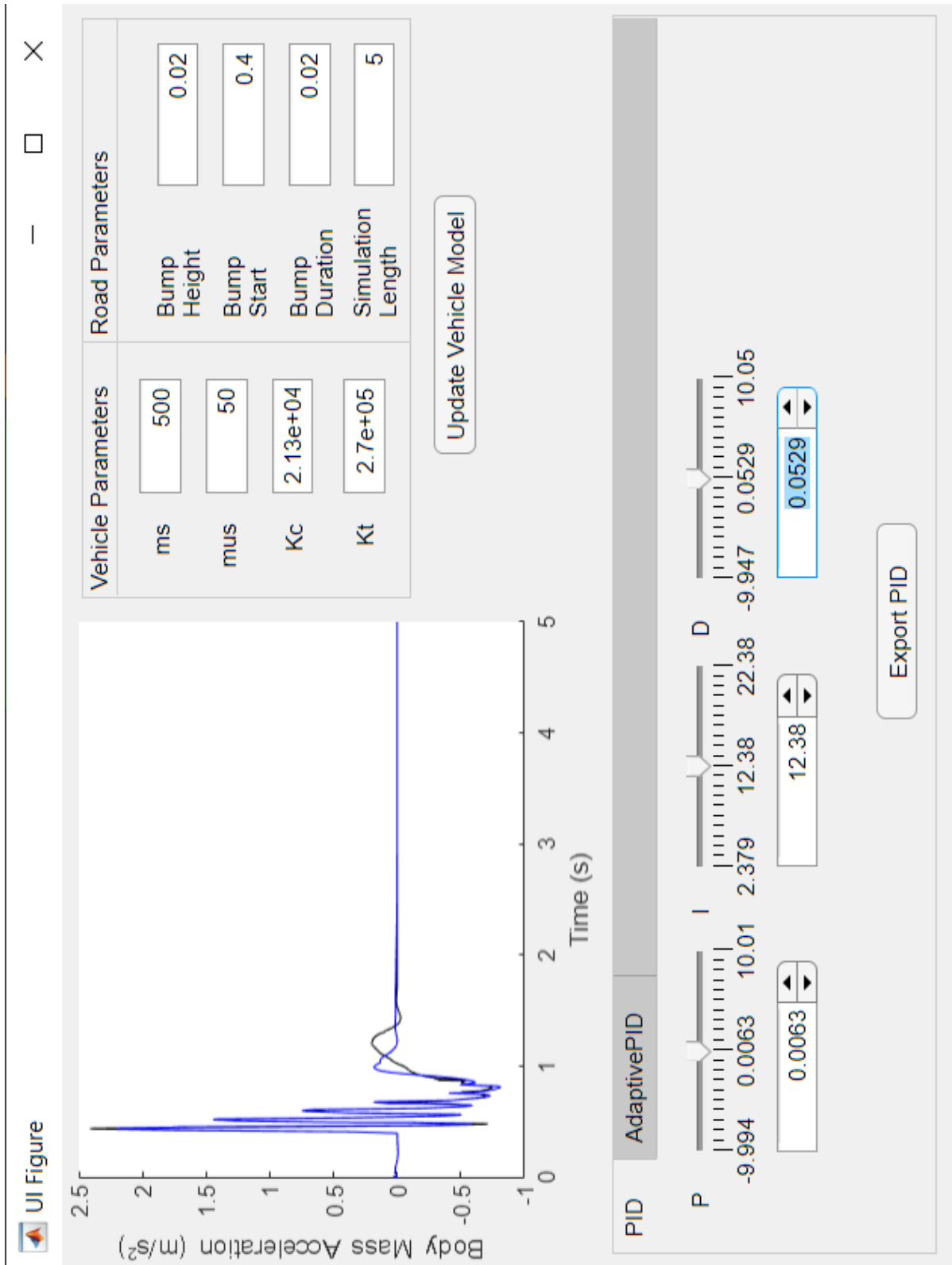


Fig. E.1 PID Tuning Application PID Page View

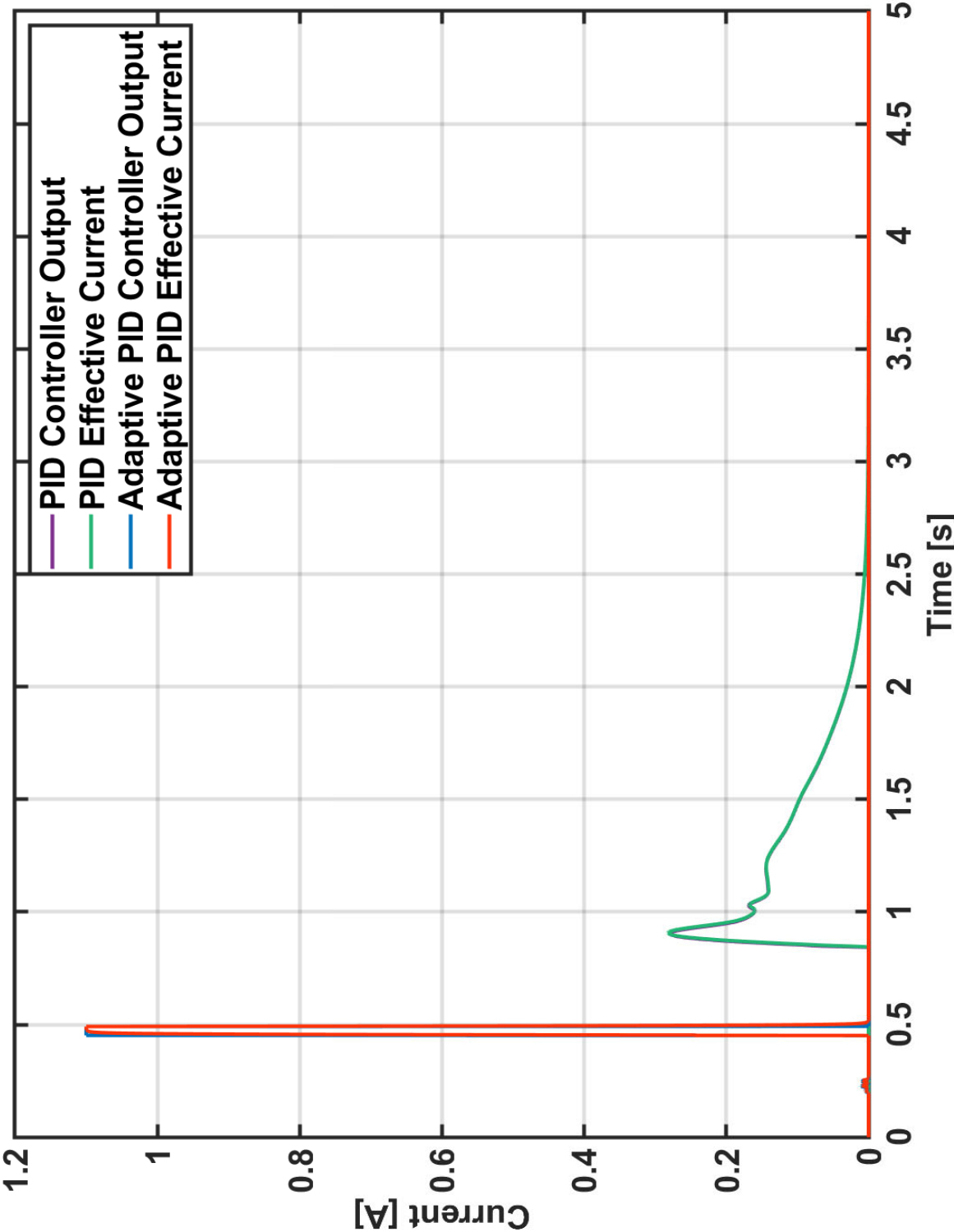


Fig. E.2 PID Tuning Application Control Current Changes

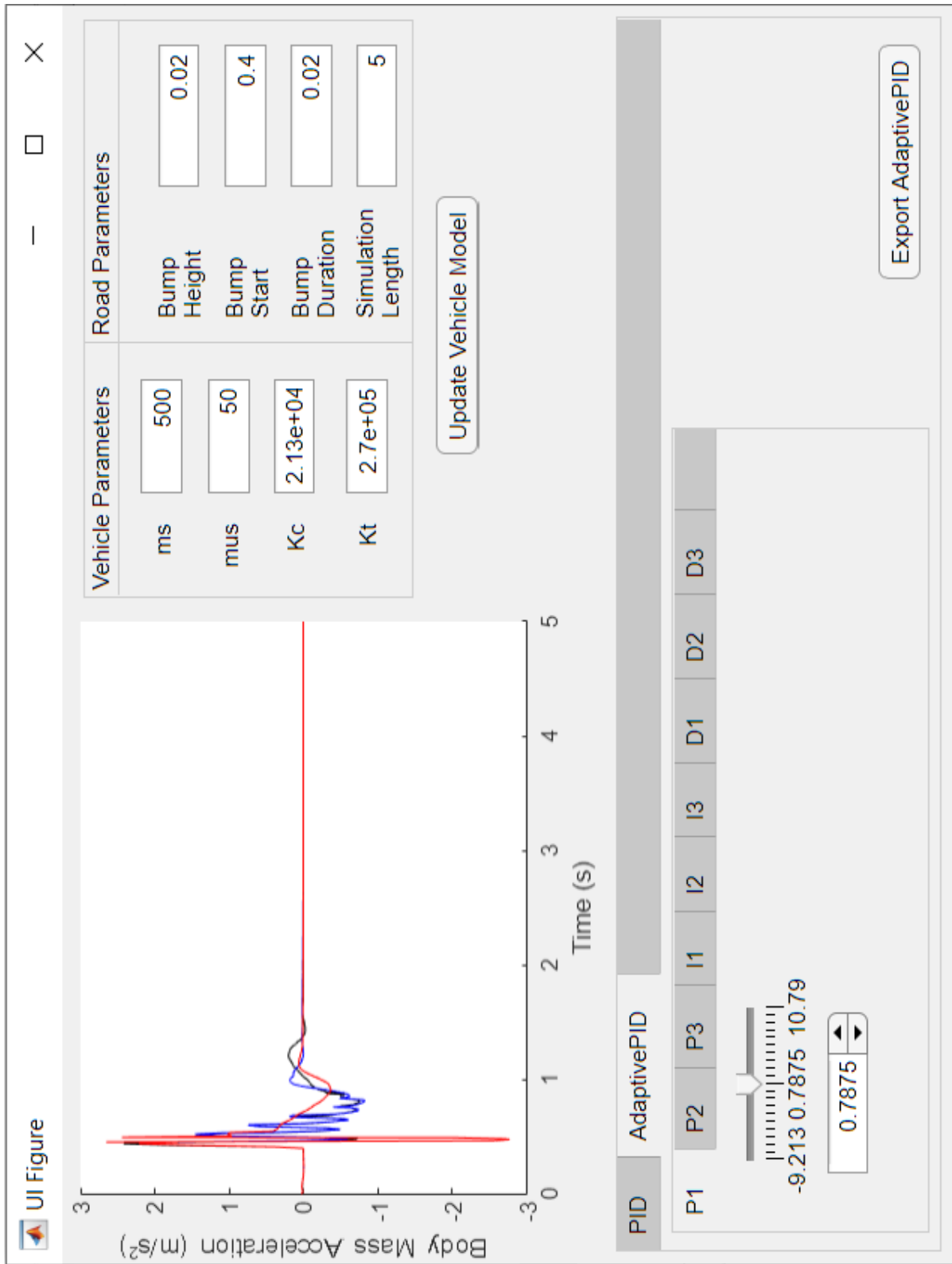


Fig. E.3 PID Tuning Application Adaptive PID Page View



# Appendix F

## NMPC Controller Iteration Limitations Supporting Evidence

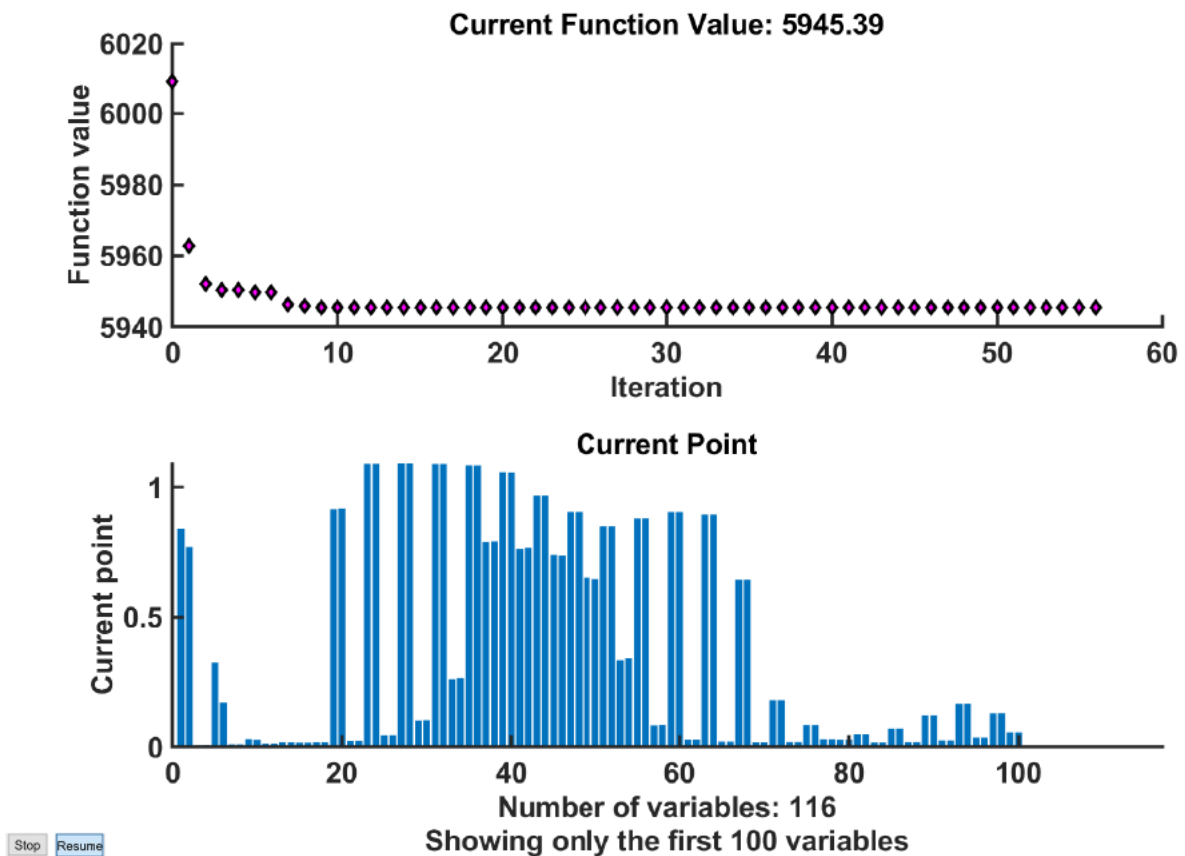


Fig. F.1 The plotfcn output for an arbitrary test case with  $N_p = 29$



# References

- Ab Talib, M. H., and Mat Darus, I. Z. (2013) 'Self-tuning PID controller for active suspension system with hydraulic actuator'. in *2013 IEEE Symposium on Computers Informatics (ISCI)*, '2013 IEEE Symposium on Computers Informatics (ISCI)' [online] held 7-9 April 2013 at Bayview Hotel Langkawi, Langkawi: IEEE, 86–91. available from <<http://dx.doi.org/10.1109/ISCI.2013.6612381>>
- Ab Talib, M. H., Mat Darus, I. Z., Mohd Samin, P., Mohd Yatim, H., Ardani, M. I., Shaharuddin, N. M. R., and Hadi, M. S. (2020) 'Vibration control of semi-active suspension system using pid controller with advanced firefly algorithm and particle swarm optimization'. *Journal of Ambient Intelligence and Humanized Computing* [online] available from <<http://dx.doi.org/10.1007/s12652-020-02158-w>>
- aftermarketNews (2021) *Tenneco to Supply CES Shock Absorbers on New Volvo XC60* [online] available from <<https://www.aftermarketnews.com/tenneco-to-supply-ces-shock-absorbers-on-new-volvo-xc60/>> [11 October 2021]
- Alexandru, C., and Alexandru, P. (2011) 'A comparative analysis between the vehicles' passive and active suspensions'. *International Journal of Mechanics* [online] 5 (4), 371–378. available from <[https://www.researchgate.net/publication/289089003\\_A\\_comparative\\_analysis\\_between\\_the\\_vehicles'\\_passive\\_and\\_active\\_suspensions](https://www.researchgate.net/publication/289089003_A_comparative_analysis_between_the_vehicles'_passive_and_active_suspensions)> [23 January 2021]
- Allen, R., Chrstos, J., and Rosenthal, T. (1997) 'A tire model for use with vehicle dynamics simulations on pavement and off-road surfaces'. *Vehicle System Dynamics* [online] 27 (sup001), 318–321. available from <<http://dx.doi.org/10.1080/00423119708969663>> [09 November 2020]
- Altinoz, O. T., and Yilmaz, A. E. (2018) 'Optimal PID Design for Control of Active Car Suspension System'. *International Journal of Information Technology and Computer Science* [online] 10 (1), 16–23. available from <<http://dx.doi.org/10.5815/ijitcs.2018.01.02>> [23 January 2021]
- Anderson, M., and Harty, D. (2010) 'Unsprung mass with in-wheel motors - myths and realities'. in *10th International Symposium on Advanced Vehicle Control (AVEC 2010)*, '10th international symposium on advanced vehicle control (avec 2010)' [online] held 22-25 August 2010 at Loughborough University, Loughborough: AVEC, 261–266. available from <<https://www.proteanelectric.com/f/2018/04/protean-Services3.pdf>> [18 January 2021]
- Bakker, E., Nyborg, L., and Pacejka, H. B. (1987) 'Tyre modelling for use in vehicle dynamics studies'. *SAE Transactions* [online] 96, 190–204. available from <<http://www.jstor.org/stable/44470677>>

- Barak, P. (1992) *Passive versus active and semi-active suspension from theory to application in North American industry SAE Technical Paper 922140*. [online] available from <<https://doi.org/10.4271/922140>> [10 November 2020]
- Bekakos, C., Papazafeiropoulos, G., O'Boy, D., and Prins, J. (2015) 'Dynamic response of rigid wheels on deformable terrains'. in *Proceedings of the 13th European Conference of the International Society for Terrain-Vehicle Systems*, '13th European Conference of the International Society for Terrain-Vehicle Systems (ISTVS 2015)' [online] held 21-23 October 2015 at National Research Council of Italy, Rome: ISTVS, 1-13. available from <[https://repository.lboro.ac.uk/articles/conference%20contribution/Dynamic\\_response\\_of\\_rigid\\_wheels\\_on\\_deformable\\_terrains/9220859/1](https://repository.lboro.ac.uk/articles/conference%20contribution/Dynamic_response_of_rigid_wheels_on_deformable_terrains/9220859/1)> [18 January 2021]
- Bekakos, C., Papazafeiropoulos, G., O'Boy, D., Prins, J., and Mavros, G. (2016a) 'Dynamic response of rigid wheels on deformable terrains'. *Journal of Advances in Vehicle Engineering* 2 (4), 210-218. available from <[https://repository.lboro.ac.uk/articles/Dynamic\\_response\\_of\\_rigid\\_wheels\\_on\\_deformable\\_terrains/9223589](https://repository.lboro.ac.uk/articles/Dynamic_response_of_rigid_wheels_on_deformable_terrains/9223589)> [09 November 2020]
- Bekakos, C., Papazafeiropoulos, G., O'Boy, D., Prins, J., and Mavros, G. (2016b) 'Off-road tire-terrain interaction: An analytical solution'. *SAE International Journal of Commercial Vehicles* [online] 9 (2), 244-251. available from <<http://dx.doi.org/10.4271/2016-01-8029>> [09 November 2020]
- Bekker, M. G. (1962) 'Mechanics of off-the-road locomotion'. *Proceedings of the Institution of Mechanical Engineers: Automobile Division* [online] 16 (1), 25-44. available from <[http://dx.doi.org/10.1243/pime\\_auto\\_1962\\_000\\_009\\_02](http://dx.doi.org/10.1243/pime_auto_1962_000_009_02)> [09 November 2020]
- Besselink, I., Pacejka, H., Schmeitz, A., and Jansen, S. (2005) 'The mf-swift tyre model: Extending the magic formula with rigid ring dynamics and an enveloping model' 26, 245-252
- Bhise, A. R., Desai, R. G., Yerrawar, R. N., Mitra, A. C., and Arakerimath, R. R. (2016) 'Comparison between passive and semi-active suspension system using matlab/simulink'. *IOSR Journal of Mechanical and Civil Engineering* [online] 13 (04), 01-06. available from <<http://dx.doi.org/10.9790/1684-1304010106>> [10 November 2020]
- Bilstein (2021) *PERFECTLY TAILORED TO HIGH PERFORMANCE AND COMFORT* [online] available from <<https://www.bilstein.com/sg/en/blog/perfectly-tailored-high-performance-comfort/>> [11 October 2021]
- Blundell, M., and Harty, D. (2014) *The Multibody Systems Approach to Vehicle Dynamics* 2nd edn., Netherlands: Elsevier
- Braz-César, M., and Barros, R. (2013) 'Experimental and numerical analysis of MR dampers'. in Papadrakakis, M. and Papadopoulos, V. and Plevris, V. eds. *Proceedings of the International Conference on Computational Methods in Structural Dynamics and Earthquake Engineering (COMPDYN)*, 'International Conference on Computational Methods in Structural Dynamics and Earthquake Engineering (COMPDYN)' [online] held 12-14 June 2013 at Kos International Convention Centre (KICC), Kos: IEEE, 3672-3690. available from <<http://dx.doi.org/10.7712/120113.4769.c1590>>

- Bruyne, S. D., der Auweraer, H. V., Anthonis, J., Desmet, W., and Swevers, J. (2012) 'Preview control of a constrained hydraulic active suspension system'. in *2012 IEEE 51st IEEE Conference on Decision and Control (CDC)*, '51st IEEE Conference on Decision and Control (CDC 2012)' [online] held 10-13 December 2012 at the Grand Wailea, Maui: IEEE, 4400–4405. available from <<http://dx.doi.org/10.1109/CDC.2012.6425847>> [09 November 2020]
- Çalışkan, K., Henze, R., and Küçükay, F. (2016) 'Potential of road preview for suspension control under transient road inputs'. *IFAC-PapersOnLine* [online] 49 (3), 117–122. available from <<http://dx.doi.org/10.1016/j.ifacol.2016.07.020>> [09 November 2020]
- Canale, M., Milanese, M., and Novara, C. (2006) 'Semi-active suspension control using "fast" model-predictive techniques'. *IEEE Transactions on Control Systems Technology* [online] 14 (6), 1034–1046. available from <<http://dx.doi.org/10.1109/tcst.2006.880196>>
- Canale, M., Milanese, M., Novara, C., and Ahmad, Z. (2005) 'Semi-active suspension control using "fast" model predictive control'. in *Proceedings of the 2005, American Control Conference*, 'American Control Conference 2005 (ACC2005)' [online] held 8-10 June 2005 at Hilton Portland & Executive Tower, Portland: IEEE, 274–281. available from <<http://dx.doi.org/10.1109/acc.2005.1469945>>
- Cardinale, M., and Pope, M. (2003) 'The effects of whole body vibration on humans: Dangerous or advantageous?' *Acta Physiologica Hungarica* 90 (3), 195–206. available from <<http://dx.doi.org/10.1556/aphysiol.90.2003.3.2>>
- Casavola, A., Di Iorio, F., and Tedesco, F. (2018) 'A multiobjective  $H_\infty$  control strategy for energy harvesting in regenerative vehicle suspension systems'. *International Journal of Control* [online] 91 (4), 741–754. available from <<http://dx.doi.org/10.1080/00207179.2017.1293298>>
- Chan, B. J., and Sandu, C. (2014) 'Development of a 3-d quasi-steady-state tyre model for on-road and off-road vehicle dynamics simulations: Part ii off-road rigid wheel model'. *International Journal of Vehicle Systems Modelling and Testing* [online] 9 (2), 107–136. available from <<http://dx.doi.org/10.1504/IJVSMT.2014.061427>> [09 November 2020]
- Chen, C., Chan, Y. S., Zou, L., and Liao, W.-H. (2018) 'Self-powered magnetorheological dampers for motorcycle suspensions'. *Proceedings of the Institution of Mechanical Engineers, Part D: Journal of Automobile Engineering* 232 (7), 921–935. available from <<http://dx.doi.org/10.1177/0954407017723761>>
- Clayton, C. R. I., Steinhagen, H. M., Powrie, W., Terzaghi, K., and Skempton, A. W. (1995) 'TERZAGHI'S THEORY OF CONSOLIDATION, AND THE DISCOVERY OF EFFECTIVE STRESS. (COMPILED FROM THE WORK OF K. TERZAGHI AND A.W. SKEMPTON)'. *Proceedings of the Institution of Civil Engineers - Geotechnical Engineering* 113 (4), 191–205. available from <<http://dx.doi.org/10.1680/igeng.1995.28015>> [24 January 2021]
- Clearmotion Inc. (2014) *Distributed active suspension control system*. [online] United States Patent US 2014/0297117A1. available from <<https://patents.google.com/patent/US20140297117A1/en>> [09 November 2020]

- ClearMotion Inc (2021) *The most advanced ride On Earth* [online] available from <<http://www.clearmotion.com/technology>> [12 October 2021]
- Cook, J. R., Petts, R. C., and Rolt, J. (2013) *Low Volume Rural Road Surfacing and Pavements A Guide to Good Practice*. OTB Engineering UK LLP, London, [online] available from <<https://www.gov.uk/research-for-development-outputs/low-volume-rural-road-surfacing-and-pavements-a-guide-to-good-practice>> [23 January 2021]
- Cooper, G., and Harper, R. (1969) 'The use of pilot ratings in evaluation of aircraft handling qualities'. *NASA Ames Technical Report*
- Cosin Scientific Software AG (2020) 'Ftire' [online] available from <<https://www.cosin.eu>>
- Cosin Scientific Software AG (2021) *FTire - Flexible Structure Tire Model Modelization and Parameter Specification* [online] available from <[https://www.cosin.eu/wp-content/uploads/ftire\\_model.pdf](https://www.cosin.eu/wp-content/uploads/ftire_model.pdf)> [14 October 2021]
- Cranfield University (2021) *Soil Classification System for England and Wales* [online] available from <<http://www.landis.org.uk/downloads/classification.cfm>> [15 October 2021]
- Crosby, M. J., and Karnopp, D. C. (1973) 'THE ACTIVE DAMPER - A NEW CONCEPT FOR SHOCK AND VIBRATION CONTROL'. *The Shock and Vibration Bulletin* [online] , 119–133 available from <[https://www.google.co.uk/books/edition/The\\_Shock\\_and\\_Vibration\\_Bulletin/R7EjAQAAMAAJ?hl=en&gbpv=0](https://www.google.co.uk/books/edition/The_Shock_and_Vibration_Bulletin/R7EjAQAAMAAJ?hl=en&gbpv=0)>
- Dangor, M., Dahunsi, O. A., Pedro, J. O., and Ali, M. M. (2014) 'Evolutionary algorithm-based PID controller tuning for nonlinear quarter-car electrohydraulic vehicle suspensions'. *Nonlinear Dynamics* 78 (4), 2795–2810. available from <<http://dx.doi.org/10.1007/s11071-014-1626-4>>
- Deshpande, V. S., Bhaskara, M., and Phadke, S. B. (2012) 'Sliding mode control of active suspension systems using a disturbance observer'. in *2012 12th International Workshop on Variable Structure Systems*, '12th International Workshop on Variable Structure Systems' [online] held 12-14 January 2012 at Indian Institute of Technology Bombay, Mumbai: IEEE, 70–75. available from <<http://dx.doi.org/10.1109/VSS.2012.6163480>> [09 October 2020]
- Desikan, A., and Kalaichelvi, V. (2015) 'Design for a preview control of semi-active suspension system using fuzzy-logic and image processing techniques'. in *2015 IEEE International Conference on Electro/Information Technology (EIT)*, 'IEEE International Conference on Electro/Information Technology (EIT2015)' [online] held 21-23 May 2015 at Northern Illinois University, Dekalb: IEEE, 224–229. available from <<http://dx.doi.org/10.1109/EIT.2015.7293426>> [09 November 2020]
- Dimock, G. A., Yoo, J. H., and Wereley, N. M. (2002) 'Quasi-steady bingham biplastic analysis of electrorheological and magnetorheological dampers'. *Journal of Intelligent Material Systems and Structures* [online] 13 (9), 549–559. available from <<http://dx.doi.org/10.1106/104538902030906>> [09 November 2020???

- Dowds, P., and O'Dwyer, A. (2005) 'Modelling and control of a suspension system for vehicle applications'. in *Proceedings of the 4th Wismarer Automatisierungs Symposium*, '4th Wismarer Automatisierungs Symposium' [online] held 22-23 September 2005. available from <<https://arrow.dit.ie/engscheleart/17/>> [09 November 2020]
- dSPACE GmbH (2020) 'Automotive simulation models' [online] available from <[https://www.dspace.com/en/ltd/home/products/sw/automotive\\_simulation\\_models.cfm#144\\_26315](https://www.dspace.com/en/ltd/home/products/sw/automotive_simulation_models.cfm#144_26315)>
- Du, H., Yim Sze, K., and Lam, J. (2005) 'Semi-active  $H_\infty$  control of vehicle suspension with magneto-rheological dampers'. *Journal of Sound and Vibration* [online] 283 (3), 981 – 996. available from <<http://dx.doi.org/https://doi.org/10.1016/j.jsv.2004.05.030>>
- Du, H., and Zhang, N. (2008) 'Designing  $H_\infty$ / $G/H_2$  static-output feedback controller for vehicle suspensions using linear matrix inequalities and genetic algorithms'. *Vehicle System Dynamics* [online] 46 (5), 385–412. available from <<http://dx.doi.org/10.1080/00423110701407013>> [09 November 2020]
- Dyke, S. J., Spencer, B. F., Sain, M. K., and Carlson, J. D. (1998) 'An experimental study of MR dampers for seismic protection'. *Smart Materials and Structures* [online] 7 (5), 693–703. available from <<http://dx.doi.org/10.1088/0964-1726/7/5/012>>
- Ekoru, J. E. D., Dahunsi, O. A., and Pedro, J. O. (2011) 'PID control of a nonlinear half-car active suspension system via force feedback'. in *IEEE Africon '11*, 'AFRICON 2011' [online] held 13-15 September 2011 at The Falls Resort and Conference Centre, Livingstone: IEEE, 1–6. available from <<http://dx.doi.org/10.1109/AFRCON.2011.6071979>> [09 November 2020]
- Encyclopedia of Mathematics (2021) *Least absolute residuals procedure: Encyclopedia of Mathematics* [online] available from <[http://encyclopediaofmath.org/index.php?title=Least\\_absolute\\_residuals\\_procedure&oldid=39268](http://encyclopediaofmath.org/index.php?title=Least_absolute_residuals_procedure&oldid=39268)> [05 November 2021]
- Fallah, M. S., Bhat, R., and Xie, W. (2010) ' $H_\infty$  robust control of semi-active macpherson suspension system: new applied design'. *Vehicle System Dynamics* [online] 48 (3), 339–360. available from <<http://dx.doi.org/10.1080/00423110902807714>>
- Fenton, J. (2013) *Handbook of Automotive Design Analysis* Elsevier Science & Techn. available from <[https://www.ebook.de/de/product/23258254/handbook\\_of\\_automotive\\_design\\_analysis.html](https://www.ebook.de/de/product/23258254/handbook_of_automotive_design_analysis.html)>
- Fischer, D., and Isermann, R. (2004) 'Mechatronic semi-active and active vehicle suspensions'. *Control Engineering Practice* [online] 12 (11), 1353–1367. available from <<http://dx.doi.org/10.1016/j.conengprac.2003.08.003>>
- Gallrein, A., and Bäcker, M. (2007) 'Cdtire: a tire model for comfort and durability applications'. *Vehicle System Dynamics* [online] 45 (sup1), 69–77. available from <<http://dx.doi.org/10.1080/00423110801931771>>
- Giorgetti, N., Bemporad, A., Tseng, H. E., and Hrovat, D. (2006) 'Hybrid model predictive control application towards optimal semi-active suspension'. *International Journal of Control* [online] 79 (5), 521–533. available from <<http://dx.doi.org/10.1080/00207170600593901>>

- Gohrle, C., Schindler, A., Wagner, A., and Sawodny, O. (2013) ‘Model predictive control of semi-active and active suspension systems with available road preview’. in *2013 European Control Conference (ECC)*, ‘2013 European Control Conference (ECC2013)’ [online] held 17-19 July 2013 at ETH Zurich, Zurich: IEEE, 1499–1504. available from <<http://dx.doi.org/10.23919/ecc.2013.6669185>>
- Gohrle, C., Schindler, A., Wagner, A., and Sawodny, O. (2014) ‘Design and vehicle implementation of preview active suspension controllers’. *IEEE Transactions on Control Systems Technology* [online] 22 (3), 1135–1142. available from <<http://dx.doi.org/10.1109/TCST.2013.2272342>>
- Göhrle, C., Schindler, A., Wagner, A., and Sawodny, O. (2015) ‘Road profile estimation and preview control for low-bandwidth active suspension systems’. *IEEE/ASME Transactions on Mechatronics* [online] 20 (5), 2299–2310. available from <<http://dx.doi.org/10.1109/tmech.2014.2375336>> [09 November 2020]
- Göhrle, C., Wagner, A., Schindler, A., and Sawodny, O. (2012) ‘Active suspension controller using mpc based on a full-car model with preview information’. in *American Control Conference 2012*, ‘American control conference 2012’ [online] held 27-29 June 2012 at Hotel Fairmont The Queen Elizabeth, Montréal: IEEE, 497–502. available from <<http://dx.doi.org/10.1109/acc.2012.6314680>> [09 November 2020]
- Grecenko, A. (1967) ‘Binomic slip-thrust equation for tractors on predominantly frictional soils’. *Journal of Terramechanics* [online] 4 (4), 37–54. available from <[http://dx.doi.org/10.1016/0022-4898\(67\)90020-1](http://dx.doi.org/10.1016/0022-4898(67)90020-1)> [09 November 2020]
- Griffin, M. (2001) ‘Whole-body vibration’. in *Encyclopedia of Vibration*, edited by Braun, S. Oxford: Elsevier, 1570–1578. available from <<http://dx.doi.org/https://doi.org/10.1006/rwvb.2001.0082>>
- Griffin, M. J. (2007) ‘Discomfort from feeling vehicle vibration’. *Vehicle System Dynamics* [online] 45 (7-8), 679–698. available from <<http://dx.doi.org/10.1080/00423110701422426>>
- Guglielmino, E., Sireteanu, T., Stammers, C. W., Ghita, G., and Giuclea, M. (2008) *Semi-active Suspension Control* Springer London. available from <<http://dx.doi.org/10.1007/978-1-84800-231-9>>
- Guiggiani, M. (2018) *The Science of Vehicle Dynamics* Springer International Publishing. available from <<http://dx.doi.org/10.1007/978-3-319-73220-6>>
- Guo, J. W. W., Ashasi-Sorkhabi, A., Mercan, O., and Christopoulos, C. (2017) ‘Real-time hybrid simulation of structures equipped with viscoelastic-plastic dampers using a user-programmable computational platform’. *Earthquake Engineering and Engineering Vibration* [online] 16 (4), 693. available from <<http://dx.doi.org/10.1007/s11803-017-0408-7>> [09 November 2020]
- Guo, S., Li, S., and Yang, S. (2006a) ‘Semi-active vehicle suspension systems with magnetorheological dampers’. in *2006 IEEE International Conference on Vehicular Electronics and Safety*, ‘2006 IEEE International Conference on Vehicular Electronics and Safety’ [online] held 13-15 December 2006, Shanghai: IEEE, 403–406. available from <<http://dx.doi.org/10.1109/ICVES.2006.371624>> [09 November 2020]

- Guo, S., Yang, S., and Pan, C. (2006b) 'Dynamic modeling of magnetorheological damper behaviors'. *Journal of Intelligent Material Systems and Structures* [online] 17 (1), 3–14. available from <<http://dx.doi.org/10.1177/1045389X06055860>> [09 November 2020??]
- Harnisch, C., Lach, B., Jakobs, R., Troulis, M., and Nehls, O. (2005) 'A new tyre–soil interaction model for vehicle simulation on deformable ground'. *Vehicle System Dynamics* [online] 43 (sup1), 384–394. available from <<http://dx.doi.org/10.1080/00423110500139981>> [09 November 2020]
- Hassan, S. (1986) 'Fundamental studies of passive, active and semi-active automotive suspension systems' [online] Unpublished PhD thesis. Leeds: University of Leeds. available from <<https://core.ac.uk/download/pdf/9257269.pdf>>
- Hegazy, S., and Sandu, C. (2013) 'Experimental investigation of vehicle mobility using a novel wheel mobility number'. *Journal of Terramechanics* [online] 50 (5-6), 303–310. available from <<http://dx.doi.org/10.1016/j.jterra.2013.09.005>> [09 November 2020]
- Heißing, B., and Ersoy, M. (eds.) (2010) *Chassis Handbook* Vieweg+Teubner Verlag. available from <<http://dx.doi.org/10.1007/978-3-8348-9789-3>>
- Hrovat, D., Cairano, S. D., Tseng, H. E., and Kolmanovsky, I. V. (2012) 'The development of model predictive control in automotive industry: A survey'. in *IEEE International Conference on Control Applications (CCA), 2012*, 'Ieee international conference on control applications 2012 (cca 2012)' [online] held 3-5 October 2012, Dubrovnik: IEEE, 295–302. available from <<http://dx.doi.org/10.1109/cca.2012.6402735>> [09 November 2020]
- Hu, Y., Chen, M. Z., and Hou, Z. (2015) 'Multiplexed model predictive control for active vehicle suspensions'. *International Journal of Control* [online] 88 (2), 347–363. available from <<http://dx.doi.org/10.1080/00207179.2014.953589>>
- Ikenaga, S., Lewis, F. L., Campos, J., and Davis, L. (2000) 'Active suspension control of ground vehicle based on a full-vehicle model'. in *Proceedings of the 2000 American Control Conference*, 'American Control Conference 2000 (ACC 2000)' [online] held 28-30 June 2000 at Hyatt Regency Chicago, Chicago: IEEE, 4019–4024. available from <<http://dx.doi.org/10.1109/acc.2000.876977>> [09 November 2020]
- IPG Automotive GmbH (2020) 'Carmaker: Virtual testing of automobiles and light-duty vehicles' [online] available from <<https://ipg-automotive.com/products-services/simulation-software/carmaker/>>
- Jamil, M., Zafar, S., and Gilani, S. O. (2018) 'Designing PID controller based semi-active suspension system using MATLAB simulink'. in *Lecture Notes of the Institute for Computer Sciences, Social Informatics and Telecommunications Engineering* Springer International Publishing, 282–295. available from <[http://dx.doi.org/10.1007/978-3-319-94180-6\\_27](http://dx.doi.org/10.1007/978-3-319-94180-6_27)>
- Janosi, Z., and Hanamoto, B. (1961) 'The analytical determination of drawbar pull as a function of slip for tracked vehicles in deformable soils'. in Minerva Tecnica eds. *Proceedings of the 1st International Conference on the Mechanics of Soil-Vehicle Systems*, '1st International Conference on the Mechanics of Soil-Vehicle Systems' [online] held 12-16 June 1961, Turin: DTIC. available from <<https://apps.dtic.mil/dtic/tr/fulltext/u2/283396.pdf>> [26 January 2021]

- Kamath, G., and Wereley, N. (1997a) 'Modeling the damping mechanism in electro-rheological fluid based dampers'. *ASTM Special Technical Publication* [online] 1304, 331–348
- Kamath, G. M., and Wereley, N. M. (1997b) 'A nonlinear viscoelastic - plastic model for electrorheological fluids'. *Smart Materials and Structures* [online] 6 (3), 351–359. available from <<http://dx.doi.org/10.1088/0964-1726/6/3/012>>
- Kamath, G. M., and Wereley, N. M. (1997c) 'Nonlinear viscoelastic-plastic mechanisms-based model of an electrorheological damper'. *Journal of Guidance, Control, and Dynamics* [online] 20 (6), 1125–1132. available from <<http://dx.doi.org/10.2514/2.4167>>
- Karamihas, S. M., Gillespie, T. D., Kohn, S. D., and Perera, R. W. (1999) *Guidelines for longitudinal pavement profile measurement NCHRP Project 10-47*. University of Michigan Transportation Research Institute, [online] available from <<https://deepblue.lib.umich.edu/bitstream/handle/2027.42/1276/92023.0001.001.pdf?sequence2>> [09 November 2020]
- Koch, G., and Kloiber, T. (2014) 'Driving state adaptive control of an active vehicle suspension system'. *IEEE Transactions on Control Systems Technology* [online] 22 (1), 44–57. available from <<http://dx.doi.org/10.1109/TCST.2013.2240455>> [09 November 2020]
- Krauze, P. (2013) 'Comparison of Control Strategies in a Semi- Active Suspension System of the Experimental ATV'. *JOURNAL OF LOW FREQUENCY NOISE, VIBRATION AND ACTIVE CONTROL* [online] 32 (1), 67–80. available from <<https://journals.sagepub.com/doi/pdf/10.1260/0263-0923.32.1-2.67>>
- Kruger, V. O., W., and Spieck, M. (2004) 'Semi-active suspension systems for road and off-road vehicles - an overview'. *Journal of Middle European Construction and Design of Cars (MECCA)* [online] available from <[http://www.bozek.cvut.cz/mecca/2004/4\\_04-vaculin-en.pdf](http://www.bozek.cvut.cz/mecca/2004/4_04-vaculin-en.pdf)>
- Kurtay, T., and Reece, A. (1970) 'Plasticity theory and critical state soil mechanics'. *Journal of Terramechanics* [online] 7 (3-4), 23–56. available from <[http://dx.doi.org/10.1016/0022-4898\(70\)90004-2](http://dx.doi.org/10.1016/0022-4898(70)90004-2)> [10 November 2020]
- Kwok, N., Ha, Q., Nguyen, M., Li, J., and Samali, B. (2007) 'Bouc–wen model parameter identification for a MR fluid damper using computationally efficient GA'. *ISA Transactions* [online] 46 (2), 167–179. available from <<http://dx.doi.org/10.1016/j.isatra.2006.08.005>>
- Labuz, J. F., and Zang, A. (2012) 'Mohr–Coulomb Failure Criterion'. *Rock Mechanics and Rock Engineering* 45 (6), 975–979. available from <<http://dx.doi.org/10.1007/s00603-012-0281-7>>
- Langlois, R. G., and Hanna, D. (1991) 'Preview control algorithms for the active suspension of an off-road vehicle' Unpublished dissertation. Kingston: Queen's University
- Li, H. (2013) 'Analysis of off-road tire-soil interaction through analytical and finite element methods' [online] Unpublished PhD thesis. Technischen Universität Kaiserslautern. available from <<https://d-nb.info/1043687246/34#page42>> [05 November 2021]
- Lindler, J. E., and Wereley, N. M. (1999) 'Double adjustable shock absorbers using electrorheological fluid'. *Journal of Intelligent Material Systems and Structures* [online] 10 (8), 652–657. available from <<http://dx.doi.org/10.1106/468r-dhqm-076w-maf6>> [09 November 2020???

- Lord Corporation (2006) *LORD USER INSTRUCTIONS LORD Wonder Box Device Controller Kit* [online] available from <<http://www.lordfulfillment.com/upload/UI7000.pdf>> [15 October 2021]
- Lord Corporation (2009) ‘Lord Technical Data: RD-8040-1 and RD-8041-1 Dampers’ [online] available from <<http://www.lordmrstore.com/lord-mr-products/rd-8040-1-mr-damper-short-stroke>> [23 January 2021]
- Lyasko, M. (2010a) ‘LSA model for sinkage predictions’. *Journal of Terramechanics* [online] 47 (1), 1 – 19. available from <<http://dx.doi.org/10.1016/j.jterra.2009.06.004>> [24 January 2021]
- Lyasko, M. (2010b) ‘Slip sinkage effect in soil-vehicle mechanics’. *Journal of Terramechanics* [online] 47 (1), 21 – 31. available from <<http://dx.doi.org/https://doi.org/10.1016/j.jterra.2009.08.005>> [09 November 2020]
- Lyasko, M. I. (2010c) ‘How to calculate the effect of soil conditions on tractive performance’. *Journal of Terramechanics* [online] 47 (6), 423 – 445. available from <<http://www.sciencedirect.com/science/article/pii/S0022489810000248>> [09 November 2020]
- Ma, Z., Zhang, Y., and Yang, J. (2015) ‘Velocity and normal tyre force estimation for heavy trucks based on vehicle dynamic simulation considering the road slope angle’ 54 (2), 137–167. available from <<http://dx.doi.org/10.1080/00423114.2015.1122817>>
- Macfarlane, A. B. (2016) ‘Modular electric automatic guided vehicle suspension-drive unit’ [online], Unpublished dissertation. Nelson Mandela Metropolitan University. available from <<http://dx.doi.org/10.13140/RG.2.2.20894.02885>>
- Mehra, R. K., Amin, J. N., Hedrick, K. J., Osorio, C., and Gopalasamy, S. (1997) ‘Active suspension using preview information and model predictive control’. in *Proceedings of the 1997 IEEE International Conference on Control Applications*, ‘1997 iee international conference on control applications’ [online] held 5-7 October 1997 at Sheraton Hartford Hotel, Hartford: IEEE, 860–865. available from <<http://dx.doi.org/10.1109/CCA.1997.627769>>
- Messner, B., Tilbury, D., Hill, R., and Taylor, J. D. (2021) *Control Tutorials For MATLAB & Simulink - Suspension: Simulink Modeling* [online] available from <<https://ctms.engin.umich.edu/CTMS/index.php?example=Suspension&section=SimulinkModeling>> [29 January 2021]
- Mori, T., Nilkhamhang, I., and Sano, A. (2007) ‘Adaptive semi-active vibration isolation considering uncertainties of mr damper and suspension structure’. in *2007 46th IEEE Conference on Decision and Control*, ‘46th IEEE Conference on Decision and Control 2007’ [online] held 12-14 December 2007 at Hilton New Orleans Riverside Hotel, New Orleans: IEEE, 4815–4820. available from <<http://dx.doi.org/10.1109/CDC.2007.4434973>> [09 November 2020]
- Nerbin, M. M., Gharamaleki, R. M., and Mirzaei, M. (2017) ‘Novel optimal control of semi-active suspension considering a hysteresis model for mr damper’. *Transactions of the Institute of Measurement and Control* [online] 39 (5), 698–705. available from <<http://dx.doi.org/10.1177/0142331215618446>>

- Nguyen, M. Q., Canale, M., Sename, O., and Dugard, L. (2016) 'A model predictive control approach for semi-active suspension control problem of a full car'. in *2016 IEEE 55th Conference on Decision and Control (CDC)*, '55th Conference on Decision and Control (CDC 2016)' [online] held 12-14 December 2016 at ARIA Resort & Casino, Las Vegas: IEEE, 721–726. available from <<http://dx.doi.org/10.1109/CDC.2016.7798353>>
- NIST (2013) *NIST/SEMATECH e-Handbook of Statistical Methods: 4.1.4.2. Nonlinear Least Squares Regression* [online] available from <<https://www.itl.nist.gov/div898/handbook/pmd/section1/pmd142.htm#:~:text=One%20common%20advantage%20is%20efficient,with%20relatively%20small%20data%20sets.>> [23 January 2021]
- NIST (2021) *Engineering Statistics Handbook: 2.6.5.2.2. Bisquare Weighting* [online] available from <<https://www.itl.nist.gov/div898/handbook/mpc/section6/mpc6522.htm>> [05 November 2021]
- Öhlins (2021) *CES8700* [online] available from <<https://www.ohlins.com/product/ces8700/>> [11 October 2021]
- Pacejka, H. B. (2012) *Tire and vehicle dynamics* Amsterdam Boston: Elsevier/BH
- Pacejka, H. B., and Bakker, E. (1992) 'The magic formula tyre model'. *Vehicle System Dynamics* [online] 21 (sup001), 1–18. available from <<http://dx.doi.org/10.1080/00423119208969994>>
- Paciello, V., and Pietrosanto, A. (2011) 'Magnetorheological dampers: a new approach of characterization'. *IEEE Transactions on Instrumentation and Measurement* [online] 60 (5), 1718–1723. available from <<http://dx.doi.org/10.1109/tim.2010.2102391>>
- Park, S., Popov, A., and Cole, D. (2004) 'Influence of soil deformation on off-road heavy vehicle suspension vibration'. *Journal of Terramechanics* [online] 41 (1), 41–68
- Pazooki, A., Rakheja, S., and Cao, D. (2012) 'Modeling and validation of off-road vehicle ride dynamics'. *Mechanical Systems and Signal Processing* [online] 28, 679–695. available from <<http://dx.doi.org/10.1016/j.ymssp.2011.11.006>>
- Peng, Y., Yang, J., and Li, J. (2018) 'Parameter identification of modified bouc–wen model and analysis of size effect of magnetorheological dampers'. *Journal of Intelligent Material Systems and Structures* [online] 29 (7), 1464–1480. available from <<http://dx.doi.org/10.1177/1045389X17740963>>
- Peperhowe, M., and Schindler, W. (2013) 'Efficient vehicle dynamics development via simulation-based prognosis tools' [online] available from <<https://www.dspace.com/en/ltd/home/medien/abstract.cfm?docid=1789>> [24 January 2021]
- Prokop, G., and Sharp, R. (1995) 'Performance enhancement of limited-bandwidth active automotive suspensions by road preview'. *Control Theory and Applications, IEE Proceedings* - [online] 142, 140 – 148. available from <<http://dx.doi.org/10.1049/ip-cta:19951772>>
- Rao, K. D. (2014) 'Modeling, simulation and control of semi active suspension system for automobiles under matlab simulink using pid controller'. *IFAC Proceedings Volumes* [online] 47 (1), 827 – 831. available from <<http://dx.doi.org/https://doi.org/10.3182/20140313-3-IN-3024.00094>>

- Åström, K., and Hägglund, T. (1995) *PID Controllers: Theory, Design, and Tuning* 2nd edn., Research Triangle Park, N.C: International Society for Measurement and Control
- Rathai, K. M., Alamir, M., and Sename, O. (2019) ‘Experimental implementation of model predictive control scheme for control of semi-active suspension system’. *IFAC-PapersOnLine* [online] 52 (5), 261–266. available from <<http://dx.doi.org/10.1016/j.ifacol.2019.09.042>> [10 November 2020]
- Reece, A. R. (1965) ‘Principles of soil-vehicle mechanics’. *Proceedings of the Institution of Mechanical Engineers: Automobile Division* 180 (1), 45–66. available from <[http://dx.doi.org/10.1243/PIME\\_AUTO\\_1965\\_180\\_009\\_02](http://dx.doi.org/10.1243/PIME_AUTO_1965_180_009_02)>
- Rill, G. (2020) ‘TMEASY 6.0 – A HANDLING TIRE MODEL THAT INCORPORATES THE FIRST TWO BELT EIGENMODES’. in M. Papadrakakis and M. Fragiadakis and C. Papadimitriou eds. *Proceedings of the XI International Conference on Structural Dynamics Volume I, ‘EURODYN 2020 XI International Conference on Structural Dynamics’* [online] held 23-26 November 2020, Athens: ICMES, 676–689. available from <<http://dx.doi.org/10.47964/1120.9054.18673>> [23 January 2021]
- Rill, G. (2021) *TMeasy Tire Model easy to use* [online] available from <<http://www.tmeasy.de/>> [23 January 2021]
- Rill, G., and Castro, A. A. (2020) *Road Vehicle Dynamics* CRC Press. available from <<http://dx.doi.org/10.1201/9780429244476>>
- Roscoe, K. H., Schofield, A. N., and Wroth, C. P. (1958) ‘On the yielding of soils’. *Géotechnique* [online] 8 (1), 22–53. available from <<http://dx.doi.org/10.1680/geot.1958.8.1.22>> [10 November 2020]
- Rula, A. A., Nuttall, J., and Clifford, J. (1971) *An Analysis of Ground Mobility Models (ANAMOB) Technical Report (U.S. Army Engineer Waterways Experiment Station); no. M-71-4.* [online] available from <<https://hdl.handle.net/11681/30624>> [09 November 2020]
- Sahputro, S. D., Fadilah, F., Wicaksono, N., and Yusivar, F. (2017) ‘Design and implementation of adaptive PID controller for speed control of DC motor’. in *15th International Conference on Quality in Research (QiR) : International Symposium on Electrical and Computer Engineering*, ‘15th International Conference on Quality in Research (QiR) : International Symposium on Electrical and Computer Engineering’ held 24-27 July 2017 at The Westin Resort Nusa Dua, Nusa Dua: IEEE, 179–183. available from <<http://dx.doi.org/10.1109/QIR.2017.8168478>>
- Sandu, C., Taheri, Sh., Taheri, S., and Gorsich, D. (2019) ‘Hybrid Soft Soil Tire Model (HSSTM). Part I: Tire material and structure modeling’. *Journal of Terramechanics* [online] 86, 1 – 13. available from <<http://dx.doi.org/https://doi.org/10.1016/j.jterra.2019.08.002>> [10 November 2020]
- Schofield, A., and Wroth, P. (1968) *Critical State Soil Mechanics* [online] New York: McGraw-Hill. available from <[http://www-civ.eng.cam.ac.uk/geotech\\_new/publications/schofield\\_wroth\\_1968.pdf](http://www-civ.eng.cam.ac.uk/geotech_new/publications/schofield_wroth_1968.pdf)> [10 November 2020]

- Schwanghart, H. (1968) 'Lateral forces on steered tyres in loose soil'. *Journal of Terramechanics* [online] 5 (1), 9–29. available from <[http://dx.doi.org/10.1016/0022-4898\(68\)90015-3](http://dx.doi.org/10.1016/0022-4898(68)90015-3)> [09 November 2020]
- Senatore, C., and Sandu, C. (2011) 'Off-road tire modeling and the multi-pass effect for vehicle dynamics simulation'. *Journal of Terramechanics* [online] 48 (4), 265 – 276. available from <<http://dx.doi.org/https://doi.org/10.1016/j.jterra.2011.06.006>> [09 November 2020]
- Seong, M.-S., Choi, S.-B., and Sung, K.-G. (2011) 'Control strategies for vehicle suspension system featuring magnetorheological (MR) damper'. InTech. available from <<http://dx.doi.org/10.5772/24556>>
- Shoop, S. A. (2001) *Finite Element Modeling of Tire-Terrain Interaction Technical Report ERDC/CRREL TR-01-16*. [online] available from <<https://apps.dtic.mil/dtic/tr/fulltext/u2/a398076.pdf#page28>>
- Simon, D. (1998) 'Experimental evaluation of semiactive magnetorheological primary suspensions for heavy truck applications' [online], Unpublished dissertation. Virginia Polytechnic Institute and State University. available from <<http://hdl.handle.net/10919/37032>>
- Smith, W., and Peng, H. (2013) 'Modeling of wheel–soil interaction over rough terrain using the discrete element method'. *Journal of Terramechanics* 50 (5), 277 – 287. available from <<http://dx.doi.org/https://doi.org/10.1016/j.jterra.2013.09.002>>
- Snyder, R. A., Kamath, G. M., and Wereley, N. M. (2001) 'Characterization and analysis of magnetorheological damper behavior under sinusoidal loading'. *AIAA Journal* [online] 39 (7), 1240–1253. available from <<http://dx.doi.org/10.2514/2.1466>>
- Soliman, A., and Kaldas, M. (2019) 'Semi-active suspension systems from research to mass-market – a review'. *Journal of Low Frequency Noise, Vibration and Active Control* 40 (2), 1005–1023. available from <<http://dx.doi.org/10.1177/1461348419876392>>
- Spencer, B., Dyke, S., Sain, M., and Carlson, J. (1997) 'Phenomenological model of a magnetorheological damper'. *Journal of Engineering Mechanics-asce - J ENG MECH-ASCE* [online] 123. available from <[http://dx.doi.org/10.1061/\(ASCE\)0733-9399\(1997\)123:3\(230\)](http://dx.doi.org/10.1061/(ASCE)0733-9399(1997)123:3(230))>
- Strecker, Z., Mazurek, I., Roupec, J., and Klapka, M. (2015) 'Influence of MR damper response time on semiactive suspension control efficiency'. *Meccanica* [online] 50 (8), 1949–1959. available from <<http://dx.doi.org/10.1007/s11012-015-0139-7>> [10 November 2020]
- STS (2021) *Tests on Soil Samples* [online] available from <<http://sts.com.pk/soil-testing/>> [15 October 2021]
- Szymon, T., and Harlecki, A. (2017) 'Determination of the position of the contact point of a tire model with an uneven road surface for purposes of vehicle dynamical analysis'. *Journal of Theoretical and Applied Mechanics* [online] available from <<http://dx.doi.org/10.15632/jtam-pl.55.1.3>>
- Taghavifar, H., and Rakheja, S. (2019) 'A methodology to analyze the vehicle vibration response to deformable terrain stiffness and damping properties'. *Proceedings of the Institution of Mechanical Engineers, Part D: Journal of Automobile Engineering* [online] 234 (4), 1123–1136. available from <<http://dx.doi.org/10.1177/0954407019863610>> [10 November 2020]

- Taheri, Sh., Sandu, C., Taheri, S., and Gorsich, D. (2015a) 'Hybrid Soft Soil Tire Model (HSSTM). Part 1: Tire Material and Structure Modeling'. *Journal of Terramechanics* [online] available from <<https://apps.dtic.mil/dtic/tr/fulltext/u2/a616952.pdf>> [10 November 2020]
- Taheri, Sh., Sandu, C., Taheri, S., Naranjo, S., Jayakumar, P., Ross, B., and Christ, D. (2013) 'Off-road soft soil tire model'. in *7th Americas regional ISTVS Conference Florida*, '7th americas regional istvs conference florida' [online] Florida: held 4-7 November 2013 at Tampa Convention Center and Marriott Tampa Waterside Hotel. available from <<https://www.istvs.org/proceedings-orders/7th-north-american-conf-2013-tampa>> [18 January 2021]
- Taheri, Sh., Sandu, C., Taheri, S., Pinto, E., and Gorsich, D. (2015b) 'A technical survey on terramechanics models for tire–terrain interaction used in modeling and simulation of wheeled vehicles'. *Journal of Terramechanics* [online] 57, 1–22. available from <<http://dx.doi.org/10.1016/j.jterra.2014.08.003>> [09 November 2020]
- Talatahari, S., Kaveh, A., and Rahbari, N. M. (2012) 'Parameter identification of bouc-wen model for MR fluid dampers using adaptive charged system search optimization'. *Journal of Mechanical Science and Technology* [online] 26 (8), 2523–2534. available from <<http://dx.doi.org/10.1007/s12206-012-0625-y>>
- Tenneco, I. (2021a) *Electronic Damper Technologies* [online] available from <[https://www.tenneco.com/assets/1/7/Electronic\\_Damper\\_Technologies\\_Brochure.pdf](https://www.tenneco.com/assets/1/7/Electronic_Damper_Technologies_Brochure.pdf)> [11 October 2021]
- Tenneco, I. (2021b) *Tenneco Introduces Scalable Architecture For Electronic Suspension Systems* [online] available from <<https://www.tenneco.com/news/news-detail/2013/09/11/tenneco-introduces-scalable-architecture-for-electronic-suspension-systems>> [11 October 2021]
- Terzaghi, K., Peck, R. B., and Mesri, G. (1996) *Soil Mechanics in Engineering Practice* 3rd edn., Chichester: Wiley
- The MathWorks Inc. (2021) *c2d* [online] available from <[https://uk.mathworks.com/help/control/ref/lti.c2d.html?s\\_tid=srchtitle\\_c2d\\_1](https://uk.mathworks.com/help/control/ref/lti.c2d.html?s_tid=srchtitle_c2d_1)> [05 November 2021]
- The Mathworks Inc. (2021) *Choosing the Algorithm* [online] available from <<https://uk.mathworks.com/help/optim/ug/choosing-the-algorithm.html>> [24 January 2021]
- The MathWorks Inc. (2021) *PID Controller Tuning in Simulink* [online] available from <<https://www.mathworks.com/help/slcontrol/gs/automated-tuning-of-simulink-pid-controller-block.html>> [11 October 2021]
- Uhlar, S., Heyder, F., and König, T. (2019) 'Assessment of two physical tyre models in relation to their NVH performance up to 300 hz' 59 (3), 331–351. available from <<http://dx.doi.org/10.1080/00423114.2019.1681475>>
- Upadhyaya, S., Wulfsohn, D., and Jubbal, G. (1989) 'Traction prediction equations for radial ply tyres'. *Journal of Terramechanics* [online] 26 (2), 149 – 175. available from <[http://dx.doi.org/https://doi.org/10.1016/0022-4898\(89\)90004-9](http://dx.doi.org/https://doi.org/10.1016/0022-4898(89)90004-9)> [09 November 2020]

- Ursu, I., Ursu, F., and Vladimirescu, M. (1997) 'The synthesis of two suboptimal electrohydraulic suspensions, active and semiactive, employing the receding horizon method'. *Nonlinear Analysis: Theory, Methods & Applications* [online] 30 (4), 1977–1984. available from <[http://dx.doi.org/10.1016/s0362-546x\(97\)00283-6](http://dx.doi.org/10.1016/s0362-546x(97)00283-6)>
- Wang, D. H., and Liao, W. H. (2011) 'Magnetorheological fluid dampers: a review of parametric modelling'. *Smart Materials and Structures* [online] 20 (2), 023001. available from <<http://dx.doi.org/10.1088/0964-1726/20/2/023001>>
- Wang, J., Wang, W., and Atallah, K. (2011) 'A linear permanent-magnet motor for active vehicle suspension'. *IEEE Transactions on Vehicular Technology* [online] 60 (1), 55–63. available from <<http://dx.doi.org/10.1109/TVT.2010.2089546>> [09 November 2020]
- Wen, Y. K. (1976) 'Method for random vibration of hysteretic systems'. *Journal of the engineering mechanics division* [online] 102 (2), 249–263
- Wereley, N. M., Pang, L., and Kamath, G. M. (1998) 'Idealized hysteresis modeling of electrorheological and magnetorheological dampers'. *Journal of Intelligent Material Systems and Structures* [online] 9 (8), 642–649. available from <<http://dx.doi.org/10.1177/1045389x9800900810>> [09 November 2020??]
- Wong, J. Y. (2008) *Theory of ground vehicles* 4th edn., Hoboken, N.J.: Wiley
- Wong, J. Y. (2009) *Terramechanics and Off-Road Vehicle Engineering: Terrain Behaviour, Off-Road Vehicle Performance and Design* [online] Oxford: Butterworth Heinemann. available from <<https://www.sciencedirect.com/book/9780750685610/terramechanics-and-off-road-vehicle-engineering>> [09 November 2020]
- Wong, J. Y., and Reece, A. (1967) 'Prediction of rigid wheel performance based on the analysis of soil-wheel stresses part I. Performance of driven rigid wheels'. *Journal of Terramechanics* [online] 4 (1), 81 – 98. available from <[http://dx.doi.org/10.1016/0022-4898\(67\)90105-X](http://dx.doi.org/10.1016/0022-4898(67)90105-X)> [23 January 2021]
- Xu, L., Tseng, H. E., and Hrovat, D. (2016) 'Hybrid model predictive control of active suspension with travel limits and nonlinear tire contact force'. in *2016 American Control Conference (ACC)*, '2016 American Control Conference (ACC 2016)' [online] held 6-8 July 2016 at Boston Marriott Copley Place, Boston: IEEE, 2415–2420. available from <<http://dx.doi.org/10.1109/acc.2016.7525279>> [09 November 2020]
- Xu, X., Peng, Y., Du, X., Yu, M., and Fu, J. (2017) 'Modeling of magnetorheological damper using anfis'. in *2017 29th Chinese Control And Decision Conference (CCDC)*, '29th Chinese Control And Decision Conference 2017 (CCDC 2017)' [online] held 28-30 May 2017, Chongqing: IEEE, 2133–2138. available from <<http://dx.doi.org/10.1109/CCDC.2017.7978868>> [09 November 2020]
- Yakub, F., and Mori, Y. (2013) 'Model predictive control for car vehicle dynamics system - comparative study'. in *2013 IEEE Third International Conference on Information Science and Technology (ICIST)*, '2013 IEEE Third International Conference on Information Science and Technology (ICIST 2013)' [online] held 23-25 March 2013, Yangzhou: IEEE, 172–177. available from <<http://dx.doi.org/10.1109/ICIST.2013.6747530>> [09 November 2020]

- Yao, G., Yap, F., Chen, G., Li, W., and Yeo, S. (2002) 'MR damper and its application for semi-active control of vehicle suspension system'. *Mechatronics* [online] 12 (7), 963–973
- Zeinali, M., and Darus, I. Z. M. (2012) 'Fuzzy PID controller simulation for a quarter-car semi-active suspension system using magnetorheological damper'. in *2012 IEEE Conference on Control, Systems & Industrial Informatics*, '2012 IEEE conference on control, systems & industrial informatics' [online] held 23-26 September 2012 at Bandung Institute of Technology, Bandung: IEEE, 104–108. available from <<http://dx.doi.org/10.1109/CCSII.2012.6470482>> [09 November 2020]
- ZF Sachs AG (2021a) *CDC© Continuous Damping Control* [online] available from <[https://www.zf.com/products/en/buses/products\\_51140.html](https://www.zf.com/products/en/buses/products_51140.html)> [12 October 2021]
- ZF Sachs AG (2021b) *Continuous Damping Control (CDC)* [online] available from <[https://www.zf.com/products/en/cars/products\\_29310.html](https://www.zf.com/products/en/cars/products_29310.html)> [12 October 2021]
- ZF Sachs AG (2021c) *Suspension Components and Systems For Commercial Vehicles* [online] available from <<https://www.kothros.com/media/upload-files/manual/fahrwerkkomponentenundsystemefrnutzfahrzeuge.pdf>> [12 October 2021]
- Zhang, X., Liu, S., Zeng, F., and Li, L. (2010) 'Simulation research on the semi-active heave compensation system based on h8 robust control'. in *2010 International Conference on Intelligent System Design and Engineering Application*, '2010 International Conference on Intelligent System Design and Engineering Application' [online] vol. 2, held 13-14 October 2010 at Central South University, Changsha: IEEE Computer Society, 378–382. available from <<http://dx.doi.org/10.1109/ISDEA.2010.192>> [09 November 2020]
- Zhenlei Li, Yanping Yang, Xu Gong, Yi Lin, and Guiping Liu (2008) 'Fuzzy control of the semi-active suspension with MR damper based on  $\mu$ GA'. in *2008 IEEE Vehicle Power and Propulsion Conference*, '2008 IEEE Conference on Vehicle Power and Propulsion (VPPC 2008)' [online] held 3-5 September 2008, Harbin: IEEE, 1–6. available from <<http://dx.doi.org/10.1109/VPPC.2008.4677414>> [25 January 2021]
- Zhu, Q., and Ayalew, B. (2014) 'Predictive roll, handling and ride control of vehicles via active suspensions'. in *American Control Conference (ACC) 2014*, 'American Control Conference 2014 (ACC 2014)' [online] held 4-6 June 2014 at Hilton Portland & Executive Tower, Portland: IEEE, 2102–2107. available from <<http://dx.doi.org/10.1109/acc.2014.6859037>> [09 November 2020]
- Zhu, X., Wang, W., Yao, B., Cao, J., and Wang, Q. (2015) 'Analytical modeling and optimal design of a mr damper with power generation'. in *2015 IEEE International Conference on Advanced Intelligent Mechatronics (AIM)*, '2015 IEEE international conference on advanced intelligent mechatronics (aim 2015)' [online] held 7-11 July 2015 at BEXCO (Busan Exhibition Convention Center), Busan: IEEE, 1531–1536. available from <<http://dx.doi.org/10.1109/AIM.2015.7222759>> [09 November 2020]